Rheological Characterization and Thermal Conductivity of Graphene Modified Asphalt Binder

A Thesis Submitted in fulfillment of the requirement for the award of

the Degree of

MASTER OF ENGINEERING

IN

INFRASTRUCTURE ENGINEERING

Submitted by

MOEED AHMAD NAZKI

801723013

Under supervision of

Dr. Tanuj Chopra

Assistant Professor
Thapar Institute of
Engineering & Technology
Patiala, Punjab 147004

Dr. Anush K. Chandrappa

Assistant Professor
Thapar Institute of
Engineering & Technology
Patiala, Punjab 147004

DEPARTMENT OF CIVIL ENGINEERING

THAPAR INSTITUTE OF ENGINEERING & TECHNOLOGY

(DEEMED TO BE UNIVERSITY), PATIALA, PUNJAB

JULY 2019

Dedicated to the Most Subtle and Acquainted,

my Parents, my family

and Every Teacher I have been Blessed with.

DECLARATION

I, Moeed Ahmad Nazki, hereby declare that this work which is being presented in the thesis entitled "**Rheological Characterization and Thermal Conductivity of Graphene Modified Asphalt Binder**" in the patial fulfillment of the requirement for the award of degree of **Master of Engineering** in the field og **Civil Engineering** with specialization in **Infrastructure Engineering** submitted at **Thapar Institute of Engineering & Technology (Patiala)** is authentic record of my work carried out during the period from 27.7.2018 to 15.7.2019 ubder the guidance of Dr. Tanuj Chopra and Dr. Anush K Chandrappa.

The matter embodied in this thesis has not submitted by me for the award of any degree or diploma.

Date: 15 July 2019

(Moeed Ahmad Nazki)
(801723013)

This is to certify that the above declaration made by the student concerned is correct according to the best of my knowledge and belief.

15/7/19

Dr. Tanuj Chopra
Assistant Professor
Thapar Institute of
Engineering & Technology
Patiala, Punjab 147004

15/07/19

Dr. Anush K. Chandrappa
Assistant Professor
Thapar Institute of
Engineering & Technology
Patiala, Punjab 147004

ACKNOWLEDGEMENT

This report is a collective result of past year's learning and experience at Thapar Institute of Engineering And Technology under the guidance of an esteemed class of academicians. I'm grateful to Head of Civil Engineering Department **Dr. Prem Pal Bansal** for providing such a warm and working environment, also I would like to express my utmost gratitude towards Incharge Transportation Lab **Ms. Neena Garg** for providing extra lab hours which made it possible to finish the work in stipulated time. Also I'm sincerely grateful and obliged to the faculty of civil engineering department for providing a prosperous and enlightened environment with their presence.

I would like to offer my regards and respect to my mentor **Dr. Tanuj Chopra** for his immaculate expertise of the field and ever supporting, warm, illustrious nature which expedited the Thesis work.

I would like to thank and express a heartfelt gratitude to my co-guide **Dr. Anush K Chandrappa** for his knowledgeable interactions and his astute acumen which always inspired to keep the workflow motivated and learning centric.

I would like to give my sincere Thanks to Incharge Heat and Mass transfer lab **Dr. Kundan Lal** for utilization of some sophisticated instruments in HMT lab.

I'm dearly thankful for the help and support **Mr. Sunit Kumar** and **Mr. Amarjeet Singh** has provided in the Transportation lab, by providing extra work hours and weekends just to see the work is completed on time. Also the **Heat and Mass Transfer** staff **Mr. Chanranjeet Singh** provided a flexible working environment.

Lastly I would like to express my thanks to **Anton-Paar India** for providing a wonderful experience with seminars and workshops, especially by **Dr. Thomas Mezger**. With special thanks to Head of Division Characterization Anton-Paar India **Mr**. **Dharmesh Gala** and characterization analyst **Dr**. **Satyanarayan** for their humble interactions and lectures, and area sales manager **Mr**. **Manoj Sharma** for inviting to such wonderful platforms**.**

ABSTRACT

Permanent deformation is one of the important distresses in asphalt pavements, which is greatly influenced by temperature. The phenomenon of rutting is influenced by the rheological properties of binder to an extent of 40%. With the increasing overloaded commercial vehicles, rutting is being a frequent phenomenon on highways. On the other hand, usage of high thermal conductivity materials in asphalt binder is gaining attention owing to low thermal conductivity of neat asphalt. In this study, graphene is staged as a material with future perspectives in material enhancement and uses in pavement sustainability. Graphene is an extraordinary material, which is gaining limelight for its unparalleled physical, mechanical, thermal and electrical properties. In this study, VG30 and VG40 asphalt binders were modified with graphene with four different proportions. It has proved to augment the properties of VG30 and VG40 asphalt binder for high temperature rutting parameter, keeping the storage stability in check. The asphalt binder was verified from its absolute viscosity value and the effect on viscosity and the increasing effect in the complex shear modulus due to the additive was enhanced the binder almost twice. The susceptibility to rutting for unaged control and modified binder was studied using MSCR test, also stress sensitivity of the binder was established by applying eight different stress levels instead of two. The augmentation of thermal properties of asphalt binder for different graphene dosages was observed using heat flow meter principle which gave affirmative results with 2% dosage having thermal conductance twice that of control binder.

TABLE OF CONTENTS

TABLE OF FIGURES

TABLE OF TABLES

TABLE OF EQUATIONS

Chapter 1 INTRODUCTION

1.1. BACKGROUND

The modification of asphalt binders and mixes dates back to 1873 when Samuel Whiting was awarded a patent to modify asphalt mix with latex from *balata plant* and later followed by French who started laying rubberized roads in the early 19th century, various test pavements were constructed in Britain and France by 1930. Since 1945 the modification of asphalt using polymers has been accepted as an alternative to improve the quality of the asphalt concrete pavement (Lewandowski 1994), (Terrel and Epps 1988). Therefore, strides made in the modification of asphalt binder have got a fair share of history of its own along with other advancements in the asphalt pavement technology.

The modification of asphalt binder has the capability to address various mechanical and thermal distresses developed in asphalt concrete pavement. The distresses include: deformations due to heavy vehicular traffic, temperature susceptibilities and brittlement of the pavement (Yildrim 2007).

The indent of Strategic highway research program (SHRP) changed the scope of asphalt binder by implying various grade specifications and methods to establish the degree of augmentation of the asphalt binders with various additives. To inveterate the research for advancement of pavement engineering SHRP was a five year program developed under Surface Transportation and Uniform Relocation Act (1987) in United States, the program among many highway advancement techniques and methods primarily focused on the development of a new specification grading system for asphalt binders which rather than mechanical properties highly relied on rheological properties. The need of developing an asphalt binder for region specific requirements (high temperature rutting, fatigue cracking and thermal cracking) lead to the need for modification of asphalt binder and gave a categorized model to encompass the degree of any modification of asphalt binder through a single perusal system (Petersen et al. 1987) (Coplantz et al. 1993).

The polymer modification of asphalt binders has proven to enhance the properties of asphalt binder to resist various pavement distresses to a greater extent (Yildrim 2007).

The different types of polymers used in modifying asphalt binder are; block chain polymers (*styrene butadiene styrene, ethyl vinyl acetate etc.*), synthetic and natural rubber (*polyisoprene, polybutadiene etc.*) and other (*ground tires, fibers etc.*) (Lewandowski 1994). The first two types require additives to mix and are chemically blended or cross linked with asphalt binder whereas the *others* category is not chemically blended and are added as fillers to enhance the toughness and thermal properties of the asphalt binder. Other than polymers various filler materials are utilized to tweak the properties of asphalt binder to cater a particular need. The addition of crystal bodies of nano or micro sized filler particles are providing a cheaper and if not cheaper a different alternative material properties which are difficult or expensive to harness from a polymer modification.

Graphene has been employed, since its inception, with almost every material presently significant for human use. The European Union has spent 1 billion dollar under its graphene flagship program since 2013, under this program nine companies and 46 different products have been established (Ghavanini and Theander 2015) (Jhonson 2019). In India, TATA group has taken the initiative to work on this wonder material by establishing a company and funding various research institutions across various prestigious Indian institutions. Tata Steel Graphene Business in 2016 became the first graphene producing company in the Indian corporate sector other than small scale laboratories which catered the need for graphene before that and Advanced Material Research Centre in IIT Madras and Centre for Nano and Soft Matter Science in Bengaluru are centers of excellence for graphene research and development. The highest ever recorded mechanical, thermal, electrical properties of graphene make it the strongest contender for innovating new composites in our present day research and development sector. It was discovered by Professors Andre Geim and Konstantin Novoselov at the University of Manchester in 2004 and they received a Noble prize for their work in 2010 (Zhen and Zhu 2018). From quantum computers to space elevators, graphene developed a new and unimaginable world of possibilities in any field of science, medicine and engineering, particularly it is a revolution in the material augmentation.

1.2. INTRODUCTION

Alongside global warming and population expansion one thing that has been ever growing is the need for a convenient transportation medium for people and goods. Pavement construction is one of the costliest sectors of transportation engineering the cost employed according to a Canadian research regarding the annual cost of pavements has stated that annually $150 million are being spent. In the year 2017 alone there has been a sale of 96.6 million motor vehicle units around the globe, with China leading the motor vehicle by accounting for 30% of the total vehicle sales, followed by US, Japan and India. India comprised of approximately 4% (4 million) of the total motor vehicle sale. All the transportation sectors be it air, road or shipping have witnessed a phenomenal growth in past decades. The connectivity of a region plays a vital role in the development of its economics. As per basic road statistics of India for the year 2015-2016, an annual publication of Ministry of Road Transport and Highways, the Indian road infrastructure has grown at an compound annual growth of 4.1% since 1956 to 2016, thus having a road density of 1.7 km per km^2 which is the highest road density in the world which is almost twice that of USA with 0.68 km per km^2. The development of road infrastructure in India has been of paramount importance as the investment during the last decade (2006-2016) has increased seven folds. According to (Huang 2004), 95% (2.5 *million miles*) of the pavements constructed in US consist of flexible pavements. Indian pavement infrastructure comprises of flexible pavement ~98% of the total road length and the tropical climate of the subcontinent demands for a high temperature rut resistant asphalt binder for a durable pavement design (Sinha et al. 2007) (Singh et al. 2013). The reason for adopting flexible pavements over rigid pavements chiefly rests on the low capital cost of the flexible pavements though it surpasses the maintenance costs as compared to a rigid pavement and has a lesser longevity (Jain et al. 2013). To capitalize and enhance the economic aspect of the flexible pavements it is important to augment the flexible pavement for its durability and longevity which is mainly effected by three common distresses caused in the pavement (Becker et al. 2001).

The three most common distresses caused in the flexible pavement as shown in Figure 1 are; (a) rutting *(due to high temperature),* (b) thermal cracking *(due to low temperatures)* and (c) fatigue cracking *(due to continuous load repetitions for a long duration)* . Rutting

is a groove formed along the wheel path due to the distresses caused by heavy wheel load and high temperatures (Shafabakhsh et al. 2014). It is the most common type of distress in India, the rutting of pavements is simulated using dynamic shear rheometer, dynamic material testing device, Hamburg wheel tracker test, AMPT etc., and fatigue cracking is a long term process which is caused due to the prolonged action of wheel load repetition on the pavement surface, the cracking occurs due to the aging of the bituminous binder, it can be characterized in the laboratory using dynamic shear rheometer, AMPT, Asphalt Pavement Analyser (APA) etc (Moghaddam et al. 2011). Thermal cracking usually occurs when asphalt concrete is exposed to sub-zero temperatures that is when the glass transition temperature in the asphalt binder is developed and causes cracks to develop on the surface due to very low temperatures, the thermal cracking is simulated in laboratory using bending beam rheometer, dynamic shear rheometer, direct tension tester, ABCD etc (Kim S.-S. 2005) and (Soleimani et al. 2009).

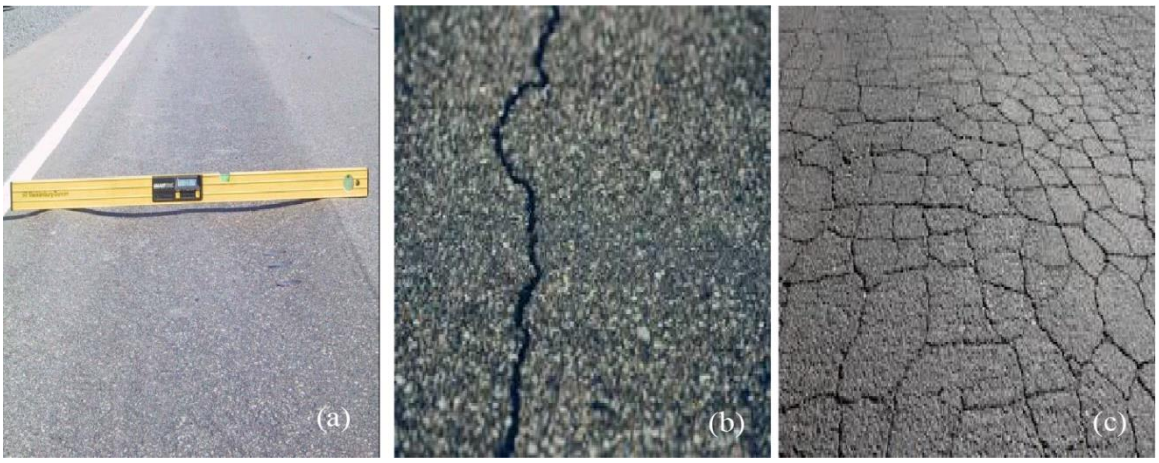

Figure 1 (a) Rutting (b) Thermal Cracking (c) Fatigue Cracking

In India due to the tropical climatic conditions rutting is of immediate importance. Rutting is caused due to inappropriate mix design or when pavement temperature rises near to softening point of the asphalt binder causing the binder to flow under the influence of gravity or getting a tacky character at the surface and getting aggravated by sticking to the vehicle tires, thus, exposing the aggregate-aggregate surface contact which in return weakens the structural integrity of the pavement layer and causing the pavement to sink along the wheel path forming a groove as shown in Figure 2 (a) (Singh et al. 2013) (Faruk et al. 2015). Also due to a weak subgrade, rutting could take place due to the influence of

compressive forces acting at the top of subgrade layer, since the soil mechanics are a bit dormant to the changes due to time and temperature, so, in most of the cases the subgrade is resilient enough to withstand the applied loads and is not the usual cause for rutting (Ebrahim and El-MaatyBehiry 2012). Figure 2 (b) shows the development of stresses in the mixture for causing rutting and the development of stresses in the subgrade for causing rutting. The current models for computing resilient modulus take into account both the parameters; mix design as well as subgrade strength. Figure 2 (c) illustrates the types of rutting caused in the pavement layers, rutting which foments the surface layer of the pavement is known as primary rutting and the rutting caused due to an insufficient durability of the subgrade often due to excess to encumbered loading rates is known as secondary rutting, therefore, a shoddy pavement develops rutting in three distinct failure types that are failure of surface layer due to inadequate or irregular mix design, base failure occurs when the rutting takes place in the granular layer and subgrade failure takes place when the rutting is in the subgrade layer of the pavement as illustrated in Figure 3 (Hjort et al. 2008). Hence, rutting dove tails with the deepest layer that is being affected and the nature of stresses generated also varies with the type of failure. The surface layer of the pavement in United States of America is comprehensively designed as per the loading time and temperature susceptibilities for a region specific ambient temperature conditions as per SHRP (Petersen et al. 1987). SHRP have developed different compacting methods *(gyratory, rolling wheel and kneading compacting)* to develop a better relationship with field results under the observations in asphalt mix performance tester (AMPT) or any testing instrument, also the verification of asphalt binder by determining its viscoelastic properties giving a strong sense of reliability of asphalt binder over the time and temperature susceptibilities. The viscoelastic behavior of the asphalt cement binder is best observed by observing its rheological properties.

Before moving towards the rheological aspect of the asphalt binder it is important to understand the chemistry behind it. Asphalt binder is a polymer consisting of a complex structure of many constituents *(Asphaltenes, Resinous components (polar aromatics,) Non-polar aromatics (naphthenic aromatics), and Saturate)* with 5 to 6 rings of polar aromatics known as Asphaltene form the maximum part of the binder and the main constituent responsible for its viscous behavior, the chemical structure of asphalt is shown

in Figure 4 (Lewandowski 1994). The asphaltenes are surrounded by polar aromatic compounds forming a ring and further the ring extends with decrease in the polarity of the compounds. Also the chemical aspects of the asphalt binder have been observed thoroughly under SHRP to understand the behavior of asphalt binder towards oxidation and to identify any hazardous compounds present in it.

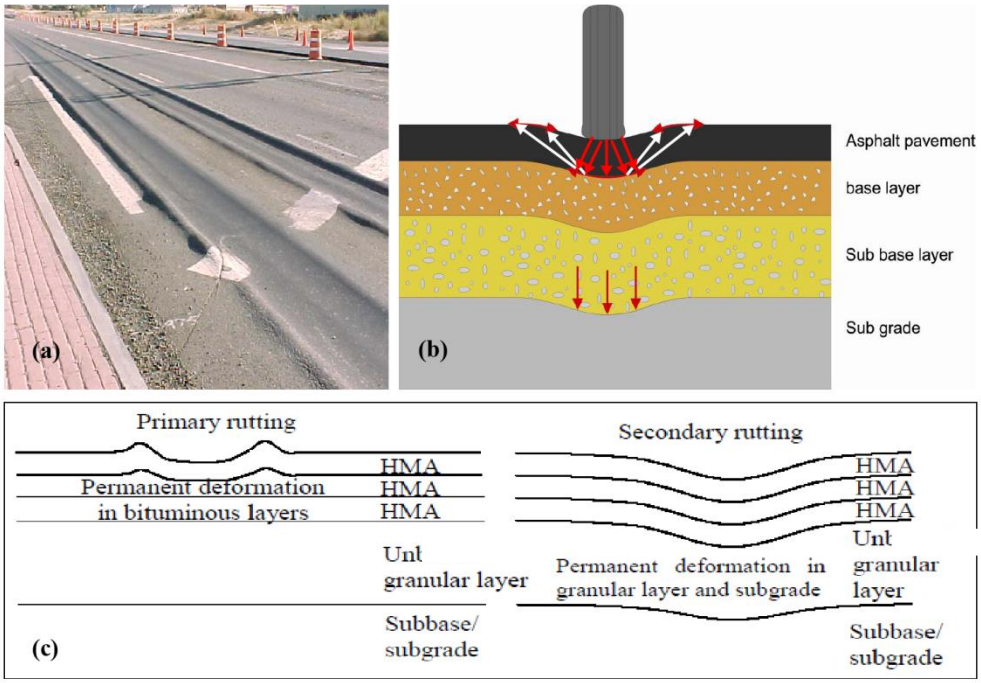

Figure 2 (a) Rutting Due To Poor Mix (b) Stress Mechanism Causing Rutting (c) Primary Rutting Caused Due to Weaker Binder or Poor Mix and Secondary Rutting Caused Due to Heavy Traffic and Poor Subgrade. (Hjort et al. 2008).

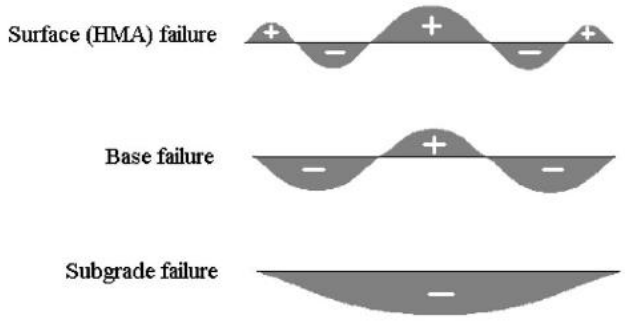

Figure 3 Stresses Generated in the Pavement Layers During Different Types of Rutting Failures (Hjort et al. 2008).

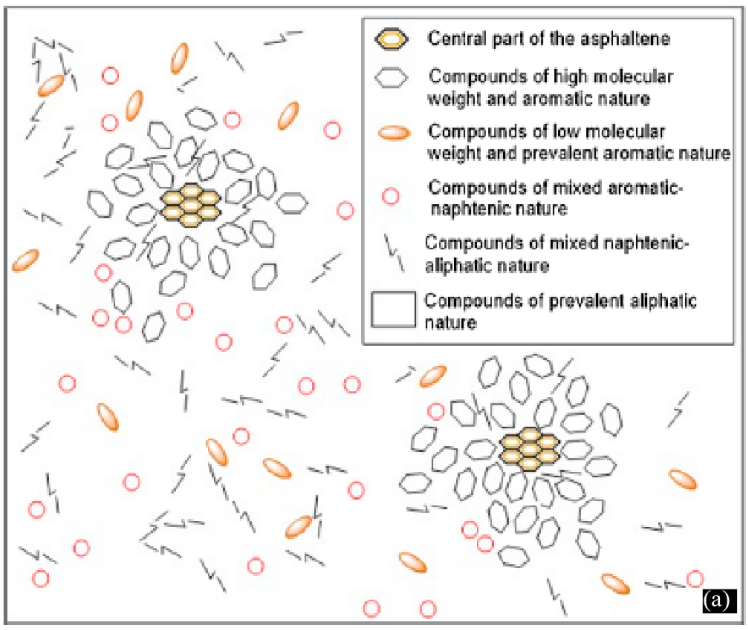

Figure 4 Asphalt Molecular Structure Diagram (Behnood and Gharehveran 2019).

Various chemical properties and the quantity of aspahltenes by asphaltene precipitation was measured and the reduced specific viscosity of different compounds in the asphalt was observed by varying the quantity of natural maltenes as the solvent and the asphaltenes as the solute to identify the dispersion and the thickness of the binder, around 50% to 60% of the asphalt constituents comprises of neutral components and rest are polar aromatic constituents, Figure 5 illustrates the different types of asphalt binders depending upon the constituents present in it, the three models that have been proposed based on the constituents of asphalt are sol type, flocculated asphaltene micelles and gel type, the results varied with different compositions of asphalt constituents and indicated that the properties of asphalt could vary with varying sources (Behnood and Gharehveran 2019). To improve the properties of the asphalt binders the observations imply to the importance of chemical structure in modifying the asphalt with different modifying agents (D'Angelo 2009).

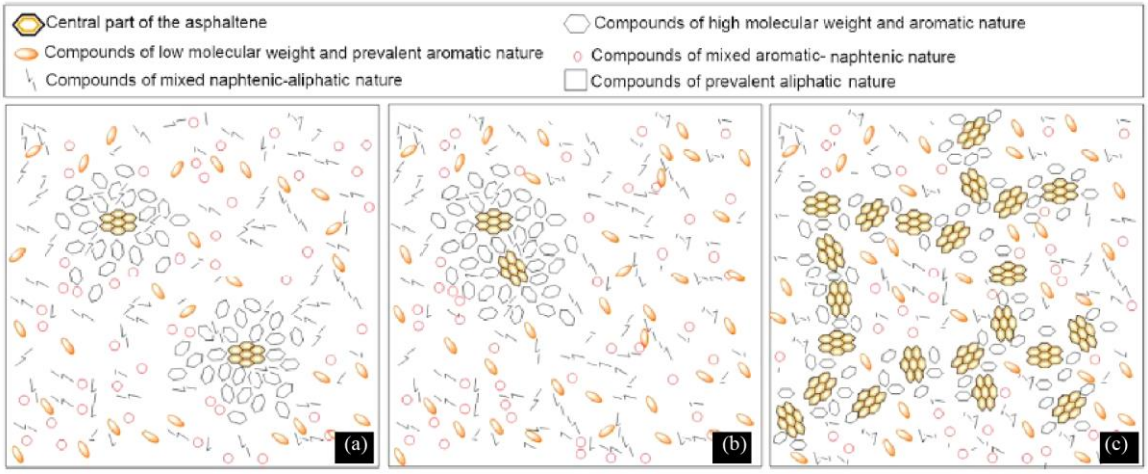

Figure 5 (a) Sol Type (b) Flocculated Asphaltene micelles (c) Gel Type (Behnood and Gharehveran 2019)

The structure of graphene as shown in Figure 6 (a) illustrates the 2D structure of graphene (*image of wrinkled graphene*) which make it possible to have a larger specific area available for bonding with the asphalt binder and the absence of open functional groups omits any interference to develop between the two materials (Eda and Chhowalla 2010) and (Chuah et al. 2014). The comparison of basic properties of graphene and other materials is given Table 1. To elicit the extraordinary properties of graphene, research in a number of scientific faculties is ongoing, since it is a nanomaterial its chemical characteristics with other materials are of paramount importance (Zhang and Zhu 2018). The FTIR analysis of graphene oxide and asphalt binder which further explained below builds upon the fact that only physical blending is possible on mixing with a high shear mixer (Li et al. 2018).

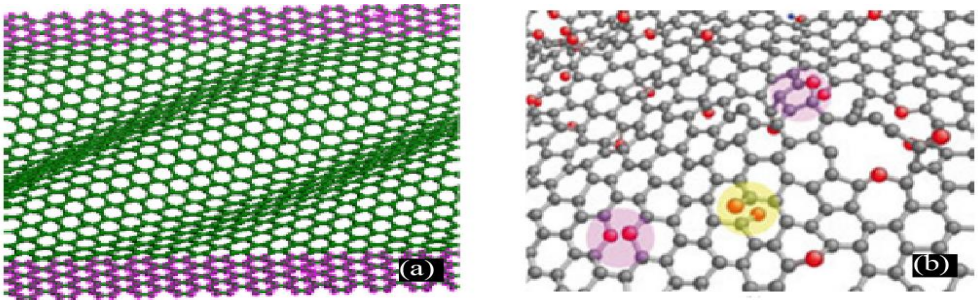

Figure 6 (a) Structure of Graphene (b) Structure of Graphene Oxide. (Chuah et al. 2014)

Though polymers usually bond due to cross linking or interactions between different polarities, the absence of any functional group make it impossible for graphene to interact chemically with the asphalt binder but in order cash out the impeccable properties of graphene chemical blended could be kept in the loop while the basic techniques are availed in case of asphalt binders (Kim et al. 2010).

To improve the durability and longevity of the binder various polymers *(Block chain, natural, others)*, agricultural or industrial waste products *(charcoal ash of various agro by-products, lignin, and plastic waste)* and fillers *(crystal structures, carbon nanotube, nano-silica, montmorillonite, graphene oxide, graphene)* have been utilized (Polacco et al. 2015). The additives enhance thermal, mechanical or chemical properties of the binder which allows the binder to resist the distresses to a higher degree than the precursor. The method to be involved in the addition of an enhancer depends on the particle size of the additive, its interactions with the asphalt binder and storage stability of the modified binder, there are two types of mixing methods:

- Wet mixing
- Dry mixing

Table 1 Comparison of Graphene with other Additives (Chuah et al. 2014)

Material	**Elastic modulus (GPa)**	**Tensile strength (GPa)**	**Elongation at break (%)**	**Density (kg/m^3)**	**Diameter/ thickness (nm)**	**Surface area (m^2/g)**
Graphene	1000	~130	0.8	2200	~0.08	2600
GO	23-42	`0.13	0.6	1800	0.67	700-1500
CNT's	950	11-63	12	1330	15-40	70-400
Carbon fiber polymeric fiber	7-400	0.4-5	1.7	1770	600-20000 18000-30000	0.134 0.225

Glass fiber	72	3.45	4.8	2540	5000-10000	0.3
Steel fiber	200	1.5	3.2	7800	50000-900000	0.02

Wet mixing is the blending of the additive directly to the asphalt cement using high shear mixers or by chemical reagents/ catalysts. Whereas dry mixing corresponds to the mixing of different modifiers into the asphalt concrete mix and are blended physically and further interacting chemically if possible with the aggregates and asphalt binder.

(Liu et al. 2018) and (Li et al. 2018) have confirmed using FTIR observations to identify that there is no chemical change in the chemical composition of asphalt binder though both differ in the case of a SBS modified asphalt binder, further study is required to address this conflict of interest as the graphene oxide (GO) used by both the researchers differs quite significantly in its specific surface area. This inability of graphene to interact with asphalt chemically make it susceptible to agglomeration as the Van der Waal's forces responsible for the bonding between asphalt and graphene make the graphene particles more attractive to each other than asphalt particles. The problem of inadequate dispersion arises with the increase in the quantity of the nanoparticles which demands a higher rate of dispersion. However the scope of this study which would be discussed in detail in the next section does not cover the improvement of dispersion techniques rather focuses mainly on the enhancement of binder properties with the addition of graphene nano-platelets.

The rheological studies of asphalt binder are opted to study the rutting behavior of asphalt binder as it emulates up to 40% for permanent deformation of the asphalt binder as shown in Figure 7 (Sybilski et al. 2013). Rutting is a nuance in the pavement industries it accounts for 80% of failure distresses in the asphalt pavement (Sha 2006). The various measuring indicators for stiffness of a binder in a rheological test are $G^*/\sin\delta$ (rutting parameter), Jnr (non-recoverable creep compliance and R% (recovery percentage), the augmentation of these parameters represents the enhancement of asphalt binder to a rut resistant binder, usually augmentation of these parameters is done by forming a composite

material of asphalt and other materials *(elastomer, plastomer, nanomaterials, mineral filler etc.)* (Yinfei et al. 2018).

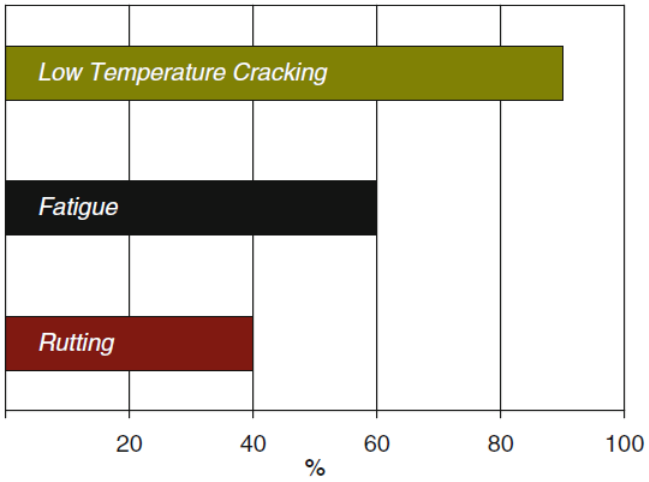

Figure 7 Relationship Between Binder Properties and Distresses in Pavements (Sybilski et al. 2013)

The strain sweep test determines complex shear modulus G^* and the phase angle δ with which rutting parameter $G^*/\sin\delta$ can be computed and also the linear viscoelastic range is determined of the binder which is necessary for conducting frequency sweep test which shall be conducted within the LVER (Airey et al. 2002). The standardization of asphalt binder at different temperatures and loading rates is possible by frequency sweep test (Santagata et al. 2012). Initial self-healing temperature (Li C. et al. 2016) and the master curve (Yin et al. 2018) could be developed from the test data. The multiple stress creep recovery (MSCR) test is fairly a new addition to the rheological testing protocol. The MSCR test is stress controlled test, in this test in regards to stiffness of binder, the permanent deformation is evaluated by observing creep and recovery cycles of asphalt (Hossain et al. 2016).

Apart from the high stiffness of the binder the thermal conductivity of the binder plays a vital role is dissipating the high temperatures as quickly as possible to ensure no heat is stored in the binder course to elevate the temperature of pavement any further. There is a thumb rule of having the pavement temperature 15℃ more than that of the air temperature, therefore to reduce this temperature differential to minimum the pavement shall be more affective in diffusing the heat energy, thus to avoid the cumulative effect of the heat energy being stored in the pavement surface. A thermally better conducive

asphalt binder helps in keeping the pavements cool and could be utilized for energy harvesting and energy storage (Mallick et al. 2009).

1.3. PROBLEM STATEMENT

The high temperatures and growing vehicular traffic of Indian subcontinent poses the problem caused due to high temperature rutting which is caused when a binder is not capable to resist high temperature and loads, this effect is usually due to the negligence to environmental conditions of a region. When a soft binder is used in a hot climatic conditions it tends deform and flow, also when a stiff binder is utilized it tends to crack in the cold temperatures. So, a need to verify an appropriate region specific binder is important to be induced in highway engineering. Since India has mostly tropical climatic conditions, the need for a stiffer and a thermally more transient binder is essential for longevity of asphalt pavements.

1.4. SCOPE AND OBJECTIVE OF RESEARCH

The objective of this study was to recognize the improvement in the rheological properties, thermal conductivity and morphological characterization of the asphalt binder modified with Graphene to produce less temperature susceptible binder. Also the stress sensitivity of the asphalt binder for a varying range of stresses other than 0.1 kPa and 3.2 kPa are observed.

This research was carried out to observe and record the improved physical properties, rheological properties, thermal conductivity and morphological changes of the asphalt binder with the addition of graphene nano-platelets. Dynamic shear rheometer MCR-52 from Anton Paar was used to observe the rheological changes of the asphalt binder and to monitor the thermal conductivity of the modified binder Thermal analyzer for building materials H112N from Pelkin Hilton was used. Scope of this study is listed as under:

1. To determine the physical properties of the asphalt binder
2. To determine the rheological properties of the asphalt binder
3. To determine the thermal conductivity of the asphalt binder

During the research work the learning curve was always growing and multi-disciplinary in nature, there were several workshops and seminars that helped in better understanding

of the subjects and expedited the research. For shear mixing of the asphalt binder and graphene a make shift mixer was engineered by combining an old mechanical stand drill with a mixing blade attached to a drill bit. The drill could be adjusted for different speeds using a gear set and could go up to 2400 rpm. The rheological testing was conducted using a DSR and the thermal conductivity of the binder was determined by using a thermal analyzer for building materials. The statistical analysis was carried out using SPSS.

Chapter 2 LITERATURE REVIEW

The literature review forms an important aspect of the research and was carefully categorized in seven different sections to discipline the research for a focused approach. The reviewing of papers was done in a manner to first identify the cause of concern in the current industrial practices and then gaining knowledge regarding the methodology to be followed. This research is multi-disciplinary in nature and attracted knowledge of different walks of science and engineering. The categorization scheme was devised of major categories, though the reviews might not be category specific due to the multi-disciplinary approach of various researchers, the categories are as follows:

1. History, Road statistics and testing protocols
2. Distresses in pavements, modification of asphalt and rheological studies
3. Utilization of nanomaterials in asphalt and other construction materials
4. Properties of graphene and its utilization in asphalt binder modification
5. Thermal behavior of asphalt binder and pavements
6. Chemical and Morphological characterization
7. Statistical Modelling

2.1.HISTORY, ROAD STATISTICS AND TESTING PROTOCOLS

- (Petersen et al. 1987) worked under the National Research Council's SHRP and gave the correlation between the chemical and physical properties of the asphalt. The research illustrates various measuring test methods and characterization processes. Also the tests and temperatures required to determine the new super pave grading through rheological studies with respect to the environmental aspects of a region are illustrated in this study.
- (Terrel and Epps 1988) study gives a record of issuance of asphalt modification patents to as early as 1843 and gives the account for various types of polymers which are used in the modification of the asphalt binder and the testing mechanism used to understand the changes in the properties of the asphalt binder due to the polymer

modification. The development of latex to form emulsions and the use of elastomers to avoid the permanent deformation are discussed in this review study.

- (Coplantz et al. 1993) carried out literature review to understand the correlation of the field results to that of the laboratory results for SHRP and it was concluded that the modified binders showed a better performance than the neat binders, also the limitation of the conventional measuring procedures was subject to question as they could not correlate to the field results.
- (Lewandowski 1994) Studied a wide vista for the advances made in asphalt modification by discussing its historical significance, chemical behavior, morphological and rheological changes or augmentations that the material has undergone. The historical account given in this study dates polymer modification to about 100 years from now and suggests that a proper modification with scientific observations were developed as early as 50 years ago. The addition of a polymer material of an order of just 3% could impart an increase in the viscosity of the modified binder by almost 2 degrees.
- (Becker et al. 2001) presented an overview of the polymer modified binder in light of Venezuelan oil market. The study described that less than 6% as a genuine polymer additive and more than 6%, it lists the modification as a high content polymer modification. The paper suggests that the initial cost of the modified pavement was high though life cycle cost of the pavement is skimmed by almost 10 times.
- (Huang 2004) mentioned in his book that as of 2001 around 95% of the pavements in US comprise of asphalt concrete pavements. United States of America constructed its very first bituminous pavement from Newark to New Jersey in 1870.
- (Singh et al. 2006) studied the rheological behavior of asphalt for Indian conditions, in which he describes use of 1.59 Hz frequency as the equivalent to a vehicle traversing the pavement at 80 km / h for a loading duration of 1 s.
- (Yildrim 2007) study illustrated the importance of a modified binder which could resist multiple stresses including moisture susceptibility, which turned out to be more economical in the long run. Also the storage stability of the modified asphalt is important as the lack of compatibility between the asphalt and modifier could result in a poor pavement.

- (Soenena et al. 2013) observed a round robin test for European MSCR standards in which the repeatability and reproducibility of the 4 binders initially and then 7 binders across different institutions were observed by computing the coefficient of variance of the data. It further suggests due to some technical fault the DSR tends to show a negative recovery. The negative recovery is a tricky concept caused due to the latency of the responsive signal.
- (Johra et al. 2014) studied the process involved in obtaining graphene, which included chemical vapor deposition, micromechanical cleavage of graphite, and exfoliation of graphite. This study solution based chemical approach was adopted. The XRD pattern shows a peak value around 26° and the Raman spectrometer shows a peak at 1600 cm^{-1} in the G band.
- (Ghavanini and Theander 2015) This report was funded by Chalmers Industriteknik to review the advances made and possible in the transportation infrastructure by inclusion of graphene. The report highlights the extraordinary properties of graphene of having highest specific surface area of 2700 m^2 / g, thermal conductivity 106 times that of copper, intrinsic mobility 100 times that of Si, most stretchable crystal (up to 20% elastically), thermal conductivity (outperforming diamond), completely impermeable (even He atoms cannot squeeze through), Conducts electricity in the limit of no electrons, lightest charge carriers (zero rest mass), Longest mean free path at room temperature (micron range)
- (Zani et al. 2017) observed that there is not a significant change in the rheological properties of the asphalt binder after storage of 3 and 5 days. The frequency sweep test determined that there was not much difference between the complex shear modulus of the different samples bound to different storing times. The resistance to polymer and asphalt separation could be taken care by maintaining the polymer modified binder at high temperatures.
- (Jeffry et al. 2018) Suggests that the coconut shell ash was used to modify the properties of the binder and had resulted in the enhancement of the physical and rheological properties of the binder. The rutting parameter had demonstrated an improvement in rutting for 70℃ and implied an optimum level of 6% coconut ash

powder of 47.7 nm particle size. The storage stability of the modified binder was well within the 2.2℃ boundary condition.

- (Jhonson 2019) European Union has spent € 1 billion and 10 years of extensive research in Graphene flagship program which garnered 9 companies, 46 products and have helped 17 commercial products. Graphene has developed some lifesaving products such as flexible wireless sensor which could be used to measure the heart rate of a patient. Among many one of the highlights of graphene products is the graphene coated commercial helmet which can resist high impacts and temperature.

2.2. DISTRESSES IN PAVEMENTS, MODIFICATION OF ASPHALT AND RHEOLOGICAL STUDIES

- (Airey et al. 2002) studied the viscoelastic criteria predefined by SHRP. The linear viscoelastic region could be determined via amplitude test and by computing the ratio of complex shear modulus at high and lowest strain percentage, the ratio shall be above 0.95 in order to qualify for a linear range. Also the strain percentage at which the frequency sweep is to be observed shall be within LVER.
- (Fanga et al. 2004) Suggests improper design, poor drainage and heavy vehicular traffic lead to the rutting of the pavement surface which could be categorized into three classes depending upon the depth at which the rutting takes place, rutting in the surface layer is usually due to the improper mix design, the base and subgrade rutting is due to the weak granular and subgrade heave, respectively. In this study, time hardening creep model using Finite Element Analysis showed that the rutting affected the surface layer immediately as the area under the layer is lesser as compared to other two layers and the top to down stress transfer mechanism of flexible pavements demand for a more robust surface layer.
- (Sha 2006) studied the effects of structural and moisture susceptibility on the asphalt concrete pavements to assimilate the nature of rutting and the measures requisite to avoid it. Further it reported that 80% of the pavement failures are due to the permanent deformation of the pavement.
- (Kim S.-S. 2005) proposed a new testing mechanism known as ABCD other than bending beam rheometer and direct tension tester. The ABCD tester marks the coefficient of thermal expansion by attaching strain gauges inside of an Aluminum

tube onto which asphalt binder is molded. Asphalt has higher values for coefficient of thermal expansion / contraction than Aluminum thus the system allows asphalt to form thermal cracks which are be monitored and recorded by strain gauges. ABCD test has many advantages as it is a fast test and as many as 60 -90 samples could be tested in a 0.036 m^3 chamber.

- (Sinha et al. 2007) Suggests that the pavement designed in accordance with Marshal test is likely to fail due to rutting despite having a thicker crust, as the other factors such as climate condition, traffic variations, slow moving traffic at the intersections or curves etc., play an important role in determining the pavement behavior. It demonstrated the superiority of crumb rubber modified bitumen mix over the unmodified bitumen mix in there thermal characteristics. The importance of taking into account a regional temperature for binder selection was reported.
- (Soleimani et al. 2009) reports that most of the pavements designed as per the North American guidelines are usually under designed for thermal cracking. Though the report mentions new Canadian standards have increased the conditioning time for BBR from 1h to 24h and from 24h to 72h which increased the accuracy of the test from 55% to 90% and 90% to 95%, respectively. In this study the tests were conducted using DSR with a torsion beam attachment and $\tan\delta$ values were analyzed.
- (Moghaddam et al. 2011) drafted a review on the fatigue and rutting behavior of asphalt mixes. The study describes various conditions leading towards rutting and the testing protocol to analyze fatigue and rutting performance of the pavement. Fatigue distress in the asphalt pavement could be characterized using Beam Fatigue Test and Indirect Tensile Fatigue Test. Rutting parameters for the asphalt mix could be analyzed using wheel tracking test, static creep test, repeated-load creep test, Marshall Quotient and indirect tensile test. Also the fatigue and rutting parameter of the asphalt pavement could be observed using the rheological properties of the asphalt by a DSR and the additives to the asphalt binder were able to prevent rutting and fatigue characteristics of the asphalt concrete by either decreasing the oxidation of asphalt or by enhancing elastic properties of the asphalt binder and allowing the asphalt to withstand the temperature changes as well. This study explains that the varying amount of wax is responsible for the varying properties of the asphalt and an

appropriate asphalt grade shall be verified as per its penetration grade or the complex modulus observed using DSR.

- (Ebrahim and El-MaatyBehiry 2012) the overloading of the pavement causes high compressive stresses at the top of subgrade resulting in the permanent deformation or secondary rutting of the pavement. In this study BISAR software has been utilized extensively to emulate the stresses in the layers below asphalt concrete.
- (Santagata et al. 2012) studied the influence of carbon nano-tubes on asphalt binder by plotting the master curve for the 4 different proportions with difference in the ages of binder by conducting frequency sweep test. The observations indicated an improvement in the rutting parameters and also an ageing index was drafted using the data from frequency sweep test.
- (Jain et al. 2013) analyzed that flexible pavements are more economical than rigid pavements as these can be constructed in stages as per demand, also flexible pavements are recyclable. Though overall life cycle cost for rigid pavements is 30 – 40% less but initial cost of rigid overlay is 15% - 60% more than the flexible pavement.
- (Sybilski et al. 2013) compiled a state of the art report on the binder testing and the role of binder properties which come into picture in emulating the distresses in the asphalt concrete pavement. It suggests that the rheological characterization of the asphalt binder tends to project 40%, 60% and 90% assimilations on the rutting, fatigue and thermal cracking, respectively.
- (Singh et al. 2013) reported that Indian pavement infrastructure consists of 98% of flexible pavements and further narrates the importance of an appropriate mix design to achieve necessary strength. The aggregate selection imparts an important part of the mix design of the pavement as the interfacial bonding between asphalt binder and aggregate is of paramount importance. The study establishes a firm ground to determine that the polymeric modification of asphalt binder with a plastomeric 3D polymer (EVA) enhances the interfacial bonding and enhances the rheological rutting parameter $G^*/\sin\delta$ for the asphalt binder.

- (Shafabakhsh et al. 2014) Suggested that a rut resistant asphalt binder is required to avoid rutting which results in wheel track grooves which hampers the road safety and causes the pavement to permanently deform. The study employed the use of powdered tire rubber to enhance the anti-rut properties of the pavement and also it suggests augmentation of flexibility of the pavement layers to avoid distresses developed in the pavement due to heavy load and extreme thermal conditions.
- (Polacco et al. 2015) reviewed the modification of asphalt by virtue of polymeric addition using high shear mixer. The study reports that there are 75% elastomers, 15% plastomers and 10% other natural rubber or categorized as *other*. Further it states that the colloidal matrix of the asphalt binder shall not encounter any swelling of the additive or else it might retain the properties of an unmodified binder.
- (Faruk et al. 2015) highlighted the importance of HMA mix design in order to prevent rutting of pavement caused due to shear deformation in the surface layer. In this study, Simple Punching Shear Test *(SPST),* a new laboratory testing was considered which embarked on some positive statistical results by demonstrating 95% reliability value by Tukey's test and the coefficient of variance was under 30% boundary value.
- (Saboo and Kumar 2015) suggested that the permanent deformation of the pavement is associated with the binder performance towards temperature and time including stresses or strains. The study points out the inability of the Super-Pave parameter $G^*/\sin\delta$ to simulate the exact nature of permanent deformation of the pavement whereas MSCR test determining the creep compliance and recoverable nature of asphalt determines better results. Four different stress levels were utilized to establish the creep compliance of the polymer modified binder. The PMBs tend to have a superior response towards the temperature and stress susceptibilities than the unmodified asphalt.
- (Vissche et al. 2016) reported the findings of the round robin test conducted by task group *TGI* in 2012 and 2014 with 25 participants to draft the testing protocols for the European practices for MSCR testing. In this study it was found that the binder tends to exhibit negative value when the machine is unable to send the block signal at appropriate time to stop the creep and allow the recovery of the sample. In order to get

better statistical results in terms of coefficient of variance the negative values were replaced by ‘zero’.

- (Li C. et al. 2016) suggested the use of mineral filler in asphalt binder could enhance its self-healing and observed the phenomena using the concept of flow behavior of asphalt binder by developing a flow behavior index via power law. Elevated values of the flow coefficient *n* were reported nearing to 1 which signified a Newtonian flow profile.
- (Hossain et al. 2016) studied the recovery behavior of the polymer modified asphalt and illustrated high recovery behavior of the modified binder. The polymeric modification elevates the stiffness of binder by minimizing the permanent deformation of the asphalt binder.
- (Yinfei et al. 2018) reviewed the preventive measures and tests observed for rutting of asphalt concrete pavements. The study lists the different modifiers to enhance the asphalt binder and testing parameters that should be considered in assessing the rutting behavior of the asphalt pavement. Various solutions are described in detail to avoid any compromise to the rutting of the asphalt pavement.
- (Moghaddam and Baaj 2018) Studied high modulus asphalt mix developed using three different asphalt binders (PG 58-28 + Elastomers, PG 82-29 and PG 88-28) and the correlation between the microstructure of the binder and its rheological properties was established, also the comparison of the viscoelastic properties of the asphalt binders and the mixes was evaluated using 2S2P1D model. The linear viscoelastic tests were conducted to maintain the linear behavior of the asphalt and two sets of temperature (2 - 35 and 40 – 90) were used with a varied angular frequency of 1 – 100 rads /sec (*viz. frequency* 0.159 – 15.9 Hz) to check the augmentation in the linear behavior of the asphalt by modification. The morphological studies suggested that the denser the micro-structure of the binder the lower its phase angle will be. The denser micro-structure of PG 88-28 than the PG 58-28 showcased higher stiffness and the Cole – Cole diagram illustrated that the phase angle for PG 58-28 at 90℃ is highest suggesting that the energy dissipation will be highest.
- (Shirzad et al. 2019) In this study the rheological aspects of asphalt were observed using DSR and BBM, also self-healing behavior of the asphalt binder was monitored

using its rheological properties with self-healing polymer additives. The self-healing polymer enhanced the elastic properties of the asphalt binder even on the addition of recycled asphalt binder the stiffness of the self-healing polymer modified binder was higher. The modified binder showed decrease in the recovery percentage and a decrease in the Jnr values. The UV exposed samples showed a better fatigue resistant performance in LAS test.

- (Liu et al. 2018) studied the high viscous behavior of polymer modified binder was accounted to, which is not favorable for mixing and compaction as they require low viscosities and to attain a lower viscosity higher energy would be required. The complex modulus and phase angle of the asphalt binder are augmented with SBS polymer though due to the dense formation of molecules the viscosity increases. To decrease the viscosity values, polyphosphoric acid (PPA) was added which decreased the viscosity value and its effect in augmenting complex modulus and phase shift was negligible.
- (Yin et al. 2018) suggested the construction of master curve by *time-temperature superposition principle-TTS,* master curve could be plotted for varying frequencies and temperatures . Various mathematical curve fitting methods could be employed in developing a master curve. The most widely used *cf* method is William-Landel-Ferry *(WLF)* theory.

2.3. UTILIZATION OF NANOMATERIALS IN ASPHALT AND OTHER CONSTRUCTION MATERIALS

- (Chuah et al. 2014) highlighted the superiority of 2D structure of graphene over other nanomaterials in forming composites with cement binder in order to enhance its workability, durability and increase in hydration rate. The paper emphasize on the improvement of microstructure by virtue of bridging the micro-cracks.
- (Karnati et al. 2019) suggested silica nano-particles are highly efficient in reducing the ageing process of the asphalt binder, though effectiveness of silica nano-particales is limited due to difficulty in obtaining a proper dispersion. The nano-particles tend to form agglomerates in a poor dispersion.

2.4. PROPERTIES OF GRAPHENE AND ITS UTILIZATION IN ASPHALT BINDER MODIFICATION

- (Baochang et al. 2009) suggests that dispersion is of two types, intercalated and exfoliated. They had described the gaps or interlayer space between two Silicate layers as the gallery of a interlayer distance of about 1nm. If the phase angle 2θ lies in the range of this gallery in the XRD pattern then the modifier has been intercalated in the mixture. Else if the phase angle lies outside this phase angle gallery of silicate then the modifier is exfoliated.
- (Kim et al. 2010) reviewed reports the features of top down production of graphene to augment the scalability of graphene production and it attributes to form a better composite with the polymer than the bottom up production method. The authors point out that the graphene sheets might restack in a polymer dispersion which delivers poor result, to avoid this phenomena surfactants could be employed. Monomeric grafting could be taken into account by virtue of activated functional groups interacting with the polymeric chains.
- (Eda and Chhowalla 2010) suggests the oxygen containing functional groups are attached at the edges of graphene oxide. Generally oxygen is present in graphene oxide in the form of OH and epoxy groups on basal plane, however smaller amounts of other functional groups such as carbonyl, phenol, lactone, carboxyl and Quinone are present primarily at the sheet edges. Graphene oxide ranges with chemical compositions from $C_8O_2H_3$ to $C_8O_4H_5$ and corresponds to a C/O ratio of 4:1 to 2:1. The structure depends on the method of preparation.
- (Wei and Qu 2012) Graphene is the thinnest and strongest material ever measured in the entire universe, discovered in 2004 by K. S. Novoselov and A. K. Geim. It is used only as filler in polymers. Graphene has garnered astute response from scientific society regarding its exceptional physical properties, which are electronic, electrical, mechanical, optical and thermal properties. Despite extraordinary behavior of graphene it has not been possible to harness the full potential of graphene, due to the inability to achieve a reliable dispersion of graphene. For a better dispersion though graphene oxide (GO) is better than graphene but it loses its extraordinary mechanical,

electrical and thermal strength due to the loss of π–conjugated structure of graphene. Also GO is hydrophilic irrespective of hydrophobic nature of graphene. Though GO has excellent electronic and luminance properties due to the band gaps created by the missing π-electron structure.

a. Thermal properties

Graphene has an intrinsic thermal conductivity one order higher than that of copper ($K_{(g)}$ = 5000 W mK^{-1} whereas copper has $K_{(C)}$ = 400 W mK^{-1}). The interfacial resistance is overcome by coupling of graphene with the polymer. A well dispersed graphene improves the thermal conductivity of the polymer.

b. Mechanical properties

Graphene has the highest ever recorded young's modulus of 1 TPa, with an intrinsic strength of 130 GPa but oxidation of graphene proved to decrease the decrease the mechanical properties of graphene. Oxidation occurs due to the functionalization, cross linking and assembly of graphene sheets.

c. Photothermal Effect

Graphene's optical absorption in the near to infrared (NIR ~ 700 nm – 1100 nm) has proven it to be useful for materials which lack the property to absorb in near to infrared region, for this it has been helpful in various biological studies as most of the flora and fauna lack the ability to absorb NIR. Graphene has been used in oncological studies and also it has been studied for its use in curing Alzheimer's disease. The medical benefits are attributed to its ability to induce hyperthermia.

- (Ghavanini and Theander 2015) This report was funded by Chalmers Industriteknik to review the advances made and possible in the transportation infrastructure by inclusion of graphene. The report highlights the extraordinary properties of graphene of having highest specific surface area of 2700 m^2 / g, thermal conductivity 106 times that of copper, intrinsic mobility 100 times that of Si, most stretchable crystal (up to 20% elastically), thermal conductivity (outperforming diamond), completely impermeable (even He atoms cannot squeeze through), Conducts electricity in the limit of no electrons, lightest charge carriers (zero rest mass), Longest mean free path at room temperature (micron range)

- (Zhen and Zhu 2018) observed the lamellar structure of Graphene and founded by sp^2 hybrid structure forming a hexagonal grid pattern. Graphene has this basic structure of any carbon allotrope *e.g.* graphite, C60 etc. Unlike CNT's, graphene form a 2D planar structure and its discovery paved the way for Andre Geim and Konstantin Novoselov for a Noble prize in 2010.
- (Zhang and Zhu 2018) reviewed the unique applications of graphene with an endless spectra of prospects for graphene composites. The author emphasis on the memory retaining behavior of graphene which enables it to encompass any ordinary material for knitting textiles for the energy storage. The graphene coated fiber sensors are highly sensitive and are also utilized for medicinal purposes. The aerogels developed with the indentation of graphene call for a super hydrophobic behavior with all regards to its light weight and high specific surface area. Graphene is being explored and observed by scientists as a material of high avail for the human race.
- (Liu et al. 2018) used performance grade (PG) 64-22 and (PG) 58-34 asphalt binders. Graphene oxide (GO) having an extremely high specific area of 2600 m^2/g and zeta potential of -30mV. Concluding that after 0.05% GO dosage bundling/ agglomeration of nanomaterial takes place.

  Characterization of GO interaction with Asphalt was carried out using

  a. *Fourier Transform Infrared-Spectroscopy (FTIR)*

  The FTIR results indicated that the non-modified asphalt (PG 64-22) involves in both chemical reactions as well as physical blending whereas modified asphalt *SBS* (PG 58-34) undergoes only physical blending.

  b. *Differential Scanning Calorimetry (DSC)*

  GO modified bitumen will not significantly change the T_g of the investigated bitumen, but can improve their crosslinking degree (and more effectively for non-modified). The modification of bitumen resulted in lowering the transition temperature T_g value by 3.25% in 0.05% GO modified bitumen. The endothermic energy value was 19.8% lower in 0.05%GO, indicating that the crosslinking density of bitumen was increased by the addition of GO. The crosslinking network generated by physical & chemical actions of Graphene Oxide in bitumen restricted the movement of bitumen molecules. The addition of Graphene Oxide enhanced the high-temperature property of the non-

modified (PG 64-22) asphalt binder and had a slight impression in lowering its low-temperature property. Adding Graphene Oxide in unaged or short-term aged bitumen binder will not significantly change the T_g of the binder (especially for SBS modified asphalt), but it will increase the crosslinking degree of the asphalt.

Physical properties test

a. Rotational viscosity (RV) test

Viscosity was highest at GO value of 0.05% and 0.2% for non-modified and modified bitumen respectively, the decline in viscosity on increasing the GO quantity is due to agglomeration of GO.

b. Rheological performance

From the G*/sinθ and T results, it is observed that for the non-modified bitumen binder, Graphene Oxide addition can greatly enhance the high-temperature performance of bitumen binder, and the amount of Graphene Oxide should not exceed 0.05%; further addition of Graphene Oxide may see less beneficial effects on the mechanical performance and make it uneconomical for modification.

Failure temperature is defined as the point which indicates the G*/sinθ value to be exactly 1 kPa (for un-aged binder) or 2.2 kPa (for RTFO aged binder).

c. Creep test

R-value i.e. elastic component of the bitumen can be improved by a small amount of GO of 0.05% and is increased substantially as the dose is increased. Whereas J_{nr} value i.e. unrecoverable creep compliance shows an opposite trend it reduces with addition of graphene oxide.

- (Li et al. 2018) Studied the graphene oxide modified 90A (80/100 penetration grade) and SBS-MA *(Styrene-Butadiene-Styrene Modified asphalt*) asphalt binders at addition of 1% and 3% GO by weight of bitumen. GO with 5-10 layers, 95% purity and specific area of 100-300 m^2/g, structural crystallite of 43.2 and lamella diameter of 10 μm to 50 μm.

Characterization of GO interaction with Asphalt was carried out using

a. *Fourier Transform Infrared-Spectroscopy (FTIR)*

The test suggested that there is no change in the functional groups of both the asphalt binders. Thus GO does not have any chemical reaction with either of the asphalt binders.

b. *X-ray Diffraction test (XRD)*

The lamella structure is completely alleviated as diffraction peak of GO is not observed in the XRD images of the 90A + 3% & SBS-MA + 3%. This could be attributed to the enhancement of viscosity due to the addition of GO, thus there is a poor crystallization of the saturated carbon as a bigger barrier is to be crossed during crystallization process.

c. *Gas chromatography-mass spectrometer (GC-MS) test*

The gas mass spectrometer indicates that there is a peak at the mass charge ratio of 44 inferring the gas to be CO_2. It shows that the gas released is in the range of 2.5 minutes to 4.5 minutes and after which no gas is released. The amount of CO_2 is limited due to the limited presence of oxygen containing functional groups.

d. *Differential Thermal Analysis and Thermo Gravimetric test*

The loss rate of 1% in GO starts at 154℃ and the range of first stage reaction is between 154℃ to 334℃ with a mass loss of 21.52% followed by second stage having a range between 334℃ to 629℃ with a mass loss of 35.15%. The maximum losses occur at 208℃ and 478℃. Since the mixing temperature of bitumen is less than 200℃, therefore stage 1 is a pivotal point for defining the influence and interaction between GO and Asphalt. The inference of the tests is as follows

i. GO (1%) – is not effective for thermal stability
ii. GO (3%) – effective for thermal stability

These observations could be explained by the fact that the combustion temperature of the GO (154℃) is much lower than asphalt. Therefore the stage 1 acceleration of mass loss is caused due to the combustion of graphene oxide, which implies and relates to

the phenomena that the higher initial combustion temperature and the bigger the R_{700} (residual mass ratio), better the thermal stability.

Physical properties test

a. *Separation test*

The test indicated the difference between the top and the bottom softening points of the asphalt. The difference between top and bottom softening points of the specimens is not more than 1℃. Therefore the modification of asphalt by GO does not affect the storage stability. The storage stability could be attributed to the presence of oxygen containing functional groups present at the edges of the graphene oxide structure. The GO-3% improves the thermal stability of 90A and SBS-MA and the GO-1% improves the thermal stability of 90A, while it decreases that of SBS MA.

b. *Penetration, Ductility and Softening Point*

Penetration and ductility tend to decrease whereas softening point tends to increase with the modification of asphalt with GO.

c. *Viscosity*

The viscosity of both the GO modified binders increase with increase in the dosage of the GO and also the increment in SBS-MA is more as compared to the control binder. For control binder there is an increment of 1.5% for minimum viscosity value and 4.5% for maximum viscosity value at GO dosage of 1%, whereas at 1% GO dosage there is an increment of 1.1% for minimum and 6.5% for maximum viscosity value for SBS-MA. At 3% dosage the increment in the viscosity values increases.

d. *Rheological properties*

Two tests were used DSR and BBR, where latter was used for measuring creep properties at low temperature. For high temperature sweep (30–80℃) GO improves the anti-rutting performance of SBS-MA and 90A as it reduces the phase angle δ and increases the complex modulus. The FFT results indicated that the GO can improve the anti-fatigue performance of the binders utilized. For low temperature sweep (-10 –

0℃) there is not a significant effect of the anti-fatigue performance of GO modified bitumen but the softening is more pronounced than hardening, although GO comes under the category of inorganic nanomaterials which should harden the asphalt but due to the presence of CO_2 gas the softening takes the leading role at low temperatures. The BBR test results suggest that the anti-cracking performance at low temperatures is improved in GO modified asphalt.

- (Yuan et al. 2019) states that carbon has around 500 allotropes with carbon C60, CNT's, diamond and graphene having sp^3 / sp^2 hybridized carbon, diamond, graphene and C60 poses extraordinary electrical, mechanical, thermal, intrinsic mobility, light transparency and biocompatibility. The purity and the crystallinity of the graphene highly govern the thermal conductivity which ranges from10 W m^{-1} K^{-1} to 5000 W m^{-1} K^{-1}.

2.5.THERMAL CONDUCTIVITY OF ASPHALT BINDER

- (Mallick et al. 2009) suggested that due to the black spectra of the asphalt binder it absorbs huge amounts of solar radiation and due to its poor thermal diffusivity it radiates the heat back into the atmosphere increasing the temperature of ambient location, this phenomenon is known as urban heat island effect (UHI). Further the study suggests use of absorptive paints, thermally conducive aggregates and water pipes running underneath the pavement to harvest the heat energy.
- (Zhang et al. 2019) suggested the use of asphalt binder modified by phase changing materials to dissipate heat energy rapidly from the mixture. Thus forming an active temperature control to alleviate UHI. The thermal conductivity of the asphalt binder increased three folds by the induction of phase changing material. The temperature gradient of binder and the pavement is reduced by increasing the quantity of EP-CPCM in the mixture. "The amount of heat needed that is needed to change the unit temperature of a substance with unit volume or mass is known as specific heat", the specific heat increases with increase in the quantity of EP-CPCM. EP-CPCM is a phase change material and it gives a good thermal storage capacity to the binder. For the study of rheological properties such as high temperature sweep tests for temperature range 52℃ to 82℃ were carried out to determine rutting parameter $G^*/\sin\delta$ with a frequency of 10 Hz and a strain of 0.5 %. Also intermediate

temperature sweep tests for temperature range 16℃ to 40℃ were carried out to determine fatigue parameter $G^* \times \sin\delta$ with a frequency of 10 Hz and a strain of 0.05%. The rutting parameter $G^*/\sin\delta$ improves as EP-CPCM acts as filler in the binder and improves the anti-rutting performance only when the EP-CPCM is 10% or more. For fatigue resistant mixture the temperatures below 30℃ asphalt develops no special attributes but after reaching 30℃ which is phase changing temperature of the EP-CPCM the G^*value increases and the δ value decreases.

- (Wang et al. 2017) studied the self-healing properties of asphalt binder modified with graphene. The radiation from sunlight was considered as the source for heating the pavement and it was observed that the near to infra-red region of the asphalt binder was augmented with the modification of graphene. Also the thermal conductivity of the asphalt binder increased with the modification of graphene and activation energy required for approaching a particular viscoelastic state reduced. The asphalt binder were also observed to have increased the near to infrared region absorption band of the asphalt binder which implies that the absorption window has been widened in comparison to control binder. The thermal conductivity of the binder was augmented for both asphalt binder as well as the asphalt concrete mix as well.

  The light absorbance of control binder plummeted from 4 a.u to 0.512 a.u as the wavelength of the testing light exceeded 690 nm, for graphite flake modified asphalt and graphene modified asphalt it showed an elevated absorption range, that is 860 nm and 700 nm respectively.

2.6.CHEMICAL AND MORPHOLOGICAL CHARACTERIZATION.

- (Lee et al. 2008) Studied the micromechanical properties of graphene using AFM and Nano-indentation techniques. The AFM of sample gave the bulk properties of the material therefore, multilayer graphene was analyzed using tap mode and concentrating the tip within 50 nm of the center. The study reported an intrinsic strength of = 42 ± 4 N m^{-1} and Young's modulus of 1.0 ± 0.1 TPa.
- (Behnood and Gharehveran 2019) suggested that a polymer modified binder is modified with one or more polymers, the study further describes importance of the structure of asphalt which comprises of the constituents of the asphalt binder as per SARA analysis as saturates, aromatics, resins and asphaltenes, constituting the asphalt

in the ascending order as listed [S < A < R < A]. Asphaltene is considered as the major constituent of the asphalt binder and has a significant impact on the viscoelastic and rheological properties of the asphalt binder along with some influence from the resins. For long time, asphalt binder was considered as a colloidal containing micelles as was first proposed by Rosinger in which the asphaltenes are considered as the center of micelles enveloped by lighter molecular weighted hydrocarbons and dispersed in an oil phase. Thus developing a nucleic structure of asphalt engulfed by higher molecular weighted and aromatic hydrocarbons. There three types of asphalt structures sol type, flocculated asphaltene micelles and gel type. In sol type the asphaltenes are stabilized in the oily phase by the polar interactions due to the resins and nucleic structure is formed. In flocculated asphaltene micelles polar model is followed which considers varying molecular sizes and polar functionalities continuously distributed as the constituents. Though there is a consensus of asphalt binder can't exist as a colloidal structure as asphaltenes are soluble in the maltenes. Also the unusual rheological behavior could be attributed to the molecular weight distribution of the polar molecules. Further in a gel type asphalt model the polarization of various constituents could be attributed to electric polarization as an interaction between the aromatics. Aggregation interactions of the asphaltene dipoles play a vital role in structuring the asphalt binder and are known as oligomers after forming high molecular weight molecules. The asphalt binder with lower asphaltene content forms the sol type asphalt (5% - 10%) which has high mobility for asphaltene micelles and high susceptibility towards high temperature. Due to higher presence of non-interacting micelles the asphalt behaves more like a Newtonian Fluid and has lower rates of age hardening, higher ductility and little recovering properties. Whereas gel type asphalt has higher asphaltene content (20% - 35%) In this system micelles tend to form elaborative networks with higher degree of continuity in micelle interactions developing inter-micellar voids for lighter components. Gel type structure is susceptible to low temperature, lower ductility, rapid ageing and a prominent recovery. In pavement construction most of the binders are sol type and showcase a colloidal structure formed by super-micelles and giant super-micelles.

- (D'Angelo 2009) verified the use of Polyphosphoric acid (PPA) across different sources of asphalt and different additives with varying mixing processes. The augmentation of the neat binder was similar across all the sources but the magnitude of enhancement was dependent on the constituents of the source as shown in Figure 8. Though PPA was considered to devalue the stiffness of the binder but the induction of PPA augmented the stiffness of *SBS* modified binder by encouraging the cross linking behavior of the elastomeric polymer. In response to a physically blended hydrated lime the PPA tend to have no response at all but the chemically blended hydrated lime + asphalt binder tends to enhance the stiffness of the binder.
- (Tyson et al. 2011) studied the behavior of nanomaterials forming bundles or agglomerates in the composites. To measure the degree of dispersion and agglomeration a model was developed. The level of dispersion plays an important role in determining the properties of the composite material.

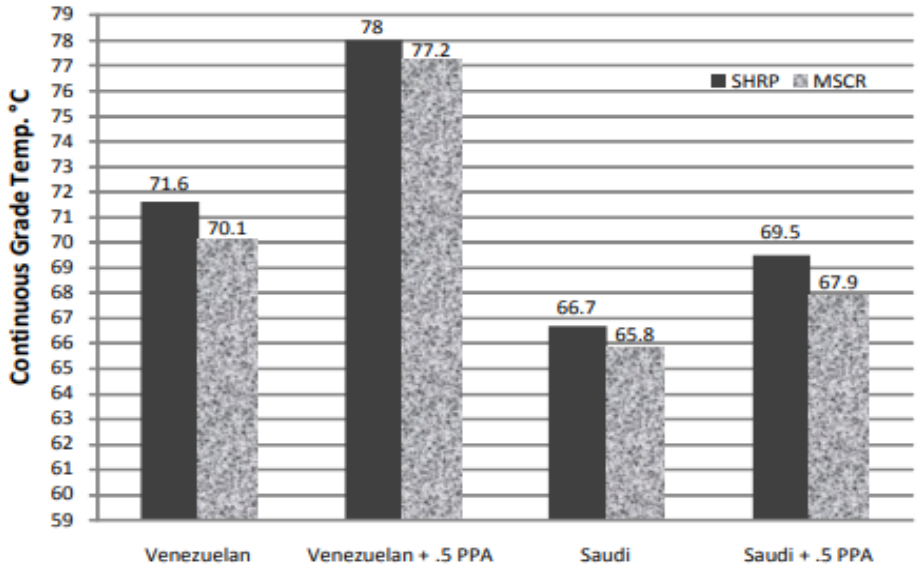

Figure 8 Impact of PPA across various sources of asphalt binders (D'Angelo 2009)

2.7.STATISTICAL MODELING

- (Kruskal and Wallis 1952) suggests the advantages of using ranks instead of observed data and the variance of samples in a population does not necessarily account to the differences in samples in a population but a mere chance of variation in random variables. Use of ranks simplifies the computations of statistical analysis as the only

assumption prerequisite to rank a observations of a sample is that the observations are independent.

- (Toothaker and Newman 1994) suggests concerns regarding the fulfillment of parametric assumptions by two-way ANOVA and studied various non-parametric tests which could be implement in a two-way analysis.
- (Peters 2001) suggests that results from a parametric test could be erroneous and are not authentic when failing to comply to any assumptions made for the parametric test. To analyze population which is not normally distributed or does not comply to any assumptions made non-parametric tests establish a better and correct understanding of the data because non-parametric tests do not analyze the observed data of a sample but devise it in ranks.
- (Ali et al. 2018) determined the significant difference between the sample means across the asphalt binder grade and the wax additives using two- way ANOVA. The effect of each additive to each grade and the significance of difference in the mean of each asphalt grade was established using least square difference (LSD) method.

Chapter 3 METHODOLOGY AND MATERIAL

The study focusses on the rheological, thermal and morphological modifications that occur in the asphalt binder. The following step by step methodology was followed as illustrated in Figure 9, which provides the research outline of the study

The literature review was carried out to understand the historical background and the complexity of asphalt binder to interact with various additives. The review gives an idea of the sheer size of the road pavement infrastructure and the concerns involved in the development and longevity of the pavement which plays a vital role in the economics of road infrastructure.

The most important thing in this study was to get an appropriate mixing machinery and procedure. The mixture of asphalt binder and graphene was prepared by wet mixing as shown by schematics in Figure 10. The samples of 750 g each were prepared with an addition of 0.5%, 1.0%, 1.5% and 2.0% of graphene by weight of bitumen. A total of 10 samples of 750 g each were prepared by shear mixing in which five samples each consisted of VG30 and VG40 grade asphalt.

To determine the transition temperature from solid to molten state of the asphalt binder, softening point was conducted with the help of ring and ball test. The importance of the softening point is to give an idea of the binder under various temporal conditions. Also the storage stability of the modified binder was determined by performing separation test on the asphalt binder. The rheological properties were determined using various testing protocols and procedures as lined by the ASSHTO and ASTM codes. The thermal conductivity was observed to determine the augmentation in the thermal behavior of the modified asphalt binder to behave as better heat sink to the heat energy generated by the solar energy stored in the pavement.

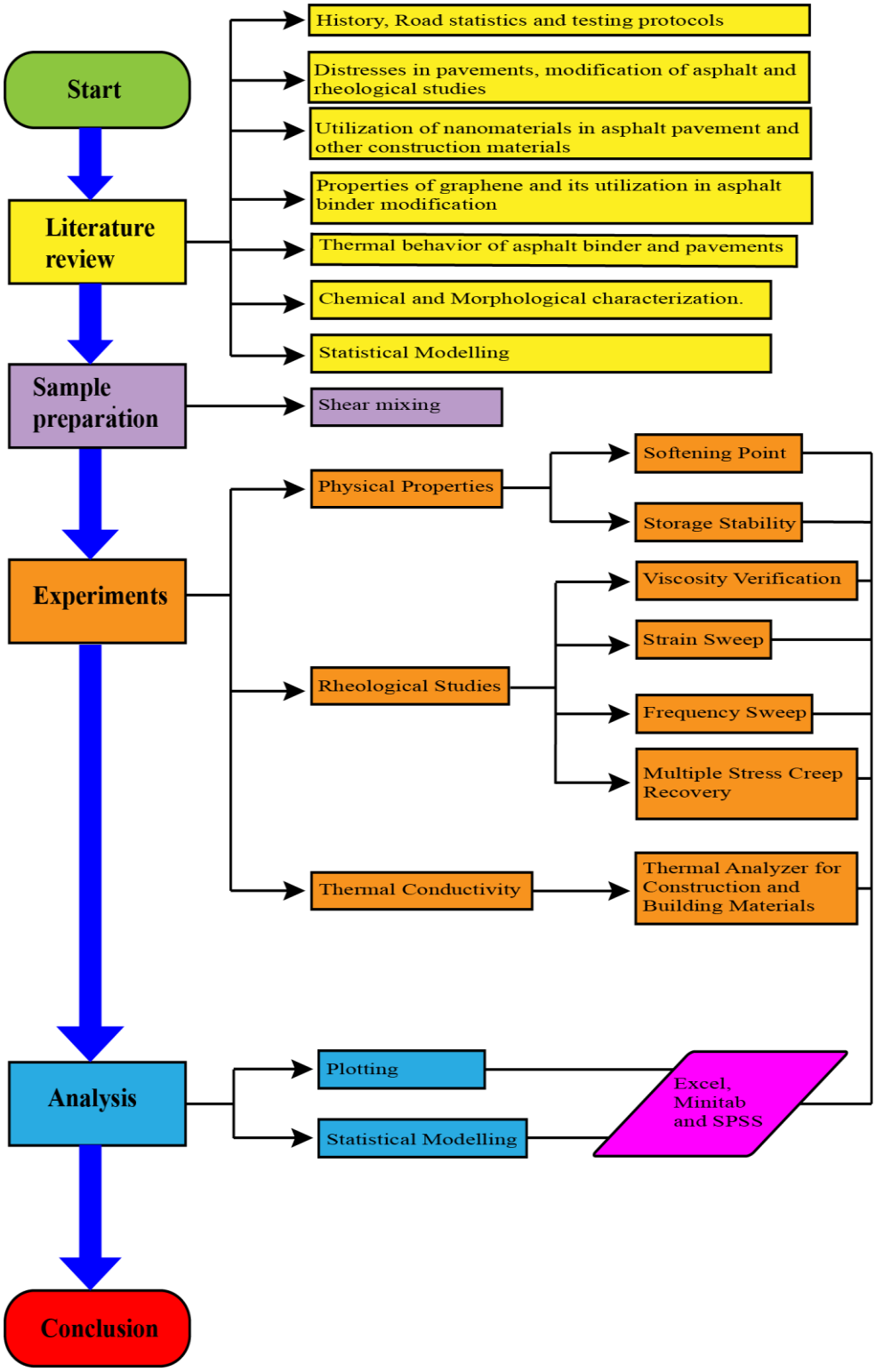

Figure 9 Flowchart of the Methodology Utilized

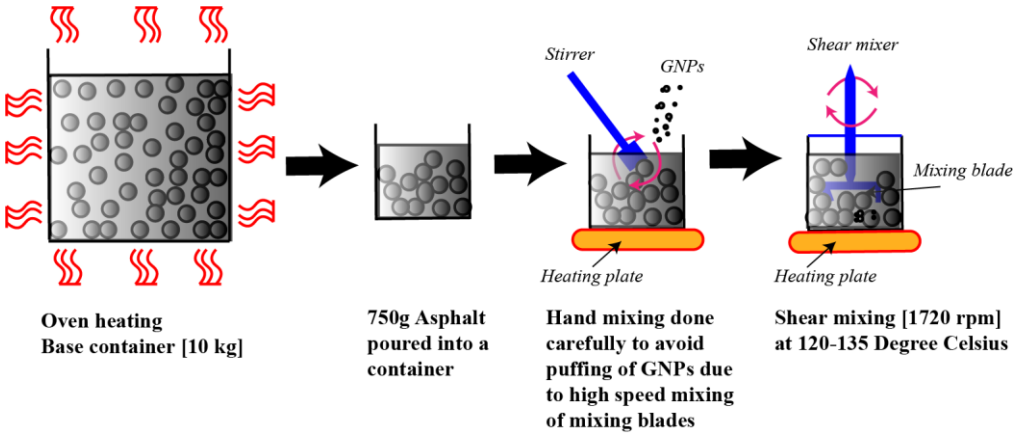

Figure 10 Mixing Schematics

3.1.LITERATURE REVIEW

The literature review encompassed various multi-disciplinary approaches that were sort out to study the properties of the asphalt binder. The disciplines involved materials science, chemistry, physics, chemical engineering, mechanical engineering and civil engineering researchers from where the different aspects of the asphalt binder were studied to get a fair understanding of the asphalt binder.

3.2.SAMPLE PREPARATION

The samples of the graphene modified asphalt binder were prepared using wet mixing method with a shear mixer which was operated at a high speed of 1720 rpm. The shear mixer was engineered during the current research using a standing drill machine as shown in the Figure 11 (a). The drill bit to be attached to the drill machine was attached with a mixing blade. The mixing temperature was maintained using a heater of 1500 W and to maintain a temperature of 120℃ - 135℃ a thermometer was used. To avoid the puffing of the nanomaterial due to the high seed of the spindle care was taken to stir the nanomaterial manually with a stirrer and then immediately was followed by the high shear mixer. All the samples including the control binders were undergone the same procedure of mixing for 40 minutes. The mixing procedure is shown in Figure 11 (b) and the samples prepared are shown in Figure 11 (c).

Figure 11 (a) Make Shift Mixer (b) Mixing with a Metallic Lid (c) Ten Samples of 750 g each Produced

3.3.EXPERIMENTAL WORK

The experimental work has varied from the basic/ conventional testing to an advanced spectrum of testing procedures for the asphalt binder. The various aspects engaged in this study are: physical properties, rheological properties, thermal properties and morphological characterization.

3.3.1.Physical Properties

The physical properties of the asphalt binder are subjected to the conventional testing methods and help to observe the qualifying parameters of the asphalt binder. The softening point test and the separation test was conducted to determine the transition temperature from solid to molten state and the storage stability of the modified asphalt respectively.

3.3.1.1. Softening Point

The softening point of the asphalt binder was observed by employing the ring and ball test, the apparatus used to determine the ring and ball test is shown in the Figure 12. Softening point determines the transition temperature at which asphalt will behave more like a liquid than solid, since asphalt does not have a distinct melting point. The softening point of the binder has been determined using ring ball test conforming to IS 1205:1978.

The apparatus utilized in the test are:

a. Standard ring and ball apparatus
b. Two steel balls each 9.5 mm in diameter and 3.5 +/- 0.05 g
c. Two brass rings tampered
d. Thermometer
e. Water bath

The procedure of the ring and ball test as per IS 1205:1978 is as follows:

a. Heat the material to a temperature of 75℃ to 100℃ and keep on stirring until it behaves completely like a Newtonian fluid and free of any moisture or air.
b. Place the rings on a plate coated with glycerin and pour the molten material into the rings.
c. Remove the excess material with a warm sharp knife after cooling it for 30 minutes in air.
d. Assemble the apparatus and place it in the bath, fill the bath with water and maintain a temperature of 5℃ for 15 minutes.
e. Now apply the heat at a rate of 5 +/- 0.5℃ until the material softens and balls are allowed to pass through the rings.
f. Record the temperature at the instant when both the balls touch the bottom plate of the apparatus.

Figure 12 (a) Ring and Ball Apparatus (b) Setup Heated with the Thermometer Monitoring (c) Both The ballsTouching the Bottom Plate

3.3.1.2.Storage Stability

The storage stability of the modified binder is of paramount importance as it qualifies the binder to be fit for the long durations before utilizing it for the pavement construction. Storage stability is determined by the separation test conforming to IS 15462: 2004. Separation test is used to determine the stability of modifier and asphalt during hot storage. The separation of the modifier and the asphalt is determined by comparing the softening point of top and bottom portion of a 136.7 mm x 25.4 mm tube containing asphalt. The tube is heated for 48 hours at a temperature of 163℃ and then frozen for 4 hours at a temperature of -6.7℃. The tube is then cut into three equal parts and the

softening point of the top and bottom portion is evaluated using ring and ball test. The step by step procedure of the test is illustrated in Figure 13. The apparatus used for the separation test are:

a. Aluminum tubes – 25.4 mm diameter and 136.7 mm length.
b. Oven
c. Freezer
d. Spatula and Hammer

The procedure followed to determine the storage stability of the modified binder by separation test is given as under:

a. Heat the sample and seal one of the ends of the tube.
b. Place the sealed end in a beaker containing sand to hold the tube vertically in the oven.
c. Place the container inside the oven for 24 hours and then place it in a freezer for 4 hours to solidify, ensuring that the sample remains vertically at all the time.
d. Cut the tube into three equal parts and mark the top and bottom portion.
e. Heat the tubes in two different containers and as per IS 1205:1978 evaluate the softening point of the samples. With top and bottom portion asphalt forming a pair for each ring and ball test.

Figure 13 (a) Pouring of Asphalt Binder into the Tube (b) Shifting the Sample in the Oven for 24 Hours (c) Freezing the Sample in the Freezer to Stabilize the Constituents (d) Cutting the Sample into Three Equal Pieces (e) Heating the Top and the Bottom Half to Perform Ring and Ball Test

3.3.2.Rheological properties

The rheological tests were conducted to determine the flow behavior of the binder, rheology as it may be defined is the science of studying the flow behavior of the material

and rheometry is the art of measuring the flow characteristics. The rheological behavior of the asphalt was determined using dynamic shear rheometer (DSR) MCR-52 from Anton-Paar using parallel plate geometry with a 25 mm diameter and 1 mm sample thickness. The instruments utilized to observe the rheology of the asphalt binder are illustrated in Figure 13. The sample preparation and testing schematics are illustrated in Figure 14. Conforming to protocols are as per ASSHTO, ASTM and IS codes (AASHTO T315), (ASTM D7175) and (IS SP-53).

Figure 14 DSR Assembly

The rheological studies involved two testing procedures:

a. Rotational Test

b. Oscillatory Test

The rotational test was used to determine the absolute viscosity by virtue of which asphalt binder is verified as per the viscosity grade specifications given in IS 73:2013. The spindle tends to apply a particular shear rate by taking complete rotations to unwind the polymeric chains of the asphalt binder to determine its resistance to flow i.e. viscosity at a particular shear rate. The oscillatory tests comprise of two testing mechanisms based on the application of external agencies; controlled shear strain and controlled shear stress. The schematics of the rotational and oscillatory test are illustrated in Figure 15.

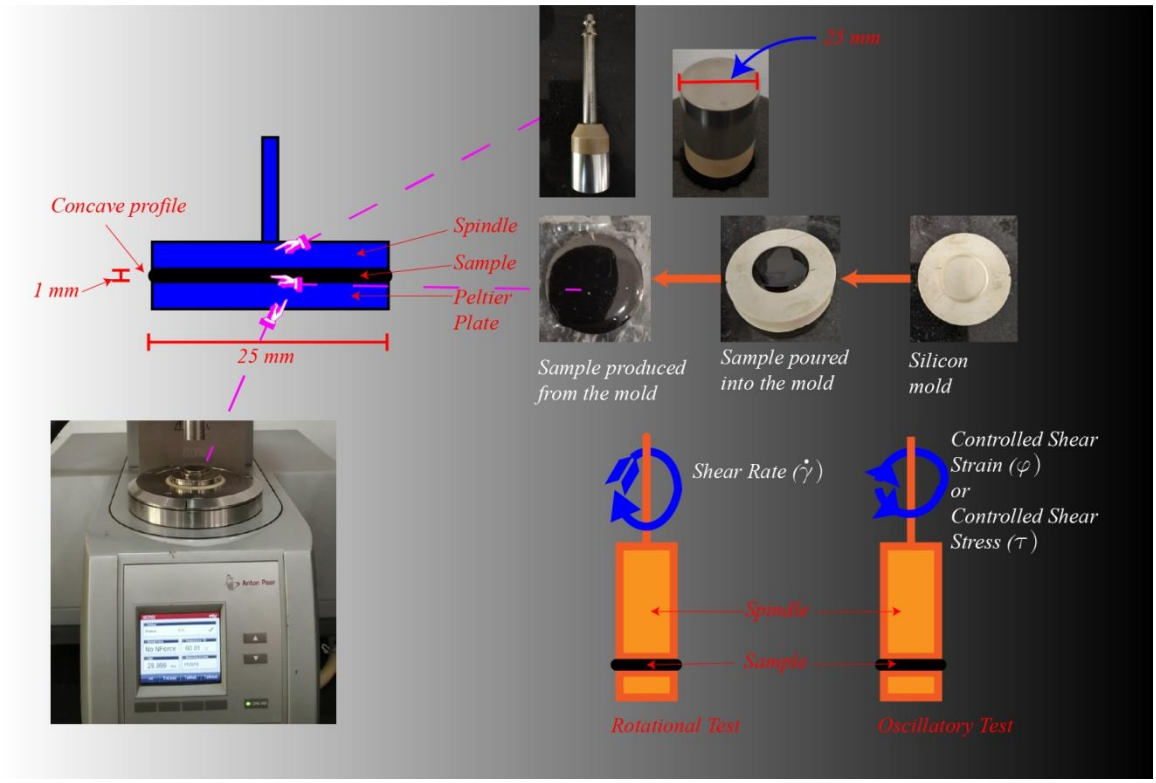

Figure 15 Schematics Diagram DSR

The oscillatory tests are used to stimulate the temperature and vehicular load applied on the pavement. In this study the rheological parameters at various temperatures and stress / strain generated conditions are examined. The various testing methodologies employed in the oscillatory test are; strain sweep, frequency sweep and multiple stress creep recovery test (MSCR). The frequency chosen for the strain sweep test and MSCR was 10 rads / sec [1.59 Hz] which corresponds to a vehicle with a speed of 55 mph (Singh et al. 2006). To check the binder for temporal susceptibilities the binder was tested at 60℃ and 65℃ for strain sweep and 65℃ for MSCR test. Since the study is not focused on the grade modifications of the binder therefore further temporal investigation was not deemed to suit the time constraints in the research. Also the frequency sweep at 4% shear strain was conducted to determine the binder susceptibilities corresponding to varying frequencies and temperatures. Note that all these tests are conducted within the linear viscoelastic range (LVER) only, therefore these tests will offer only the temperature susceptibility of the binder and will not serve as a measure to susceptibility of the binder by the applied load. To test the binder beyond the linear viscoelastic region linear amplitude sweep

(LAS) is conducted which requires shear strain to be applied beyond the scope of our instrument.

3.3.1.1.Rotational Test

The test was conducted to determine the viscosity of the asphalt binder by employing a shear rate via the rotational moving profile of the instrument. The test is an empirical implication of the Newton's law of viscosity which states that the ratio of shear stress to the rate of shear strain directly proportional to the viscosity of the material involved. The rate of shear strain employed is measured from the gap between the base of spindle and the Peltier plate and the diameter of the base of the spindle as illustrated in the Figure 16.

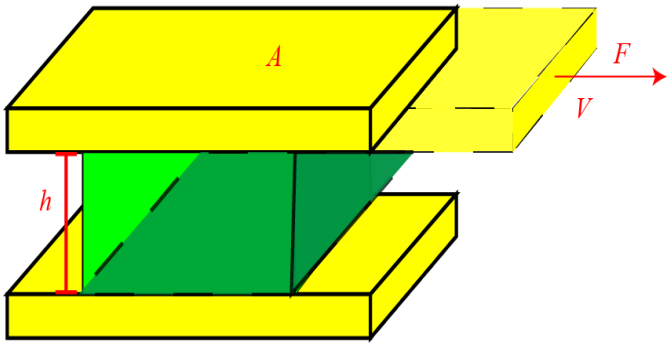

Figure 16 Newton's Law of Viscosity

The viscosity law is measured in the following manner and it is described mathematically by the equations (*SI Units)* given below:

$$\dot{\gamma} = \frac{V}{h} \qquad \textbf{Equation 1}$$

Where,

$\dot{\gamma}$ *Shear rate* [s^{-1}]

V *Speed of the moving plate* [m/s]

h *Distance between the plates* [m]

$$\tau = \frac{F}{A} \qquad \textbf{Equation 2}$$

τ *Shear Stress* [N/mm^2]

$\boldsymbol{F}$ *Force applied* [N]

$\boldsymbol{A}$ *Area of the plate* [mm^2]

These values are calculated by the software and the output value depends on the type of test to be used; controlled shear strain or controlled shear stress. The viscosity is given by Equation 3 (*SI Units*).

$$\boldsymbol{\eta} = \frac{\boldsymbol{\tau}}{\dot{\boldsymbol{\gamma}}} \qquad \textbf{Equation 3}$$

$\boldsymbol{\eta}$ *Viscosity* [$Pa.s$]

$\boldsymbol{\tau}$ *Shear stress* [N / mm^2]

$\dot{\boldsymbol{\gamma}}$ *Shear rate* [s^{-1}]

Procedure

a. Heat the sample to 100℃ to 120℃ and pour it into a silicon mold and let it cool.
b. Initialize the DSR and use the parallel plate assembly for measuring absolute viscosity of the asphalt binder.
c. Using the asphalt verification template in the *Rheocompass* software initiate the project and set temperature of the machine to 60℃, and set zero gap, the procedure used in the software is described in detail further in this section.
d. After attaining the temperature equilibrium place the sample on the plate and close in the measuring system to 1 mm gap, trim off the extra binder and enclose the sample environment by the thermal cap provided.
e. Wait for 10 minutes and run the test.
f. After finishing the test clean the spindle and the Peltier plate with a cloth by raising the temperature and then using a volatile liquid *(petrol, toluene etc.)* wipe off the plate.

The procedure followed in the *rheocompass* is illustrated in Figure 17, the procedure followed is as follows:

a. After setting and placing the sample, wait for waiting for 10 minutes and click “Start” to initialize the test. *(Note: before starting the test operator should make sure you have set the required shear rate to be used).*

b. A diagram and a table shall be generated simultaneously as the results are recorded and analyzed by the *Rheocompass.*

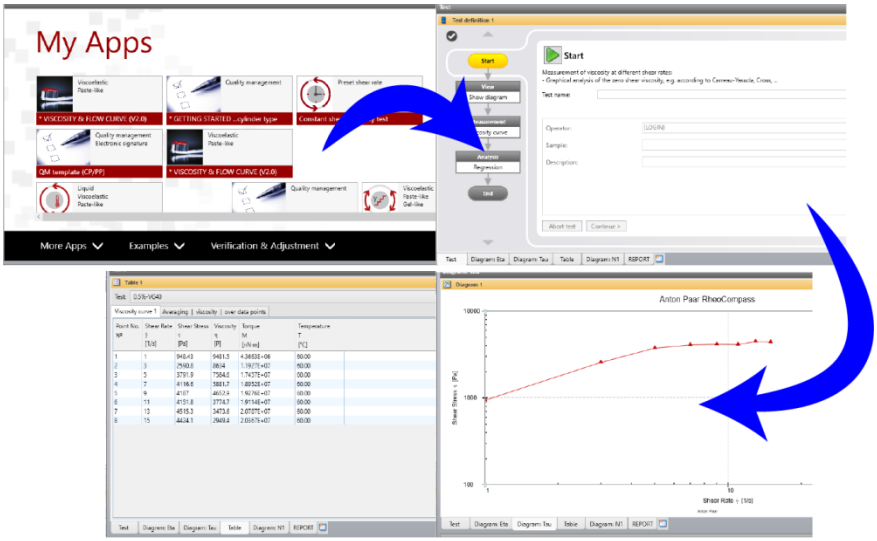

Figure 17 Operating *Rheocompass* Software For Rotational Absolute Viscosity Test

3.3.1.2.Oscillatory Test

The tests operated under the umbrella of oscillatory test are; strain sweep, frequency sweep and multiple stress creep recovery (MSCR) test. Both strain sweep and the frequency sweep are controlled shear strain tests. The strain sweep is used to determine the linear viscoelastic region of the binder, the complex moduli and the phase angle of the binder whereas frequency sweep is used to determine the time-temperature susceptibility of the asphalt binder by varying the applied temperature and the frequency by the DSR. However, the MSCR test is fairly a latest test than strain sweep and frequency sweep tests and differs in the input function of the DSR as it is controlled shear stress test. MSCR test has a better correlation with the field results of the modified asphalt binders as it takes into account the recovery behavior of the asphalt which was initially tried to be included for the asphalt binder by virtue of thixotropic methodology but the method did not provide suitable results. The initial sample placing and the waiting period is same for all the test types though the parameters observed and moving profile application of the DSR differ for the three test types, and are discussed later in this chapter.

The oscillatory test tends to depend on the response recorded off the shear strain applied and shear stress generated in the material as illustrated in Figure 18. The stiff/ solid

material tends show no lag between the applied strain and responsive stress whereas the viscoelastic material tends lag in the degree of response in the shear stress to the applied shear stress.

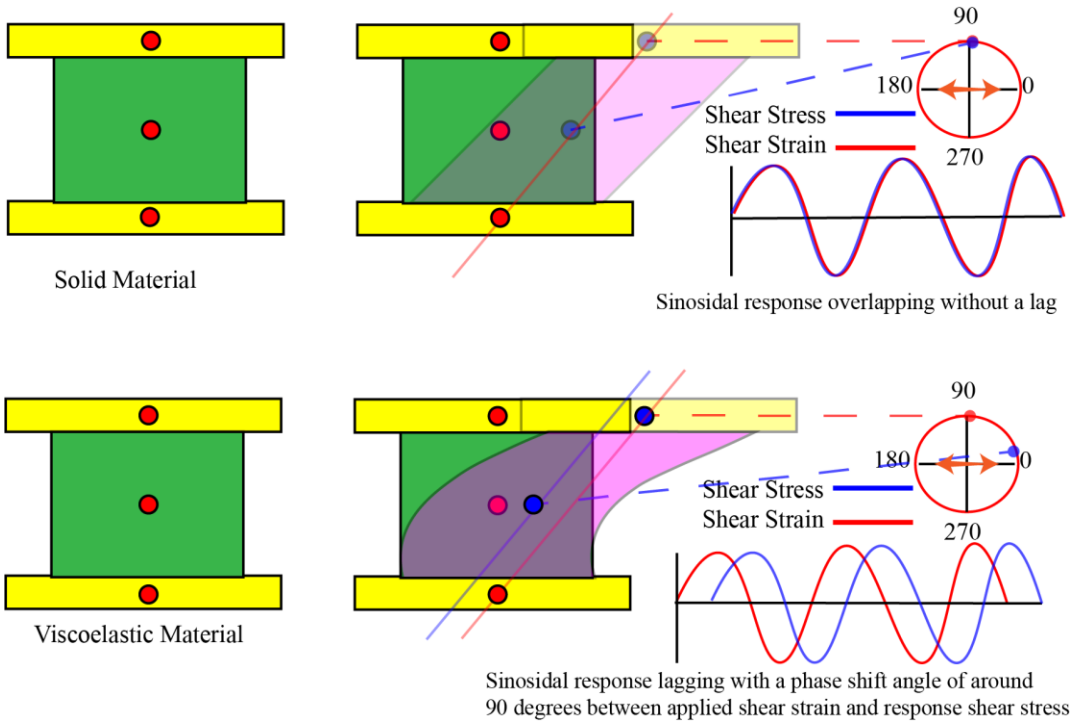

Figure 18 Diagram Illustrating Principle of Oscillatory Test

The strain sweep test was conducted at 60℃ and 65℃ for 8 different shear strain percentages, ranging from 2% to 16% with a step of 2%, the test conducted to measure the variation in the linear viscoelastic range, complex shear modulus, phase shift angle, energy dissipation ($\tan\delta$) and the rutting parameter at two different temperatures. The linear viscoelastic range as per AASHTO T-315 corresponds to the ratio of the complex shear modulus at a particular shear strain percentage to the complex shear modulus at zero complex shear modulus i.e. the lowest shear strain rate applied in this study that refers to 2% shear strain percentage as given in Equation 4. The ratio shall be equal to or greater than 0.95 which implies that the applied shear strain percentage to be within the linear viscoelastic range.

$$\text{LVER} = \frac{G^*}{G_0^*} \geq 0.95 \qquad \textbf{Equation 4}$$

The complex shear modulus is the ratio of applied/ observed shear stress to the applied/ observed shear strain as given in Equation 2 (*SI Units*). The asterisk symbol denotes that the measured property is dynamic in nature.

$$G^* = \frac{\tau^*}{\gamma^*} \qquad \textbf{Equation 5}$$

The phase shift angle is the lag in the response time of the material to the applied entity and is denoted by δ. The storage modulus *G'* and loss modulus *G''* could be represented mathematically as the components of the complex shear modulus as given in equation 6 (*SI Units*).

$$|G^*| = \sqrt{G'^2 + G''^2} \qquad \textbf{Equation 6}$$

The ratio of loss modulus (*G'')* and storage modulus (*G')* defines the energy dissipation in the material which is denoted by $\tan\delta$ as given in Equation 7, $\tan\delta$ corresponds to the energy dissipated or energy loss in the material. Since the viscoelastic material follows a spring and a dash pot model as illustrated in the Figure 19, a portion of the stress or strain is stored in the spring forming the elastic response of the material and a portion is lost in the dashpot.

$$\tan\delta = {}^{G''}/_{G'} \qquad \textbf{Equation 7}$$

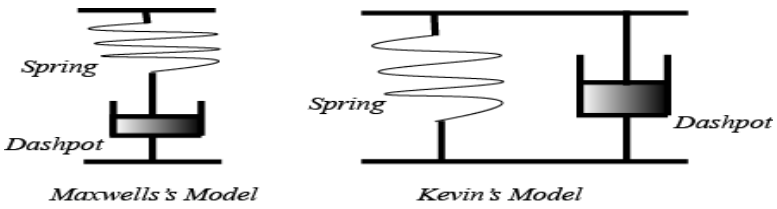

Figure 19 Viscoelastic Models

The frequency sweep test was conducted to check the time-temperature susceptibilities of the material. The frequency sweep was conducted on 4% strain at seven different temperatures (25℃ to 85℃ ∀ 10℃ interval) and an angular frequency ranging from 0.1 to 628 rad/s (0.0159 Hz to ~100 Hz).

The flow behavior index was computed using Equation 8 (*SI U*nits), in order to identify the initial self-healing behavior of the asphalt binder.

$$\eta^* = m\omega^{n-1} \qquad \textbf{Equation 8}$$

η^* is the complex viscosity, *m* and *n* are the fitting parameters and ω is the frequency at which the sample is subjected to, the frequency values ranging from 1 Hz to 100 Hz was analyzed. The value **n** determines the flow behavior of the asphalt binder as represented by the power law equations. The fluid is to follow a Newtonian flow behavior if the value of $n = 1$, since asphalt binder is viscoelastic liquid it behaves like a Newtonian fluid at temperatures around 70℃ – 80℃. The analysis is carried out in order to determine the temperature at which the asphalt binder follows a Newtonian profile by having *n* value closer to 1 in order to behave as a self-healing material by filling up the microcracks in the asphalt binder by following at elevated temperatures induced into the pavement.

The plot of the observed entities to the frequency gives a spline profile which can be standardized to a particular temperature which is useful for production purposes in industrial sector. Figure 20 illustrates the self-healing process.

Figure 20 Self-Healing of Asphalt Pavement by IR Induction

The MSCR test is a controlled shear stress in which particularly two stress levels 0.1 / 3.2 kPa are engaged to simulate the strains generated in the asphalt binder. The test employs a 10 second cycle consisting of 1s creep and 9s recovery time for a continuous loop of 10 cycles as illustrated in Figure 22 The test procedure and analysis complied to (AASHTO TP-70) but the stress levels were tweaked by introducing eight different stress levels to observe the stress sensitivity of asphalt binder in between the stress levels of 0.1/ 3.2 kPa. Also instead of 10 cycles the asphalt binder was engaged in a 30 cycle loop to develop the correlation to observe the repeatability of the test. The test was conducted for 3 trials each

and the mean value was used to arrive at the final parameter value. Calculations are carried out as per AASHTO TP-70 which includes the calculation of:

a. Percentage recovery of each stress level

b. Non-recoverable creep compliance for each stress level

c. Percentage Recovery difference and Percentage difference in non-recoverable creep compliance between 0.1 kPa and 3.2 kPa

Usually this test is conducted on RTFO aged binder but in this study unaged binders were observed since unaged show more susceptible towards rutting. The equations used to determine the recovery percentage and non-recoverable creep compliance (Jnr) are illustrated in Figure 21.

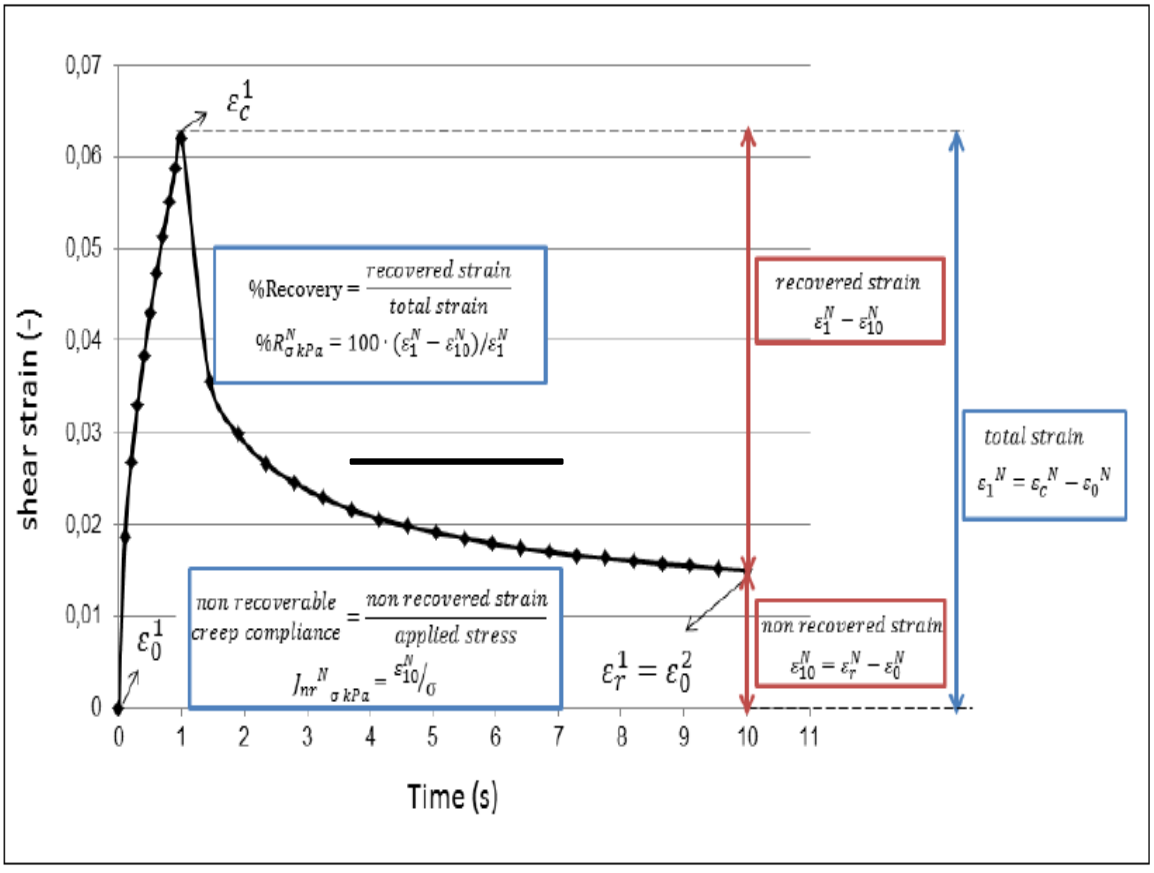

Figure 21 MSCR Principle and Equations (Soenena et al. 2013)

The procedure for placing the sample is shown in Figure 22 and the test protocol is as follows:

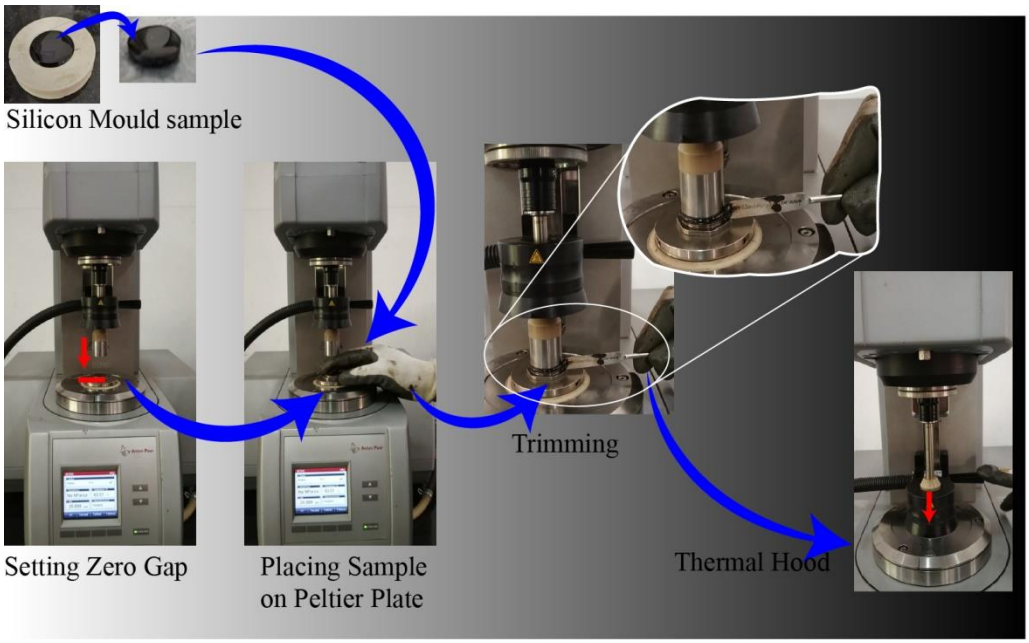

Figure 22 Sample Preparation and DSR Preparation

a. Heat the sample to up to 100℃ to 120℃ and pour it into a silicone mold of 25 mm and let it to cool.
b. Run the *Rheocompass* software on the desktop and initiate the rheometer, insert the measuring system in the DSR and set the plate temperature to 65℃.
c. After the temperature is attained press *'set zero gap'* in the software and the measuring system will move down, precisely leaving no gap between the spindle and the Peltier plate.
d. Now move the measuring system for about 3 cm using tools in '*Rheocompass'* and place your molded sample on the Peltier plate.
e. Set a gap of 1 mm and proceed with trimming the sample after some of it will spread outwards due to the press from the measuring system. Be cautious while trimming to avoid skimming out extra sample which may lead to a gap between the measuring system and the Peltier plate, which can cause a variation in the results.
f. Lower down the temperature controlling hood to induce and maintain the temperature around the sample
g. Now start the test, attain temperature equilibrium of the sample by following a wait time of 10 minutes which is included in the *rheocompass* as a default which complies in accordance to AASHTO and ASTM guidelines.

h. The raw data could be copied to MS-Excel for further analysis.

3.3.3.Thermal Properties

The augmentation of the thermal conductivity of the asphalt binder was observed using a thermal analyzer for building materials from Pelkin Hilton H112N. The instrument is used to measure the thermal conductivity of insulators by heat flow rate principal. A heat flow meter measures the flow of thermal energy through the sample by developing a temperature differential at the top and bottom of the specimen. In this instrument the top plate gets heated and the bottom plate is cooled with the help of a water cooling system. The heat flow meter method is a quick and doesn't require any sophisticated equipment, the method is described in ISO 8301: 1991. The hot and cold plate are allowed to attain thermal equilibrium i.e., the temperature is allowed to stabilize and to monitor the temperature of these plates the readings from surface thermocouples are recorded. The thermal conductivity of the material is computed with the help of calibration constants calculated for the device. The schematics of the thermal analyzer are illustrated in Figure 23.

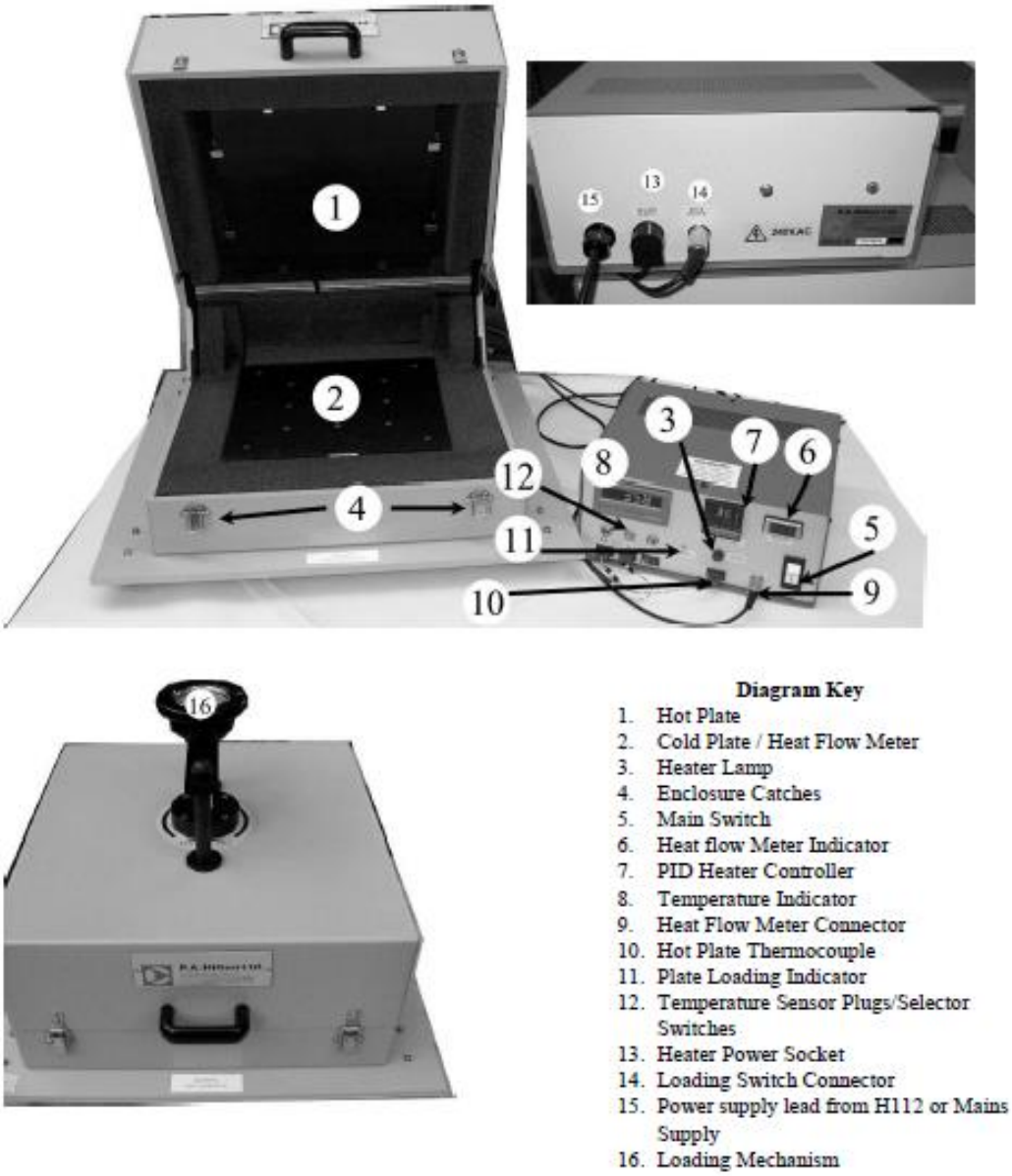

Figure 23 Schematics of the Thermal Analyzer for Building Materials

Sample Preparation

Before preparing the asphalt binder sample a mold was prepared from iron sheet and wooden beading. To form the molding of the sample a 24 gauge (3 mm) iron sheet and a 25 × 6 mm wooden beading was purchased from the market. The iron sheets were cut into 300 × 300 mm square sheets in the mechanical workshop as shown in the Figure 16 earlier. Also for the wooden beading mechanical workshop was utilized to cut the wooden beading into 6 × 6 × 300 mm cuboidal shape as shown in the Figure 16. The wood pieces were then glued to the iron sheets with the help of Fevitite as shown in Figure 16. After

engineering the mold for the asphalt binder to be tested, the asphalt binder poured into the mold at temperature of 70℃ – 90℃. The samples ready for testing are shown in Figure 24 which illustrates the timeline and the processes involved in the sample preparation.

Figure 24 Sample Preparation For Thermal Conductivity Test

Procedure

The schematics of the procedure are illustrated in Figure 25, the experiments were conducted in the heat and mass transfer lab of the mechanical department.

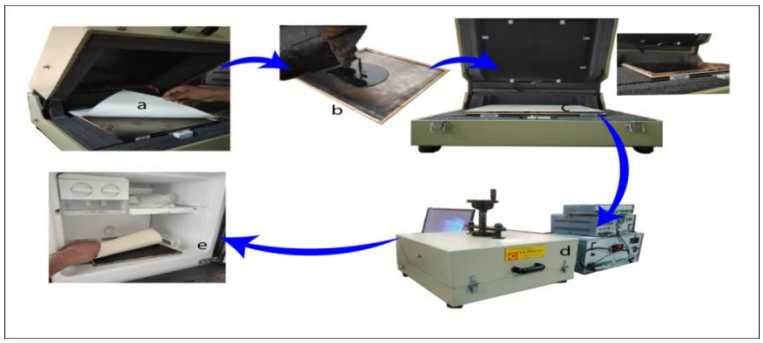

Figure 25 Thermal Conductivity Experiment Schematics

a. To begin with first the thermal conductivity of the iron sheet is observed and then a mold using the iron sheet and the wooden beading is crafted.
b. Asphalt binder is poured in the mold and let to cool off overnight at room temperature.
c. The sample is then placed in the thermal analyzer sandwiching it between the silicon sheets of 300 × 300 mm.
d. Close the lid to enclose the specimen inside and adjust the temperature with the proportional integral derivative PID heat controller for upper plate. The selector switches are used to monitor the temperature of the heat plate, bottom plate and the water circulating through the system. Also a data logger is connected to a workstation which records the data.
e. The silicon sheets are removed by cooling off the sample in the freezer for easy and clean removal.
f. Computed the thermal conductivity as per the formulae given in the manual of the instrument, Equation 12:

$$\boldsymbol{\lambda = \frac{l_s[(k_1+(k_2\times T))+\left((k_3+(k_4\times T)\right)\times HFM)+((k_5+(k_6\times T))\times HFM^2)]}{dT}}$$ **Equation 9**

λ	*Thermal conductivity* [$Wm^{-1}K^{-1}$]	k_1 = -47.2753
l_s	*Thickness of sample*	k_2 = 0.6353
HFM	*Heat flowmeter reading*	k_3 = 8.3998
dT	*Temperature difference* ($T_1 - T_2$)	k_4 = 0.0273
T	*Mean temperature of Plates* $\left(\frac{T_1+T_2}{2}\right)$	k_5 = 0.0318
		k_6 = -0.0001

The thermal conductivity of bitumen was computed by using mathematical model for series system as given Equation 10 (*SI Units*).

$$K_b = \frac{l_b(K_i \times K_T)}{K_i \times l_T - K_T \times l_i} \qquad \textbf{Equation 10}$$

K_b	*Thermal conductivity of bitumen*	$[Wm^{-1}K^{-1}]$
l_b	*Thickness of bitumen*	$\rightarrow$ *6 mm*
K_i	*Thermal conductivity of iron sheet*	$[Wm^{-1}K^{-1}]$
l_i	*Thickness of iron sheet*	$\rightarrow$ *0.3 mm (24 gauge)*
K_T	*Thermal conductivity of the system*	$[Wm^{-1}K^{-1}]$

3.4.MATERIAL

The materials utilized for the experiments were procured from Karnataka (Shimoga) and Haryana (Panipat). The asphalt binder of VG30 and VG40 grade was procured from the IOCL refineries in Panipat and graphene was procured from Shimoga via India mart. The characterization of graphene is discussed in subsequent sections.

3.4.1.Graphene

The material was supplied in a plastic container containing 200 g of the nanomaterials. The material came with the characterizations of XRD, Raman spectroscopy, SEM and TEM images. The material is verified as per the characterizations given in various literatures. There are three basic methods of preparing graphene which are chemical vapor deposition, micromechanical cleavage of graphite, and exfoliation of graphite. The supplier had used chemical vapor deposition method to prepare graphene. Graphene is a unique and the most extraordinary material available in the universe, graphene surpasses every material present to human in mechanical, thermal, electronic, photonic and electrical properties. Graphene has a Young's modulus of 1 TPa and reduced modulus of +1 GPa, Thermal conductivity of 5000 $Wm^{-1}K^{-1}$, optical transmittance of 97.7%, highest intrinsic mobility of 100 times that of Si and it has the highest specific surface area ~2700 m^2 / g (Lee et al. 2008), (Wei and Qu 2012) and (Ghavanini and Theander 2015)

Figure 26 Graphene Container and Weighing Scale with 0.5% Graphene by Weight of 750 g Asphalt

Table 2 Property Comparison of Graphene with other Materials

Properties	**Graphene**	**Competing Materials**	
Strength	130 GPa	**Steel**	0.41 GPa
Thermal Conductivity	~5000 W/m K	**Copper**	400 W/m K
Electrical Conductivity	~10 x 10^7 Siemens/ m	**Copper**	58.5 x 10^6 Siemens/m
Weight	0.002 g/m^2	**Paper**	~0.75 g/m^2

3.3.1.1.X-Ray Diffractometer and Raman Spectroscopy

The XRD provides a peak at phase angle (2θ) of 26.34° as shown in Figure 18 (a) which determines the interlayer spacing of graphene and the purity of material by crystal lattice scattering (Baochang et al. 2009). The phase angle of the modifier corresponds to that of graphene. The Raman spectroscopy of the graphene sample corresponds to a peak in the G band at 1600 cm^{-1} verifies the material as graphene, also a peak in the D brand determines a certain degree of defects in the graphene as shown in the Figure 18 (b) (Johra et al. 2014)

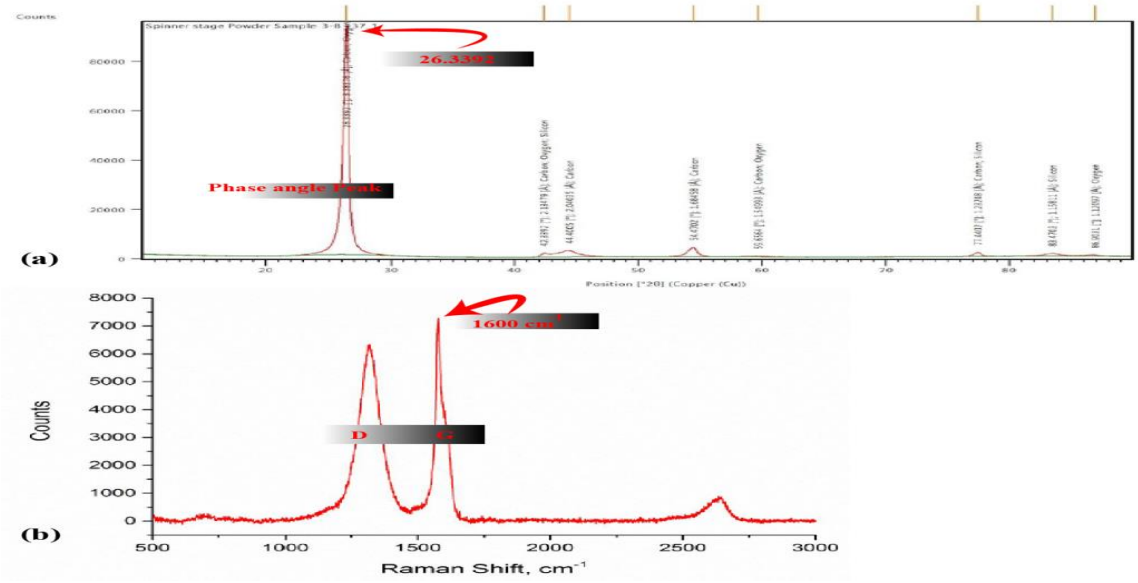

Figure 27 (a) XRD Result of Graphene (b) Raman Spectroscopy of Graphene

3.3.1.2.Scanning Electron Microscope and g Electron Microscope

The surface morphology of the material was characterized using SEM and TEM images, SEM and TEM images at 400 µm, 10 µm and 200 nm are captured as shown in Figure 19. The images are observed to illustrate the surface profile i.e. planar without any major curls, edge to edge lengths and layer thickness of graphene.

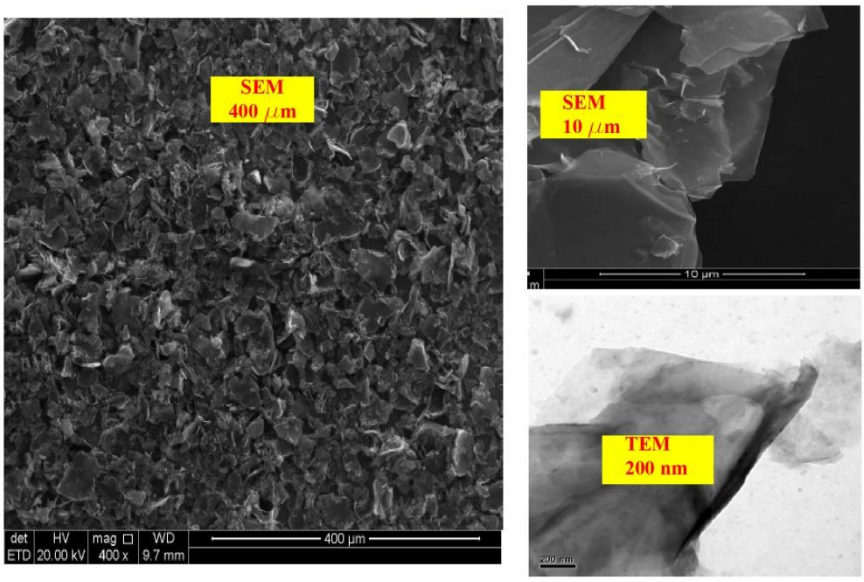

Figure 28 Scanning Electron Microscope Images (400 µm and 10 µm) and Transmission Electron Microscope Image (2 nm)

Characterization of graphene is given in Table 3.

Table 3 Characterized Properties of Graphene

Graphene	**Description**
Color	Black Powder
Purity	>99%
Average Thickness	3-8 nm
Average lateral dimension	5-10 μm
Number of layers	3-6 layers
Surface area	~180 m^2/g

3.4.2.Asphalt

Asphalt grades of VG30 and VG40 10 Kg each were procured from IOCL refinery in Panipat, Haryana which is of certified quality.

Chapter 4 RESULTS AND DISCUSSION

The results are tabulated and graphically represented in this chapter with a detailed description about the significance of the data. The chapter is divided into three subgroups each constituting to a particular aspect of asphalt binder that was observed in the laboratory.

4.1.PHYSICAL PROPERTIES

The physical properties attribute to the softening point and the storage stability of the asphalt binder.

4.1.1.Softening Point

The softening point of the asphalt binder defines the transition temperature at which a material in solid state transforms to a melt / liquid state. The softening point of VG30 and VG40 binders was verified to be above the minimum temperature of 47℃ and 50℃, respectively as per IS 72: 2013. The values observed for VG30 and VG40 are 52℃ and 58℃, the modification of asphalt binder with graphene showed a slight rise in the softening point by 2℃ for all modifying percentages. The observed values of the softening point by ring and ball test are listed below in Table 4:

Table 4 Softening Point of VG30, VG40 and Graphene Modified Asphalt Binder

VG30	**Softening point** ℃	**VG40**	**Softening point** ℃
Control Binder	52	Control Binder	58
0.5% Graphene	56	0.5% Graphene	60
1.0% Graphene	56	1.0% Graphene	60
1.5% Graphene	56	1.5% Graphene	60
2.0% Graphene	56	2.0% Graphene	60

4.1.2.Storage Stability

The storage stability of the asphalt binder is check for the stability of constituents in the asphalt binder to maintain the consistency in the asphalt binder. The storage stability was determined by separation test and the results qualified to the storage stability of 2.2℃ for

the modified asphalt binder (Jeffry et al. 2018). The results are listed in Table 5 for VG30 and Table 6 for VG40 modified asphalt.

Table 5 Storage Stability of VG 30 Asphalt Binder

Proportion	**Top portion softening point**	**Bottom portion softening point**	**Difference [^{o}C]**	**Specification** *(ASTM-D5976)*
0.5% Graphene	56	56	0	Pass <2.2
1.0% Graphene	56	56	0	Pass <2.2
1.5% Graphene	56	56	0	Pass <2.2
2.0% Graphene	56	56	0	Pass <2.2

Table 6 Storage Stability of VG40 Asphalt Binder

Proportion	**Top portion softening point**	**Bottom portion softening point**	**Difference [^{o}C]**	**Specification** *(ASTM-D5976)*
0.5% Graphene	60	60	0	Pass <2.2
1.0% Graphene	60	60	0	Pass <2.2
1.5% Graphene	60	60	0	Pass <2.2
2.0% Graphene	60	60	0	Pass <2.2

4.2.RHEOLOGICAL PROPERTIES

The rheological properties were observed by rotational and oscillatory tests using DSR. Rotational test provides viscosity as a grade indicator as per IS 73:2010. To measure the rutting and temperature susceptibilities of the asphalt binder, following tests were performed: strain sweep, frequency sweep and MSCR test (Li et al. 2018). The rheological properties show an identical trend after 1% dosage which could be attributed to the agglomeration of nanomaterial (Tyson et al. 2011). The strain sweep was used to determine the complex modulus G^*, the rutting parameter $G^*/\sin\delta$ and linear viscoelastic region (LVER). The frequency sweep was conducted on the asphalt binder to examine its

susceptibility towards various temperatures and rate of loading. The multiple stress creep recovery test establishes the permanent deformation (Jnr) and the recovery percentage (R%) of the asphalt binder.

4.2.1.Rotational Test

The rotational test adheres to the shear rate applied at 60°C corresponding to which viscosity measured defines the absolute viscosity of the asphalt binder.

3.3.1.1.Absolute Viscosity

The absolute viscosity of the binder complies in accordance to the IS 73:2013 by having values of viscosity well within the ranges at 60℃ as prescribed by the provisions provided in the code. The values of average viscosity, absolute viscosity at a given shear rate and flow behavior are illustrated in Figure 29 - 34 and the values of average viscosity and absolute viscosity are tabulated in Table 7 and Table 8 respectively. Figure 29 and 30 shows the behavior of asphalt binder at shear rates ranging from $1s^{-1}$ to $15s^{-1}$, which depicts the observation that viscosity value of 1% dosage is highest followed by 1.5%, 2% and 0.5%, respectively. Figure 31 and 32 illustrates the average of absolute viscosity for all shear rates [$1 – 15s^{-1}$] and determines somewhat an identical trend in VG30 and VG40 asphalt, the binder tends to increase viscosity value till 1% dosage and then shows a decline in the viscosity values. The flow curve depicted in Figures 28 and 29 illustrates asphalt binder as a shear thinning or pseudoplastic material.

Table 7 Average Absolute Viscosity in Poise

Proportion	**VG30**	**VG40**
Control Binder	3217.13	4595.9
0.5% Graphene	4062.87	5804.1
1.0% Graphene	7947.8	11354
1.5% Graphene	6747.16	9638.8
2.0% Graphene	5274.36	7534.8

Table 8 Viscosities at 1 s^{-1} to 15 s^{-1} Shear Rates

Absolute Viscosity [Poise]

	Shear Rate	Control Binder	0.5% Graphene	1.0% Graphene	1.5% Graphene	2.0% Graphene
VG30	1	5290.04	6637.05	14060.2	13587	9139.9
	3	4926.46	6043.8	12250.7	11732.7	8164.1
	5	4038.58	5309.22	9921.1	8912.4	7102.9
	7	3282.79	4117.19	7177.8	6177.08	5470.22
	9	2565.92	3257.03	6770.82	4866.12	4336.78
	11	2336.18	2642.29	6137.25	3132.57	3301.9
	13	1959.51	2431.52	4123	2650.76	2536.52
	15	1337.56	2064.58	3140.34	2919.7	2142.56
VG40	1	7557.2	9481.5	20086	19410	13057
	3	7037.8	8634	17501	16761	11663
	5	5769.4	7584.6	14173	12732	10147
	7	4689.7	5881.7	10254	8824.4	7814.6
	9	3665.6	4652.9	9672.6	6951.6	6195.4
	11	3337.4	3774.7	8767.5	4475.1	4717
	13	2799.3	3473.6	5890	3786.8	3623.6
	15	1910.8	2949.4	4486.2	4171	3060.8

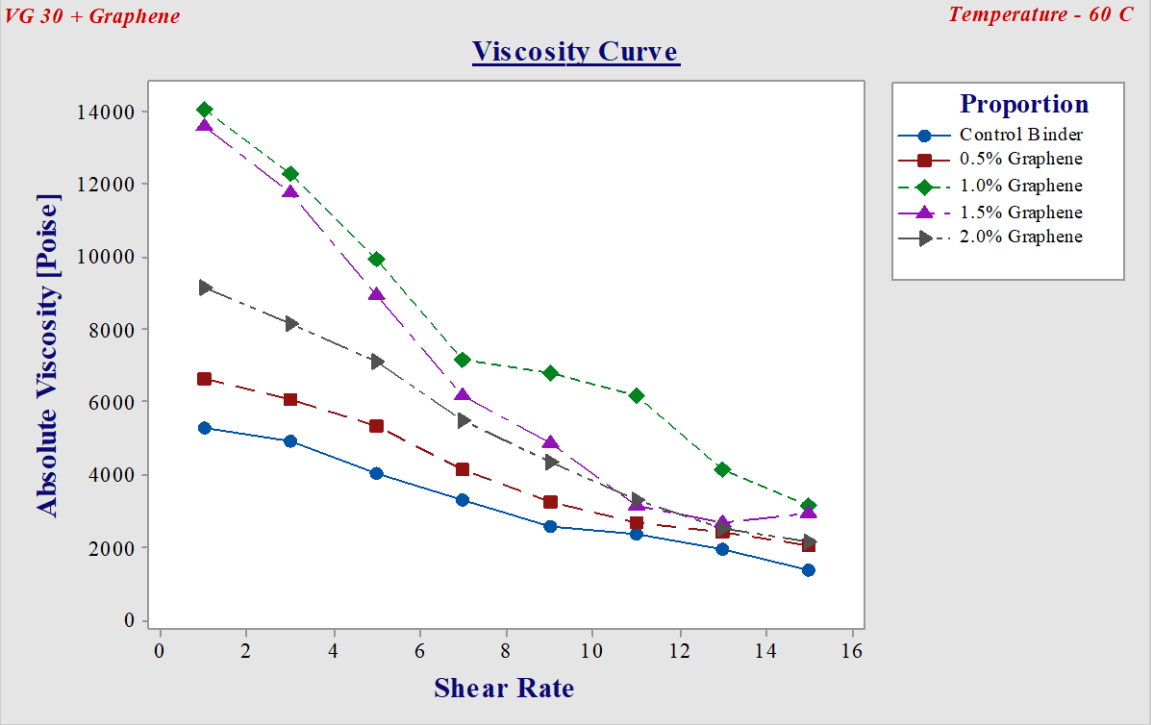

Figure 29 Viscosity Curve VG30

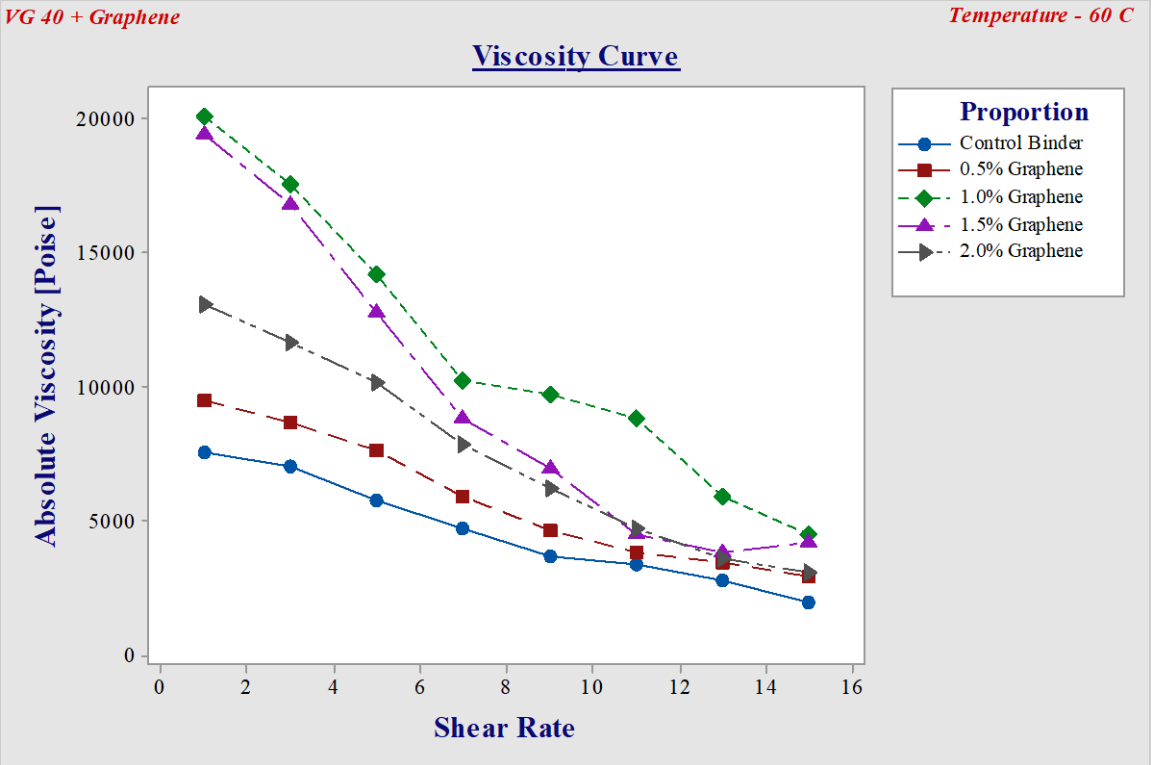

Figure 30 Viscosity Curve VG40

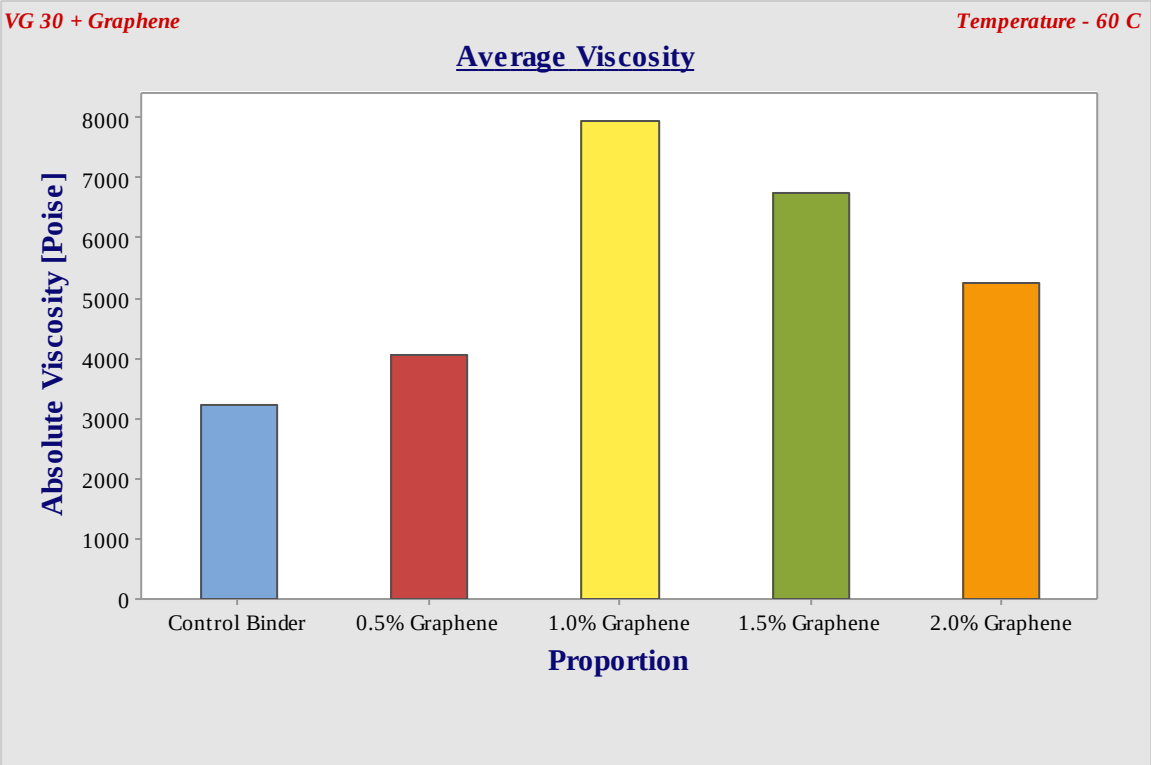

Figure 31 Average of Viscosities for all Shear Rates.

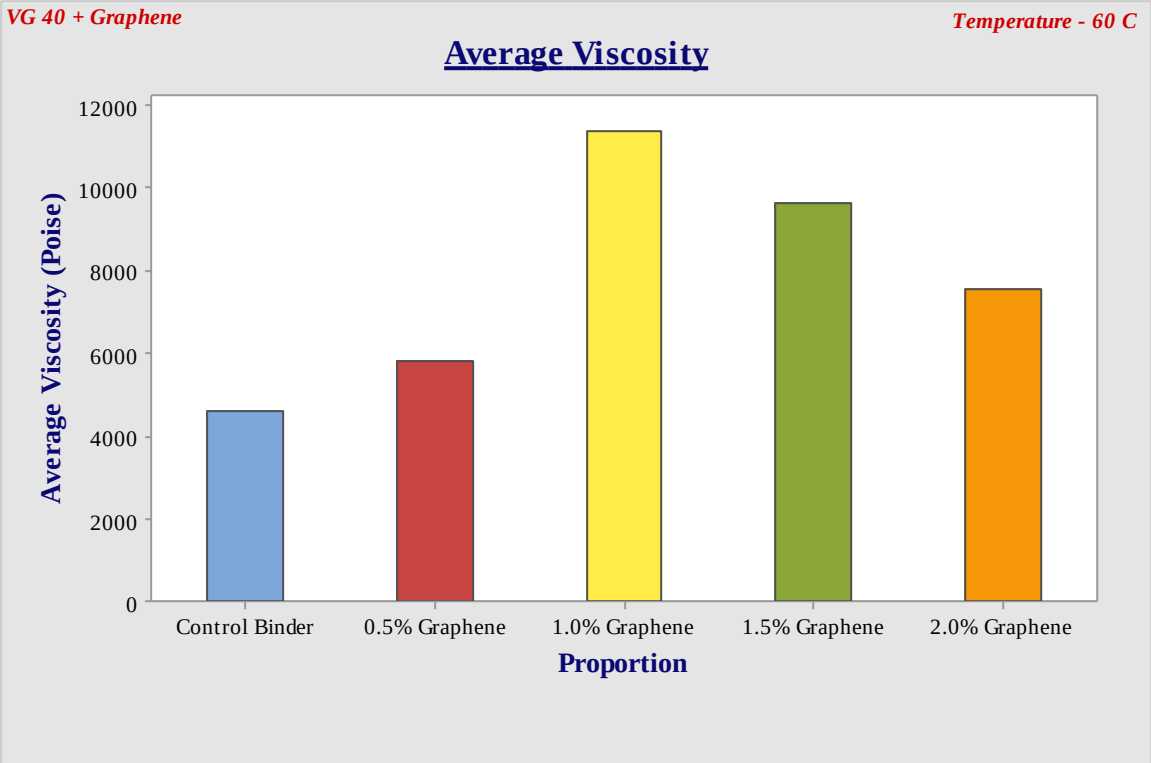

Figure 32 Average of Viscosities for all Shear Rates.

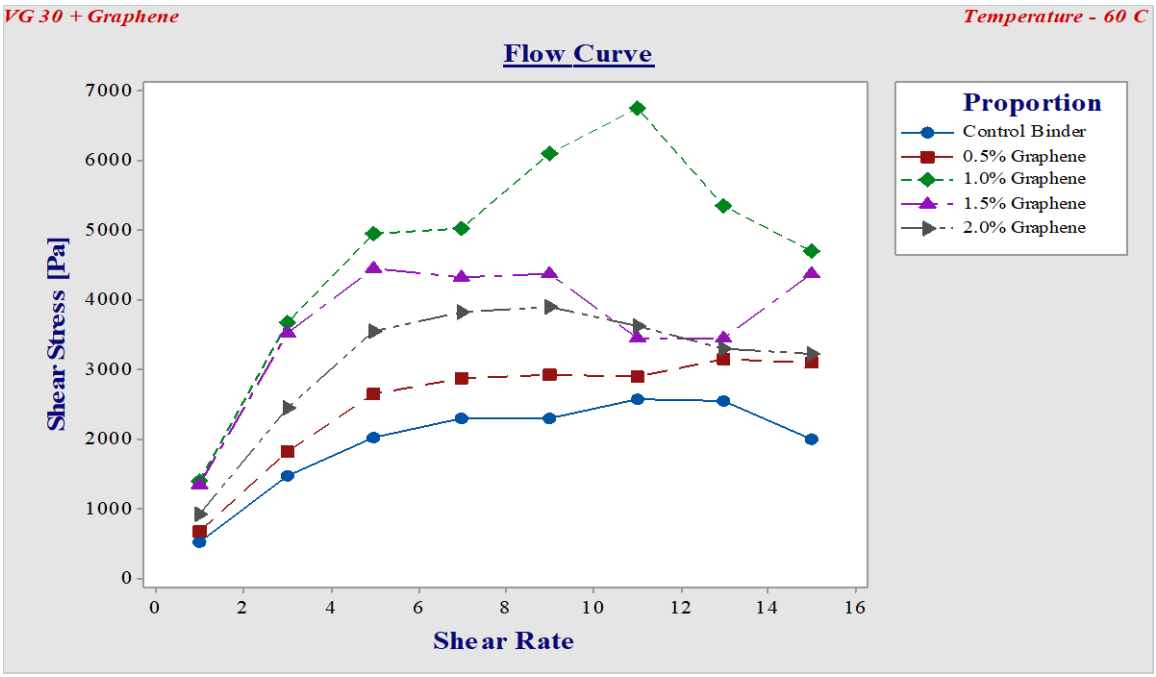

Figure 33 Flow Curve VG30

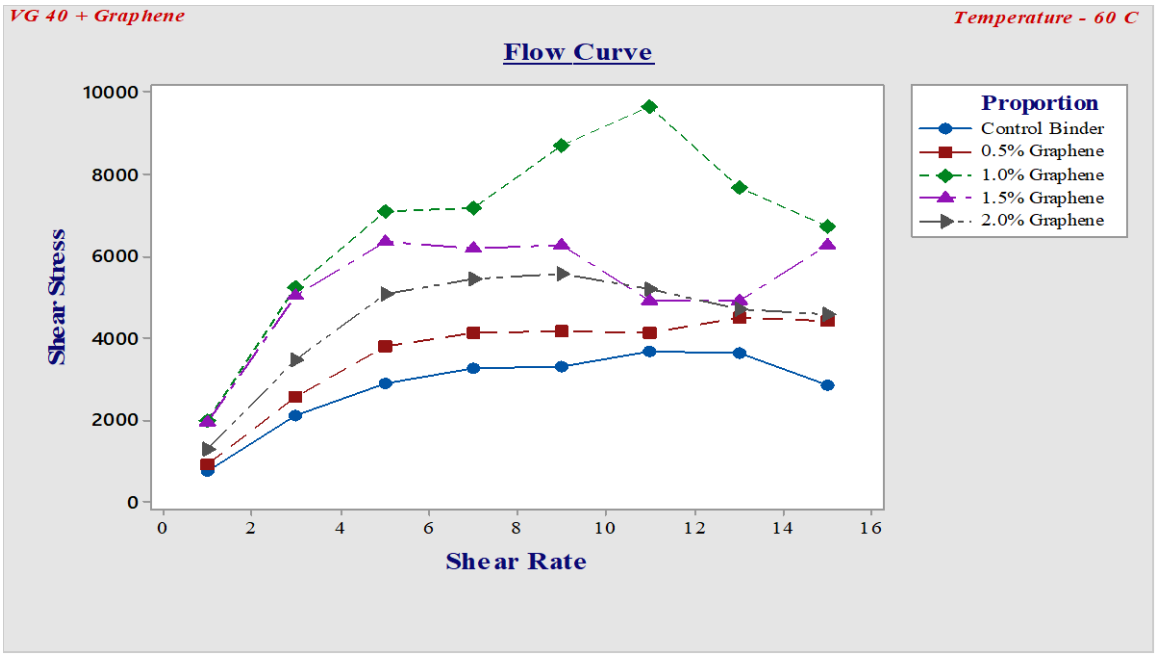

Figure 34 Flow Curve VG40

4.2.2.Oscillatory Test

Oscillatory test as the name suggests is performed in a to and fro motion and provides with a sinusoidal wave functions of stress and strain.

3.3.1.2.Strain Sweep

The strain sweep test was conducted at two different temperatures of 60℃ and 65℃ at an angular frequency of 10 rads / sec for 8 different shear strain percentages (2%, 4%, 6%, 8%, 10%, 12%, 14% and 16%). The data recorded from the strain sweep test is examined for determining the linear viscoelastic range of the binder and enhancements of the LVER hints to a more vibrant elastic component of the asphalt binder which will result in lesser energy dissipation thus indicating a robust mechanical characteristic of the asphalt binder. The values of all the parameters at 12% target strain level are tabulated in Table 9 and 10.

Figures 35 and 36 determine the linear viscoelastic region for VG30 + graphene dosages at 60℃ and 65℃, from which it could be inferred that the linear viscoelastic region at 60℃ is more than the temperature condition of 65℃. The LVER for VG30 varies in control binder from 0.96 to 0.93 and 0.943 to 0.873 for temperatures 60℃ and 65℃ respectively, for 0.5% it varies from 0.983 to 0.94 and 0.97 to 0.90 for temperatures 60℃ and 65℃ respectively, for 1% it varies from 0.991 to 0.948 and 0.972 to 0.926 for temperatures 60℃ and 65℃ respectively, for 1.5% it varies from 0.985 to 0.932 and 0.975 to 0.915 for temperatures 60℃ and 65℃ respectively and for 2% it varies from 0.986 to 0.93 and 0.972 to 0.89 for temperatures 60℃ and 65℃ respectively. 1% dosage showcases the optimum range for linear viscoelastic range.

Complex shear modulus for VG30 shows an increasing trend till 1% dosage and then shows a decline in the *G** trend as illustrated in Figures 37 and 38. The *G** tends to decline with rise in temperature by 5℃ by almost 50% for VG30. The complex shear modulus observed for eight strain percentages from lowest 2% to highest 16% varies for control binder VG30 is in the range of 6.7 to 6.3 kPa and 3.7 to 3.9 kPa for temperatures 60℃ and 65℃ respectively, for 0.5% it varies from 8.20 to 7.76 kPa and 3.94 to 3.57 kPa for temperatures 60℃ and 65℃ respectively, for 1% it varies from to 16.03 to 15.23 kPa and 7.93 to 7.35 kPa for temperatures 60℃ and 65℃ respectively, for 1.5% it varies from 12.36 to 11.55 kPa and 7.77 to 7.12 kPa for temperatures 60℃ and 65℃ respectively and for 2% it varies from 8.20 to 7.63 kPa and 5.74 to 5.14 kPa for temperatures 60℃ and 65℃ respectively. 1% dosage showcases the optimum range for linear viscoelastic range.

Phase shift angle describes the viscoelastic state of the binder, the phase shift angle $\delta <$ 45℃ signifies a viscoelastic solid and phase shift angle $\delta >$ 45℃ signifies a viscoelastic liquid. The asphalt binder above its softening point tends to behave in a molten state i.e. in a viscoelastic liquid state. This result signifies that the softening point of 60℃ is not the actual softening point, since softening point gives an idea of the transient temperature between solid and molten state therefore the values obtained during softening point cannot be treated as absolute qualifier for the binder. The phase shift angle is illustrated in Figures 39 and 40, Figure 39 shows phase shift angle increasing with the increased shear strain percentage for 60℃ with a phase angle ranging from 81.3° to 83°, 79.9° to 81.1°, 76.1° to 77°, 78° to 78.8° and 80.1° to 82° for control binder VG30, 0.5%, 1.0%, 1.5% and 2.0% respectively. By increasing temperature by 5℃, the phase shift angle tends to show a decreasing trend which signifies the binder is changing its behavior to less viscous phase. Figure 39 showcases values at different strain percentages at 65℃ having values ranging from 82.74° to 86.88°, 82.72° to 86.37°, 80.78° to 82.44°, 80.83° to 82.82° and 81.92° to 84.72° for control binder VG30, 0.5%, 1.0%, 1.5% and 2.0%, respectively.

The rutting parameter is denoted by $G^*/\sin\delta$, which shows two fold increase by the addition of graphene as illustrated in Figures 41 and 42 for 60°C and 65°C but also decreases by almost 50% with a temperature increase of 5℃, both the binder grades tend to follow a similar trend in the augmentation of the rutting parameter. Figure 40 shows $G^*/\sin\delta$ increasing with the increased shear strain percentage at 60℃ with $G^*/\sin\delta$ ranging from 6.83 to 6.38 kPa, 8.33 to 7.84 kPa, 16.56 to 15.95 kPa, 12.76 to 11.74 kPa and 8.32 to 7.71 kPa for control binder VG30, 0.5%, 1.0%, 1.5% and 2.0% respectively. Figure 41 plots the values at different strain percentages at 65 ℃ against $G^*/\sin\delta$ having values ranging from 3.74 to 3.24 kPa, 3.99 to 3.58 kPa, 8.08 to 7.44 kPa, 7.91 to 7.20 kPa and 5.82 to 5.18 kPa for control binder VG30, 0.5%, 1.0%, 1.5% and 2.0% respectively. The modification tends to increase $G^*/\sin\delta$ to its maximum value at 1% graphene dosage for both temperatures. Again the decreasing trend beyond 1% dosage is due to the agglomeration of the nanoparticles.

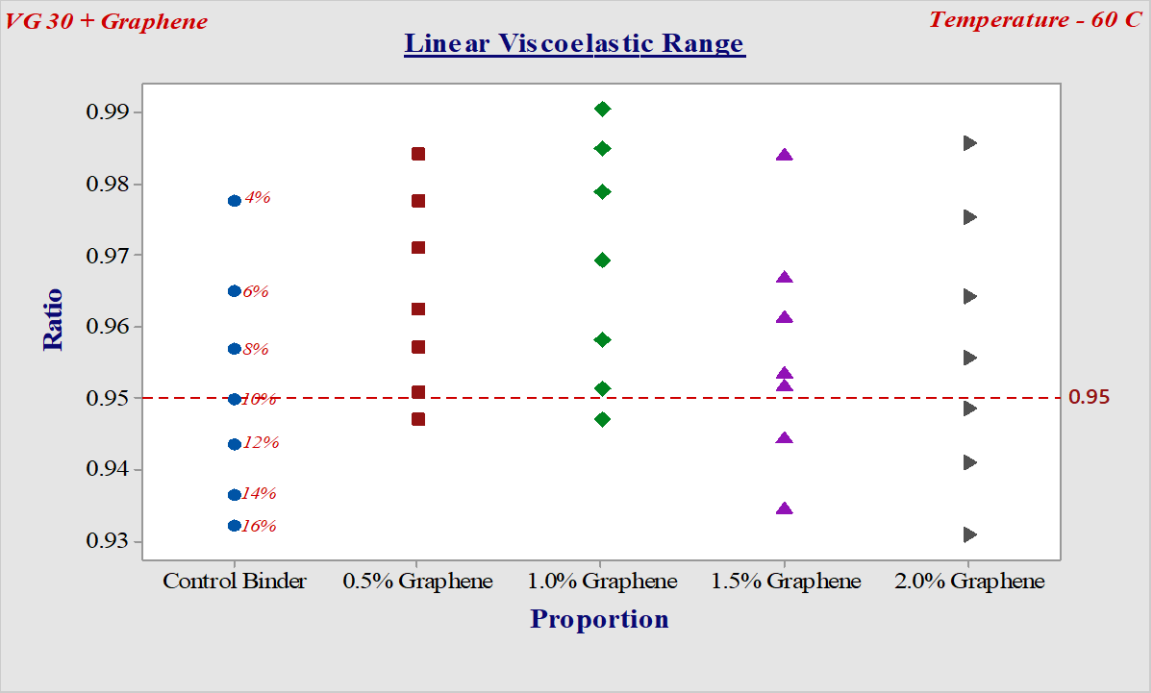

Figure 35 Linear Viscoelastic Range VG30 at 60℃

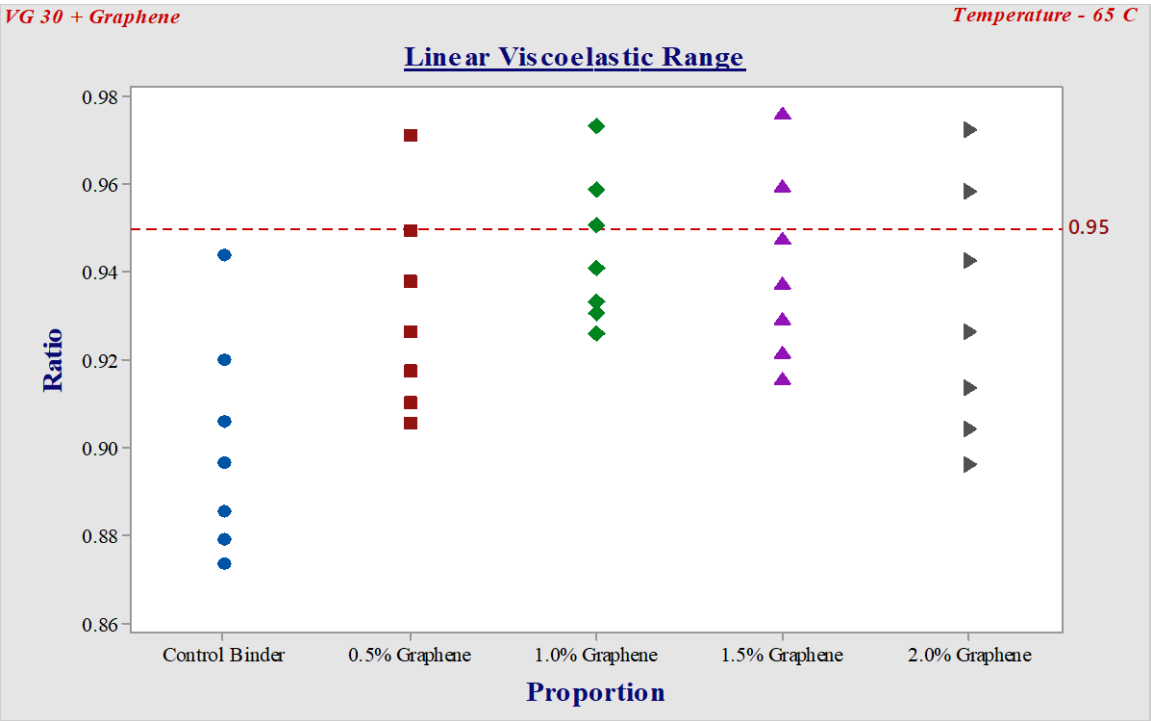

Figure 36 Linear Viscoelastic Range VG30 at 65℃

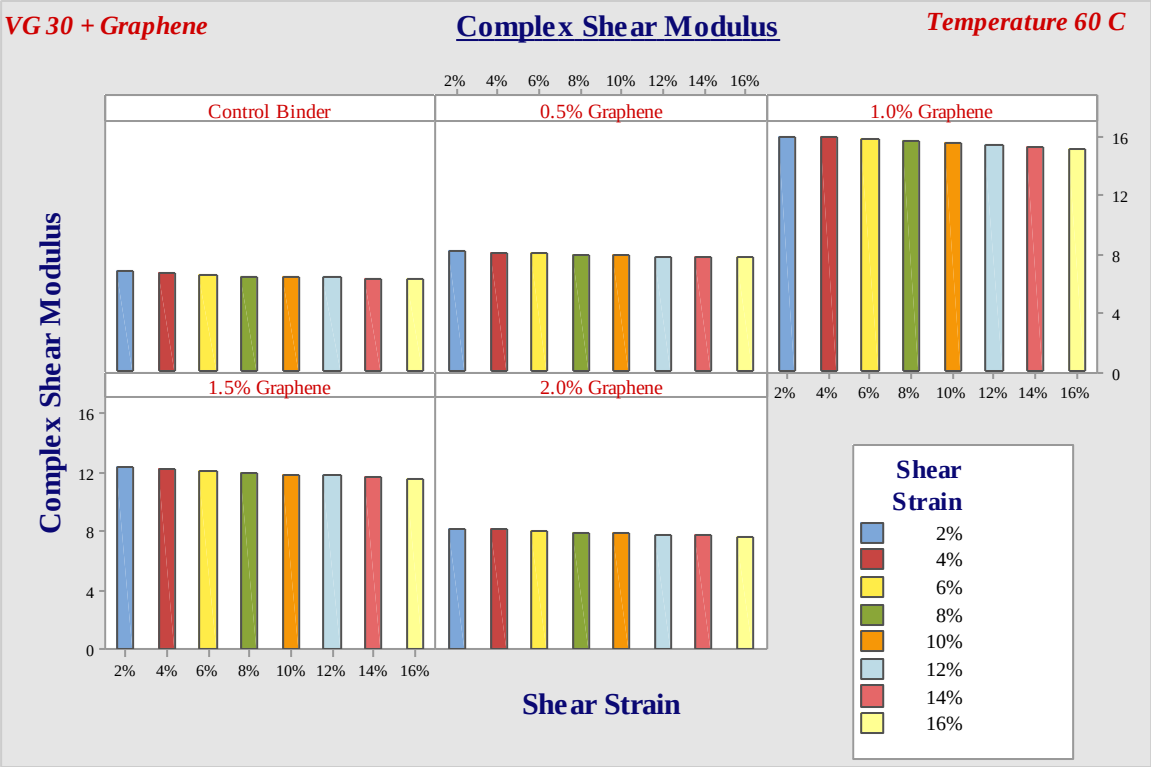

Figure 37 Complex Shear Modulus VG30 at 60℃

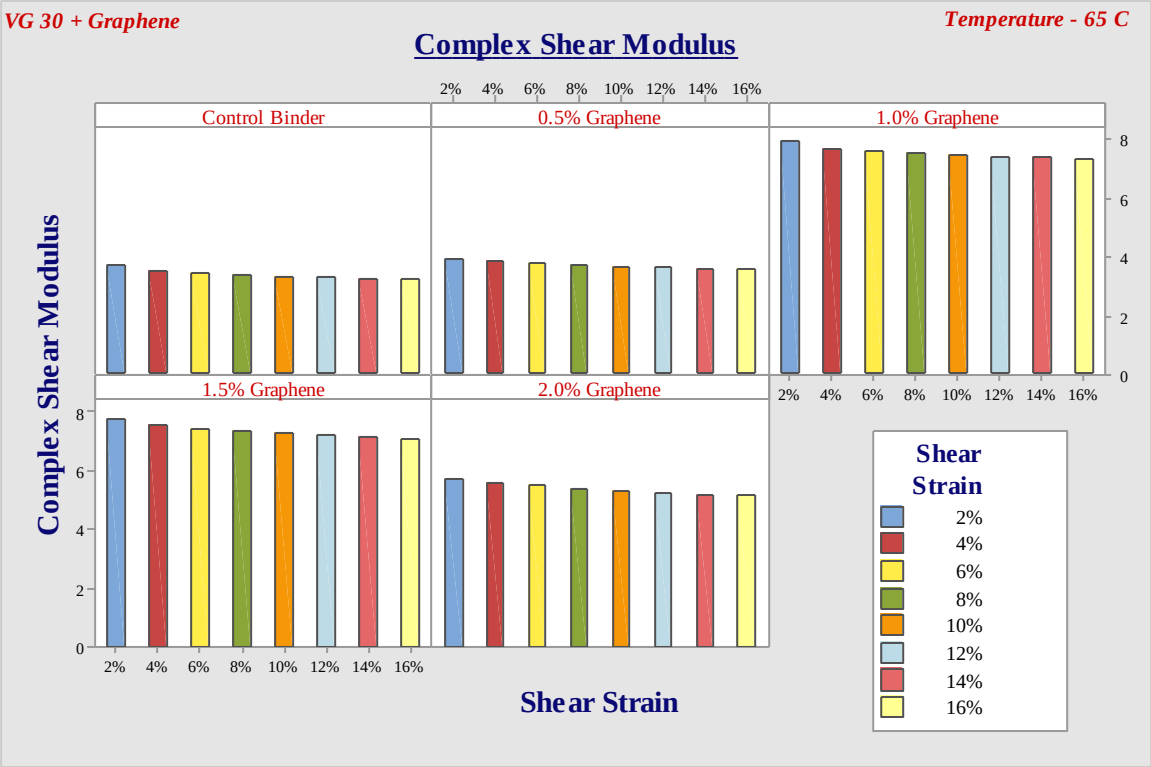

Figure 38 Complex Shear Modulus VG30 at 65℃

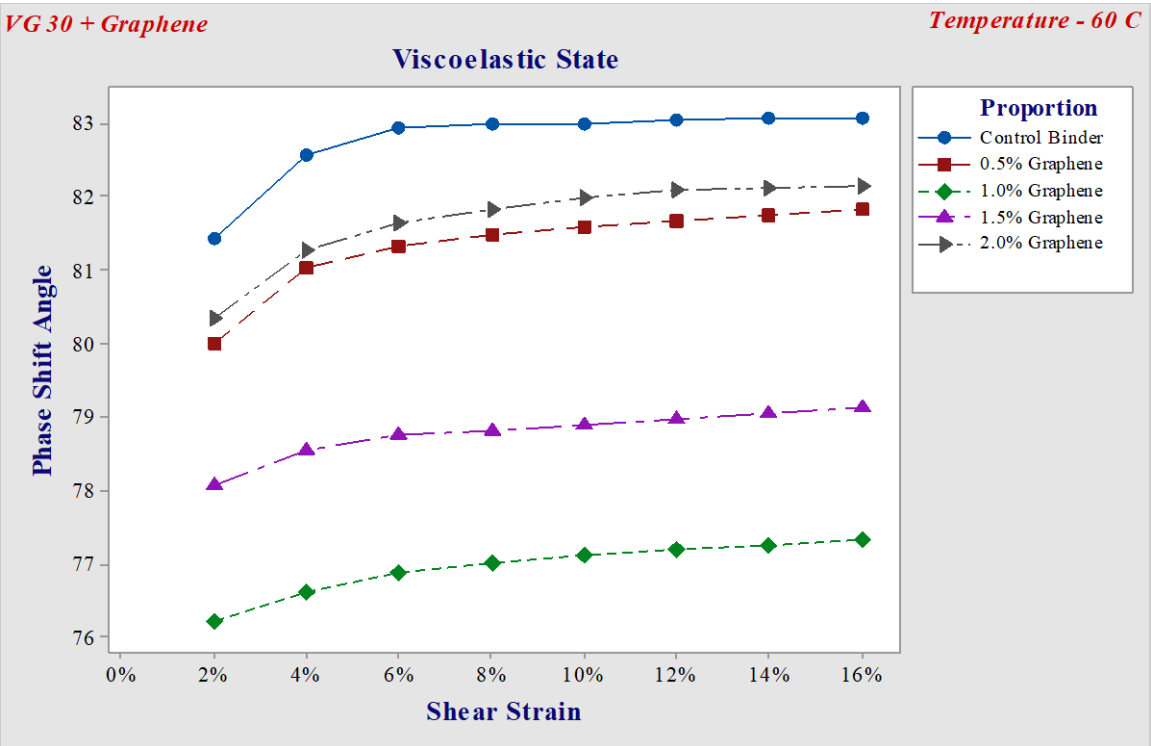

Figure 39 Phase Shift Angle VG30 at 60℃

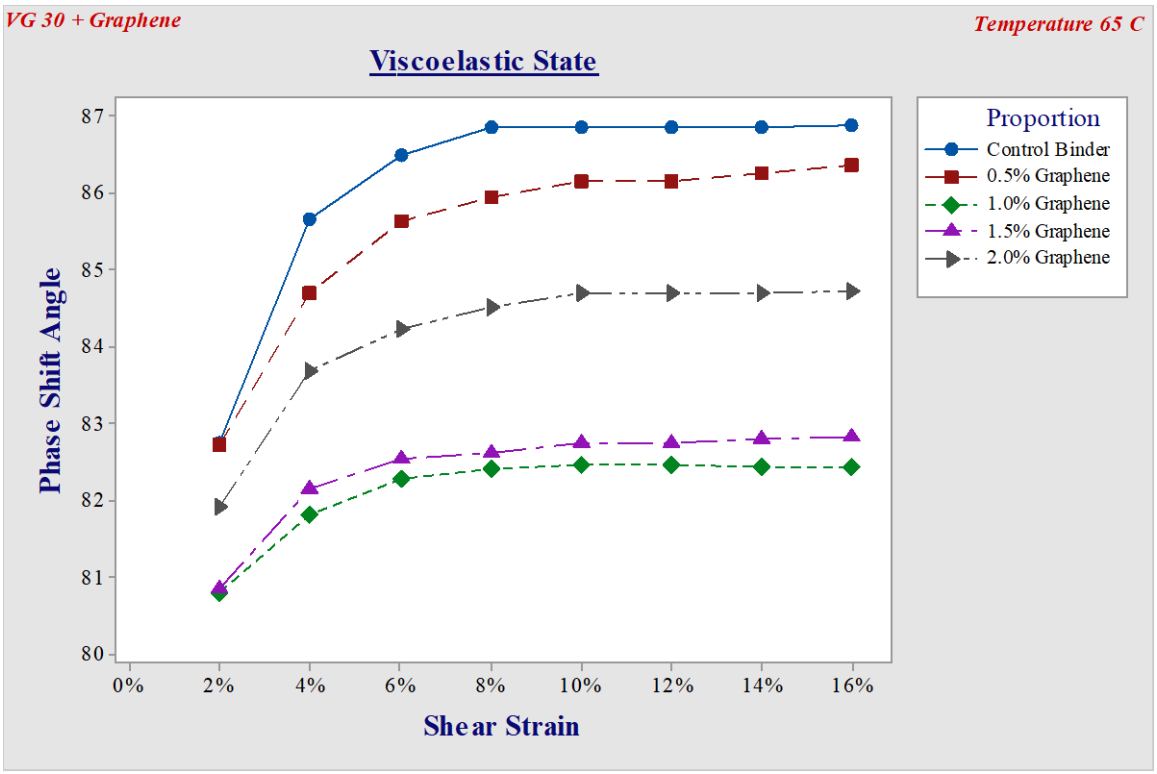

Figure 40 Phase Shift Angle VG30 at 65℃

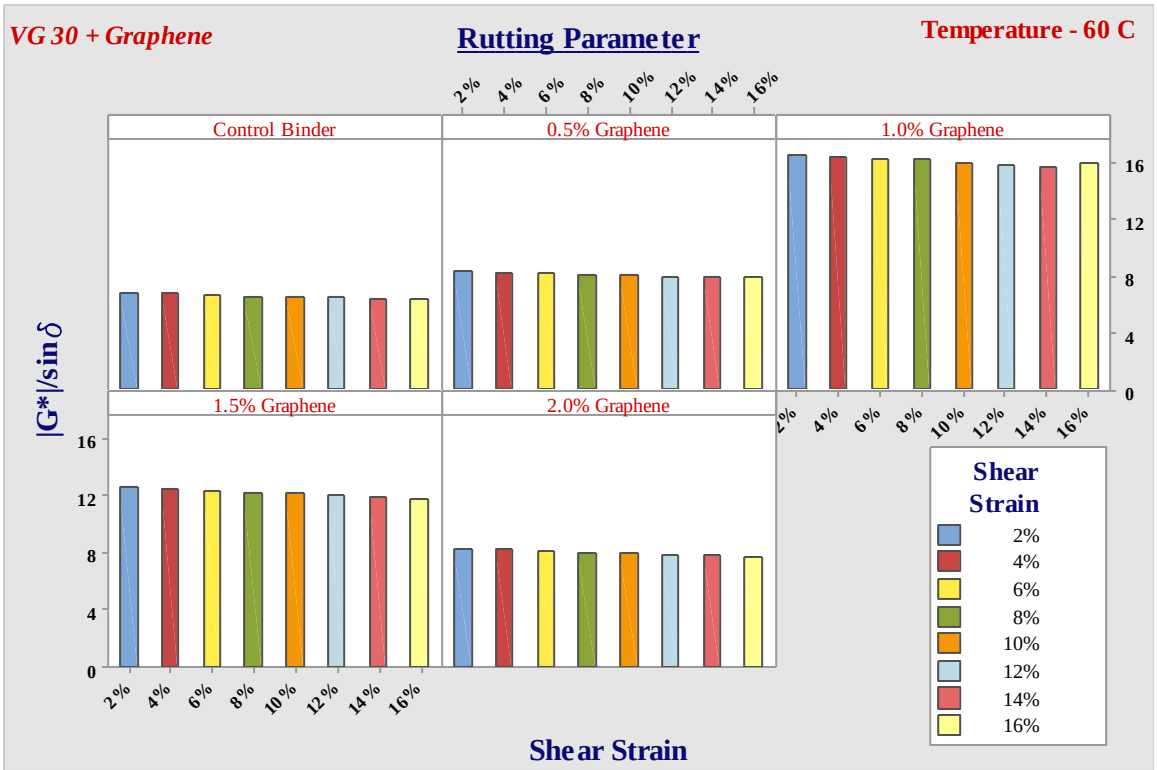

Figure 41 Rutting Parameter VG30 at 60℃

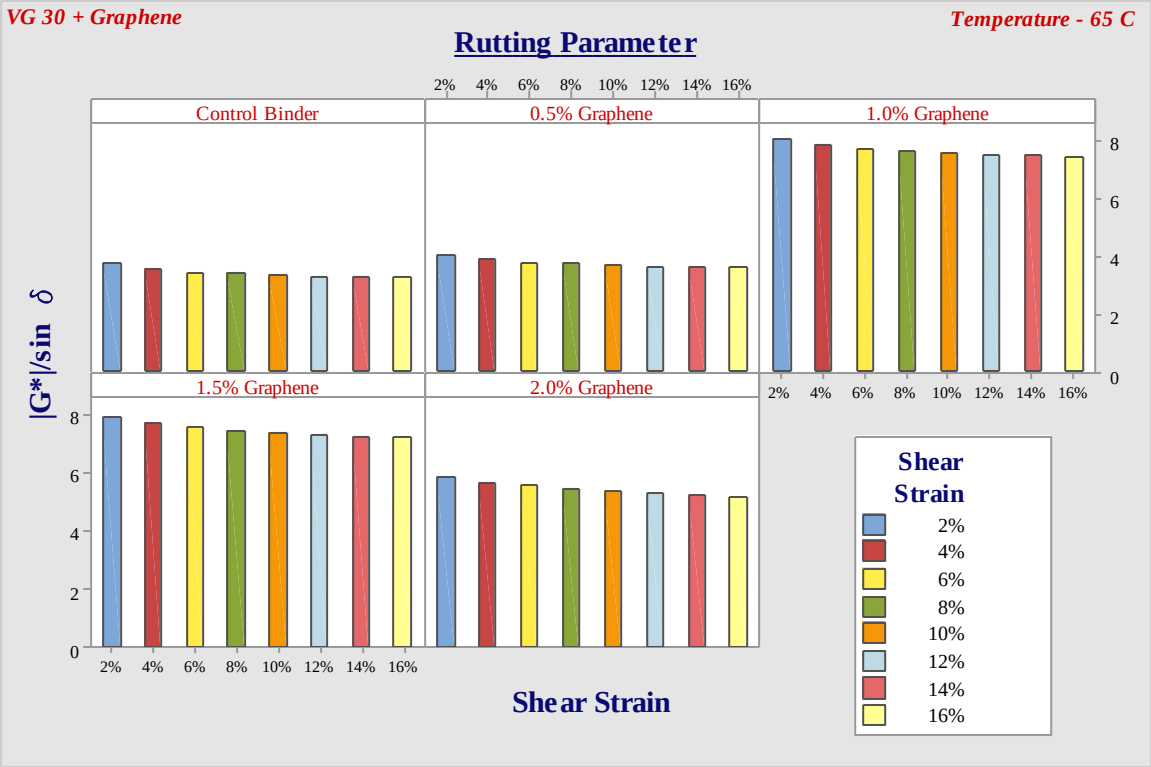

Figure 42 Rutting Parameter VG30 at 65℃

Figures 43 and 44 determine the linear viscoelastic region for VG40 + graphene dosages at 60℃ and 65℃, from signifies that the linear viscoelastic region at 60℃ is more than that of the temperature condition at 65℃. The LVER for VG40 varies in control binder from 0.97 to 0.927 and 0.94 to 0.87 for temperatures 60℃ and 65℃ respectively, for 0.5% it varies from 0.987 to 0.944 and 0.97 to 0.90 for temperatures 60℃ and 65℃ respectively, for 1% it varies from 0.989 to 0.948 and 0.974 to 0.926 for temperatures 60℃ and 65℃ respectively, for 1.5% it varies from 0.989 to 0.94 and 0.97 to 0.92 for temperatures 60℃ and 65 ℃ respectively and for 2% it varies from 0.986 to 0.93 and 0.972 to 0.90 for temperatures 60℃ and 65℃ respectively.

Complex shear modulus for VG40 signifies an increasing trend till 1% dosage and then shows a decline in the *G** trend as illustrated in Figures 45 and 46. The *G** tends to decline with rise in temperature by 5℃ by almost 50%. The complex shear modulus observed for eight strain percentages from lowest 2% to highest 16% varies for control binder VG40 is in the range of 5.7 to 5.32 kPa and 4.11 to 3.59 kPa for temperatures 60℃ and 65℃ respectively, for 0.5% it varies from 8.20 to 7.76 kPa and 4.38 to 3.97 kPa for

temperatures 60℃ and 65℃ respectively, for 1% it varies from to 16.03 to 15.23 kPa and 8.81 to 8.16 kPa for temperatures 60℃ and 65℃ respectively, for 1.5% it varies from 12.36 to 11.55 kPa and 8.64 to 7.91 kPa for temperatures 60℃ and 65℃ respectively and for 2% it varies from 8.20 to 7.63 kPa and 6.38 to 5.72 kPa for temperatures 60℃ and 65℃ respectively. 1% dosage showcases the optimum range for linear viscoelastic range.

The phase shift angle is illustrated in Figures 47 and 48, Figure 47 shows phase shift angle increasing with the increased shear strain percentage for 60 ℃ with a phase angle ranging from 81° to 84.89°, 80.92° to 82.66°, 76.69° to 77.93°, 77.42° to 77.45° and 79.26° to 80.56° for control binder VG40, 0.5%, 1.0%, 1.5% and 2.0% respectively. By increasing temperature by 5℃ the phase shift angle follows an overall decreasing trend which signifies the binder is changing its behavior to less viscous phase with temperature increase. Figure 48 showcases the values at different strain percentages at 65℃ having values ranging from 81.11° to 85°, 81° to 84.6°, 79° to 80.5°, 79.1° to 80.7° and 80.2° to 82.5° for control binder VG40, 0.5%, 1.0%, 1.5% and 2.0% respectively.

The rutting parameter is denoted by $G^*/\sin\delta$, the rutting parameter $G^*/\sin\delta$ shows two fold increase by the addition of graphene as illustrated in Figures 49 and 50 for 60℃ and 65℃ but also decreases by almost 50% with a temperature increase of 5℃, both the binder grades tend to follow a similar trend in the augmentation of the rutting parameter. Figure 49 shows $G^*/\sin\delta$ increasing with the increased shear strain percentage at 60℃ with $G^*/\sin\delta$ ranging from 5.79 to 5.34 kPa, 8.96 to 8.43 kPa, 19.83 to 18.57 kPa, 17.87 to 16.74 kPa and 13.78 to 12.74 kPa for control binder VG40, 0.5%, 1.0%, 1.5% and 2.0% respectively. Figure 50 plots the values at different strain percentages at 65℃ against $G^*/\sin\delta$ having values ranging from 4.16 to 3.60 kPa, 4.43 to 3.98 kPa, 8.97 to 8.27 kPa, 8.79 to 8.0 kPa and 6.4 to 5.76 kPa for control binder VG30, 0.5%, 1.0%, 1.5% and 2.0% respectively.

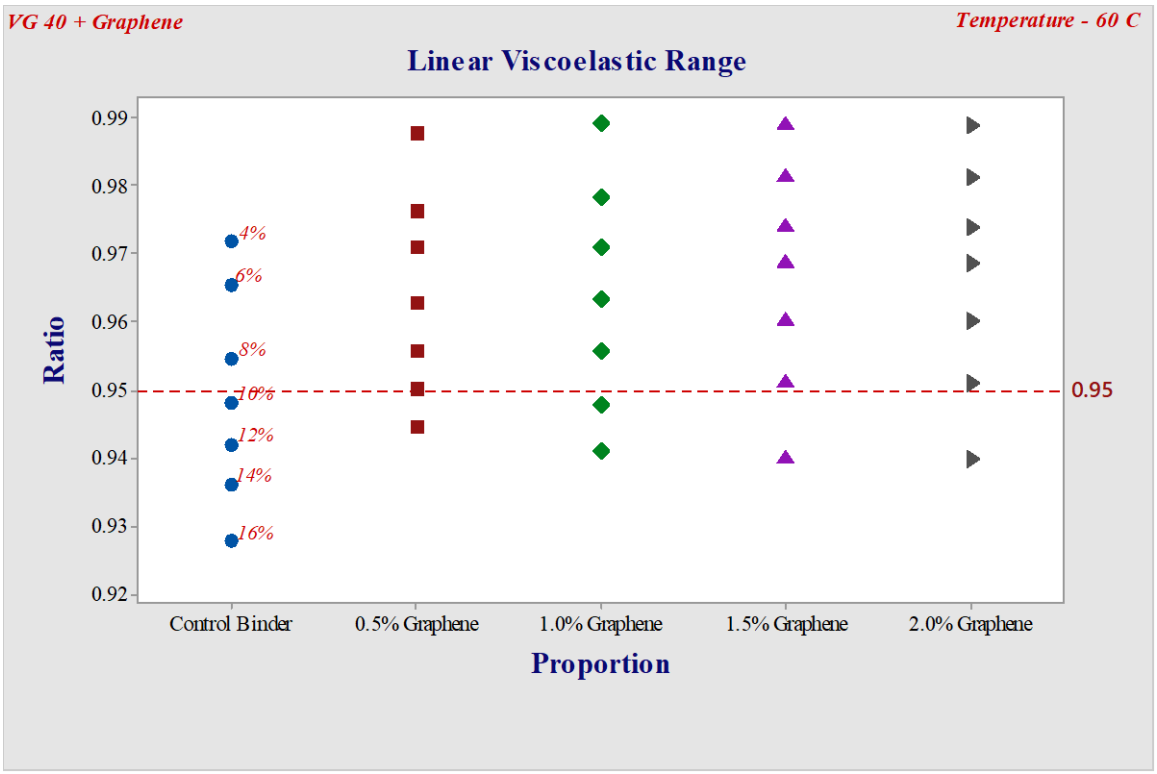

Figure 43 Linear Viscoelastic range VG40 at 60℃

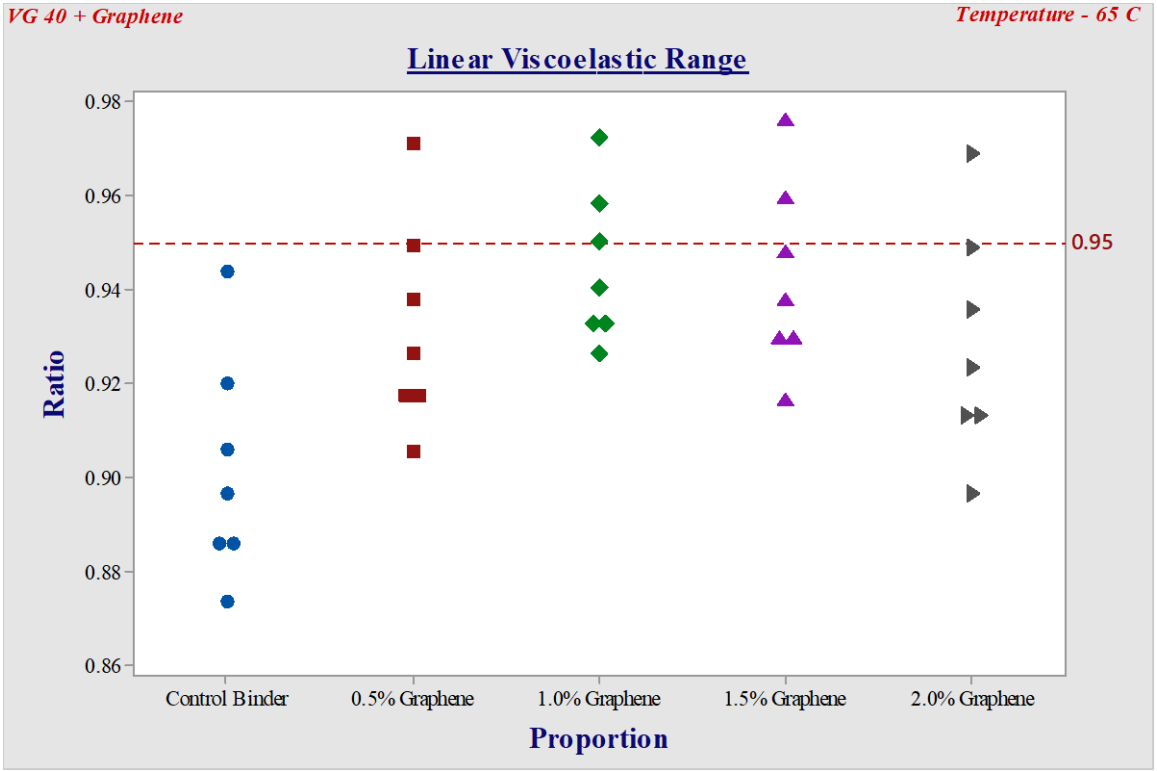

Figure 44 Linear Viscoelastic range VG40 at 65℃

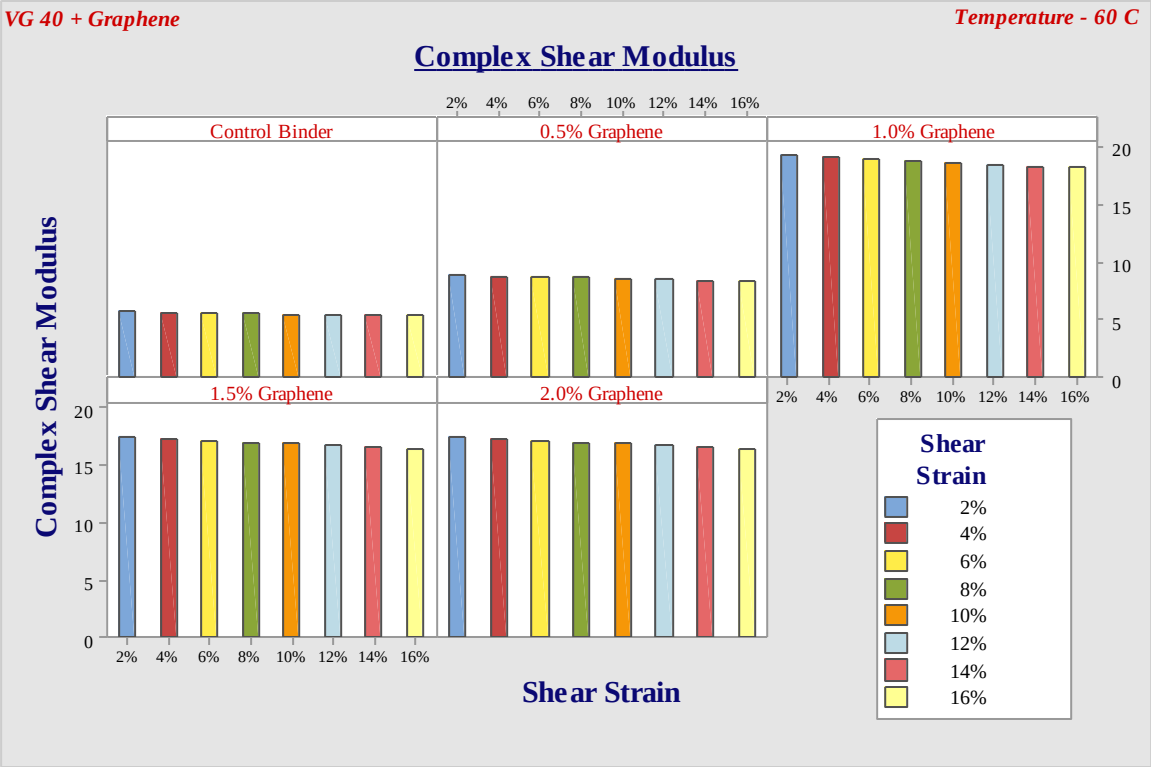

Figure 45 Complex Shear Modulus VG40 at 60℃

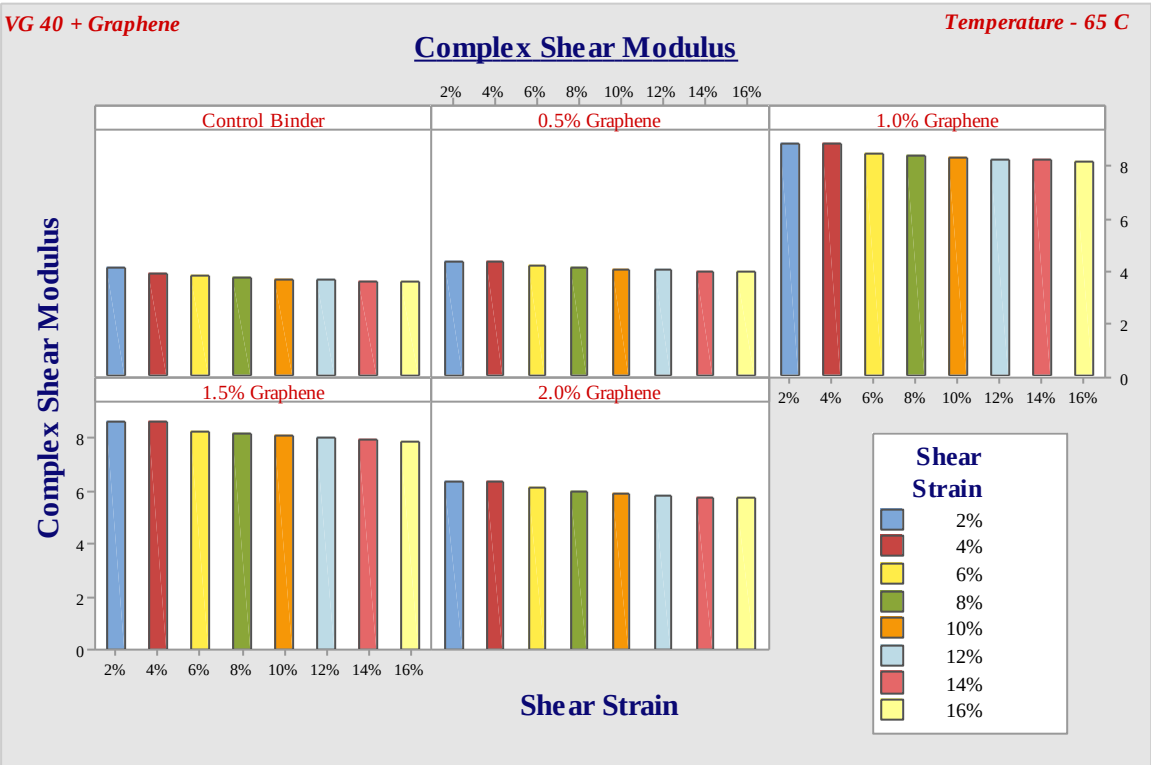

Figure 46 Complex Shear Modulus VG40 at 65℃

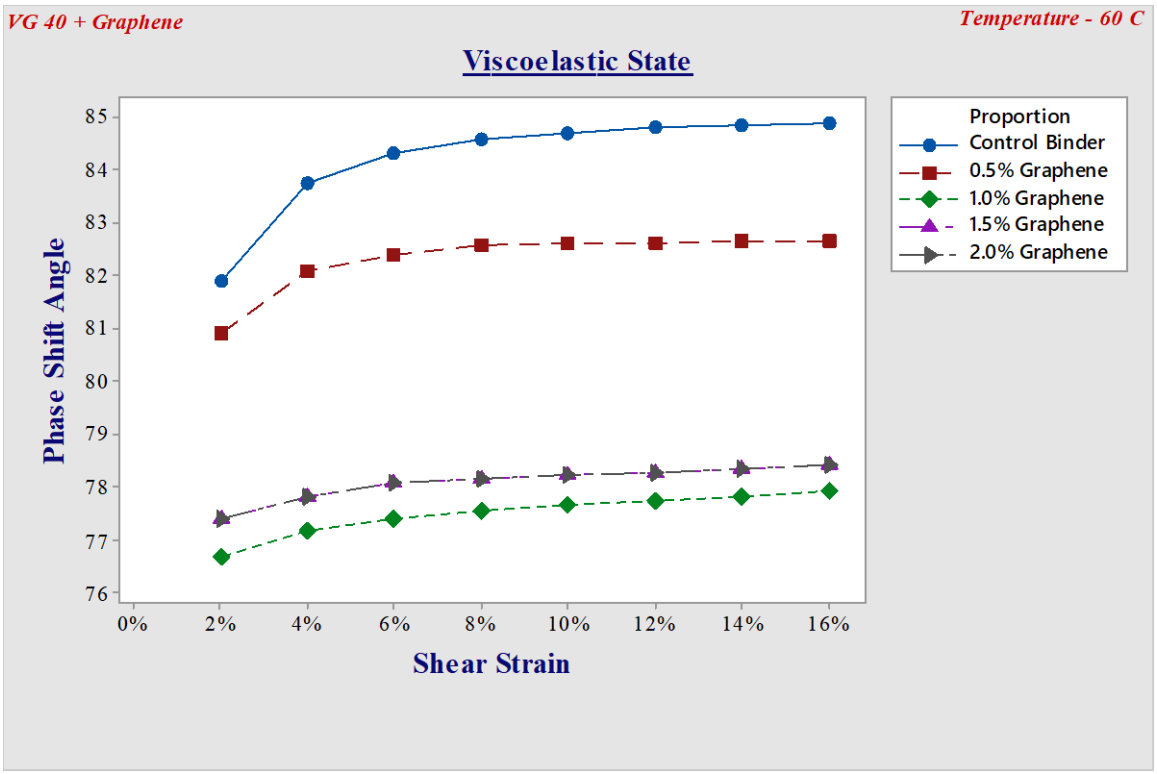

Figure 47 Phase Shift Angle VG40 at 60℃

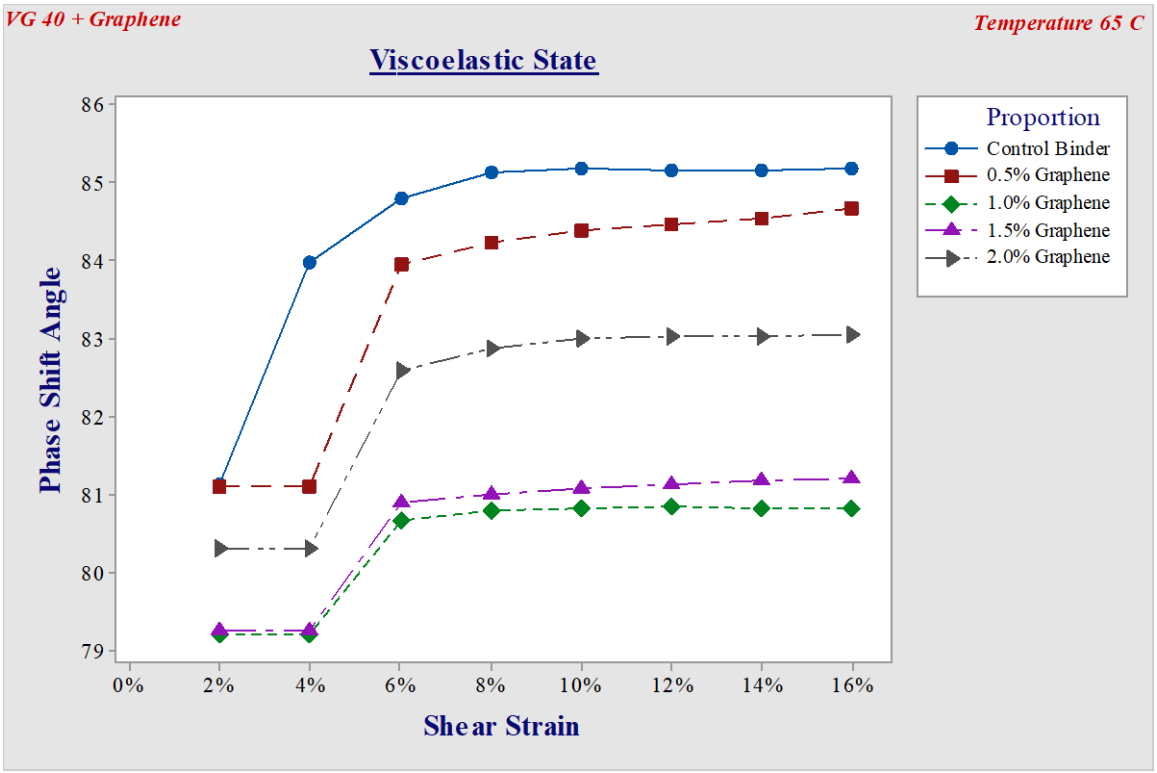

Figure 48 Phase Shift Angle VG40 at 65℃

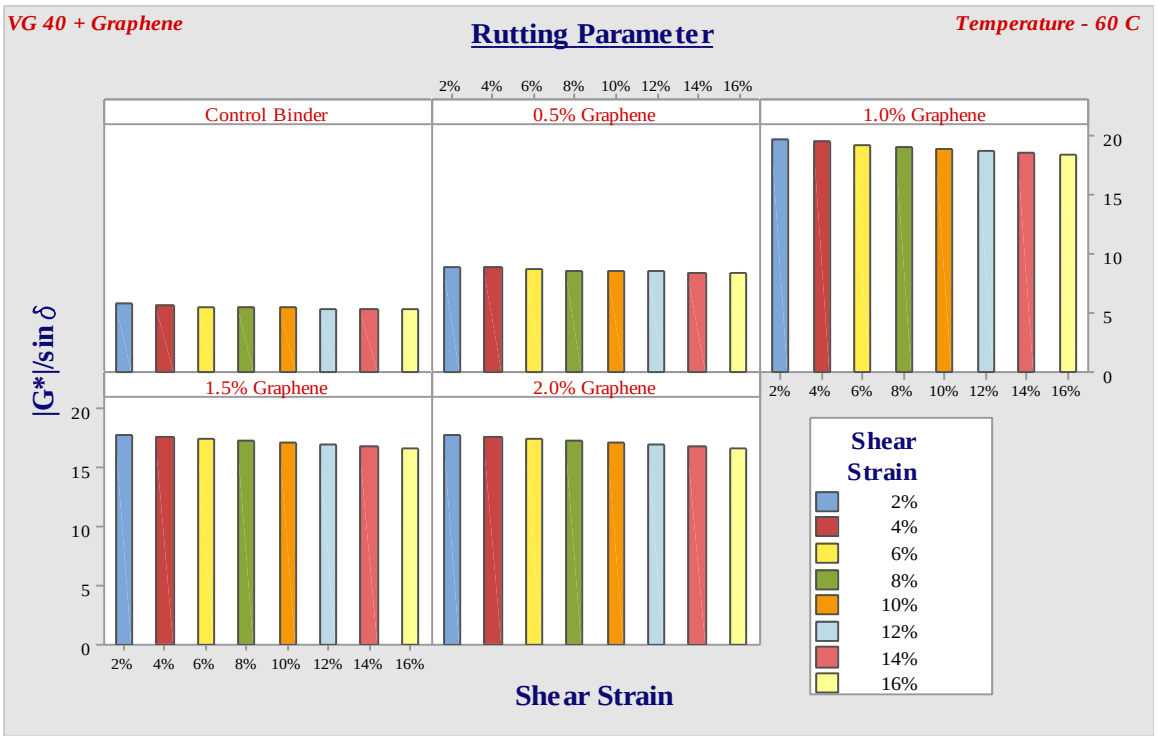

Figure 49 Rutting Parameter VG40 at 60℃

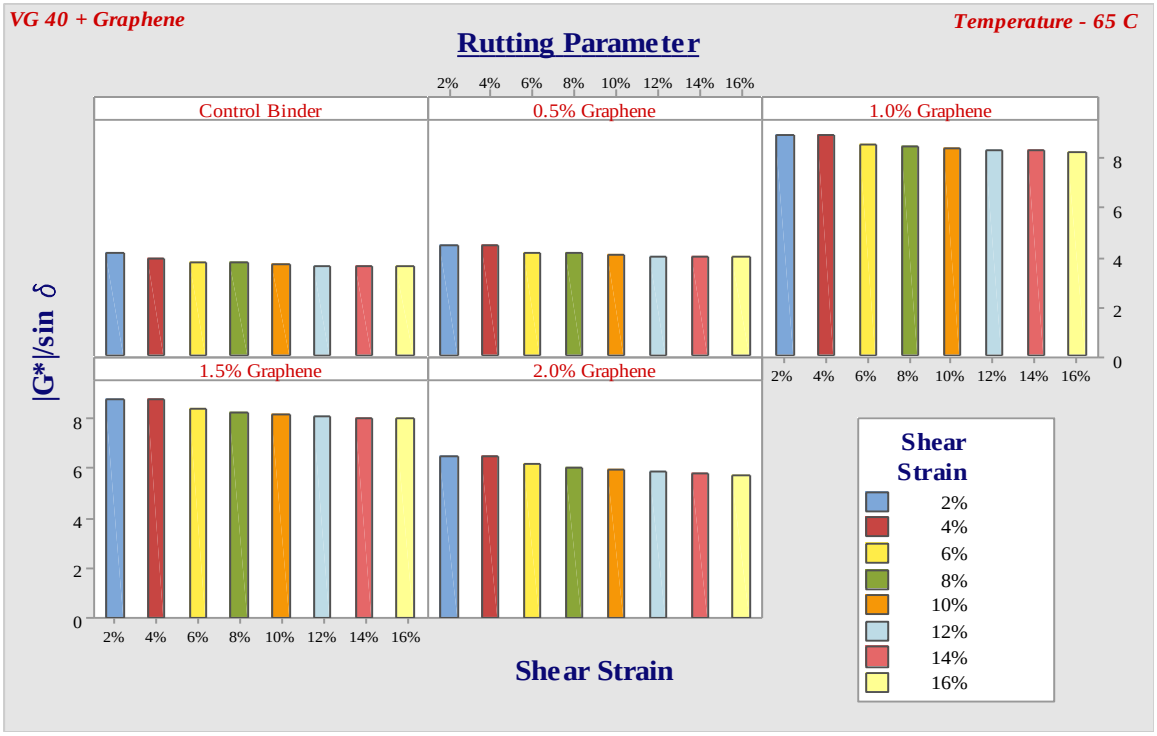

Figure 50 Rutting Parameter VG40 at 65℃

Table 9 Target Strain 12% at 60℃

VG30 – *Target strain 12%* [60℃]				
Proportion	**Complex Shear Modulus [kPa]**	G^*/G_0^*	**Phase Shift Angle [º]**	$G^*/\sin\delta$ **[kPa]**
Control Binder	6.415	0.943	83.04	6.463
0.5% Graphene	7.853	0.957	81.65	7.93
1.0% Graphene	15.416	0.958	77.20	15.80
1.5% Graphene	11.794	0.953	78.97	12.01
2.0% Graphene	7.7839	0.948	82.07	7.85
VG40 – *Target strain 12%*				
Control Binder	5.40	0.942	84.81	5.42
0.5% Graphene	8.46	0.955	82.64	8.53
1.0% Graphene	18.44	0.955	77.76	18.87
1.5% Graphene	16.75	0.960	78.30	17.10
2.0% Graphene	12.77	0.943	80.55	12.94

Table 10 Target Strain 12% at 65℃

VG30 – *Target strain 12%* [65 ℃]				
Proportion	**Complex Shear Modulus [kPa]**	G^*/G_0^*	**Phase Shift Angle [º]**	$G^*/\sin\delta$ **[kPa]**
Control Binder	3.28	0.885	86.86	3.29
0.5% Graphene	3.61	0.917	86.15	3.63
1.0% Graphene	7.38	0.930	82.43	7.48
1.5% Graphene	7.22	0.928	82.74	7.31
2.0% Graphene	5.24	0.913	84.69	5.28
VG40 – *Target strain 12%*				
Control Binder	3.64	0.885	85.16	3.65
0.5% Graphene	4.02	0.917	84.46	4.04
1.0% Graphene	8.22	0.932	80.84	8.33
1.5% Graphene	8.02	0.929	81.12	8.12
2.0% Graphene	5.83	0.913	83.03	5.87

3.3.1.3.Frequency Sweep

The frequency sweep gives the relation between the rheological parameters and frequency – temperature. As illustrated in Figures 51 – 60 the complex shear modulus tends to

decrease with decreasing frequency and vice – versa with the temperature increase. Figures 61 – 70 are called black space diagram and help to build a relationship between complex shear modulus and phase shift angle, the plot builds a pictorial representation of the isotherms which are attributed by observing the overlapping of the curves of different temperatures. The flow behavior index of both the binders was computed using the power law and it was inferred that modification of the binder doesn't help with the augmentation of the flow characteristics to improve the self-healing behavior of the asphalt binder. The flow index behavior values are tabulated in Table 11 and table 12 for VG30 and VG40 respectively. The flow index behavior for VG30 - control binder, 0.5%, 1%, 1.5% and 2% dosages ranges in the value 0.895 to 0.961, 0.893 to 0.964, 0.897 to 0.968, 0.896 to 0.968 and 0.897 to 0.969 respectively. The flow index behavior for VG40 - control binder, 0.5%, 1%, 1.5% and 2% dosages ranges in the value 0.9 to 0.967, 0.897 to 0.971, 0.887 to 0.967, 0.895 to 0.971 and 0.899 to 0.971 respectively. The values indicate that the viscoelastic state of the graphene modified asphalt binder is widened for temperatures 25℃ to 85℃ and at a higher temperature the value of **n** is $0.96 \leq n \leq 1$ which is closer to implicate a Newtonian flow (Li C. et al. 2016).

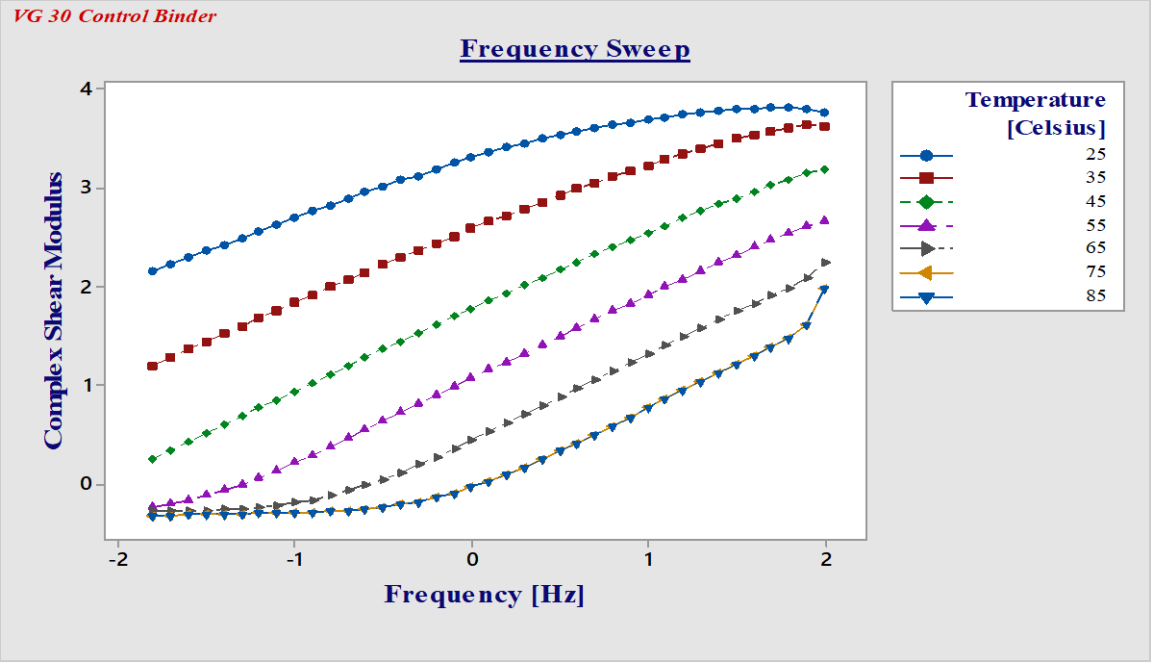

Figure 51 Frequency Sweep VG30

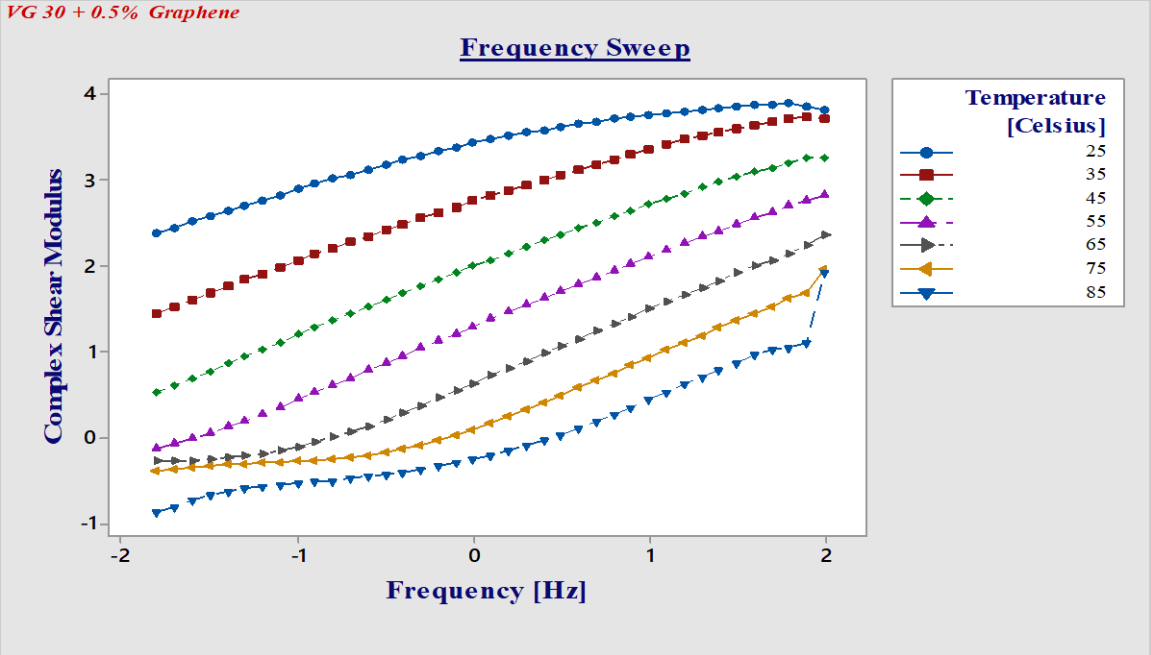

Figure 52 Frequency Sweep VG30 + 0.5% Graphene

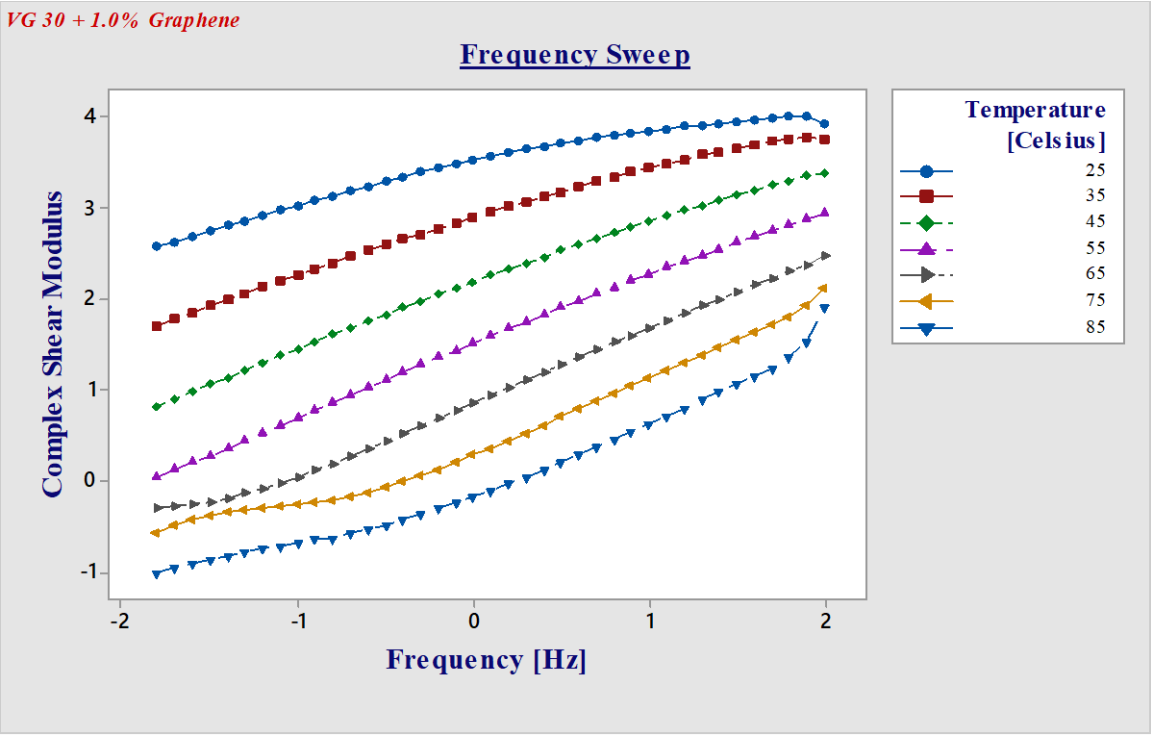

Figure 53 Frequency Sweep VG30 + 1% Graphene

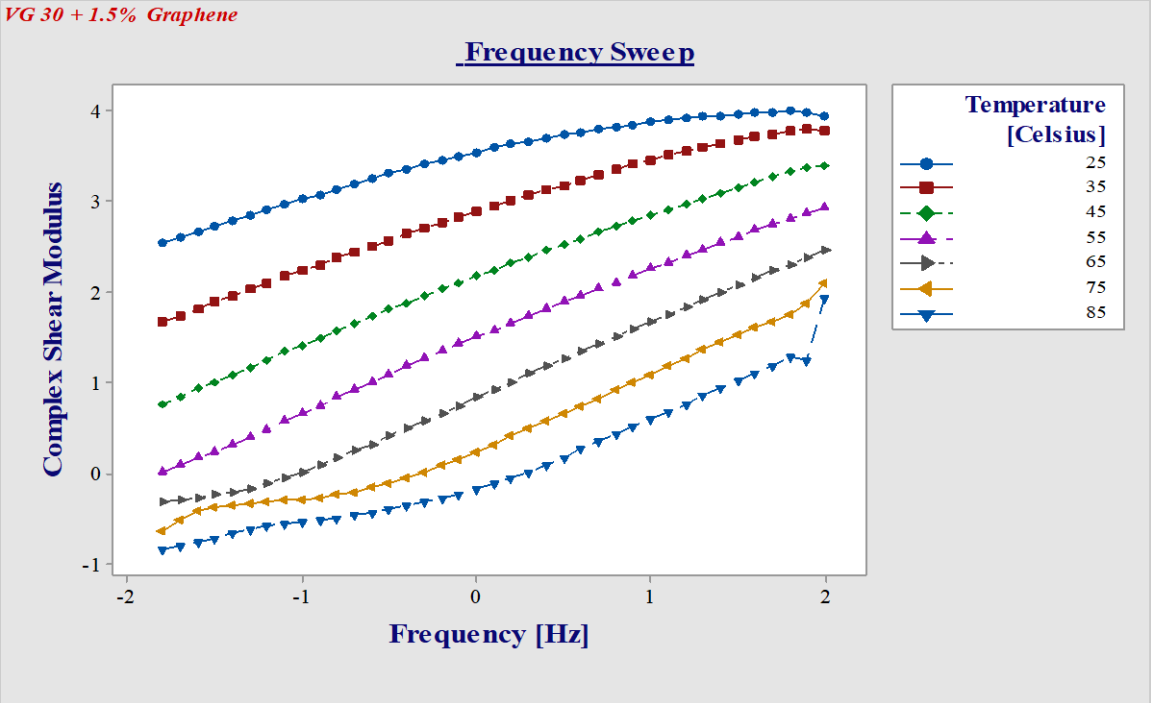

Figure 54 Frequency Sweep VG30 + 1.5% Graphene

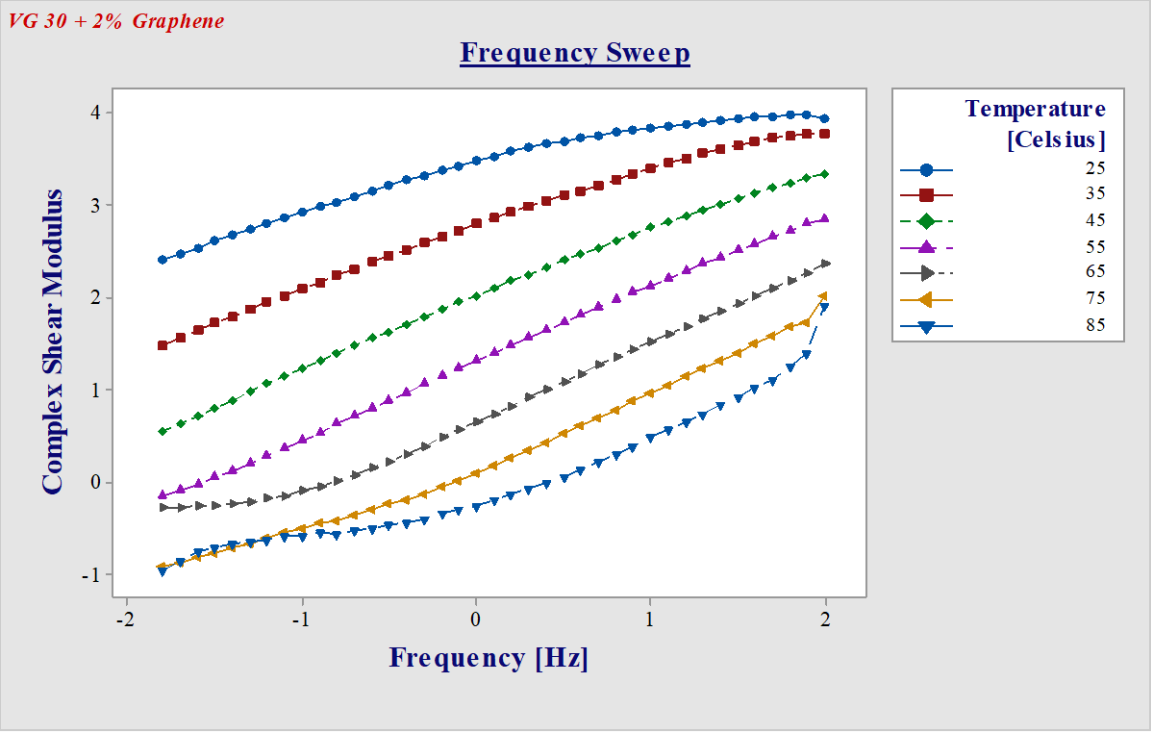

Figure 55 Frequency Sweep VG30 + 2% Graphene

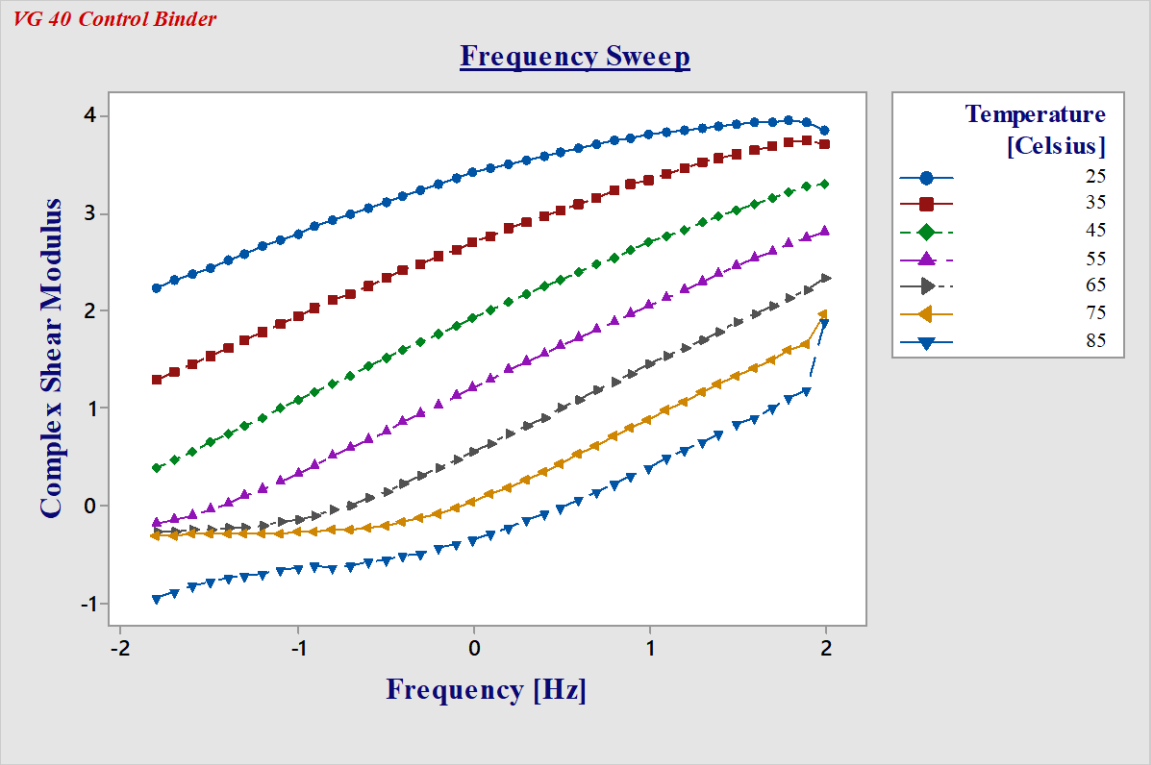

Figure 56 Frequency Sweep VG40

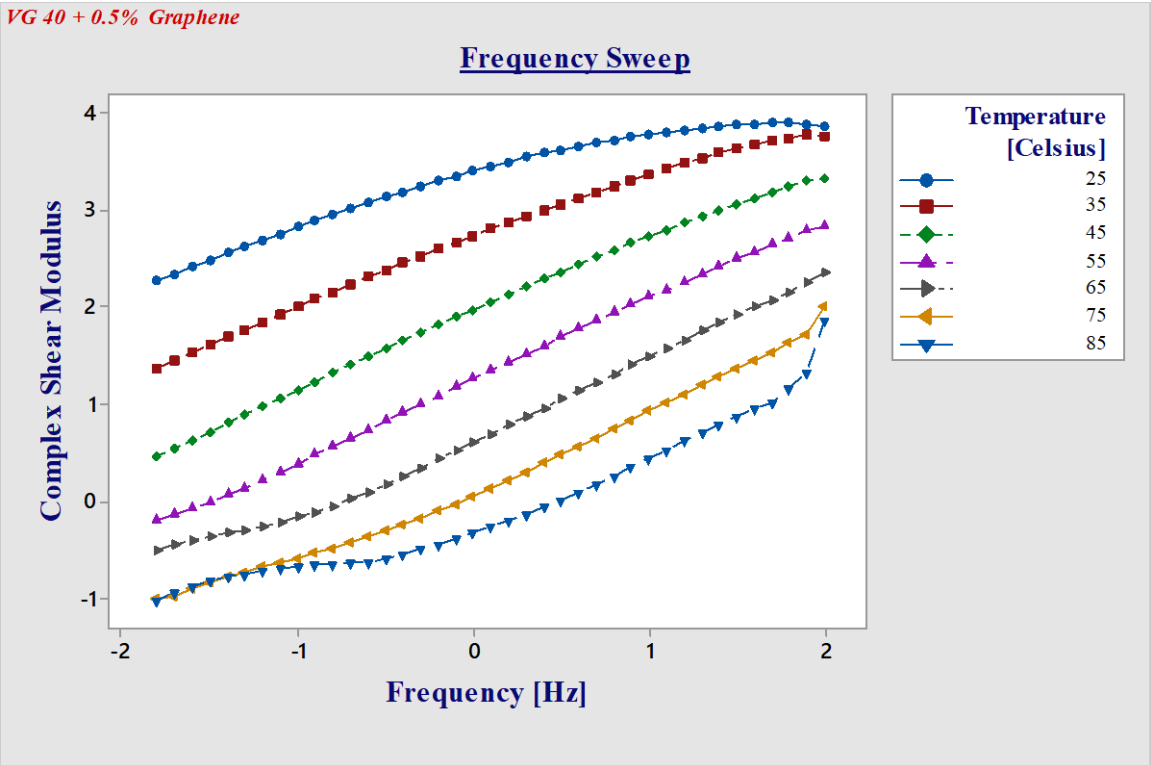

Figure 57 Frequency Sweep VG40 + 0.5% Graphene

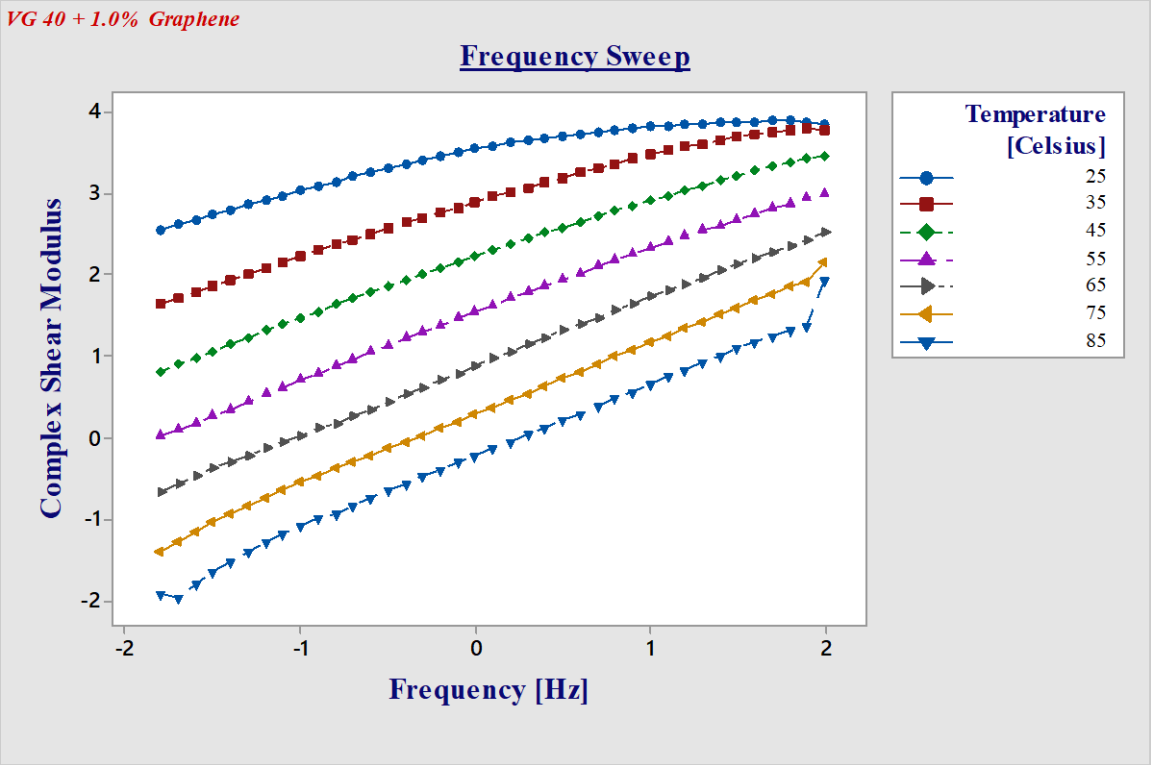

Figure 58 Frequency Sweep VG40 + 1% Graphene

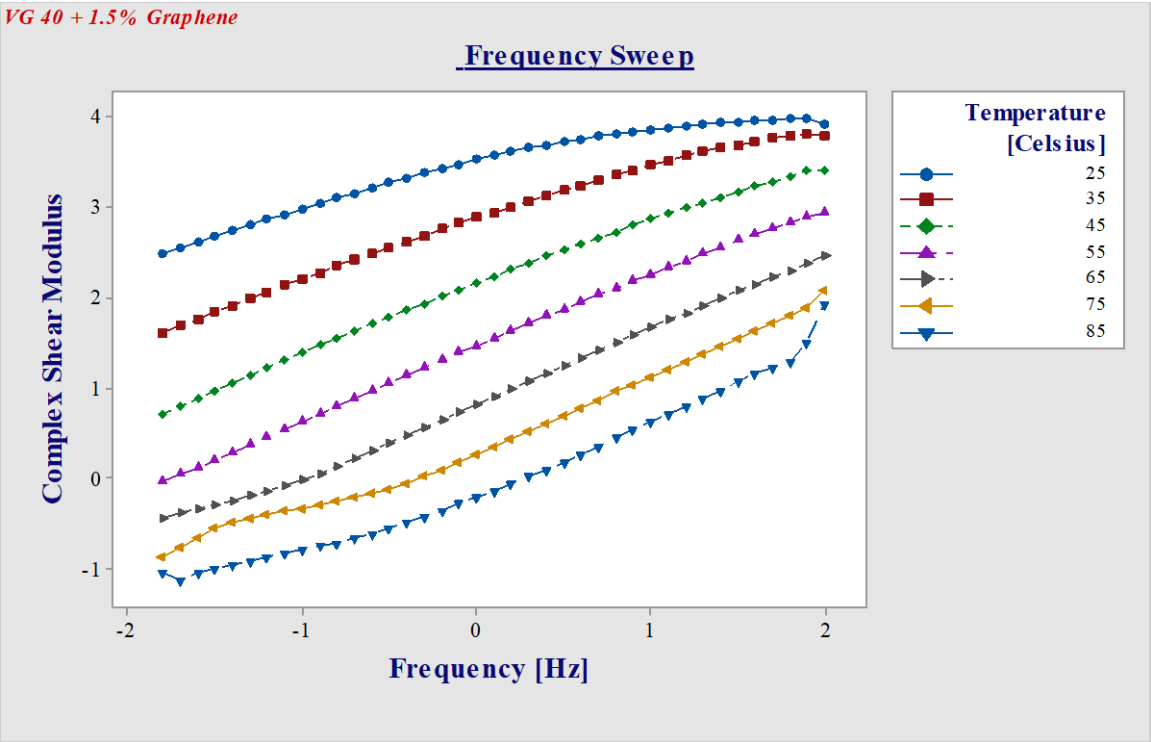

Figure 59 Frequency Sweep VG40 + 1.5% Graphene

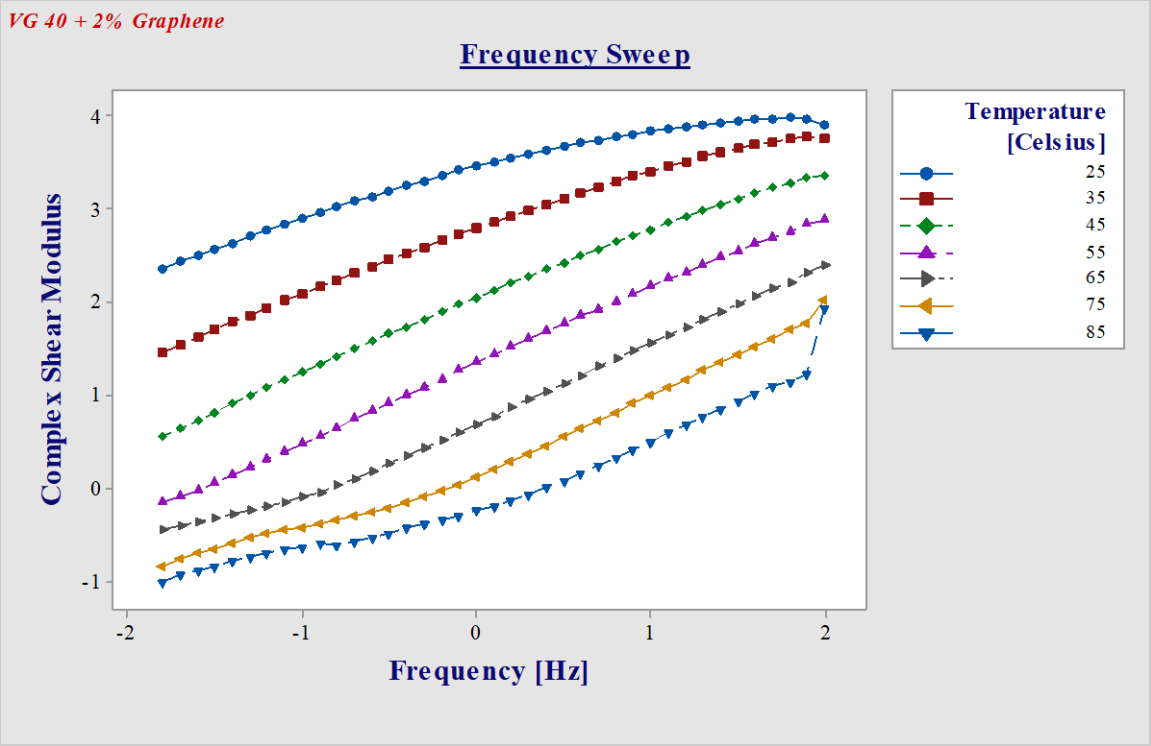

Figure 60 Frequency Sweep VG40 + 2% Graphene

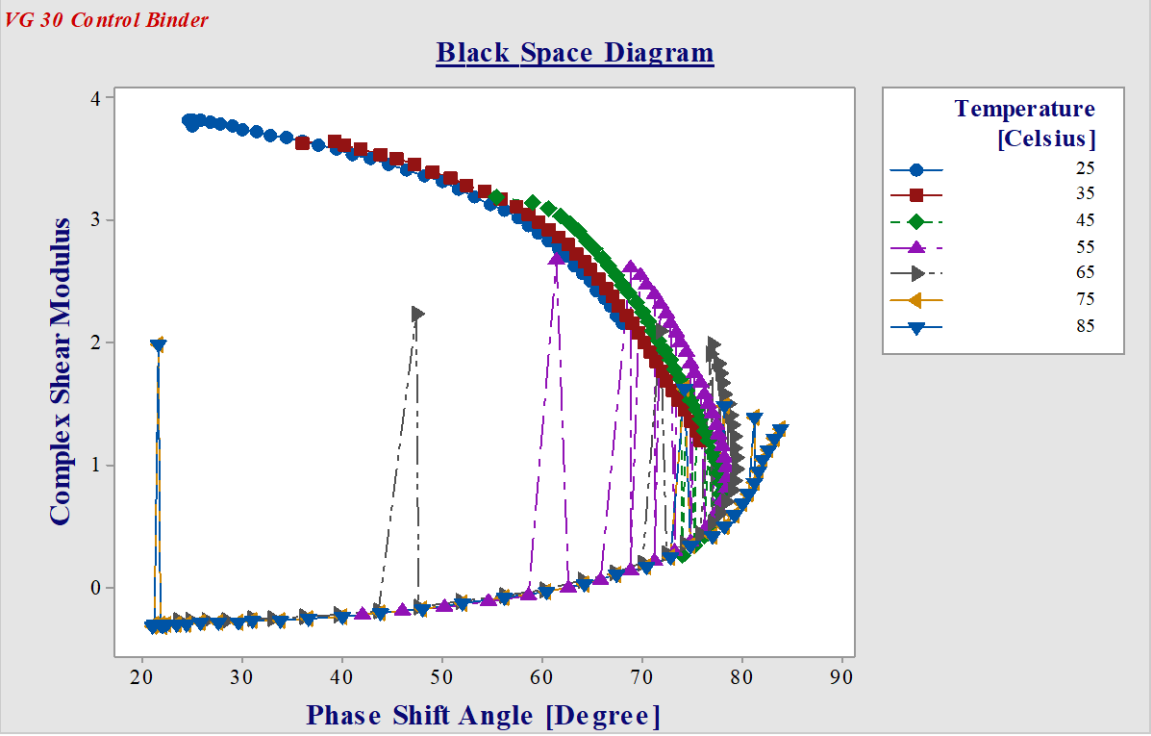

Figure 61 Black Space Diagram VG30

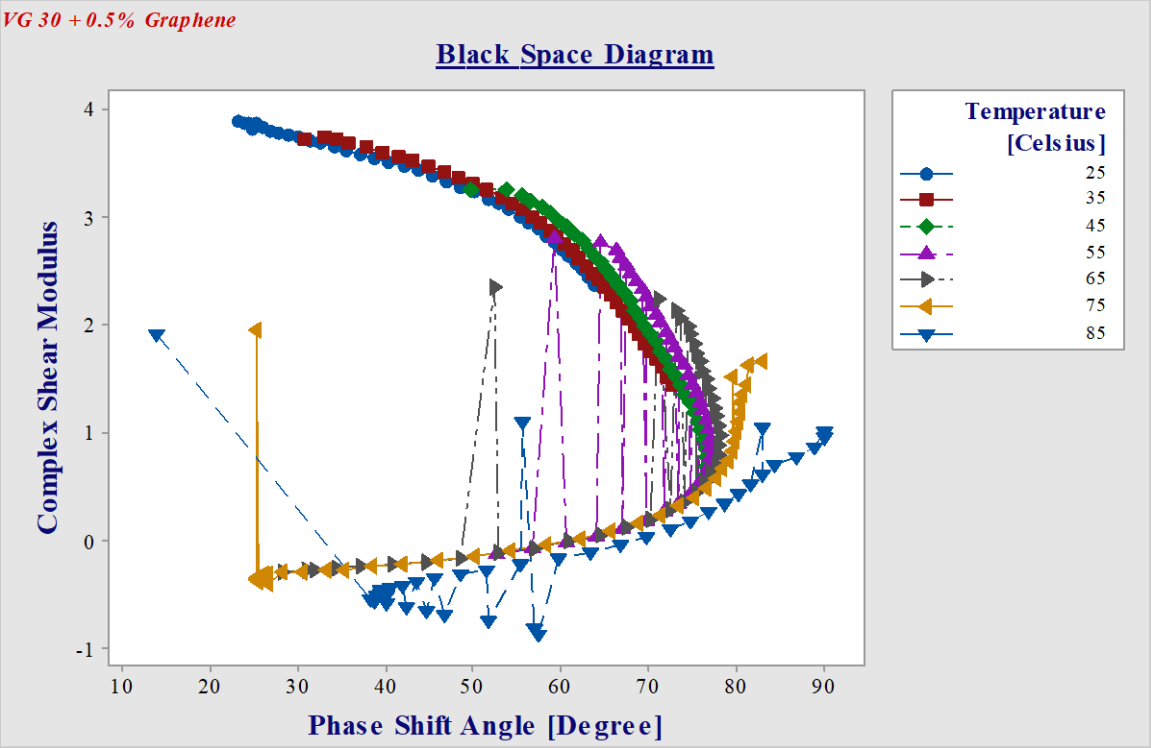

Figure 62 Black Space Diagram VG30 + 0.5% Graphene

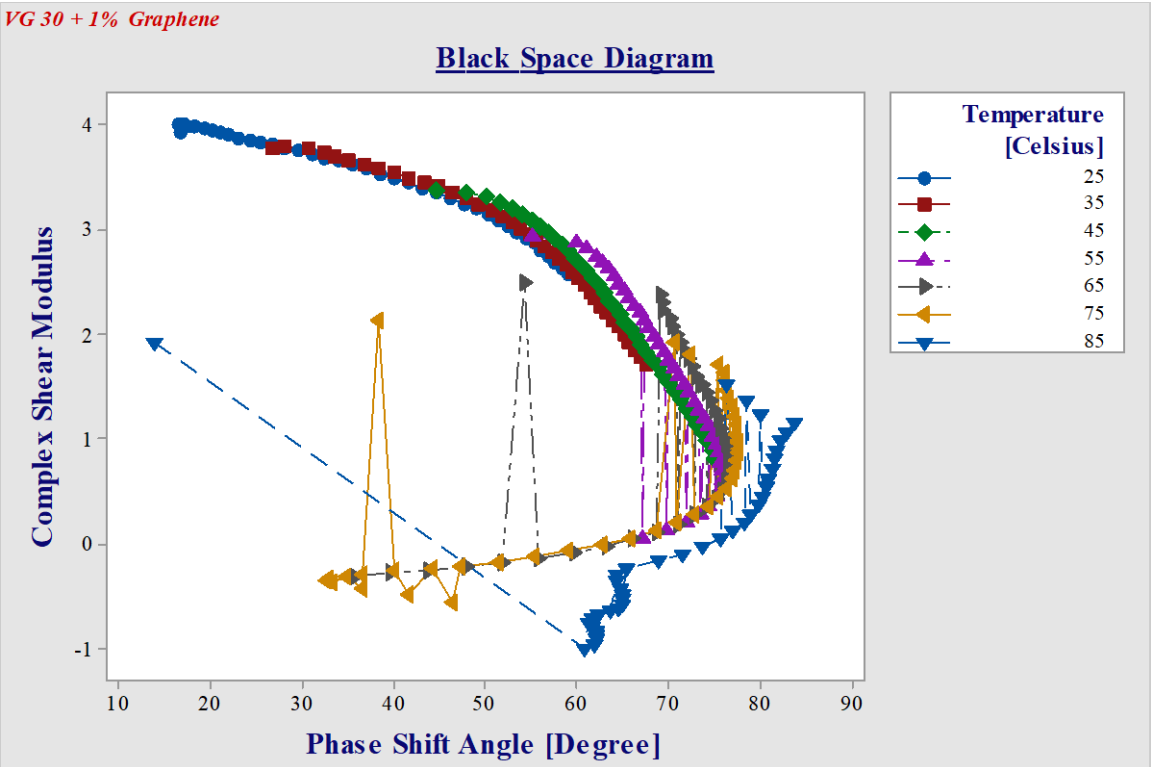

Figure 63 Black Space Diagram VG30 + 1% Graphene

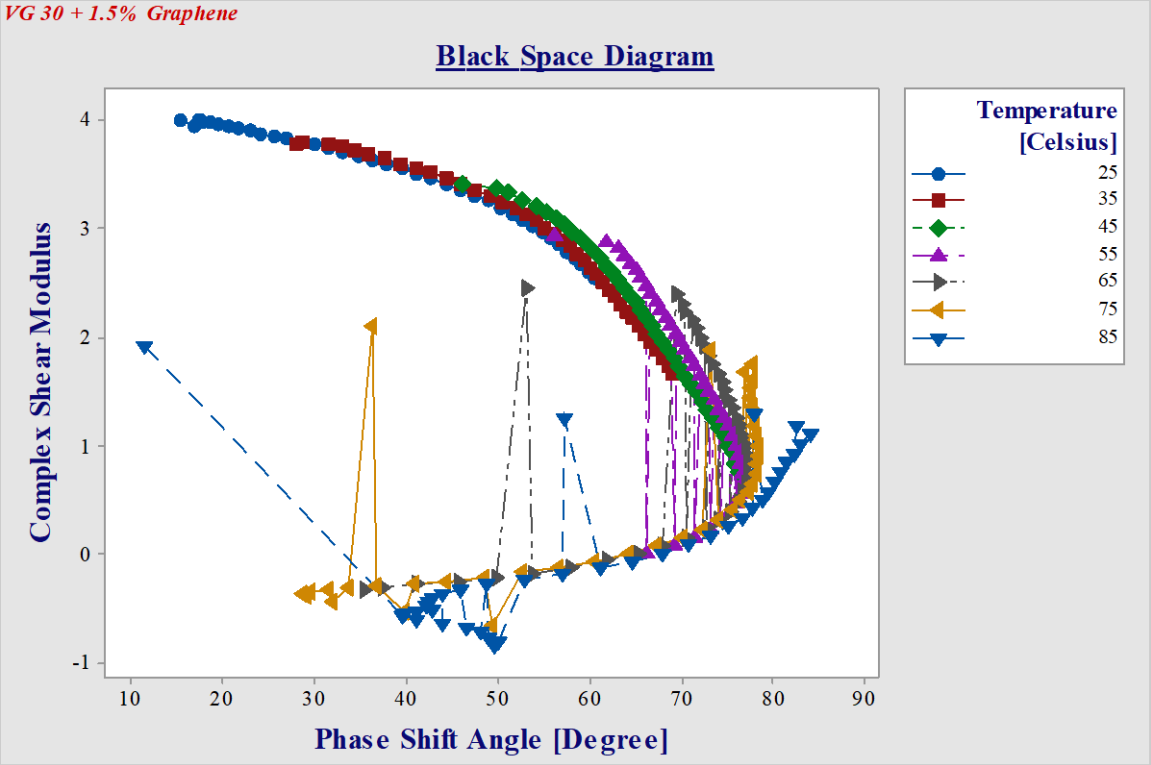

Figure 64 Black Space Diagram VG30 + 1.5% Graphene

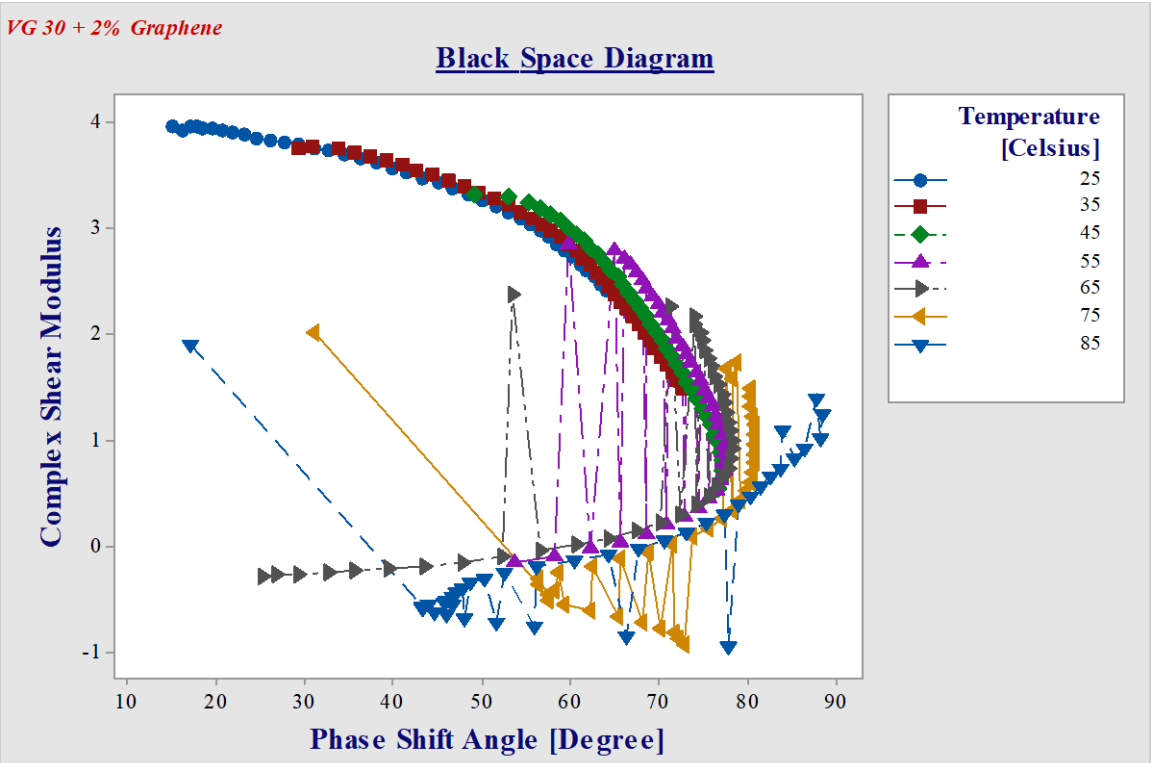

Figure 65 Black Space Diagram VG30 + 2% Graphene

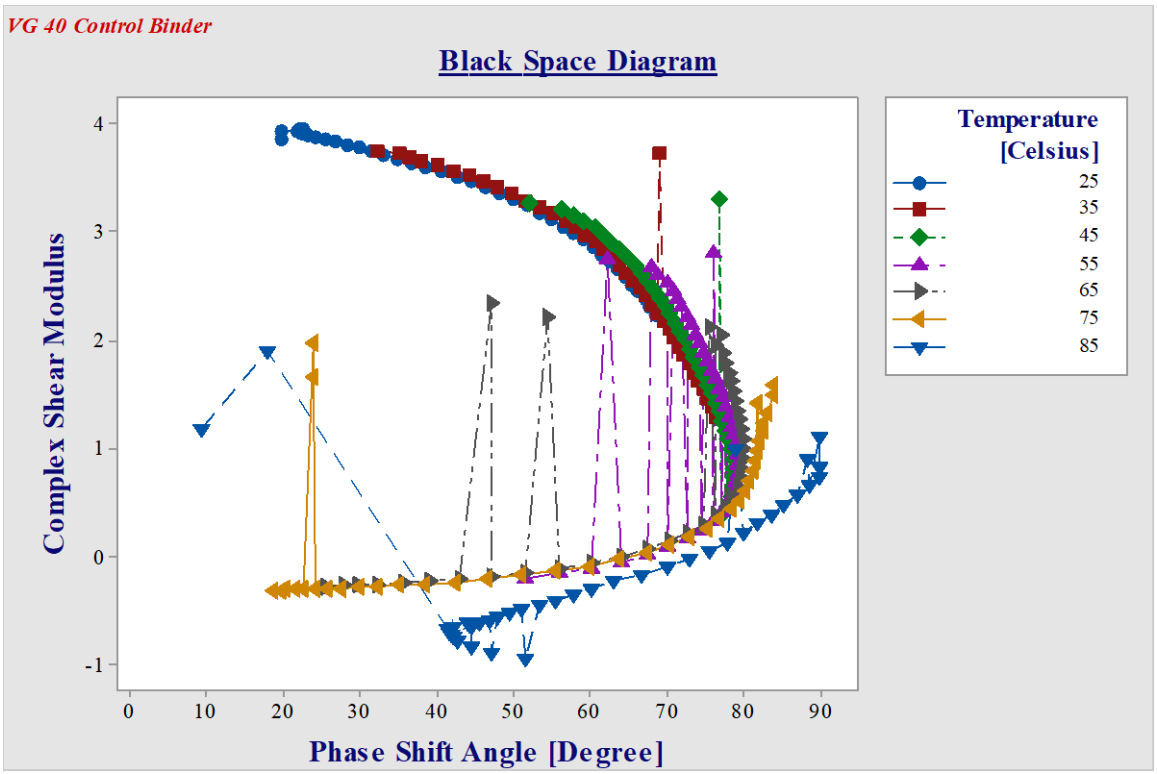

Figure 66 Black Space Diagram VG40

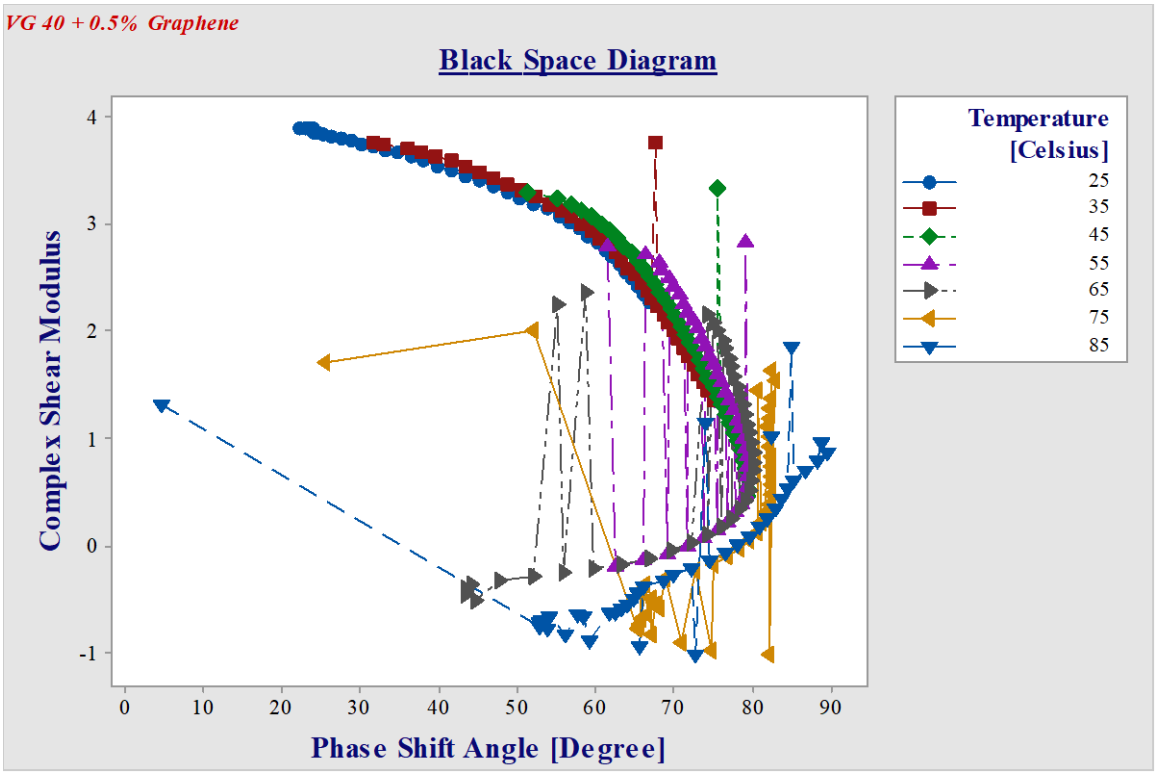

Figure 67 Black Space Diagram VG40 + 0.5% Graphene

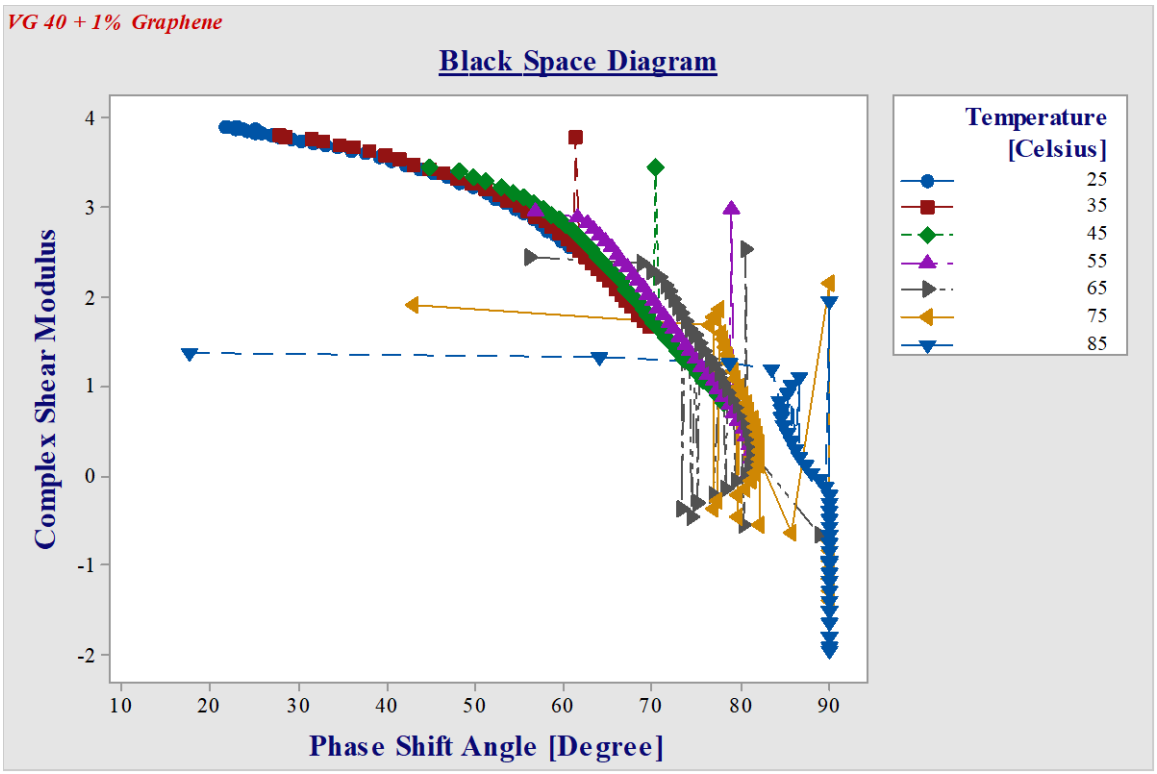

Figure 68 Black Space Diagram VG40 + 1.5% Graphene

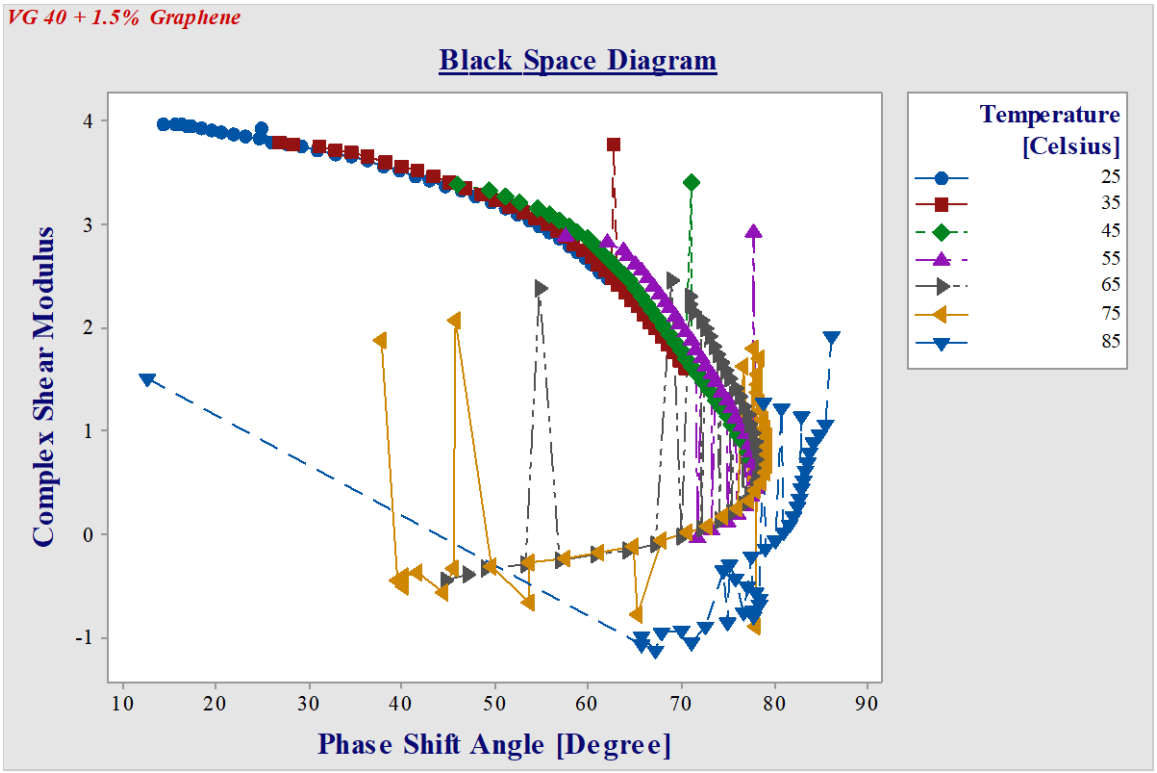

Figure 69 Black Space Diagram VG40 + 1.5% Graphene

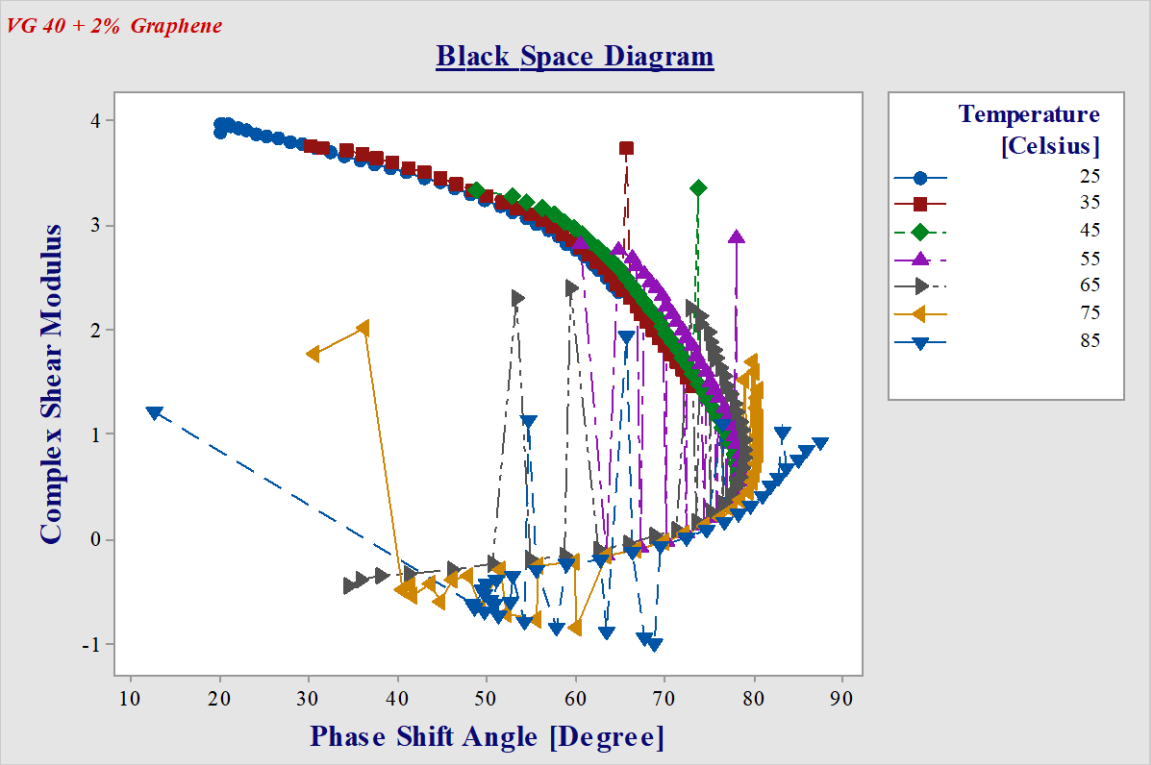

Figure 70 Black Space Diagram VG40 + 2% Graphene

Table 11 Flow Behavior Index VG30

VG30	Temperature	Fitting Equation	n-1	Flow Behavior Index [n]
Control Binder	25	$y = 4.7036x^{-0.105}$	-0.105	0.895
	35	$y = 4.3157x^{-0.068}$	-0.068	0.932
	45	$y = 3.6798x^{-0.051}$	-0.053	0.947
	55	$y = 3.0721x^{-0.04}$	-0.04	0.96
	65	$y = 2.4954x^{-0.033}$	-0.033	0.967
	75	$y = 1.9791x^{-0.034}$	-0.033	0.967
	85	$y = 1.9791x^{-0.039}$	-0.039	0.961
0.5% Graphene	25	$y = 4.7774x^{-0.107}$	-0.107	0.893
	35	$y = 4.4412x^{-0.071}$	-0.071	0.929
	45	$y = 3.834x^{-0.059}$	-0.059	0.941
	55	$y = 3.2519x^{-0.046}$	-0.046	0.954
	65	$y = 2.6661x^{-0.038}$	-0.038	0.962

	75	$y = 2.1177x^{-0.038}$	-0.038	0.962
	85	$y = 1.6508x^{-0.064}$	-0.036	0.964
1.0% Graphene	25	$y = 4.8745x^{-0.103}$	-0.103	0.897
	35	$y = 4.5116x^{-0.078}$	-0.078	0.922
	45	$y = 3.9592x^{-0.066}$	-0.066	0.934
	55	$y = 3.4027x^{-0.055}$	-0.055	0.945
	65	$y = 2.839x^{-0.046}$	-0.046	0.954
	75	$y = 2.3056x^{-0.04}$	-0.04	0.96
	85	$y = 1.8224x^{-0.032}$	-0.032	0.968
1.5% Graphene	25	$y = 4.892x^{-0.104}$	-0.104	0.896
	35	$y = 4.528x^{-0.076}$	-0.076	0.924
	45	$y = 3.9683x^{-0.062}$	-0.06	0.94
	55	$y = 3.3971x^{-0.054}$	-0.05	0.95
	65	$y = 2.8383x^{-0.044}$	-0.044	0.956
	75	$y = 2.2796x^{-0.039}$	-0.039	0.961
	85	$y = 1.7734x^{-0.032}$	-0.032	0.968
2.0% Graphene	25	$y = 4.8542x^{-0.103}$	-0.103	0.897
	35	$y = 4.4735x^{-0.07}$	-0.07	0.93
	45	$y = 3.8661x^{-0.057}$	-0.057	0.943
	55	$y = 3.2727x^{-0.045}$	-0.045	0.955
	65	$y = 2.6871x^{-0.037}$	-0.037	0.963
	75	$y = 2.1455x^{-0.035}$	-0.035	0.965
	85	$y = 1.711x^{-0.031}$	-0.031	0.969

Table 12 Flow Behavior Index VG40

VG40	**Temperature**	**Fitting Equation**	**n-1**	**Flow Behavior Index [n]**
Control Binder	25	$y = 4.8206x^{-0.1}$	-0.1	0.900
	35	$y = 4.43x^{-0.067}$	-0.067	0.933
	45	$y = 3.8226x^{-0.051}$	-0.051	0.949

	55	$y = 3.2132x^{-0.039}$	-0.039	0.961
	65	$y = 2.6212x^{-0.031}$	-0.031	0.969
	75	$y = 2.0816x^{-0.033}$	-0.033	0.967
	85	$y = 1.6222x^{-0.033}$	-0.033	0.967
0.5% Graphene	25	$y = 4.7864x^{-0.103}$	-0.103	0.897
	35	$y = 4.4528x^{-0.067}$	-0.067	0.933
	45	$y = 3.8529x^{-0.053}$	-0.053	0.947
	55	$y = 3.2521x^{-0.041}$	-0.041	0.959
	65	$y = 2.664x^{-0.034}$	-0.034	0.966
	75	$y = 2.1212x^{-0.03}$	-0.03	0.97
	85	$y = 1.6653x^{-0.03}$	-0.03	0.97
1.0% Graphene	25	$y = 4.8245x^{-0.113}$	-0.113	0.887
	35	$y = 4.541x^{-0.075}$	-0.075	0.925
	45	$y = 4.0321x^{-0.061}$	-0.061	0.939
	55	$y = 3.4621x^{-0.051}$	-0.051	0.949
	65	$y = 2.8899x^{-0.041}$	-0.041	0.959
	75	$y = 2.3491x^{-0.033}$	-0.033	0.967
	85	$y = 2.3491x^{-0.033}$	-0.033	0.967
1.5% Graphene	25	$y = 4.8679x^{-0.105}$	-0.105	0.895
	35	$y = 4.5295x^{-0.075}$	-0.075	0.925
	45	$y = 3.9753x^{-0.06}$	-0.06	0.94
	55	$y = 2.8288x^{-0.041}$	-0.041	0.959
	65	$y = 2.8288x^{-0.041}$	-0.041	0.959
	75	$y = 2.3009x^{-0.033}$	-0.033	0.967
	85	$y = 1.8313x^{-0.029}$	-0.029	0.971
2.0% Graphene	25	$y = 4.8476x^{-0.101}$	-0.101	0.899
	35	$y = 4.4746x^{-0.072}$	-0.072	0.928
	45	$y = 3.9009x^{-0.056}$	-0.056	0.944
	55	$y = 3.3106x^{-0.044}$	-0.044	0.956
	65	$y = 2.7249x^{-0.036}$	-0.036	0.964

	75	$y = 2.1794x^{-0.032}$	-0.032	0.968
	85	$y = 2.1794x^{-0.029}$	-0.029	0.971

3.3.1.4.Multiple Stress Creep Recovery Test

The MSCR test was carried out to observe the recovery behavior and the permanent deformation of the binder. Figures 71 and 72 graphically represent the MSCR test for 10 cycles at 65℃, the plot clearly shows that 1% graphene dosage shows the least strain generated and control binder containing the highest level of creep for the same stresses applied to the sample. The 10 cycles for each stress level accounted for 800 s and 8000 data points which is marginal to the 30 cycle test with 2400 s and a total of 24000 data points for each trial. Figures 73 and 74 illustrate verifies the 10 cycle test results that 1 % dosage tends to undergo least amount of strain. 30 cycle test was carried in order to check the repeatability of the test with relation to the application of stress to time. Tables 23 and 24 give the coefficient of variation in R% and Jnr between cycle 10 and cycle 30.

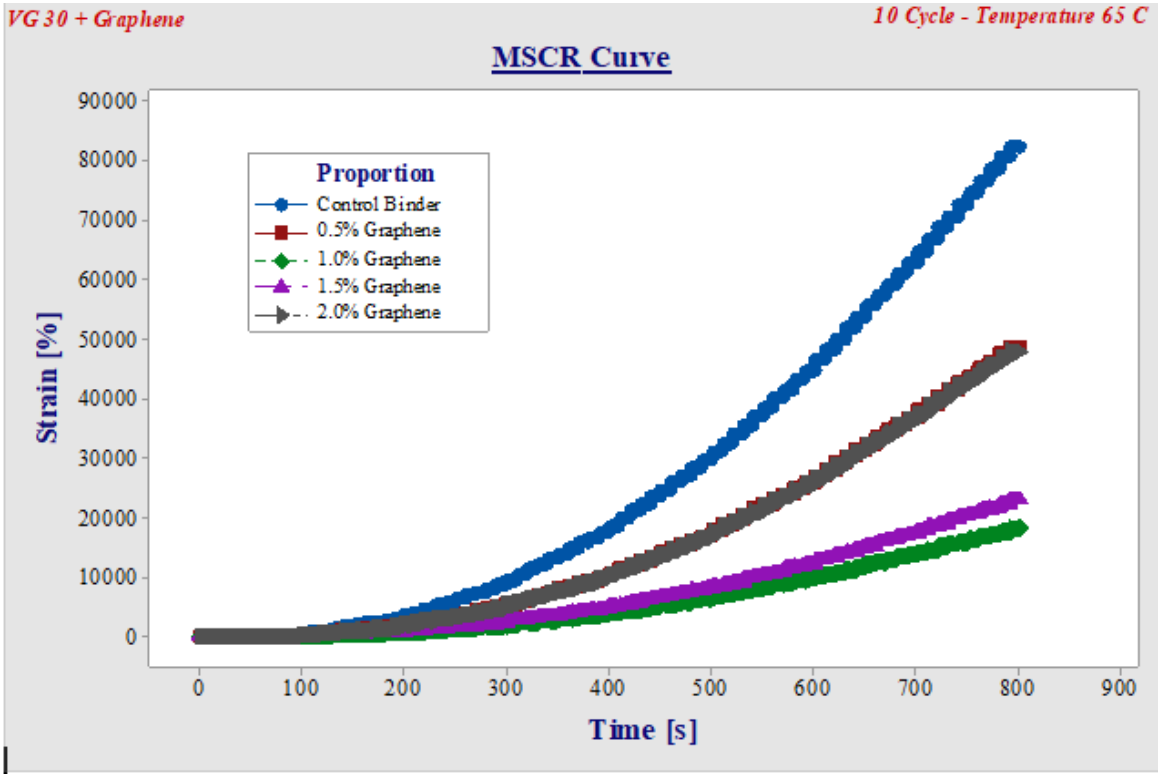

Figure 71 MSCR Curve VG30 Cycle - 10

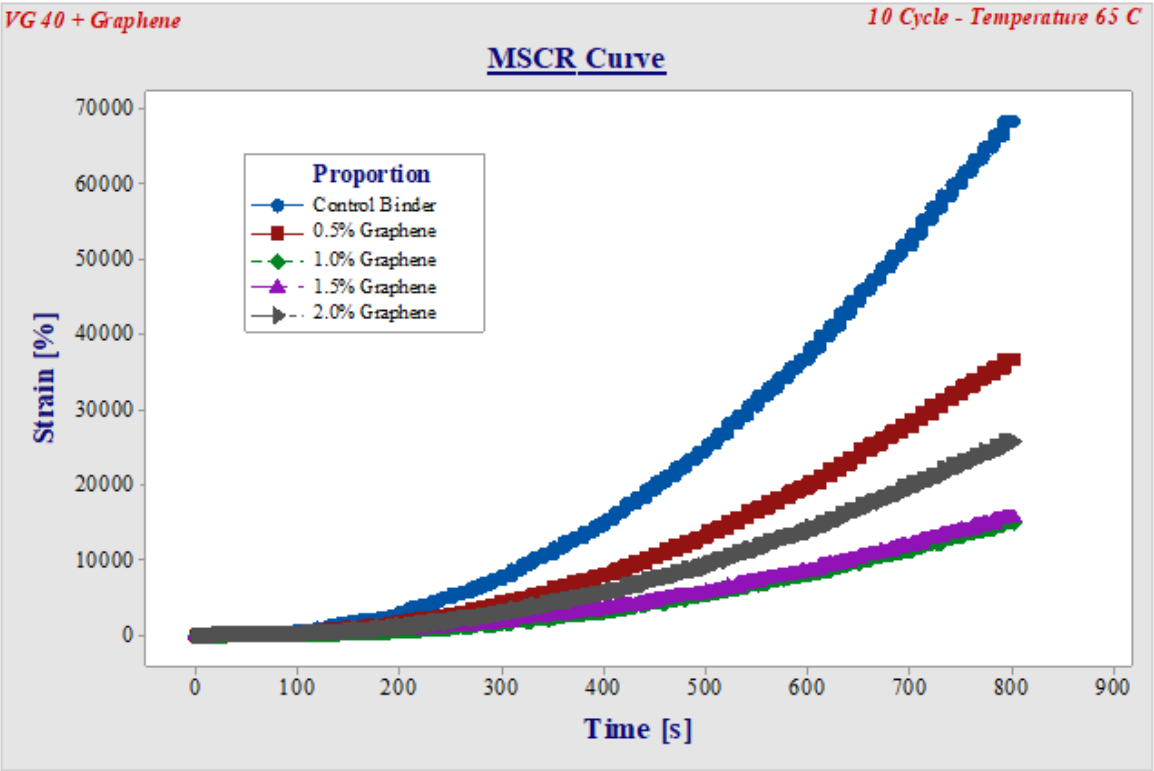

Figure 72 MSCR Curve VG40 Cycle - 10

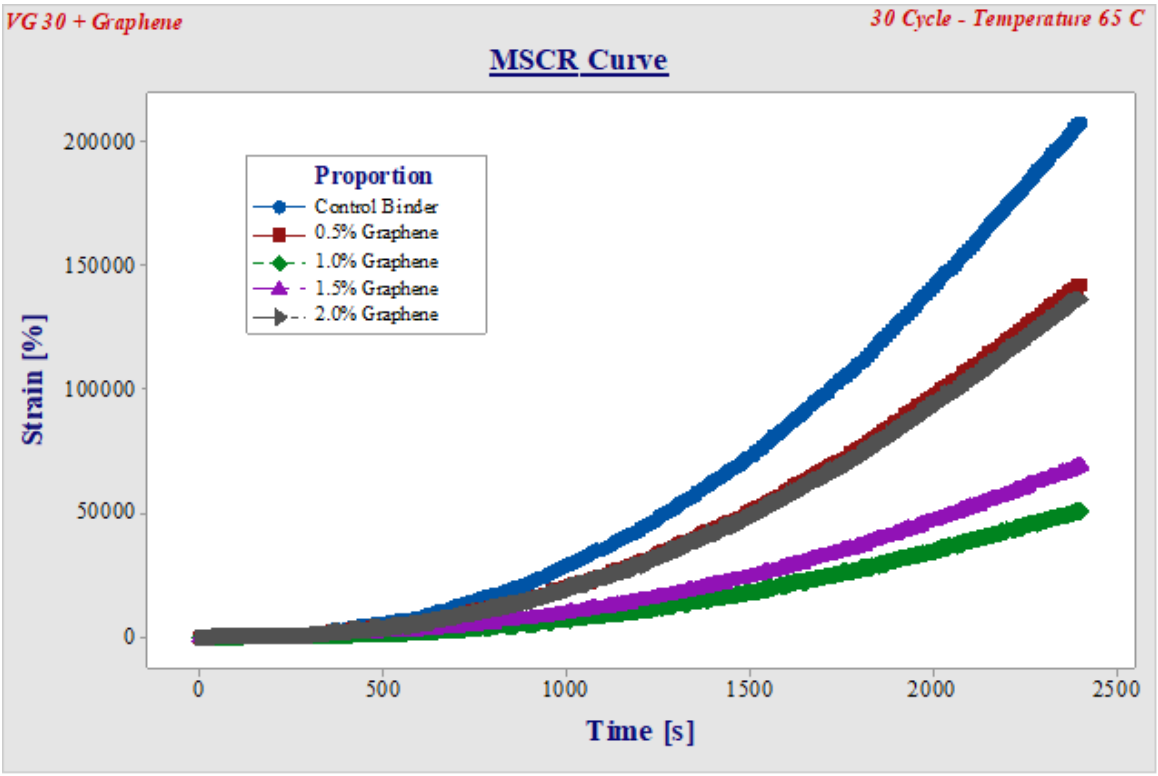

Figure 73 MSCR Curve VG30 Cycle - 30

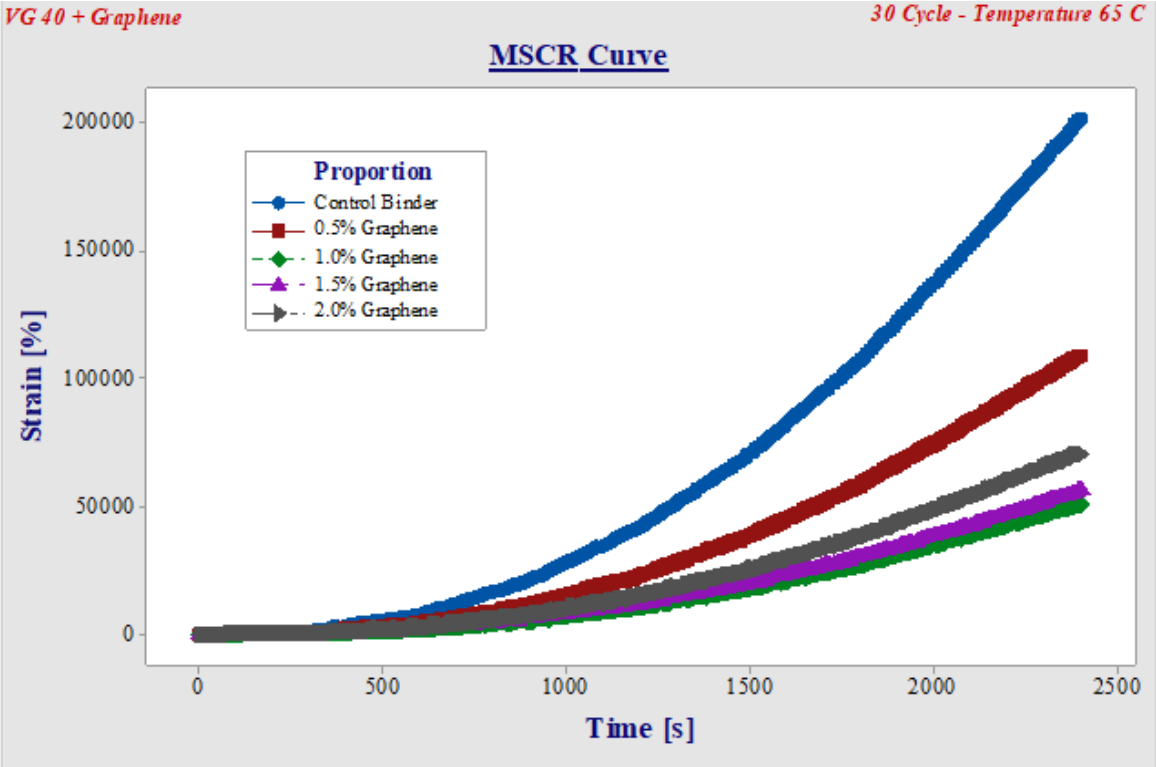

Figure 74 MSCR Curve VG40 Cycle – 30

Figures 75 – 78 illustrate the recovery percentage of the binder for 10 cycle and 30 cycle test, in these plots negative recovery of the binder could be observed which would be attributed to the delay in signal processing of the DSR (Vissche et al. 2016) (Soenena et al. 2013). Figure 75 represents the recovery percentage for VG30 - 10 cycle test showcasing the negative recovery of control binder beyond 0.1 kPa, also negative recovery could be observed for 0.5% and 2% dosages beyond 1 kPa. The highest recovery percentage was observed for 1% dosage with 14.42% at 0.1 kPa and steeply plummeting to 5.18% at 0.5 kPa and then progressing gradually declining to 1.58% at 3.2 kPa. Similar fashion is followed by other dosages with 1.5% dosage plummeting from 11.66% to 4.13% at 0.1 kPa and 0.5 kPa respectively, reaching a value of 0.677% at 3.2 kPa.

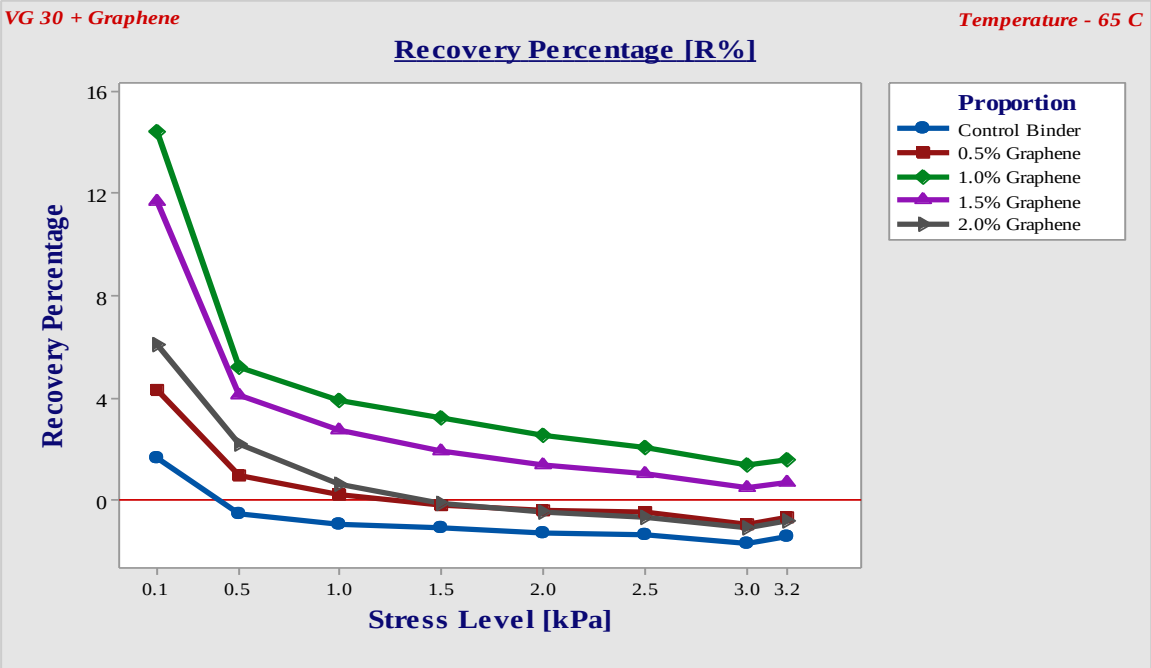

Figure 75 Recovery Percentage Plot VG30 – Cycle 10

Figure 76 illustrates the recovery behavior of the VG40 grade asphalt binder modified with graphene, also the negative recovery was observed for the VG40 sample as well since this effect is due to the electronic error in the machine. The negative recovery is indifferent to the MSCR results and was treated as an erroneous case measure and no correction is available for such an error and was out of the scope and trade of this report. The highest recovery percentage was observed for 1.5% dosage with 16.51% at 0.1 kPa but it plummets to 4.31% at 0.5 kPa with gradually decreasing to 1.48% at 3.2 kPa. Rather than highest value of recovery percentage, 1% dosage decreases in a more controlled fashion from 16.30% at 0.1 kPa to 5.41% at 3.2 kPa representing better recovery percentage than 1.5% dosage irrespective of the higher initial recovery percentage.

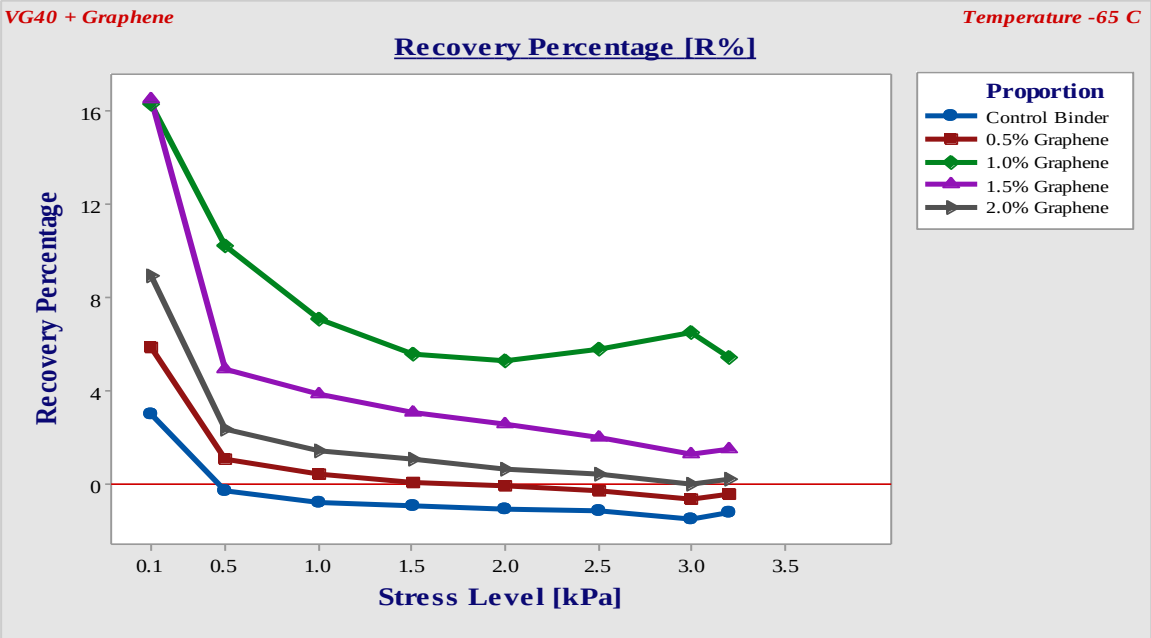

Figure 76 Recovery Percentage Plot VG40 – Cycle 10

Figures 77 and 78 are the graphical representation of the recovery percentage of the VG30 and VG40 asphalt binder for 30 cycle test. The 30 cycle test varies significantly in recovery percentage result with 10 cycle test. Though it follows a similar trend of steep decrease from 0.1 kPa to 0.5 kPa but it varies in the recovery percentage values significantly. The graphene dosage of 1% to VG30 showcases the highest level of recovery percentage 14.24% at 0.1 kPa with steep decline to 5.43% at 1 kPa and gradually decreasing to 1.70% at 3.2 kPa. Apart from 1% dosage only 1.5% dosage doesn't show any negative values. The control binder tends to show very little or insignificant amount of R% of 2.5% and tends to show negative values even before reaching a stress level of 0.5 kPa. 0.5% and 2% dosages were observed to develop a negative value beyond 1.5 kPa after showing a recovery value of 5.77% and 4.97% at 0.1 kPa, respectively. VG40 asphalt binder follows almost an identical trend for cycle 30 as in cycle 10 test, the graphene dosage of 1.5% showcases a maximum value of R% of 15.06% at 0.1 kPa and decreases steeply to 4.16% at 0.5 kPa with gradual decrease to 1.17% at 3.2 kPa. Following closely is 1% dosage which was observed to have a lesser value of around 1% (14.67%) than 1.5% graphene dosage and tends to follow the R% values of 1.5% dosage closely but at higher stress levels and completing at 1.46% at 3.2 kPa.

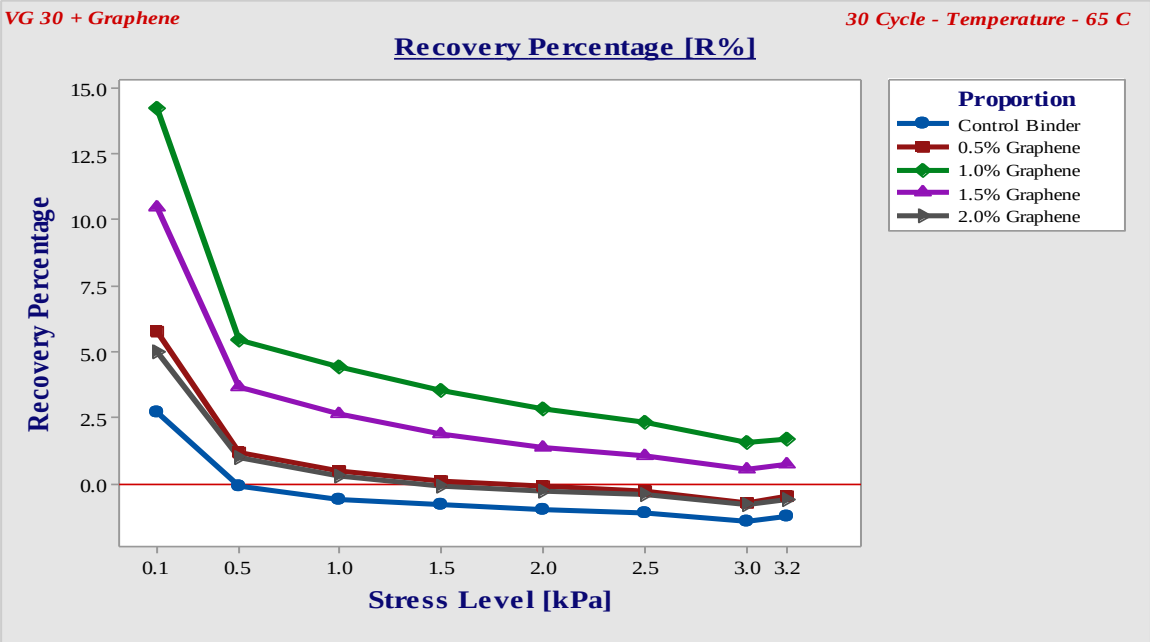

Figure 77 Recovery Percentage Plot VG30 – Cycle 30

The non-recoverable creep compliance Jnr is the measure of permanent deformation of the asphalt binder with the modification of asphalt with graphene the Jnr values tend to enhance thus indication an augmentation in the anti-rut behavior of the asphalt binder.

The Jnr value of the VG30 asphalt binder for cycle 10 test as shown in Figure 78 shows the control binder to have maximum deformation value of 527.37 kPa^{-1} at 3.2 kPa and decreased to its minimum of 120.40 kPa^{-1} at 3.2 kPa for 1% dosage of graphene. There is a 77% decrease in the permanent deformation values by graphene modification. Figure 79 represents the creep compliance value of control binder, 0.5%, 1%, 1.5% and 2% dosages at 3.2 kPa was 457.57 kPa^{-1}, 245.65 kPa^{-1}, 98.40 kPa^{-1}, 104.33 kPa^{-1} and170.85 kPa^{-1}. The Jnr value for VG40 asphalt binder decreased with graphene dosage of 1% at 3.2 kPa was 78.5% less than Jnr value of control binder.

Figures 80 and 81 illustrate the creep compliance behavior of VG30 and VG40 asphalt binder for 30 cycle test. The creep compliance value for VG30 at 3.2 kPa^{-1} was 469 kPa^{-1} , 283 kPa^{-1}, 115 kPa^{-1}, 157 kPa^{-1} and 305 kPa^{-1}. The creep compliance value for VG30 at 3.2 kPa^{-1} was 431 kPa^{-1}, 258 kPa^{-1}, 109 kPa^{-1}, 119 kPa^{-1} and 162 kPa^{-1} for control binder, 0.5%, 1%, 1.5% and 2% dosages respectively.

Figures 82 and 83 illustrate the recovery and Jnr *diff* for VG30 and VG40 for cycle 10 test. The Jnr *diff* should be less than 75% as per AASHTO TP 70. The recovery *diff* for VG30 was observed as 538.95%, 116.02%, 88.86%, 94.15% and 112.87% for control binder, 0.5%, 1%, 1.5 and 2% graphene additive. The Jnr *diff* value for VG40 was 543.29%, 42.20%, 48.84%, 49.53% and 57.031% for control binder, 0.5%, 1%, 1.5 and 2% graphene dosages.

Figures 84 and 85 represent recovery and Jnr *diff* for VG30 and VG40 for cycle 30 test. The recovery *diff* for cycle 30 test for VG30 control binder, 0.5%, 1%, 1.5% and 2% were: 144%, 109%, 88%, 93% and for VG40 control binder, 0.5%, 1%, 1.5% and 2% were: 112%, 141%, 107%, 89% and 92% respectively. The Jnr *diff* for cycle 30 test for VG30 and VG40 were: (45%, 44%, 47%, 47% and 45%) and (40%, 45%, 53%, 51% and 46%).

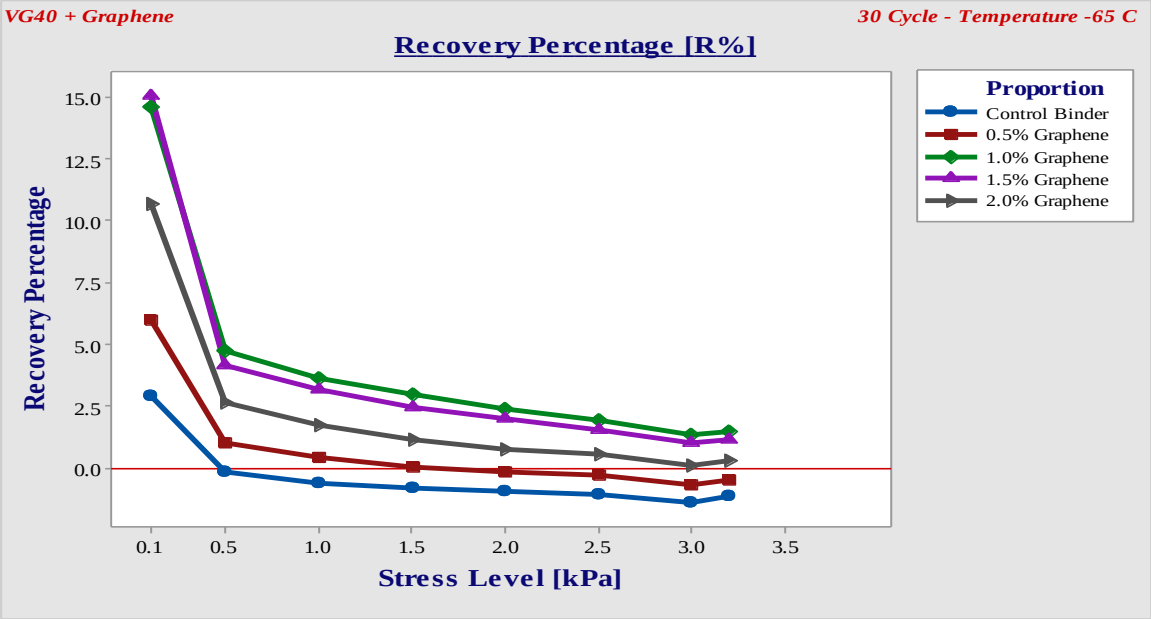

Figure 78 Recovery Percentage Plot VG40 – Cycle 10

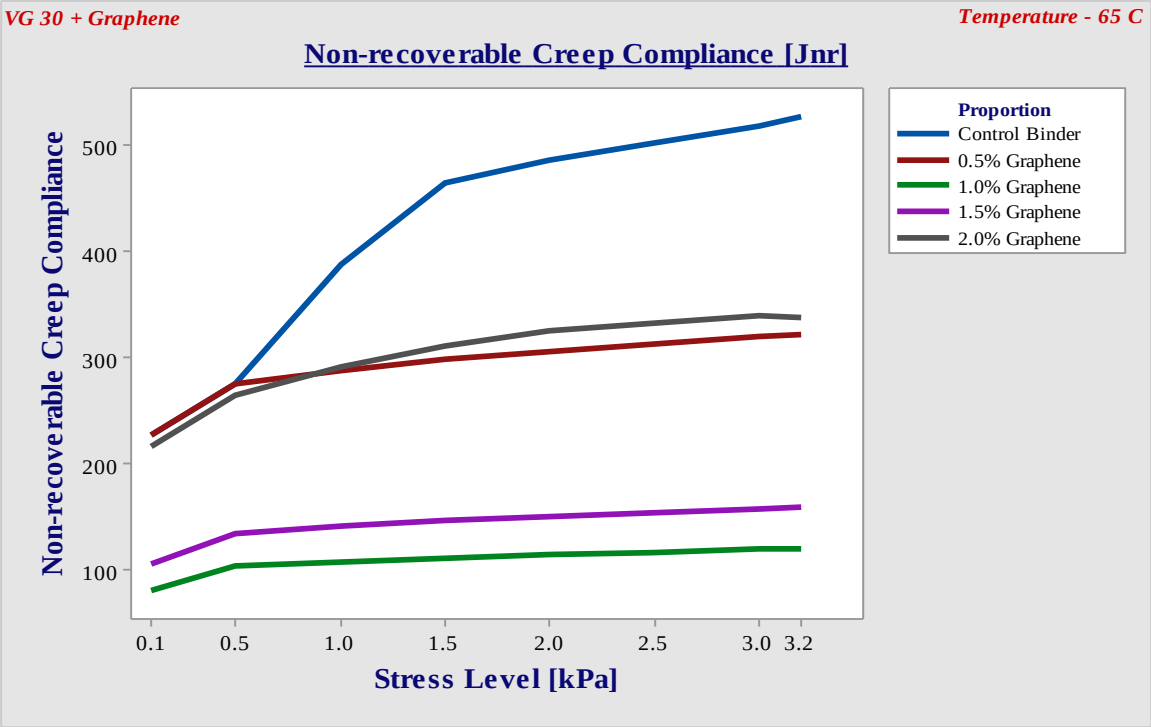

Figure 79 Non – Recoverable Creep Plot VG30 – Cycle 10

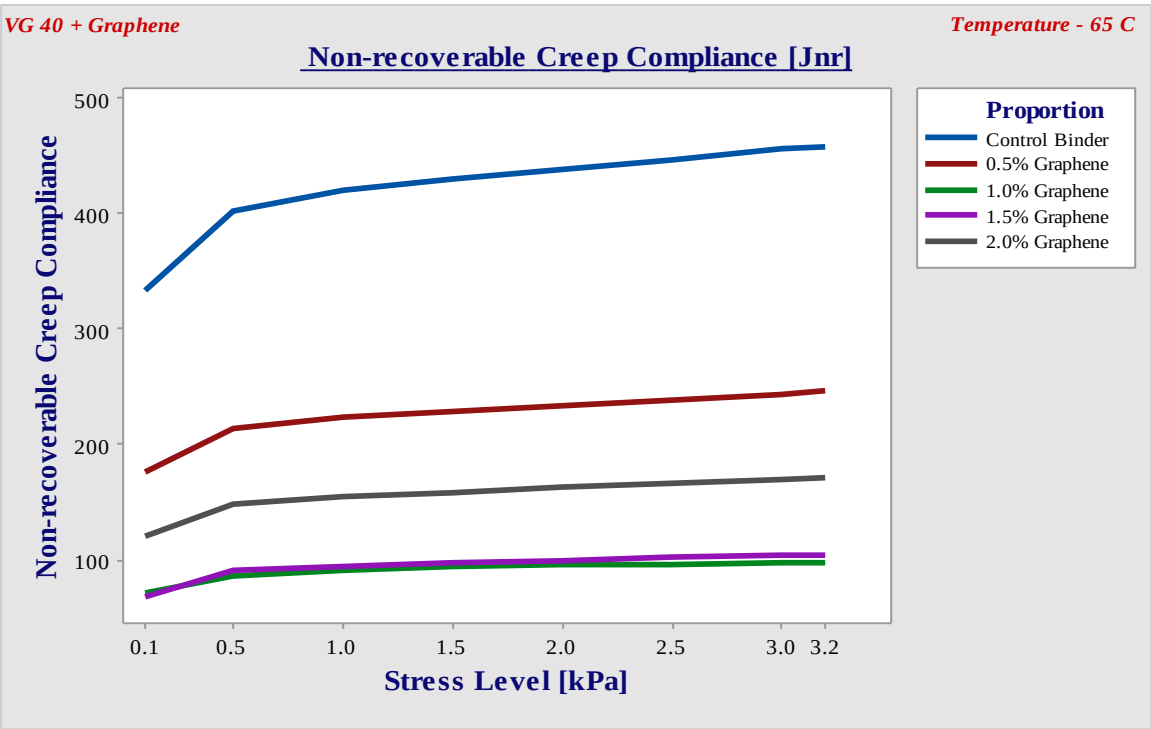

Figure 80 Non – Recoverable Creep Plot VG40 – Cycle 10

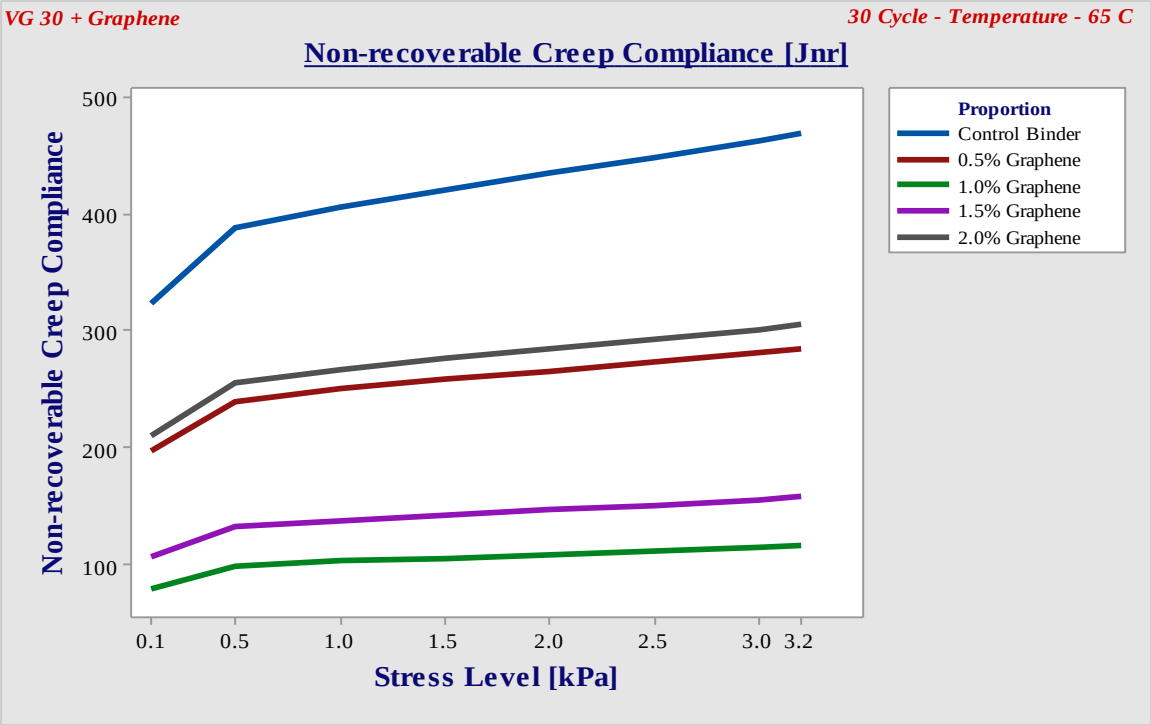

Figure 81 Non – Recoverable Creep Plot VG30 – Cycle 30

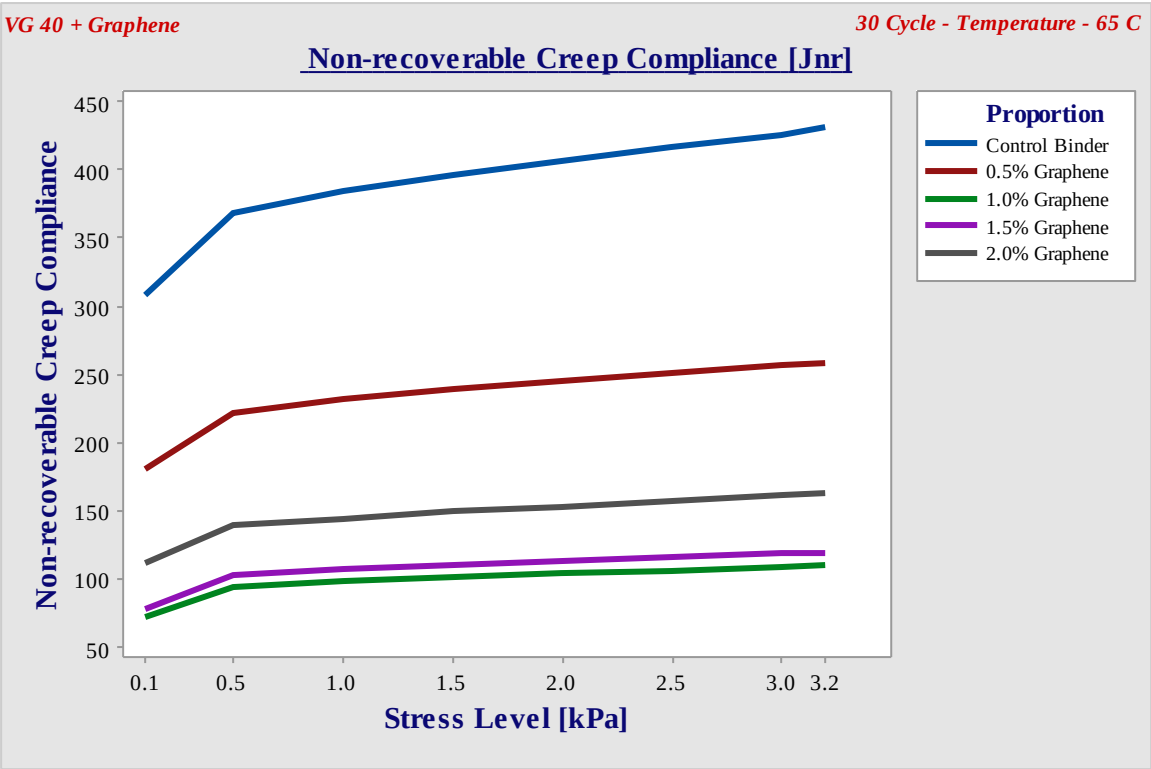

Figure 82 Non – Recoverable Creep Plot VG40 – Cycle 30

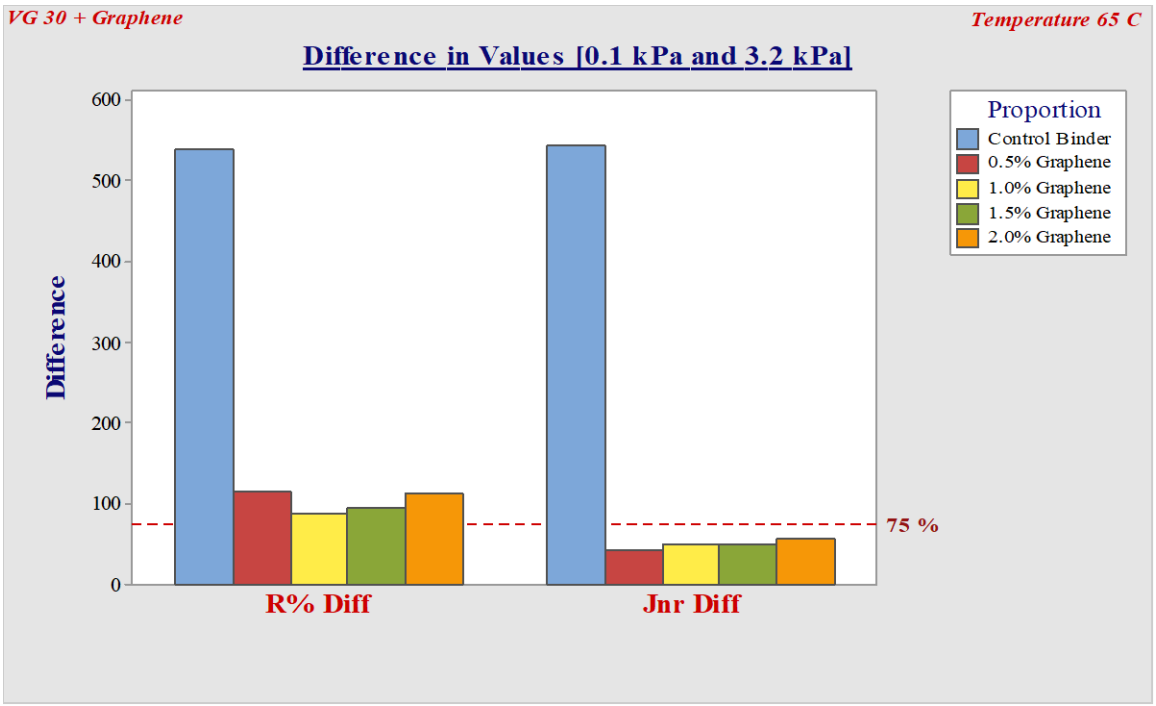

Figure 83 VG30 (Cycle 10) - Recovery Percentage and Non–Recoverable Creep [Jnr] Difference Between [0.1/3.2 kPa]

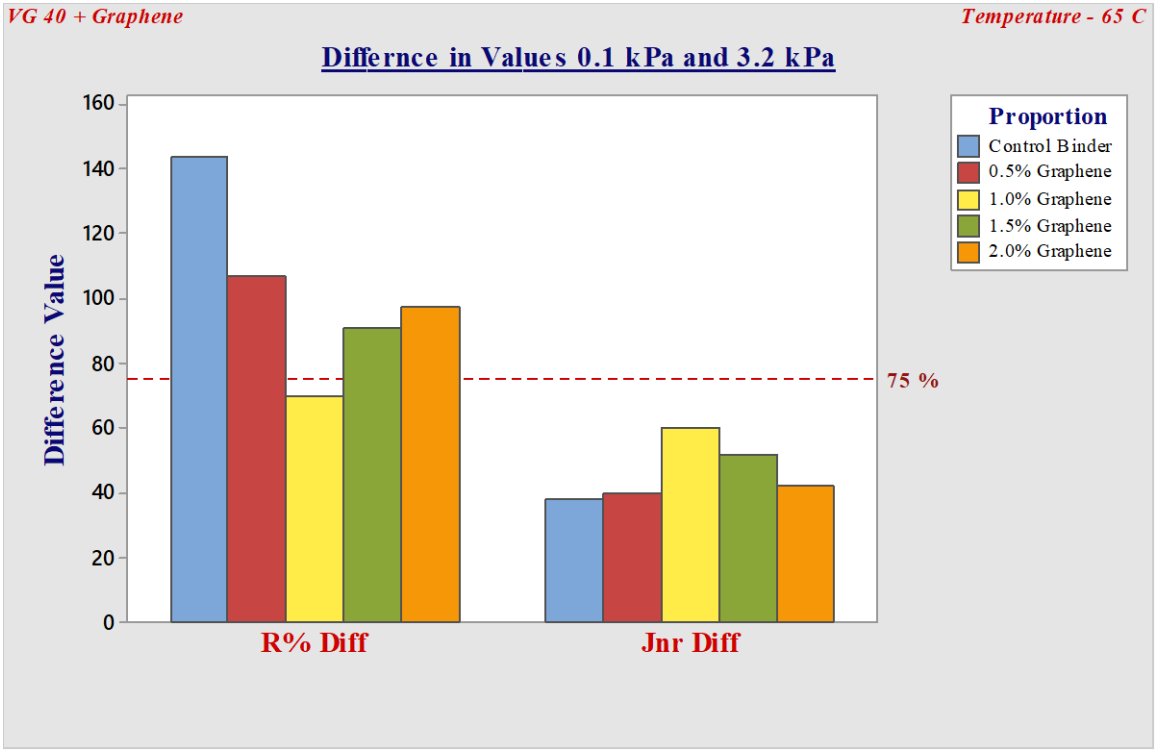

Figure 84 VG40 (Cycle 10) - Recovery Percentage and Non–Recoverable Creep [Jnr] Difference Between [0.1/3.2 kPa]

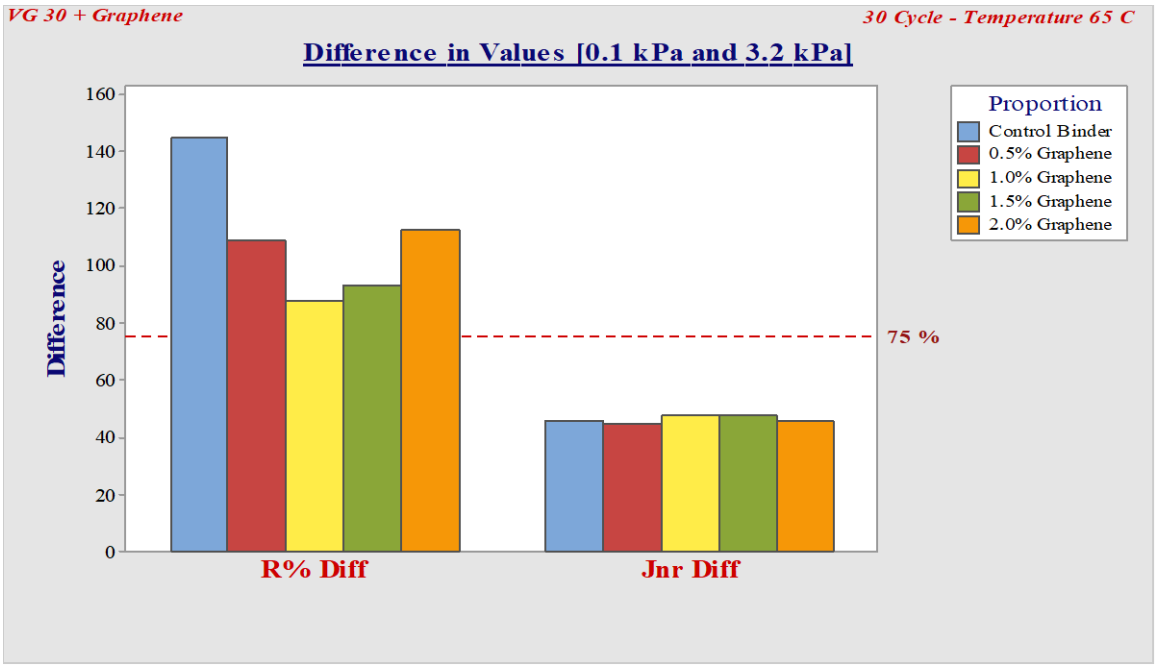

Figure 85 VG30 (Cycle 10) - Recovery Percentage and Non–Recoverable Creep [Jnr] Difference Between [0.1/3.2 kPa]

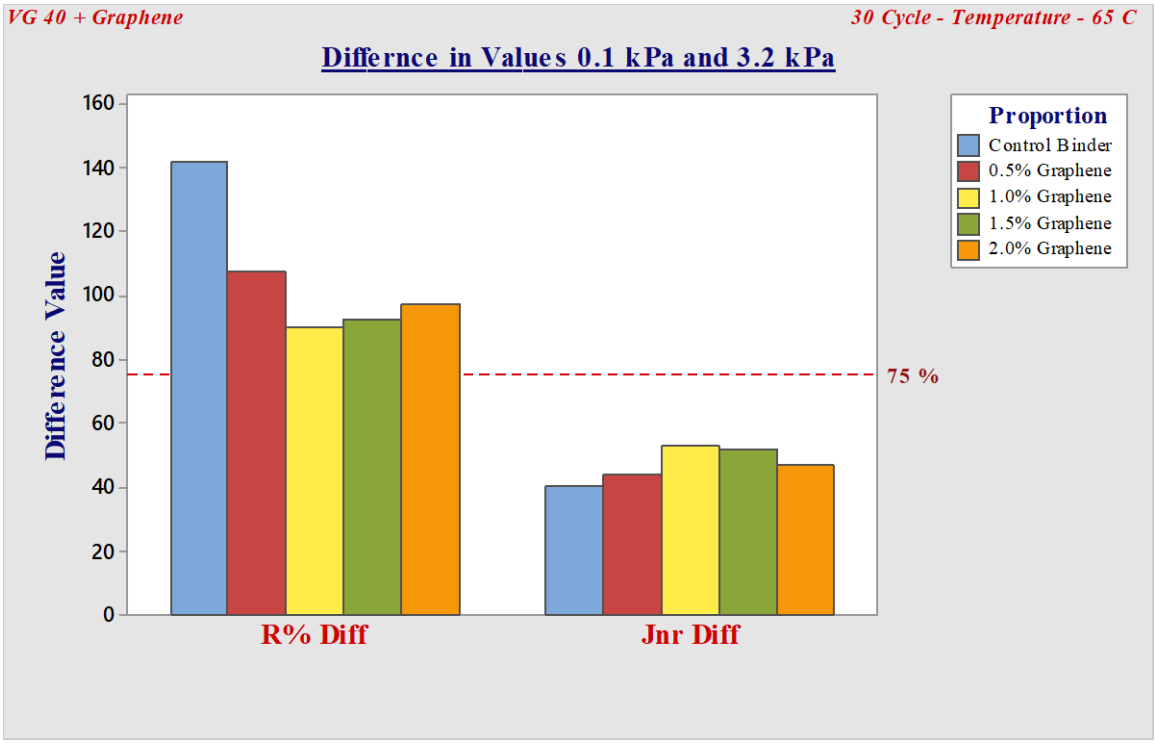

Figure 86 VG40 (Cycle 10) - Recovery Percentage and Non–Recoverable Creep [Jnr] Difference Between [0.1/3.2 kPa]

Figures 87 – 118 shows comparison between control binder and graphene dosages with stress sensitivity in different stress levels (0.1 kPa, 0.5 kPa, 1 kPa, 1.5 kPa, 2 kPa, 2.5 kPa, 3 kPa and 3.2 kPa) stress levels for R% and Jnr for cycle 10 and cycle 30 observed for each cycle. The plots show a wavy curve for 0.1 kPa stress level which signifies the transient strains observed by the DSR due to the low magnitude of the stress.

Figure 87 illustrates comparison between the stress sensitivity for VG30 control binder and 0.5% graphene, the plot shows the difference between observed R% at each cycle. The 0.5% dosage clearly shows augmented results than control binder. Figure 88 shows the comparison of Jnr value between control binder and the 0.5% dosage in each cycle and the plot delineates a clear line between the creep compliance of the two proportions. Figures 89 and 90 represent the comparison of R% and Jnr value between VG30 control binder and VG30 + 1% graphene. The plot illustrates the superiority of 1% graphene additive over the entire 10 cycles. Figure 91 and 92 illustrates the comparison between the R% and Jnr value of control binder and VG30 + 1.5% graphene, there are no negative values for 1.5% dosage in the entire 10 cycles and the R% value decreases with each stress level increase. The difference between the 0.1 kPa and 0.5 kPa shows a stark difference between the R% value and the Jnr values. Figures 93 and 94 show the comparison between control binder and VG30 + 2% graphene for R% and Jnr value in each cycle. Figures 95 and 96 illustrate the difference in the R% and Jnr values of control binder and VG40 + 0.5% graphene. At cycle 6 and cycle 8 the values of R% for control binder and 0.5% graphene tend to coincide, at cycle 9 the value of R% tends to drop lower for 0.5% graphene than control binder, the irregularities at 0.1 kPa are due to inability of the DSR to send back stop signals at appropriate delay time. Figures 97 and 98 illustrates the comparison between control binder and the VG40 + 1% graphene which shows a significant augmentation of R% value and Jnr value from control binder to 1% graphene. Figures 99 and 100 show the comparison between control binder and VG40 + 1.5% graphene for R% and Jnr values for each cycle. Figure 101 and 102 represents the difference in the control binder and VG40 + 2% graphene for R% and Jnr values with R% value as high as 12% and Jnr values below 200 kPa for each stress level and each cycle of 2% dosage. Figures 103 – 118 illustrate the comparison between the stress sensitivity of control binder and graphene dosages for 30 cycle test.

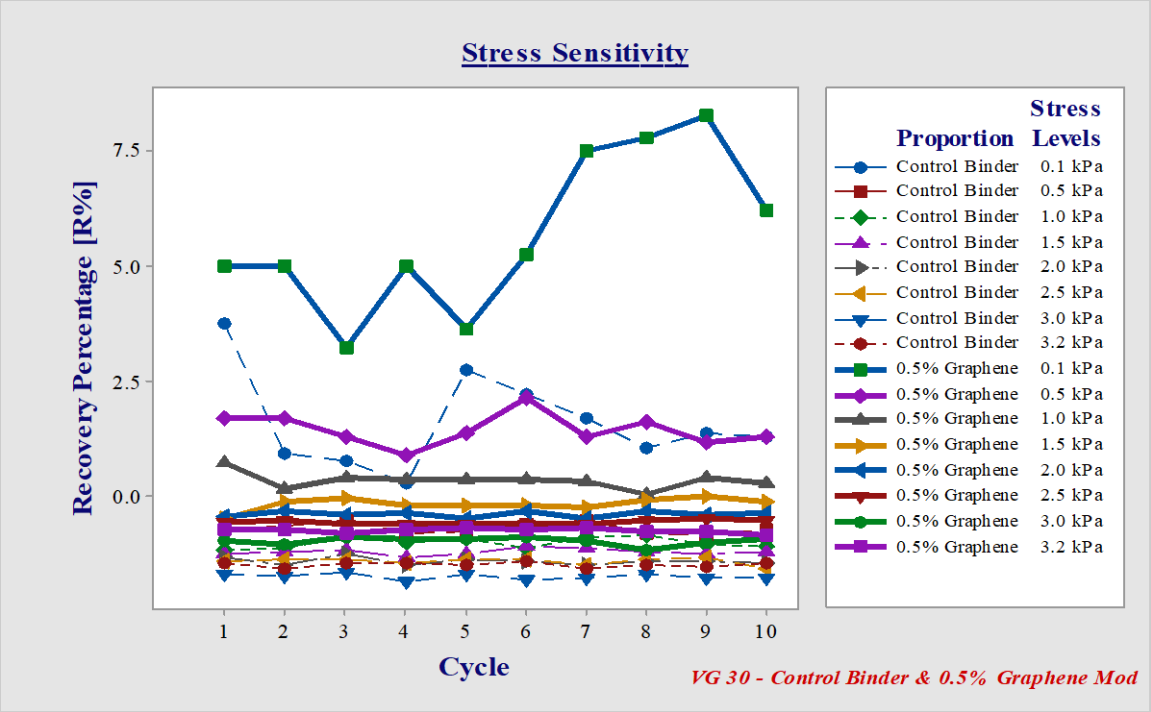

Figure 87 Stress Sensitivity for VG30 – Control Binder and 0.5% Graphene (R%-*Cycle 10)*

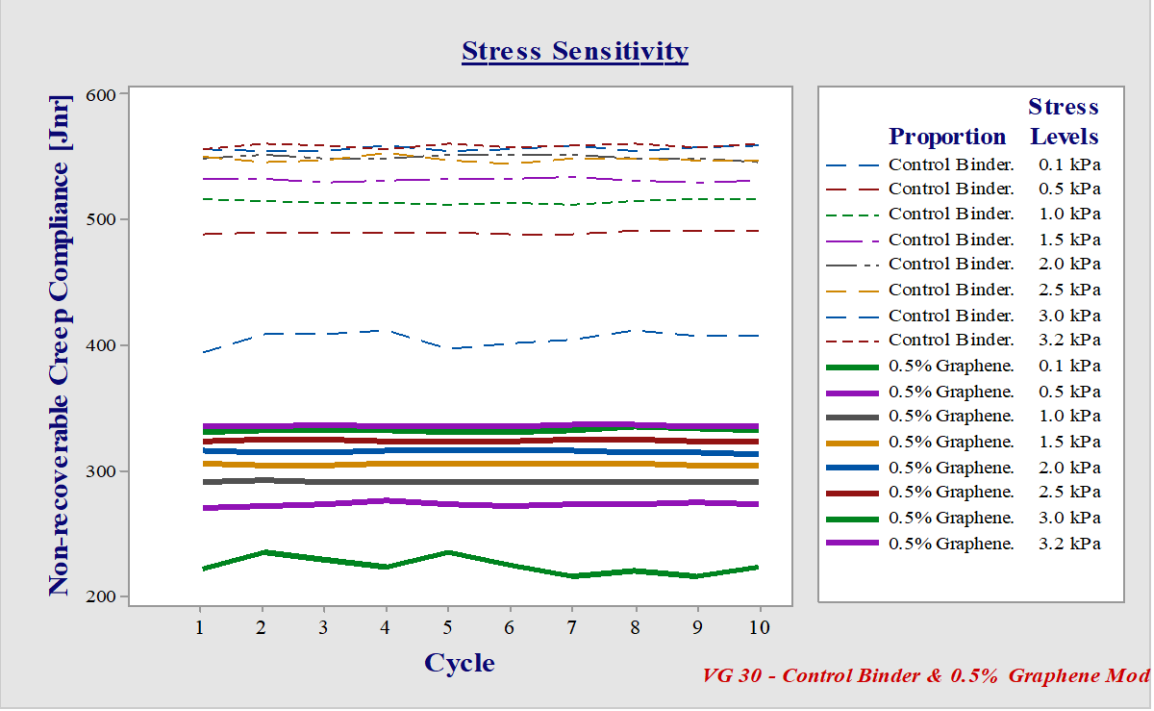

Figure 88 Stress Sensitivity for VG30 – Control Binder and 0.5% Graphene (Jnr-*Cycle 10)*

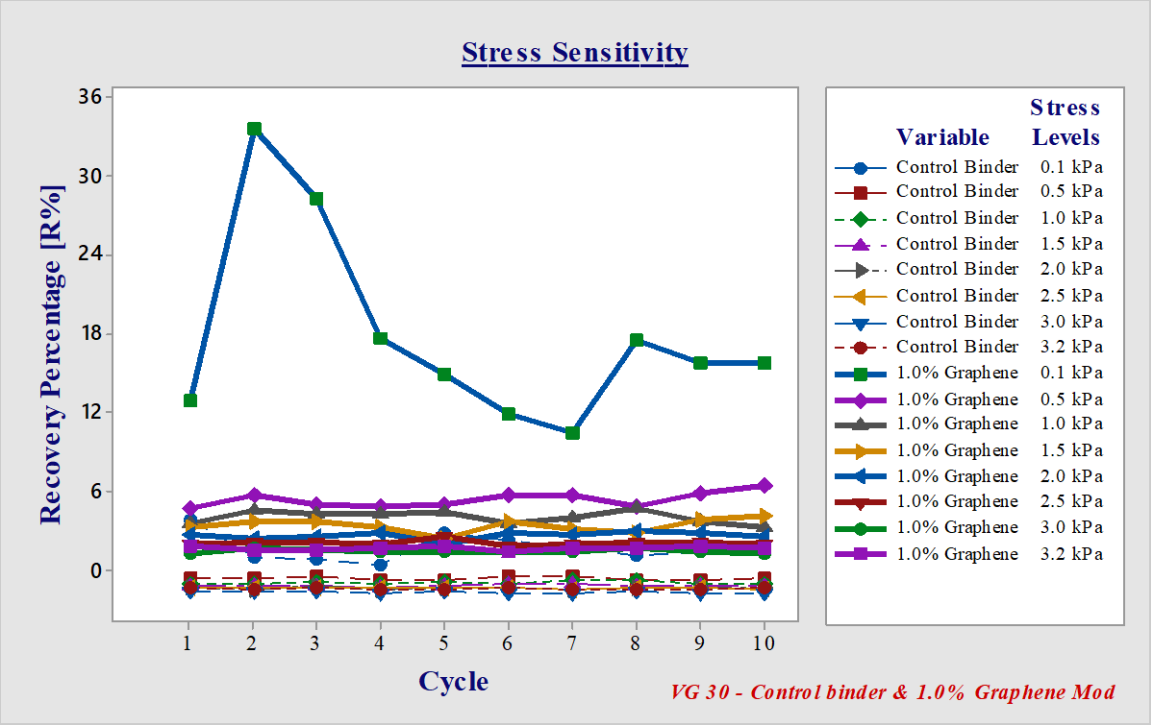

Figure 89 Stress Sensitivity for VG30 – Control Binder and 1% Graphene (R%-*Cycle 10)*

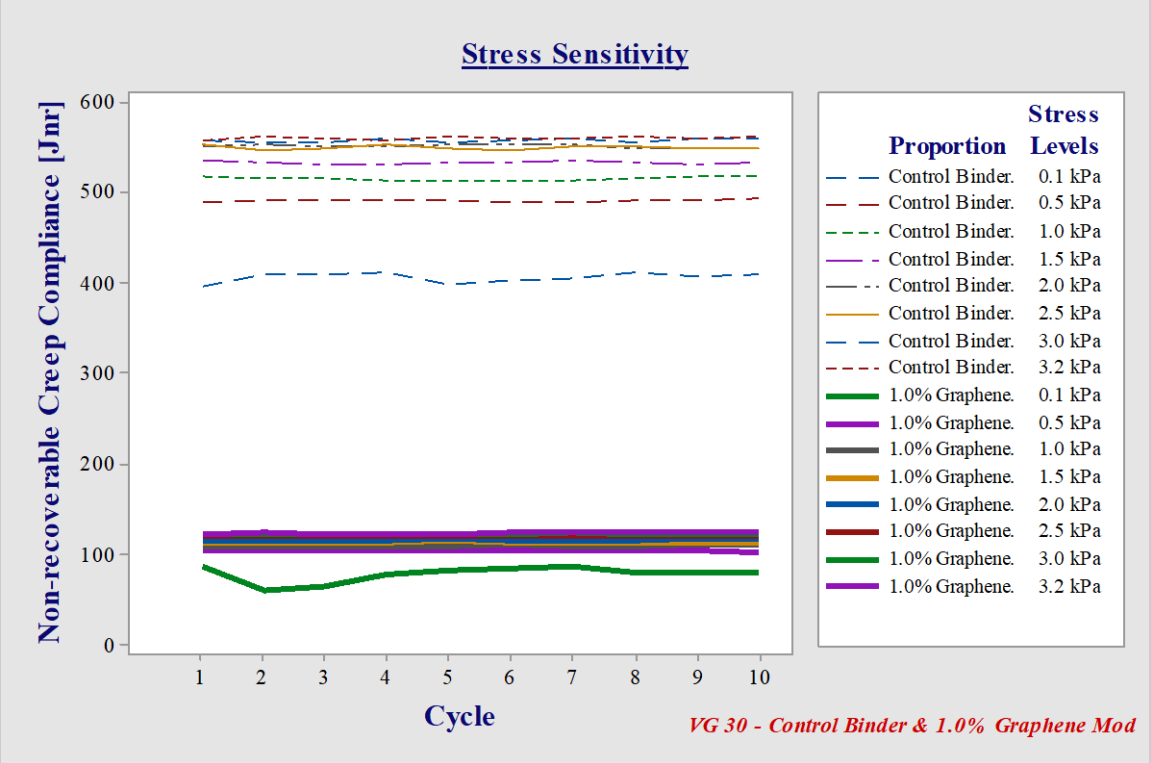

Figure 90 Stress Sensitivity for VG30 – Control Binder and 1% Graphene (Jnr-*Cycle 10)*

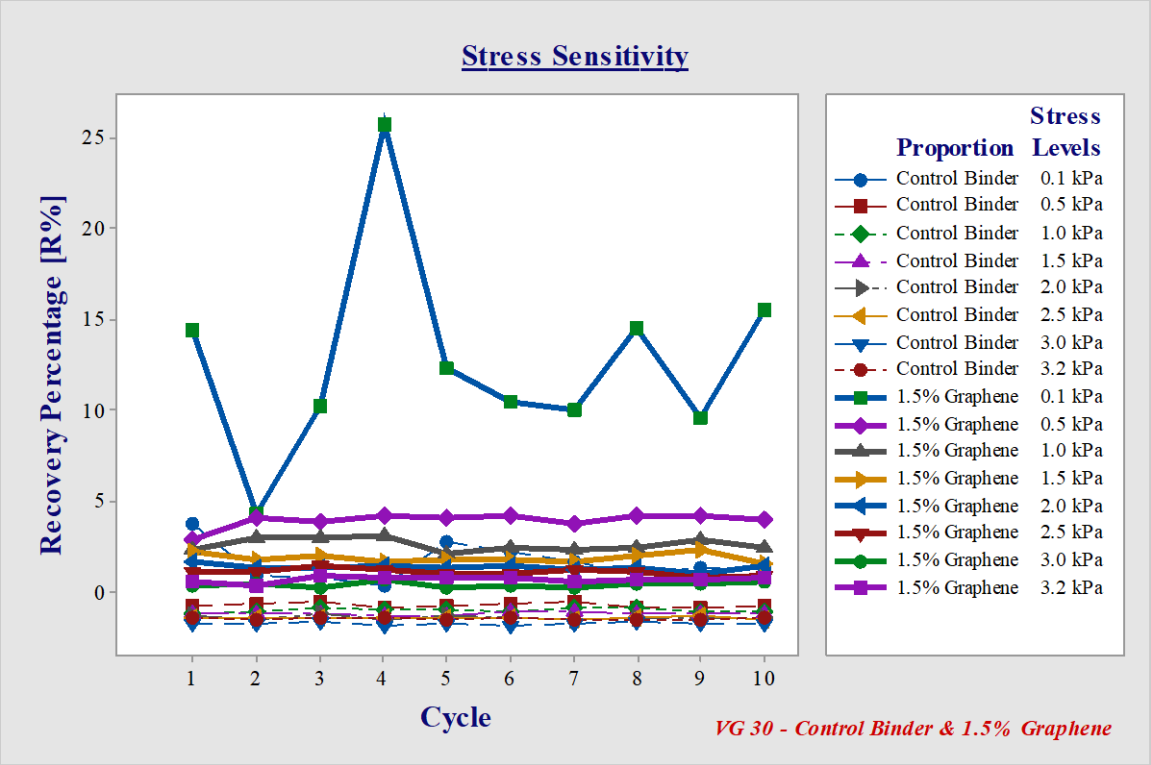

Figure 91 Stress Sensitivity for VG30 – Control Binder and 1.5% Graphene (R%-*Cycle 10)*

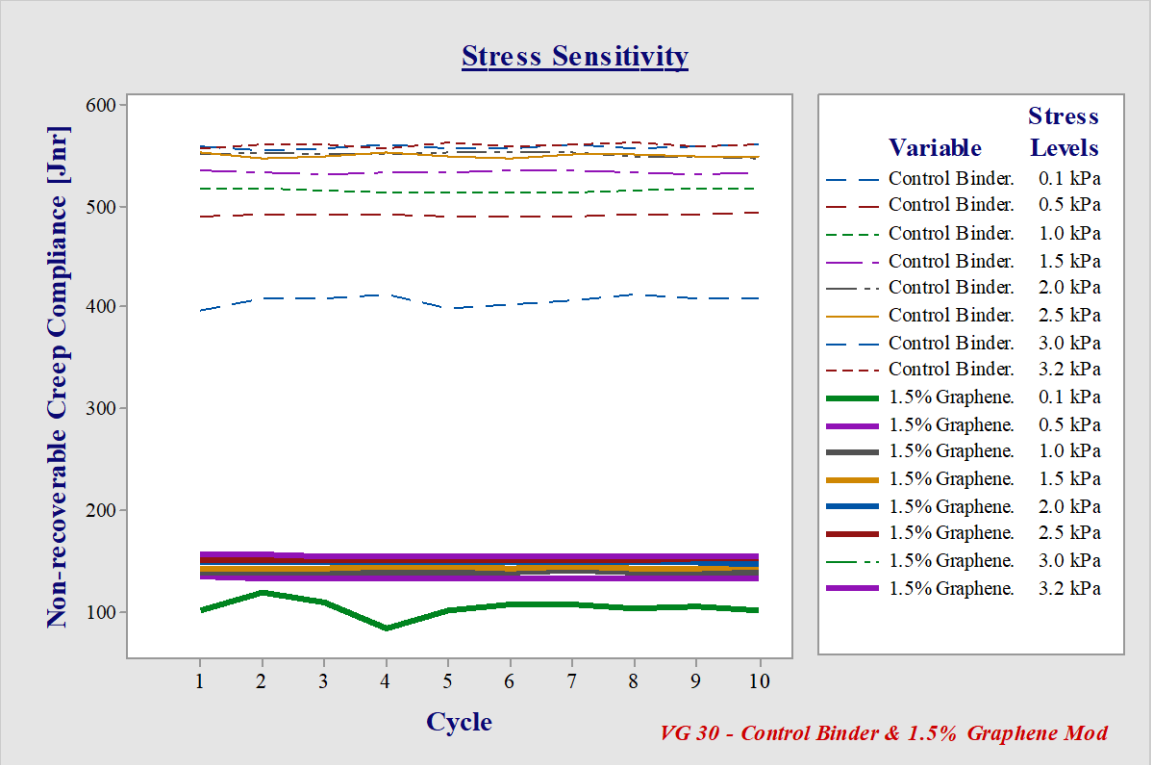

Figure 92 Stress Sensitivity for VG30 – Control Binder and 1.5% Graphene (Jnr-*Cycle 10)*

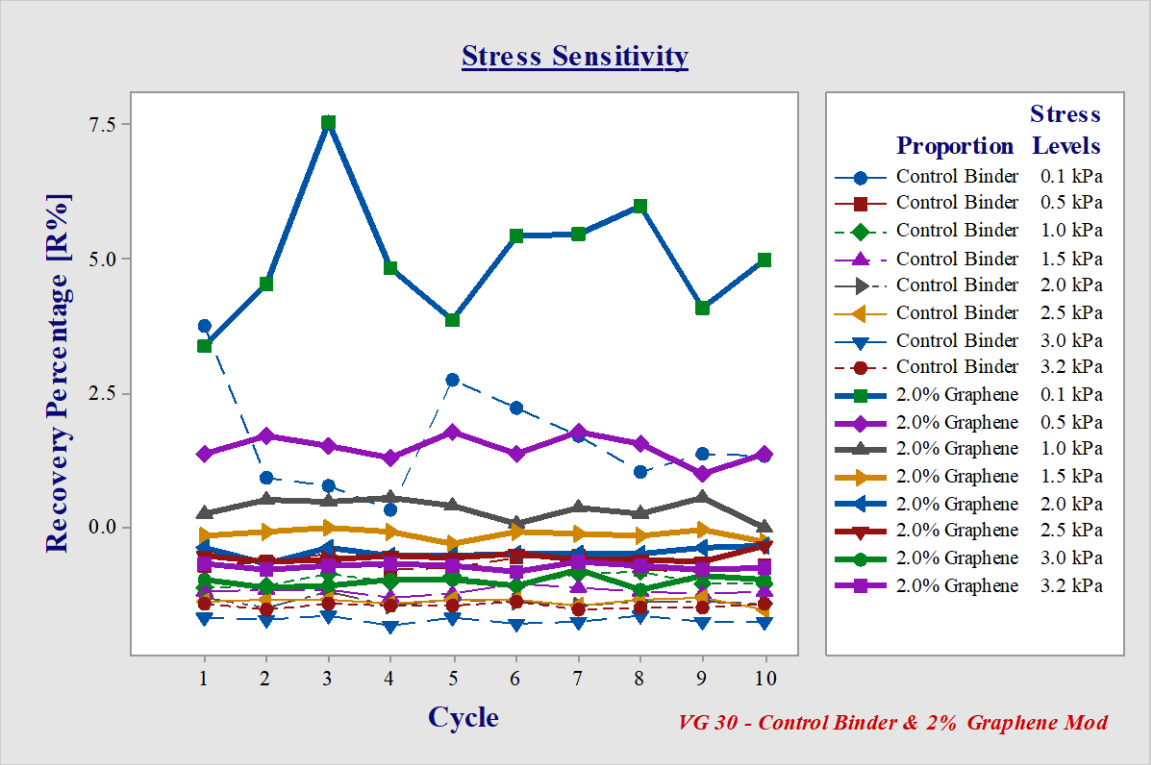

Figure 93 Stress Sensitivity for VG30 – Control Binder and 2% Graphene (Jnr-*Cycle 10)*

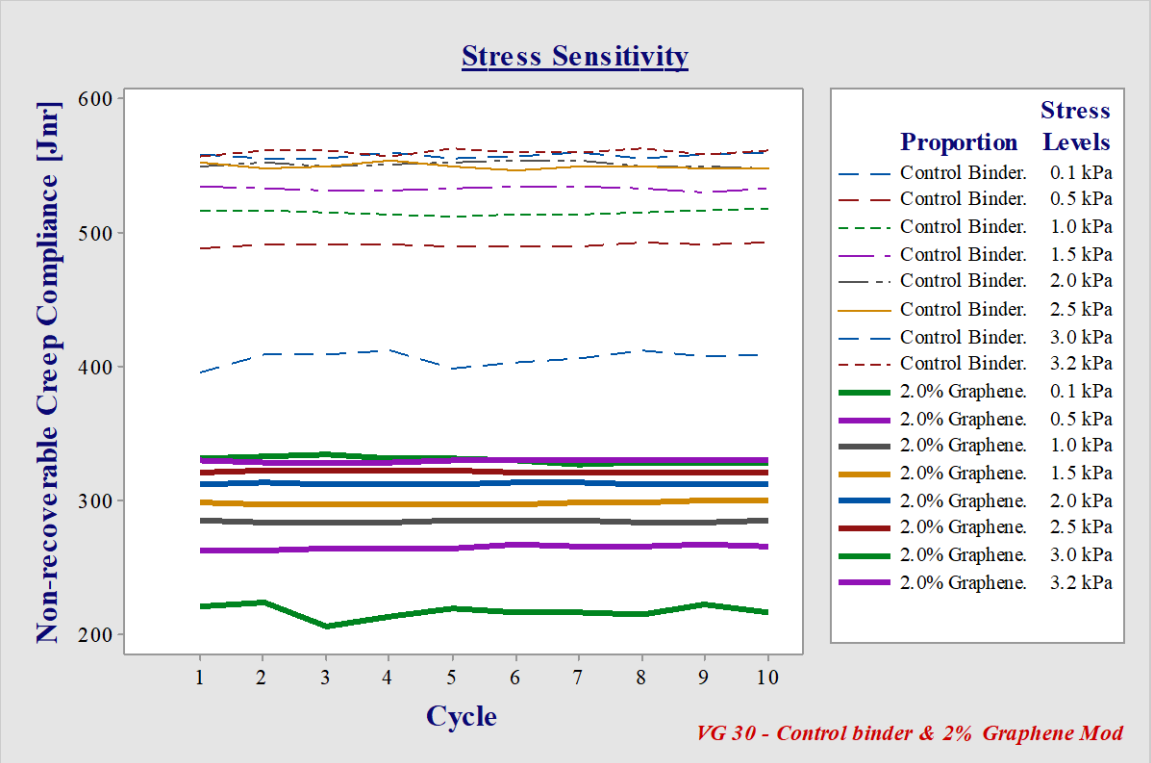

Figure 94 Stress Sensitivity for VG30 – Control Binder and 2% Graphene (Jnr-*Cycle 10)*

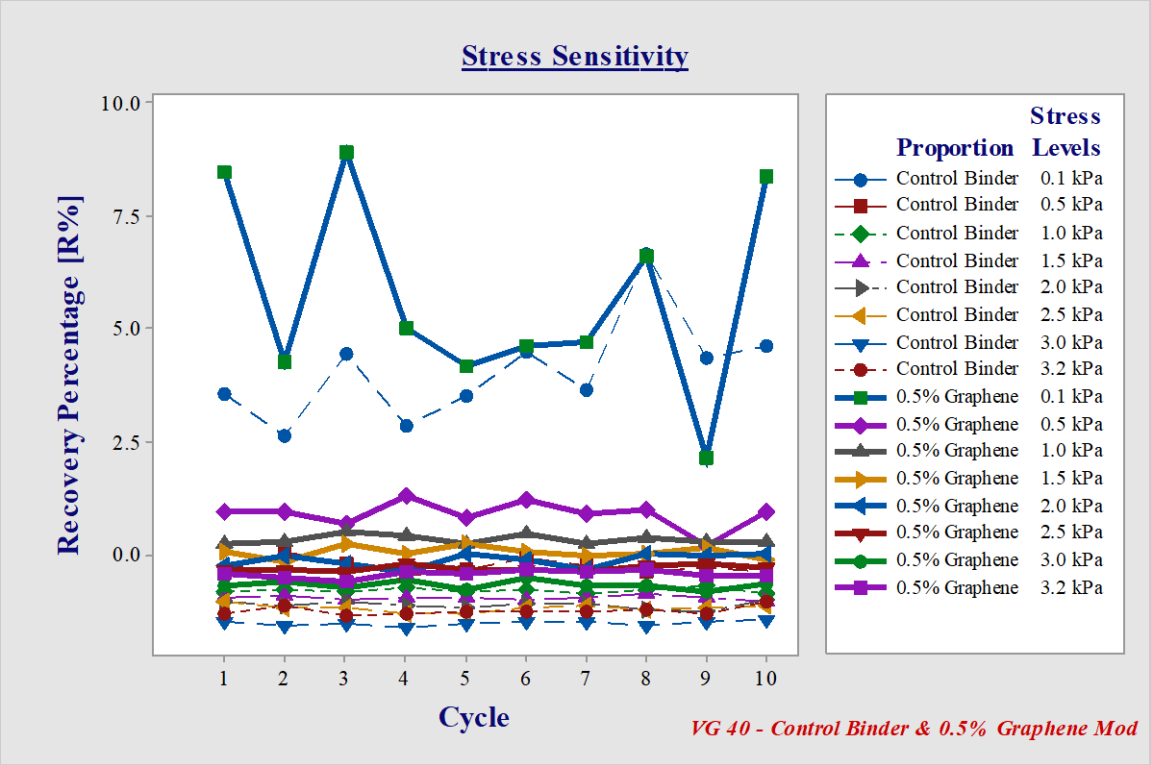

Figure 95 Stress Sensitivity for VG40 – Control Binder and 0.5% Graphene (R%-*Cycle 10)*

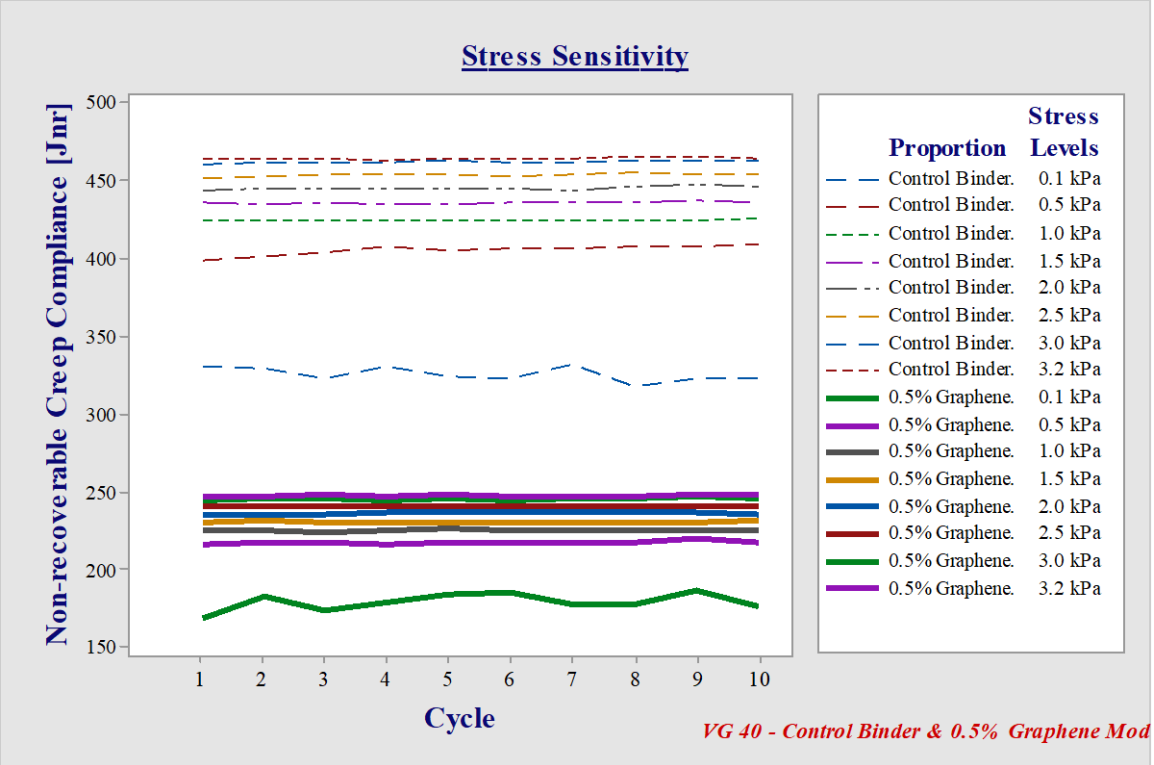

Figure 96 Stress Sensitivity for VG40 – Control Binder and 0.5% Graphene (Jnr-*Cycle 10)*

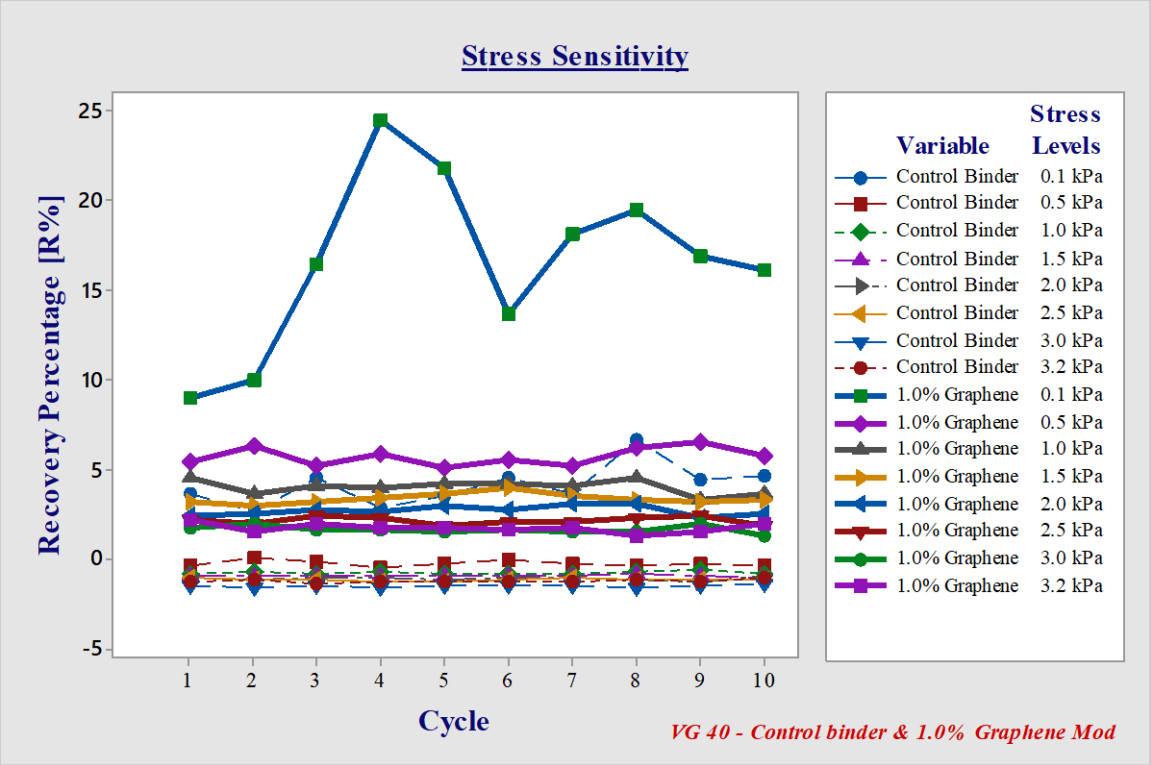

Figure 97 Stress Sensitivity for VG40 – Control Binder and 1% Graphene (R%-*Cycle 10)*

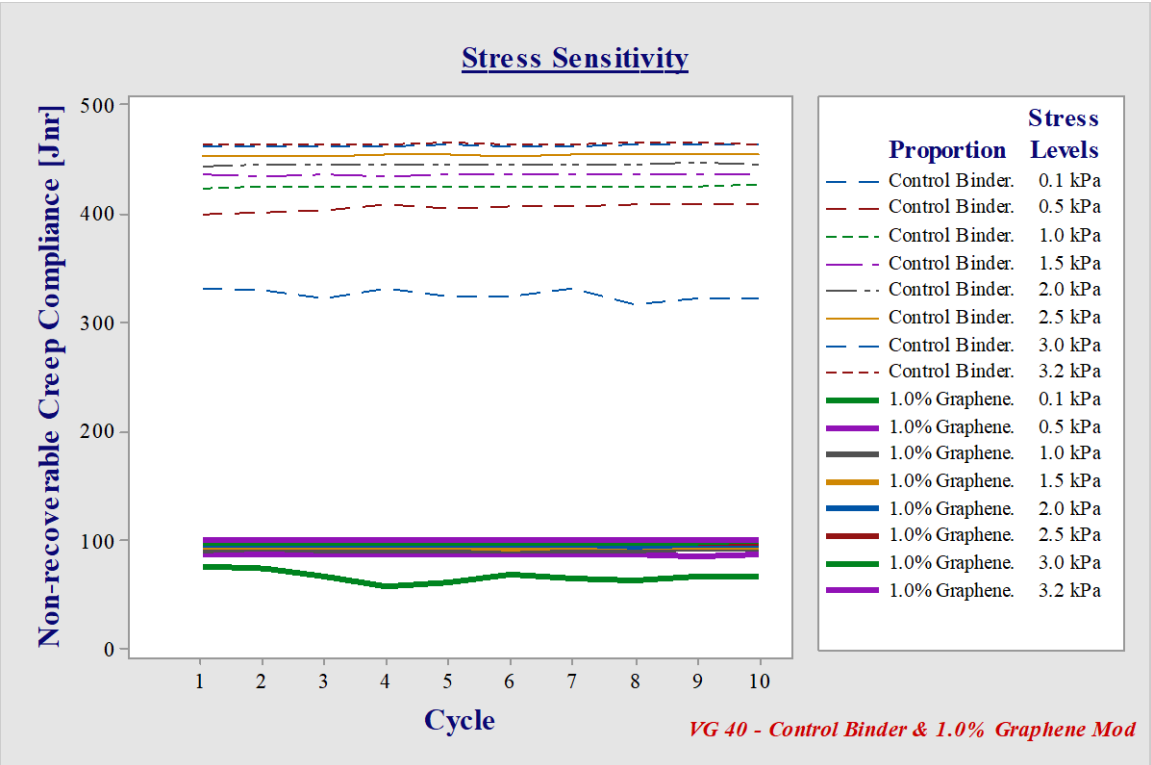

Figure 98 Stress Sensitivity for VG40 – Control Binder and 1% Graphene (Jnr-*Cycle 10)*

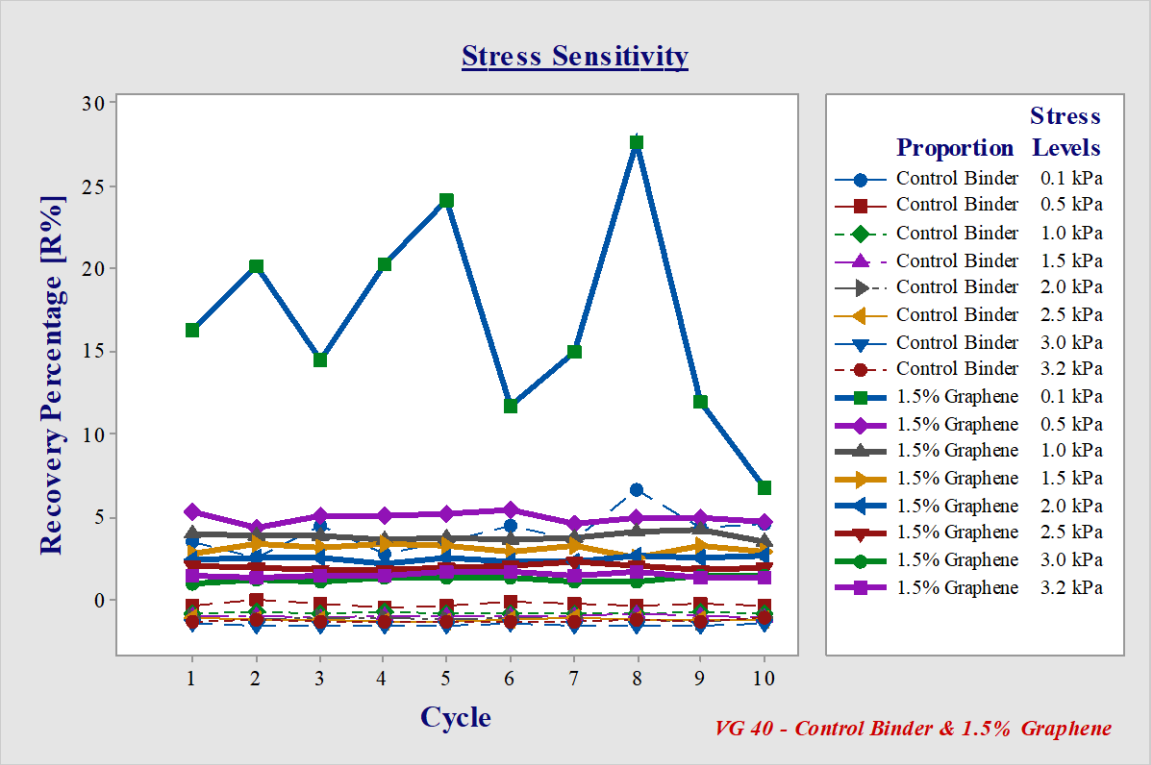

Figure 99 Stress Sensitivity for VG40 – Control Binder and 1.5% Graphene (R%-*Cycle 10)*

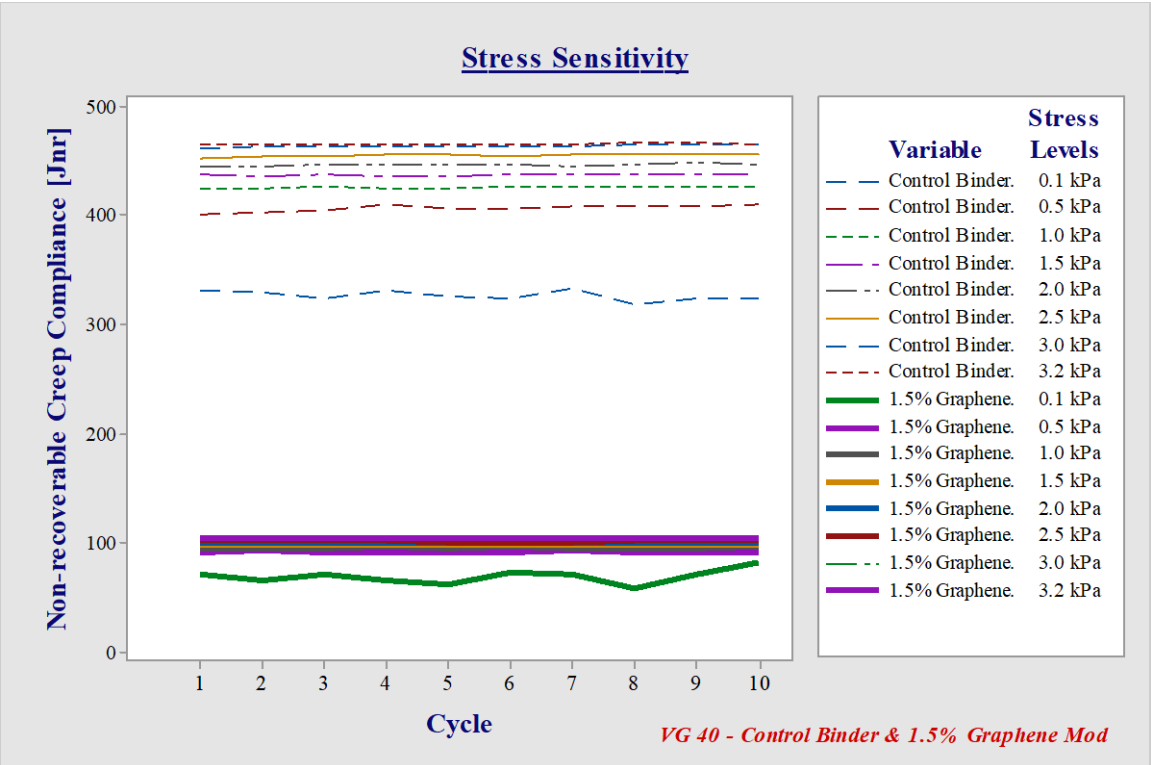

Figure 100 Stress Sensitivity for VG40 – Control Binder and 1.5% Graphene (Jnr-*Cycle 10)*

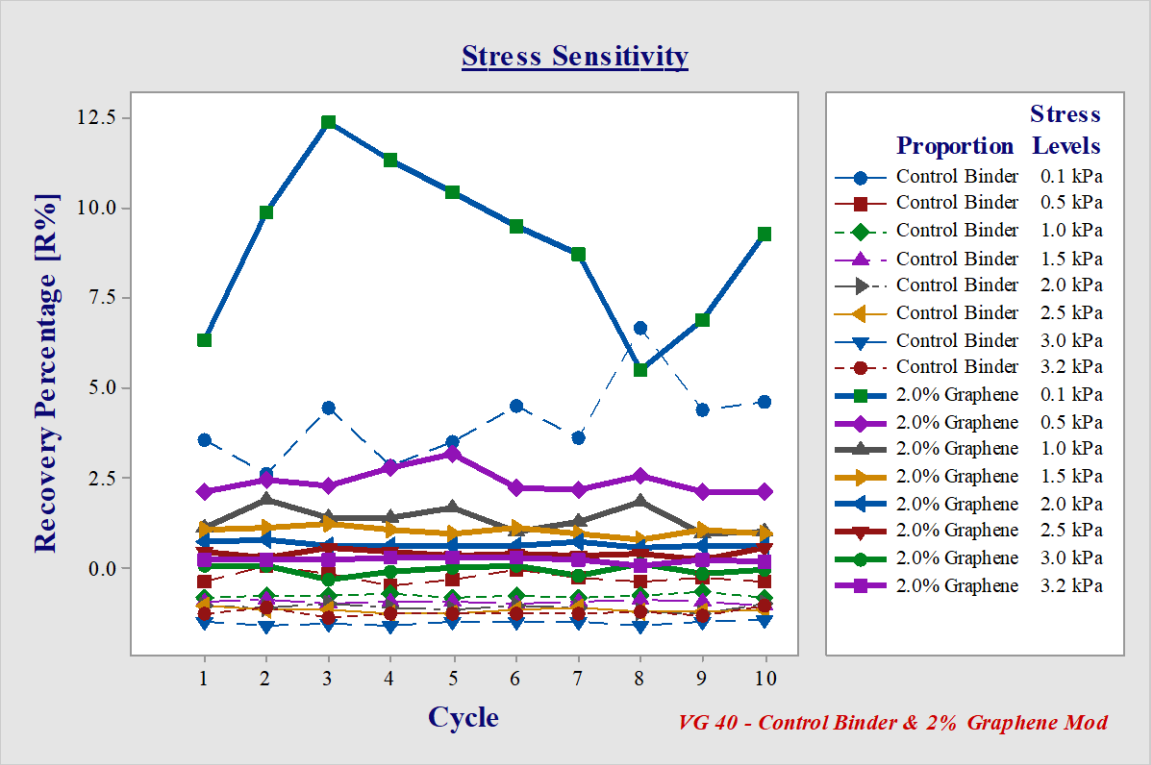

Figure 101 Stress Sensitivity for VG40 – Control Binder and 2% Graphene (R%-*Cycle 10)*

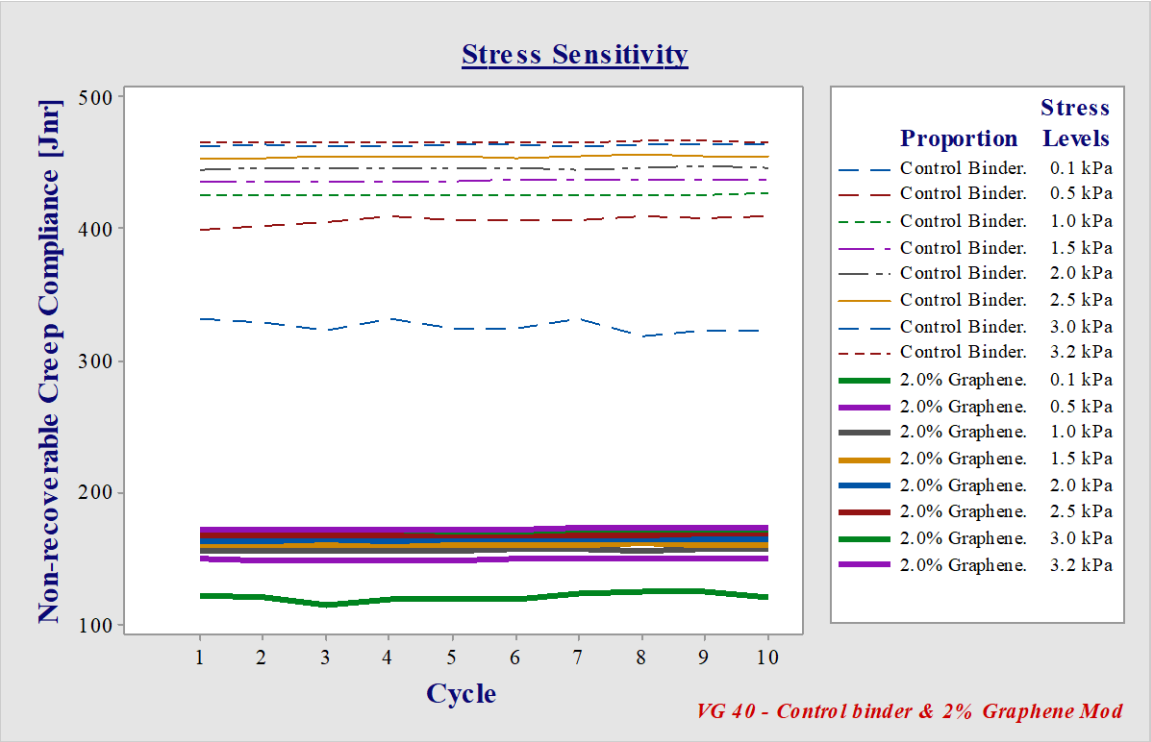

Figure 102 Stress Sensitivity for VG40 – Control Binder and 2% Graphene (Jnr-*Cycle 10)*

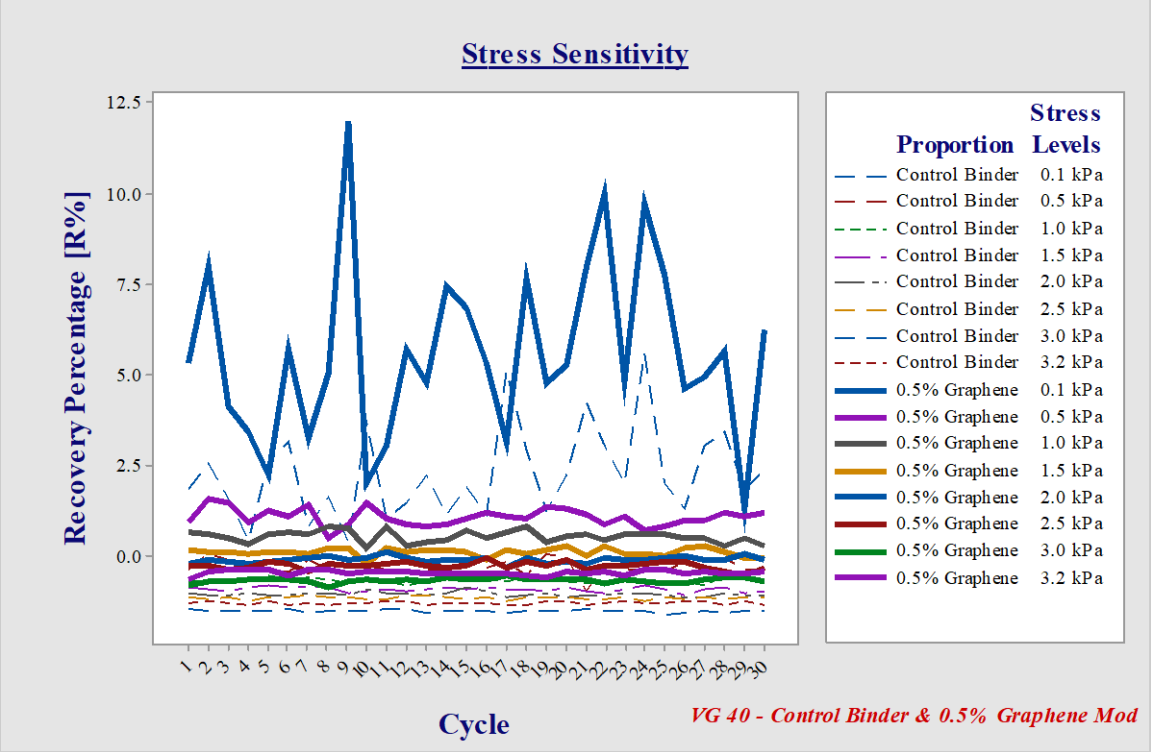

Figure 103 Stress Sensitivity for VG40 – Control Binder and 0.5% Graphene (R%-*Cycle 30)*

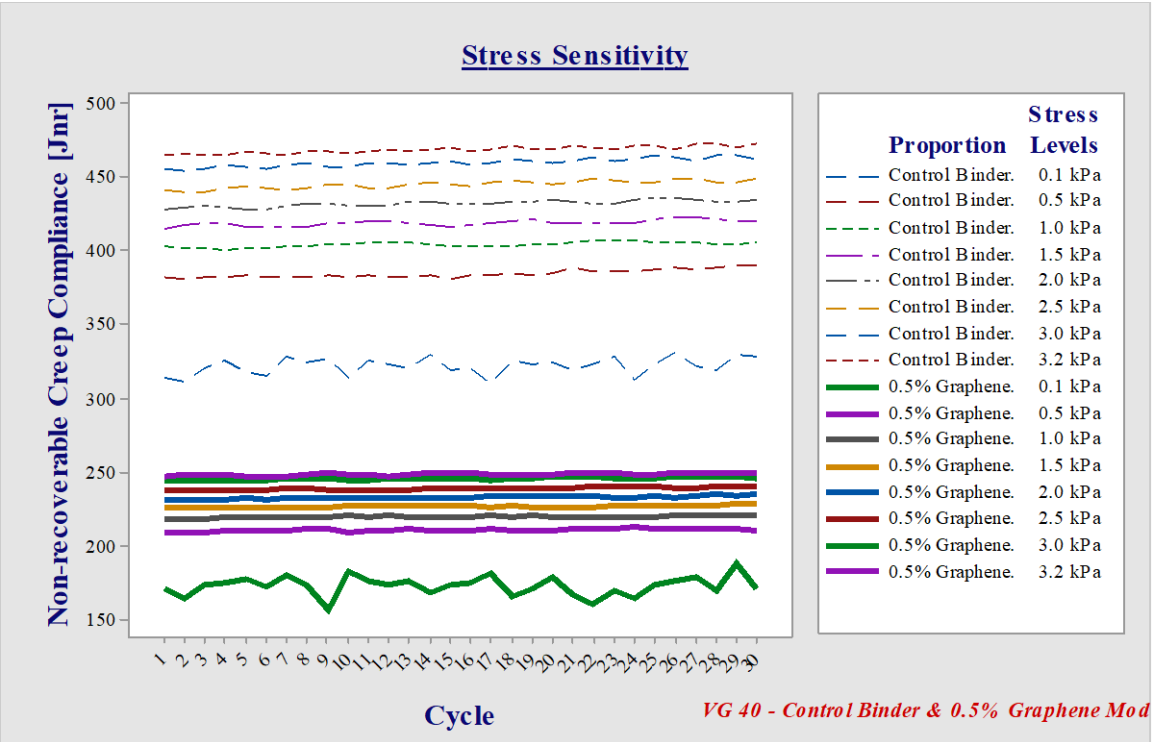

Figure 104 Stress Sensitivity for VG40 – Control Binder and 0.5% Graphene (Jnr-*Cycle 30)*

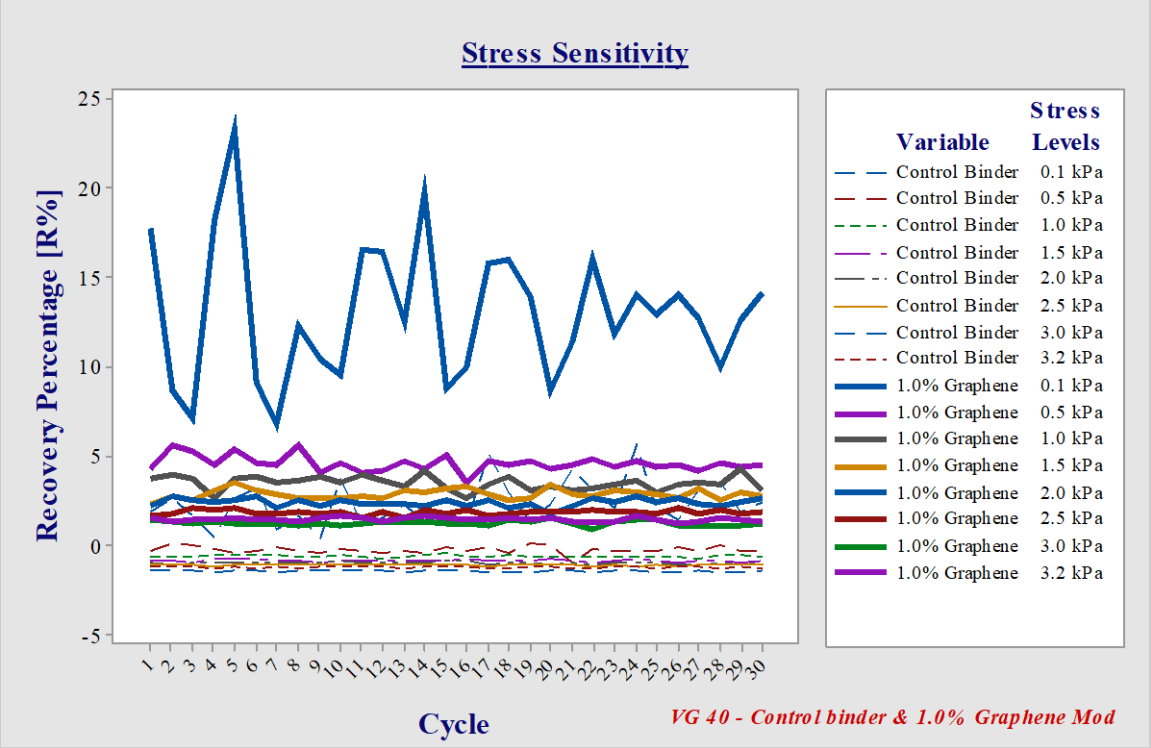

Figure 105 Stress Sensitivity for VG40 – Control Binder and 1% Graphene (R%-*Cycle 30)*

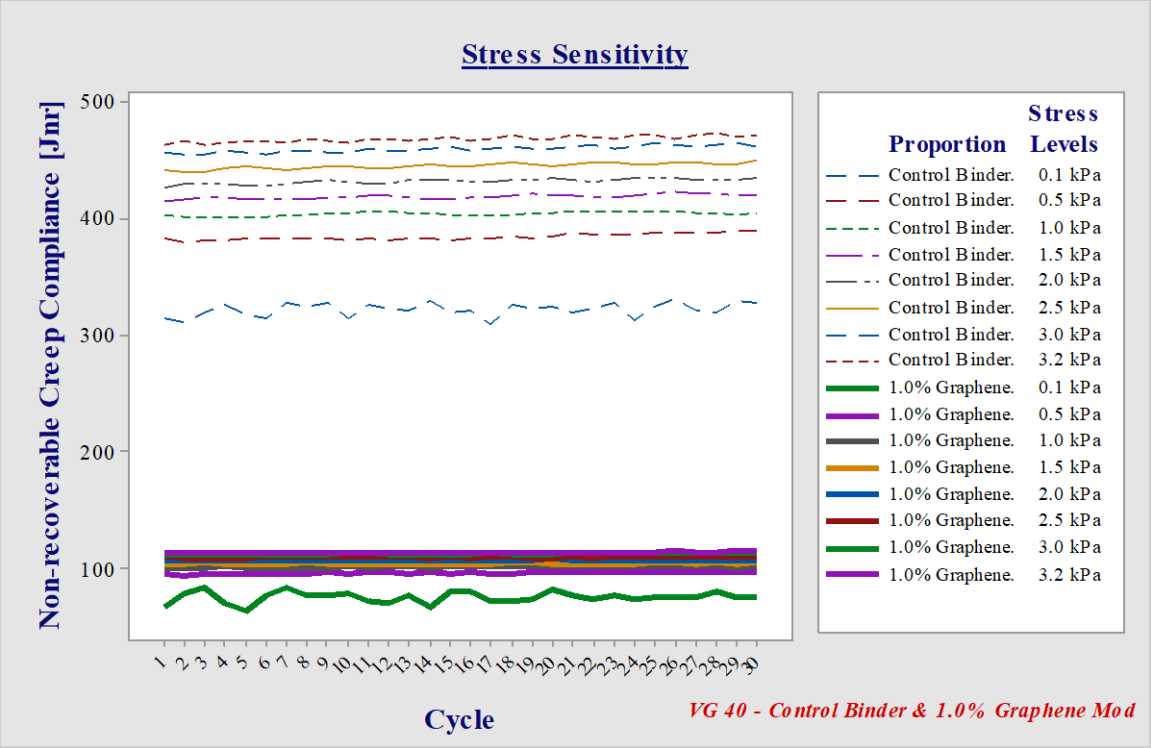

Figure 106 Stress Sensitivity for VG40 – Control Binder and 1% Graphene (Jnr-*Cycle 30)*

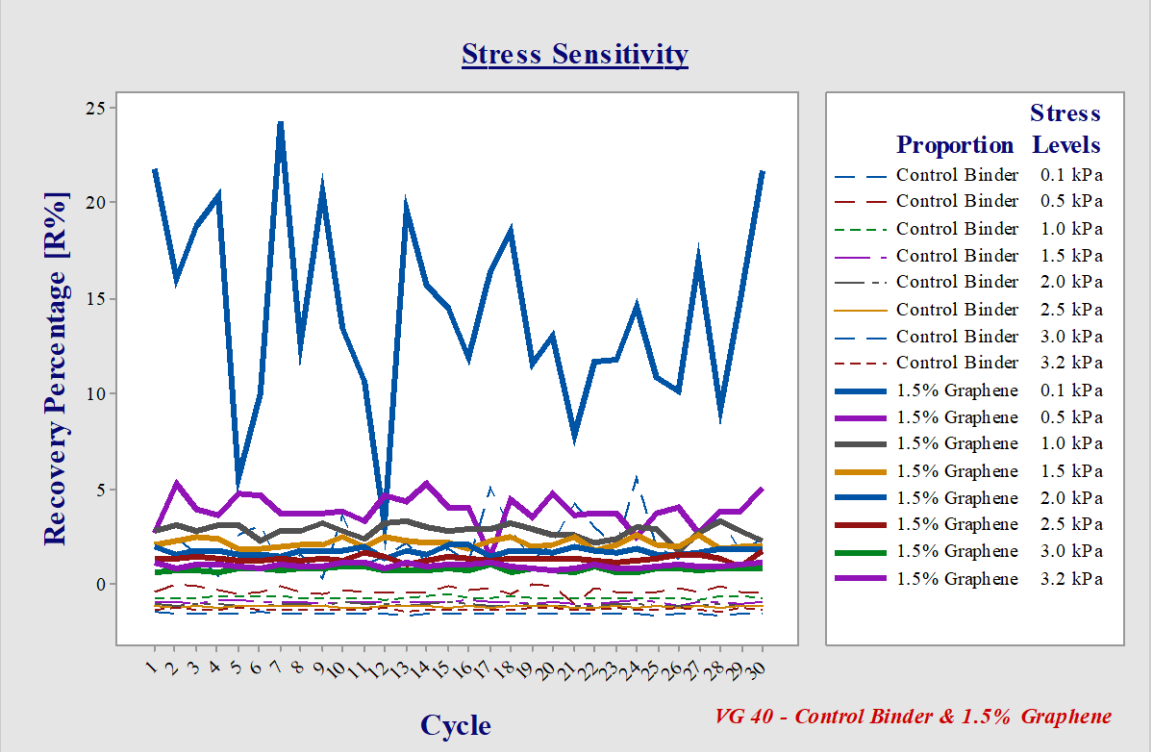

Figure 107 Stress Sensitivity for VG40 – Control Binder and 1.5% Graphene (R%-*Cycle 30)*

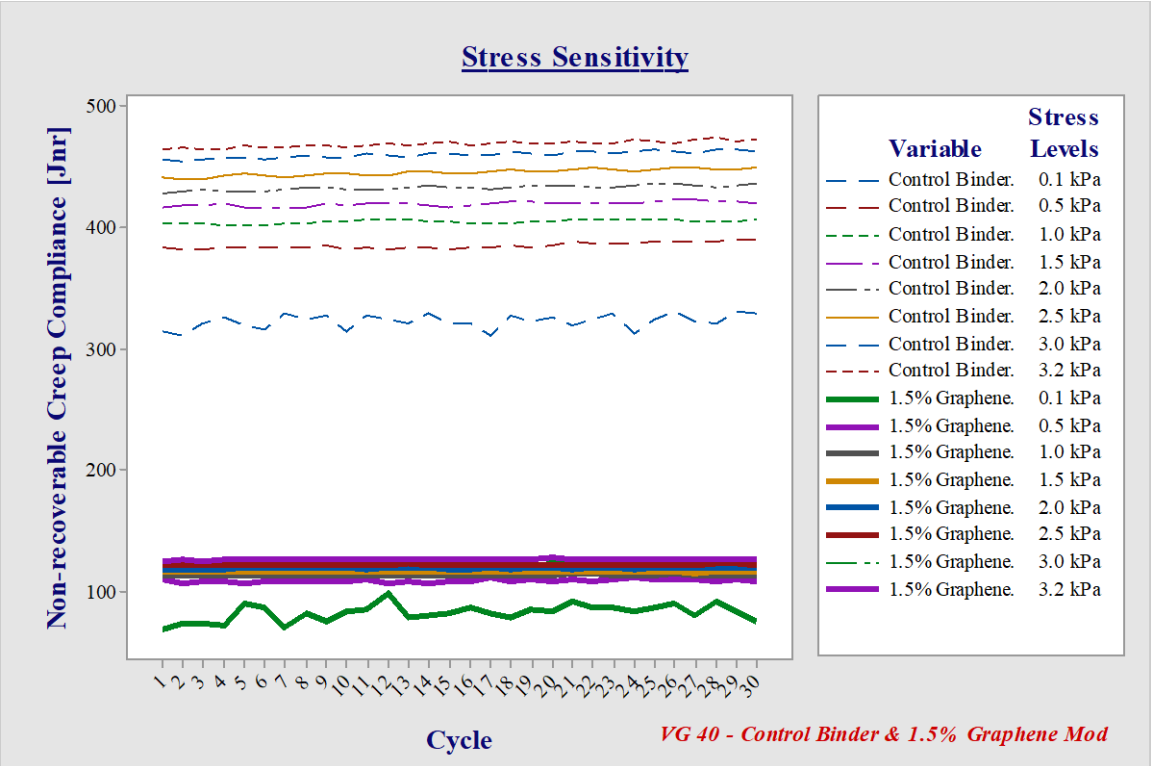

Figure 108 Stress sensitivity for VG40 – control binder and 1.5% graphene (Jnr-*Cycle 30)*

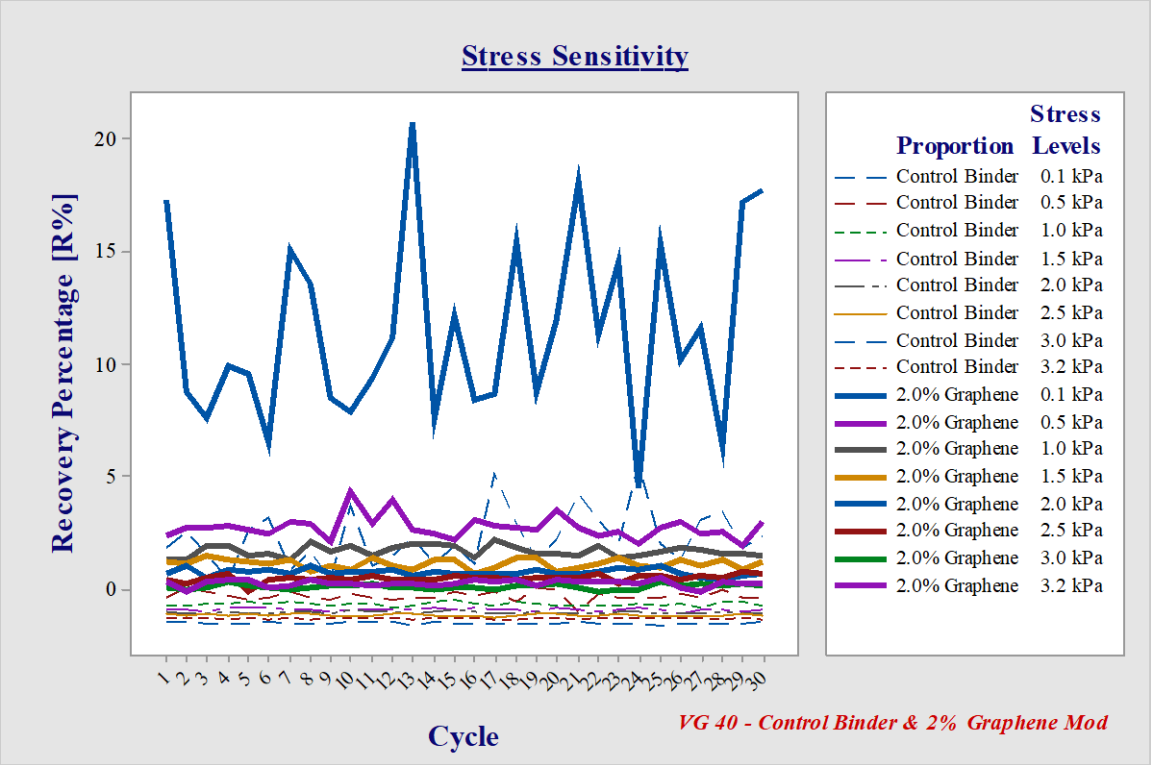

Figure 109 Stress Sensitivity for VG40 – Control Binder and 2% Graphene (R%-*Cycle 30)*

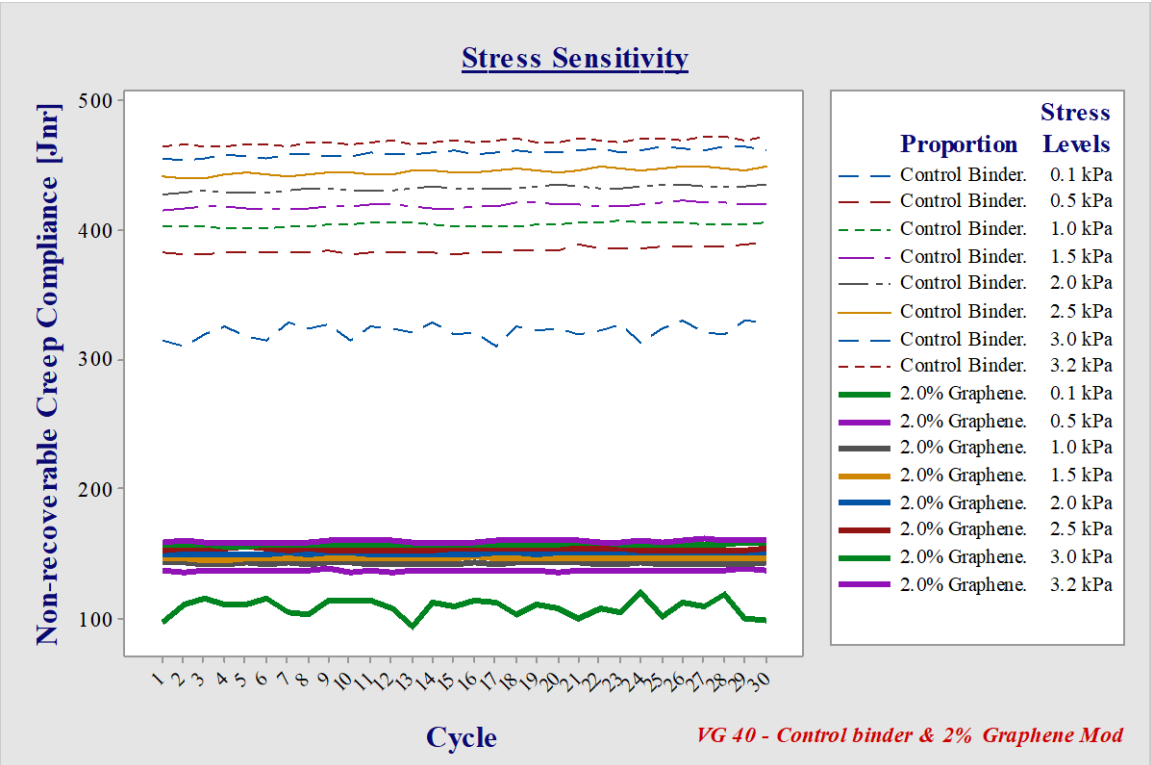

Figure 110 Stress Sensitivity for VG40 – Control Binder and 2% Graphene (Jnr-*Cycle 30)*

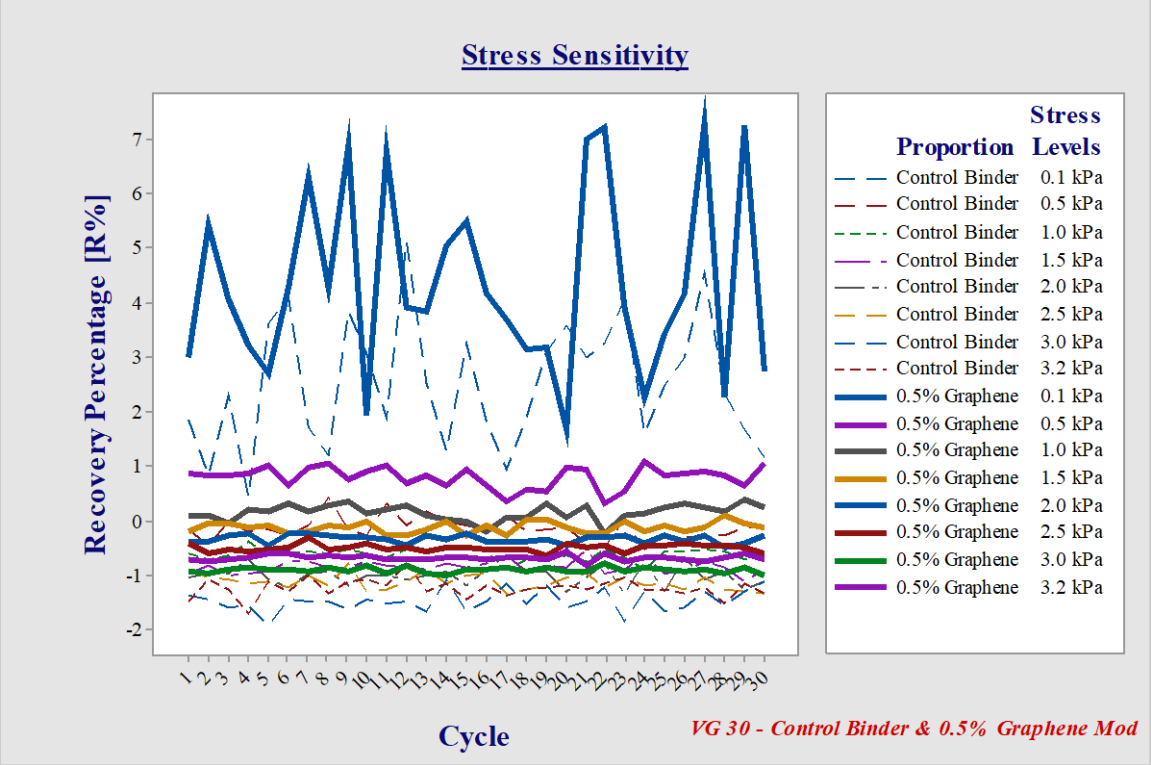

Figure 111 Stress Sensitivity for VG30 – Control Binder and 0.5% Graphene (R%-*Cycle 30)*

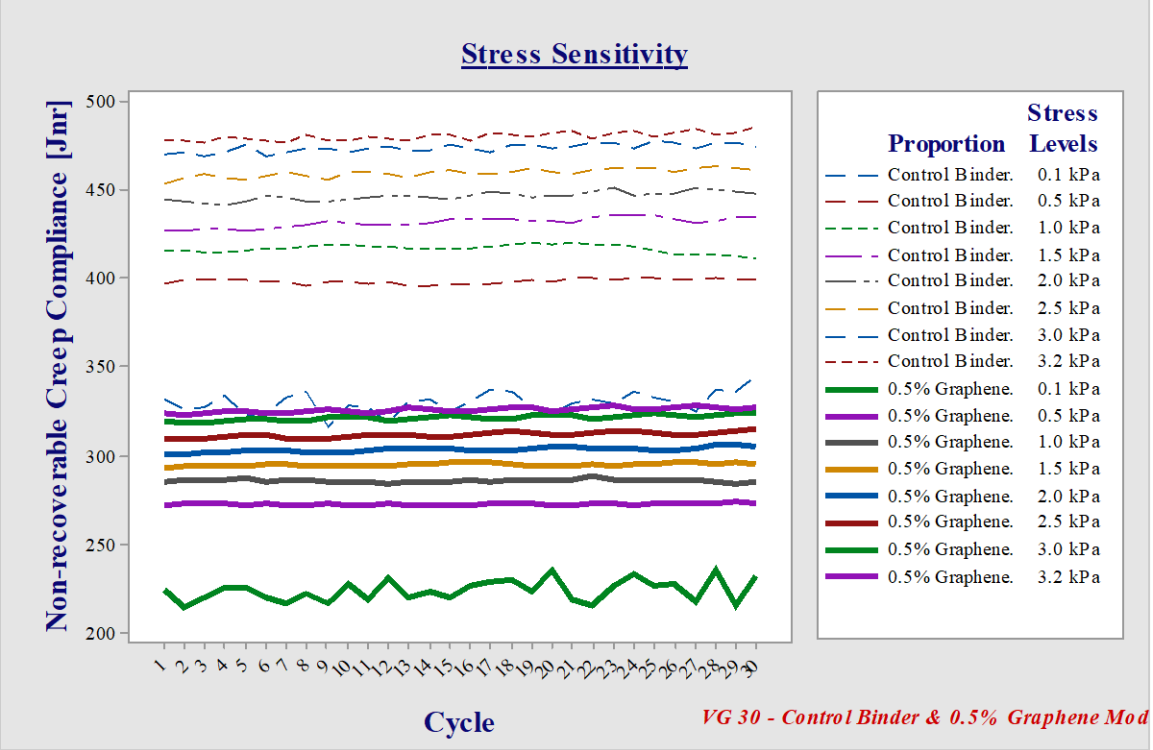

Figure 112 Stress Sensitivity for VG30 – Control Binder and 0.5% Graphene (Jnr-*Cycle 30)*

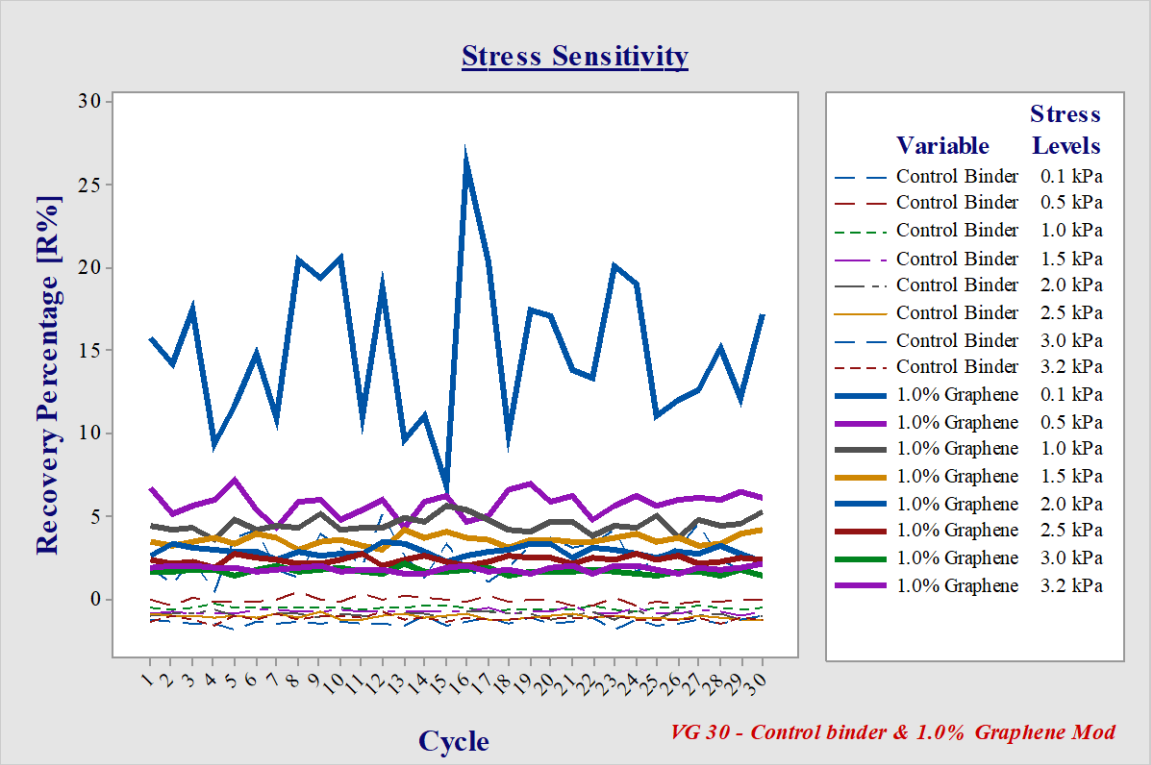

Figure 113 Stress Sensitivity for VG30 – Control Binder and 1% Graphene (R%-*Cycle 30)*

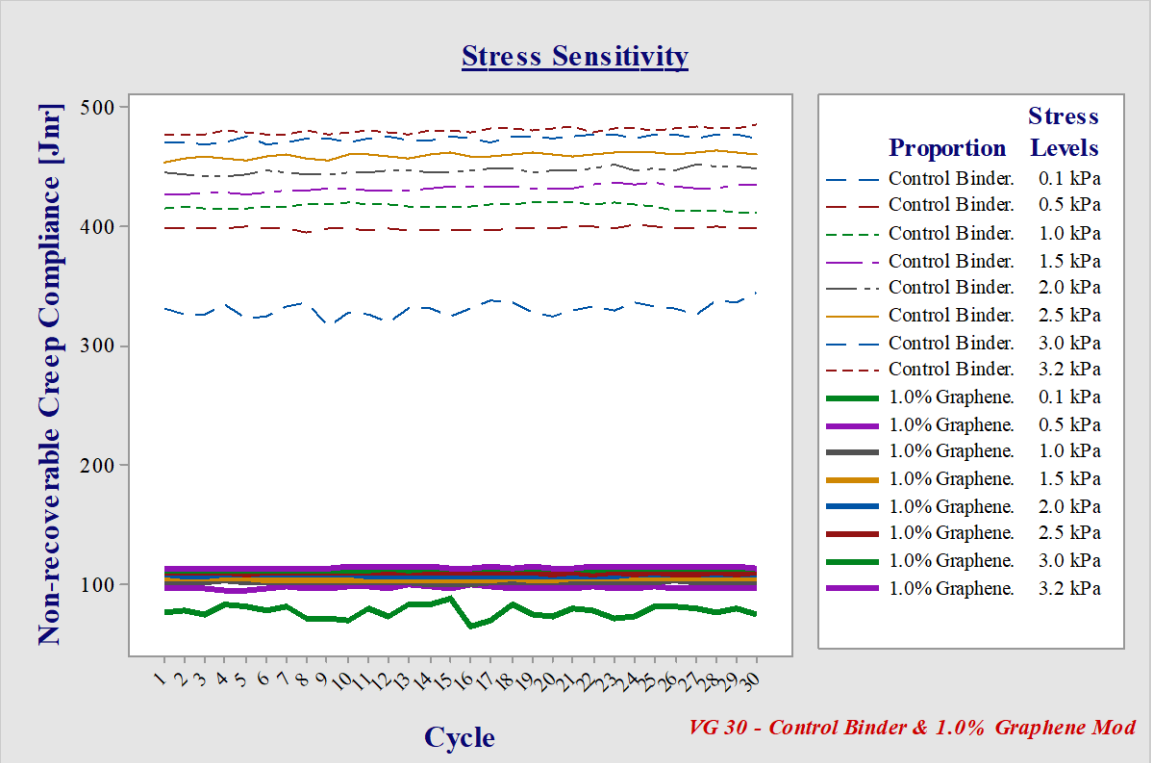

Figure 114 Stress Sensitivity for VG30 – Control Binder and 1% Graphene (Jnr-*Cycle 30)*

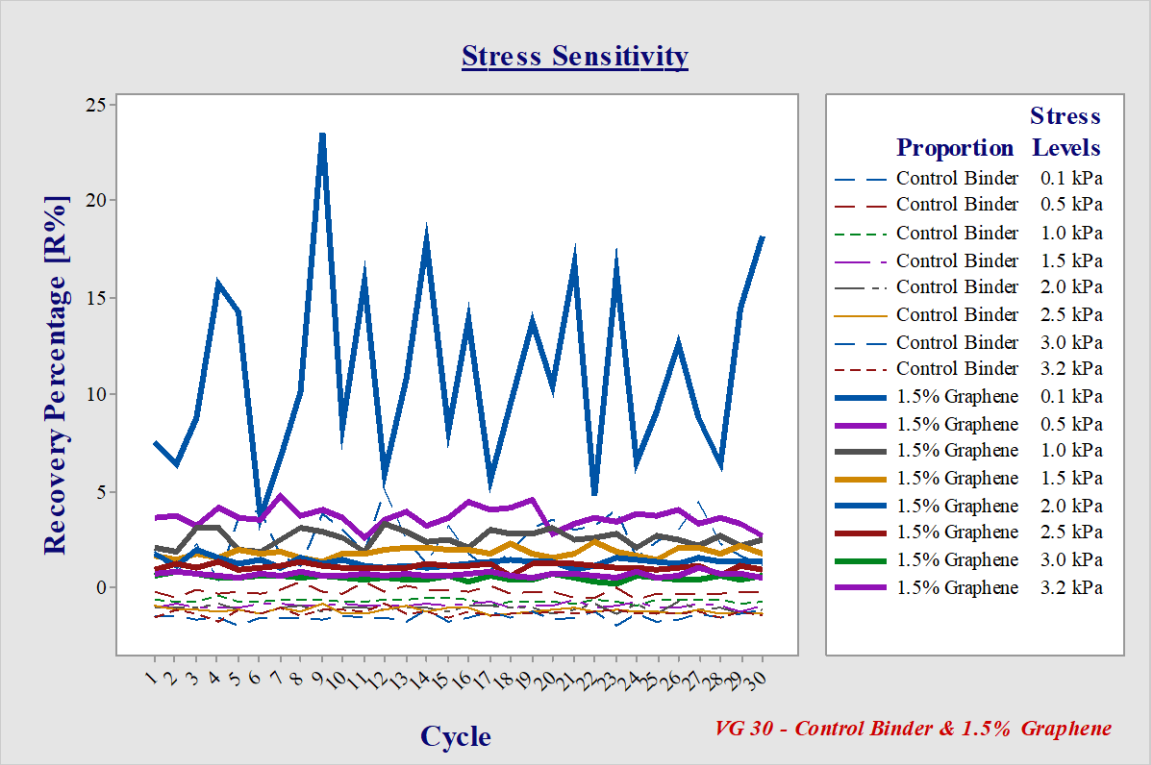

Figure 115 Stress Sensitivity for VG30 – Control Binder and 1.5% Graphene (R%-*Cycle 30)*

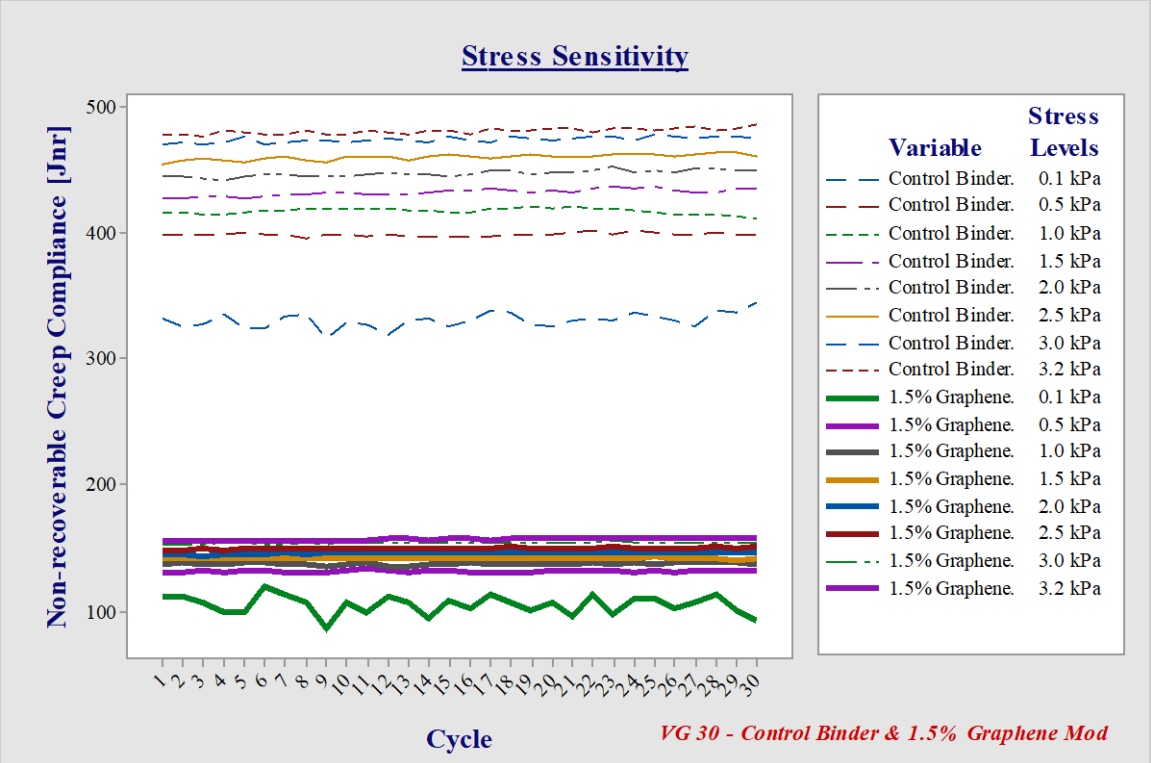

Figure 116 Stress Sensitivity for VG30 – Control Binder and 1.5% Graphene (Jnr-*Cycle 30)*

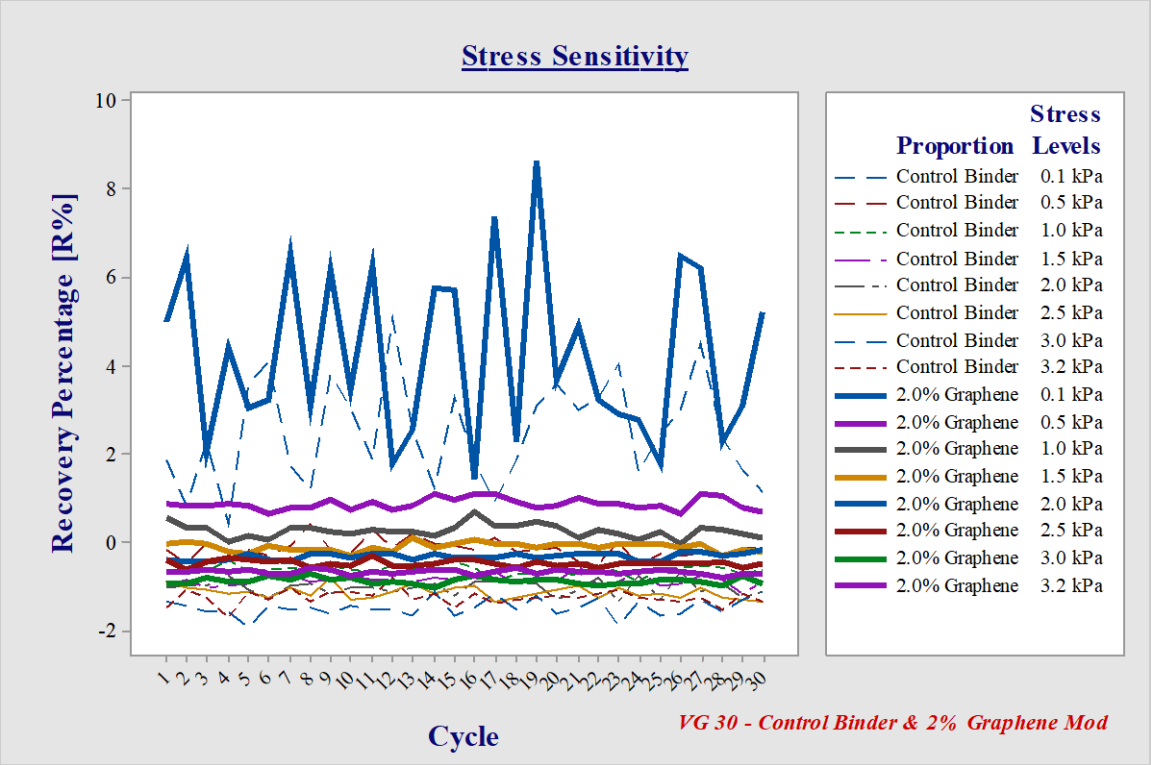

Figure 117 Stress Sensitivity for VG30 – Control Binder and 2% Graphene (R%-*Cycle 30)*

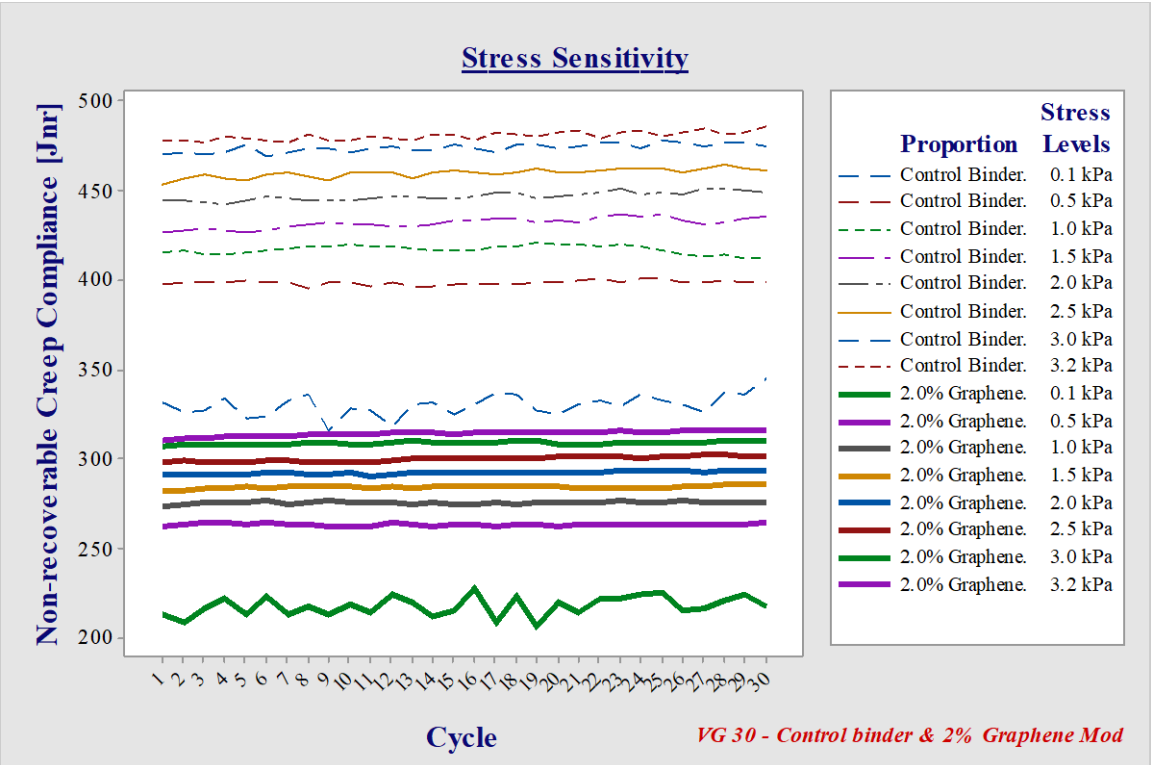

Figure 118 Stress Sensitivity for VG30 – Control Binder and 2% Graphene (Jnr-*Cycle 30)*

Tables 13 – 16 list the results for R% for VG30 and VG40 corresponding to 10 and 30 cycle test. The negative values as observed by emulating stress via DSR are listed though they won't be of any significance for the statistical analysis. Tables 17 – 20 list the Jnr values for VG30 and VG40 corresponding to 10 and 30 cycle test. As graphically illustrated the values listed in the table tend to have lower values of Jnr for 1% dosage, suggesting 1% dosage as the optimum additive. Tables 21 and 22 give R% *diff* and Jnr *diff* values for VG30 and VG40 binder corresponding to 10 cycle and 30 cycle test respectively. The value of Jnr *diff* shall be less than 75% though control binder for both VG30 and VG40 does not follow.

Table 13 VG30 – 10 Cycle (*MSCR Test*)

Stress Level [kPa]	**Recovery Percentage**				
	Control Binder	**0.5% Graphene**	**1.0% Graphene**	**1.5% Graphene**	**2.0% Graphene**
0.1	1.62	4.35	14.42	11.66	6.10
0.5	-0.50	1.00	5.18	4.13	2.21
1.0	-0.91	0.21	3.89	2.75	0.65
1.5	-1.07	-0.15	3.21	1.89	-0.12
2	-1.26	-0.36	2.53	1.38	-0.44
2.5	-1.32	-0.48	2.05	1.04	-0.63
3	-1.67	-0.90	1.38	0.49	-1.03
3.2	-1.41	-0.67	1.56	0.67	-0.77

Table 14 VG40 - 10 Cycle (*MSCR Test*)

Stress Level [kPa]	Recovery Percentage				
	Control Binder	**0.5% Graphene**	**1.0% Graphene**	**1.5% Graphene**	**2.0% Graphene**
0.1	3.018	5.84	16.30	16.51	8.92
0.5	-0.32	1.07	10.21	4.91	2.36
1.0	-0.77	0.38	7.08	3.86	1.42
1.5	-0.93	0.07	5.58	3.07	1.03
2	-1.06	-0.10	5.26	2.53	0.65
2.5	-1.16	-0.27	5.77	1.99	0.42
3	-1.50	-0.64	6.46	1.27	-0.04
3.2	-1.24	-0.41	5.41	1.48	0.23

Table 15 Recovery Percentage VG30 - 30 Cycle (*MSCR Test*)

Stress Level [kPa]	Recovery Percentage				
	Control Binder	**0.5% Graphene**	**1.0% Graphene**	**1.5% Graphene**	**2.0% Graphene**
0.1	2.73	5.77	14.24	10.49	4.97
0.5	-0.10	1.17	5.43	3.69	0.98
1.0	-0.57	0.46	4.43	2.62	0.26
1.5	-0.80	0.10	3.50	1.85	-0.06
2	-0.96	-0.10	2.80	1.34	-0.28
2.5	-1.08	-0.27	2.31	1.06	-0.42
3	-1.43	-0.69	1.57	0.56	-0.81
3.2	-1.20	-0.47	1.70	0.70	-0.61

Table 16 Recovery Percentage VG40 - 30 Cycle (*MSCR Test*)

Stress Level [kPa]	Recovery Percentage				
	Control Binder	**0.5% Graphene**	**1.0% Graphene**	**1.5% Graphene**	**2.0% Graphene**
0.1	2.92	6.00	14.64	15.06	10.68
0.5	-0.19	0.98	4.72	4.16	2.65
1.0	-0.60	0.42	3.65	3.17	1.71
1.5	-0.81	0.06	2.99	2.47	1.12
2	-0.95	-0.16	2.40	1.98	0.75
2.5	-1.05	-0.31	1.92	1.56	0.53
3	-1.40	-0.70	1.32	0.99	0.09
3.2	-1.16	-0.47	1.46	1.17	0.30

Table 17 Non – Recoverable Creep Compliance VG30 - 10 Cycle (*MSCR Test*)

Stress Level [kPa]	Non-recoverable Creep Compliance – Jnr [kPa^{-1}]				
	Control Binder	**0.5% Graphene**	**1.0% Graphene**	**1.5% Graphene**	**2.0% Graphene**
0.1	227.04	80.97	80.97	106.74	215.79
0.5	274.74	274.74	103.63	134.26	265.23
1.0	387.22	288.88	108.30	141.13	290.82
1.5	464.03	298.32	111.05	146.53	312.086
2	487.14	306.03	114.27	150.92	325.74
2.5	502.68	313.12	116.88	154.63	332.09
3	519.26	320.36	119.58	158.59	340.37
3.2	527.37	322.79	120.40	159.58	338.81

Table 18 Non – Recoverable Creep Compliance VG40 - 10 Cycles (*MSCR Test*)

Stress Level [kPa]	Non-recoverable Creep Compliance – Jnr [kPa^{-1}]				
	Control	**0.5%**	**1.0%**	**1.5%**	**2.0%**

	Binder	Graphene	Graphene	Graphene	Graphene
0.1	332.48	175.72	72.01	68.76	120.01
0.5	402.38	213.79	85.94	91.26	147.86
1.0	419.02	223.16	91.27	95.04	154.54
1.5	429.61	228.14	94.63	97.62	158.70
2	437.96	233.20	96.45	99.83	162.64
2.5	446.27	237.91	96.71	101.89	166.00
3	454.90	243.47	96.96	104.06	169.64
3.2	457.57	245.65	98.40	104.33	170.85

Table 19 Non – Recoverable Creep Compliance VG30 - 30 Cycle (*MSCR Test*)

Stress Level [kPa]	**Non-recoverable Creep Compliance – Jnr [kPa^{-1}]**				
	Control Binder	**0.5% Graphene**	**1.0% Graphene**	**1.5% Graphene**	**2.0% Graphene**
0.1	322.55	196.55	78.22	106.80	209.99
0.5	388.31	239.98	98.67	131.92	255.21
1.0	406.52	251.32	102.80	138.01	267.47
1.5	421.22	259.09	105.61	142.36	276.38
2	435.60	265.86	108.28	146.59	284.54
2.5	448.74	272.84	110.82	150.58	292.31
3	462.71	280.54	114.07	155.22	300.42
3.2	469.70	283.91	115.57	157.78	305.45

Table 20 Non – Recoverable Creep Compliance VG40 - 30 cycle (*MSCR Test*)

Stress Level [kPa]	**Non-recoverable Creep Compliance – Jnr [kPa^{-1}]**				
	Control Binder	**0.5% Graphene**	**1.0% Graphene**	**1.5% Graphene**	**2.0% Graphene**
0.1	307.55	179.89	71.87	78.39	110.98
0.5	368.44	221.69	94.51	102.95	139.33
1.0	384.42	231.54	98.70	107.05	144.56
1.5	396.24	238.30	101.43	110.09	149.37
2	406.36	244.56	103.95	112.79	153.31
2.5	415.73	250.50	106.18	115.29	156.77
3	425.34	257.22	108.78	118.22	160.87
3.2	431.22	258.65	109.95	119.09	162.95

Table 21 Recovery *Diff* and Jnr *Diff Cycle 10* (*MSCR Test*)

10 Cycle					
Recovery *Diff*					
Grade	**Control Binder**	**0.5% Graphene**	**1.0% Graphene**	**1.5% Graphene**	**2.0% Graphene**
VG30	538.95	116.02	88.86	94.15	112.87
VG40	143.76	107.07	69.82	91.00	97.36
Jnr *Diff*					
VG30	543.29	42.20	48.84	49.53	57.03
VG40	37.67	39.85	60.16	51.72	42.35

Table 22 Recovery *Diff* and Jnr *Diff* - *Cycle 30* (*MSCR Test*)

30 Cycle					
Recovery *Diff*					
Grade	**Control Binder**	**0.5% Graphene**	**1.0% Graphene**	**1.5% Graphene**	**2.0% Graphene**
VG30	144.83	109.04	88.00	93.24	112.55
VG40	45.62	44.37	47.75	47.76	45.46
Jnr *Diff*					
VG30	141.99	107.84	89.93	92.28	97.15
VG40	40.19	43.73	53.00	51.76	46.82

Coefficient of variance was computed in this test as illustrated in Figures 119 – 122 and the negative values of the recovery percentage were treated with no significance in the analysis, representing zero recovery percentage value (Soenena et al. 2013). Figure 120 illustrates the coefficient of variance for VG30 binder for recovery percentage between the three trials of cycle 10 and cycle 30 each and the coefficient of variance between results of cycle 10 and cycle 30 tests. The samples of control binder, 1% and 1.5% tends to variate 4%, 8% and 8% respectively which less than 10% but 0.5% and 2% dosages show a higher variation. Dosage 0.5% dosage shows a higher degree of variation of 18% and 12%, whereas 1%, 1.5%,then 2% vary under 10%. Figure 121 is a graphical representation of the coefficient of variation for the VG30 binder for Jnr across three trials and the cycle 10 – cycle 30 results. Figure 122 illustrates the coefficient of variance for VG40 binder for recovery percentage between the three trials of cycle 10 and cycle 30 each and the coefficient of variance between results of cycle 10 and cycle 30 tests. . Figure 123 is a graphical representation of the coefficient of variation for the VG40 binder for Jnr across three trials and the cycle 10 – cycle 30 results. The results are tabulated in Tables 23 and 24.

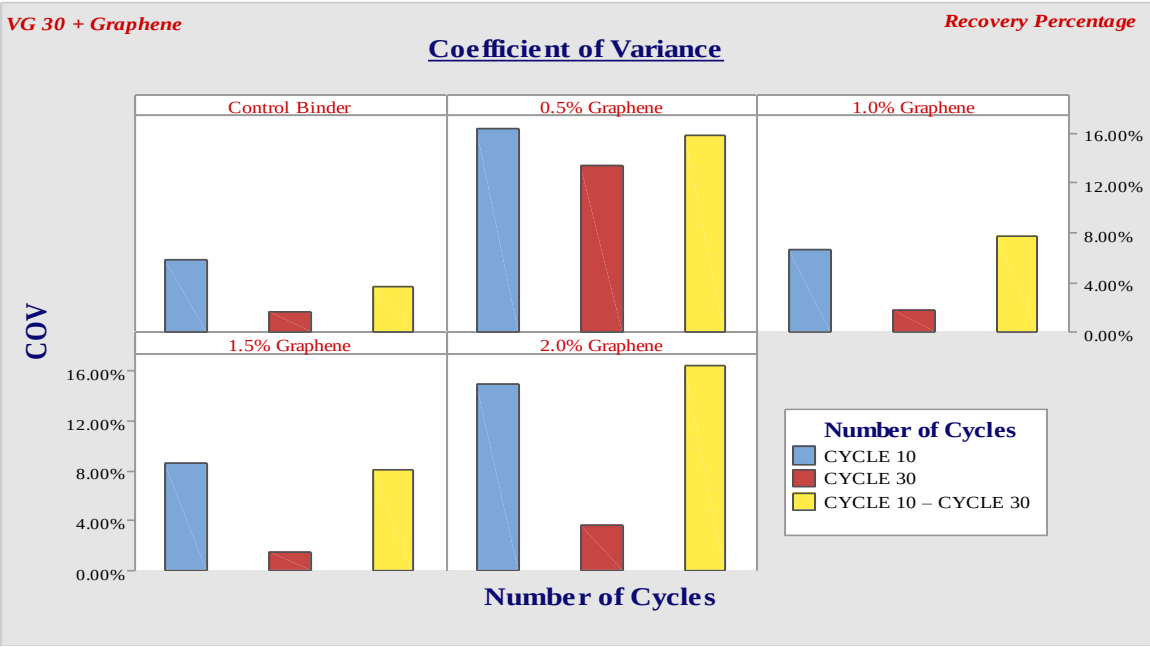

Figure 119 Coefficient of Variation VG30 – R%

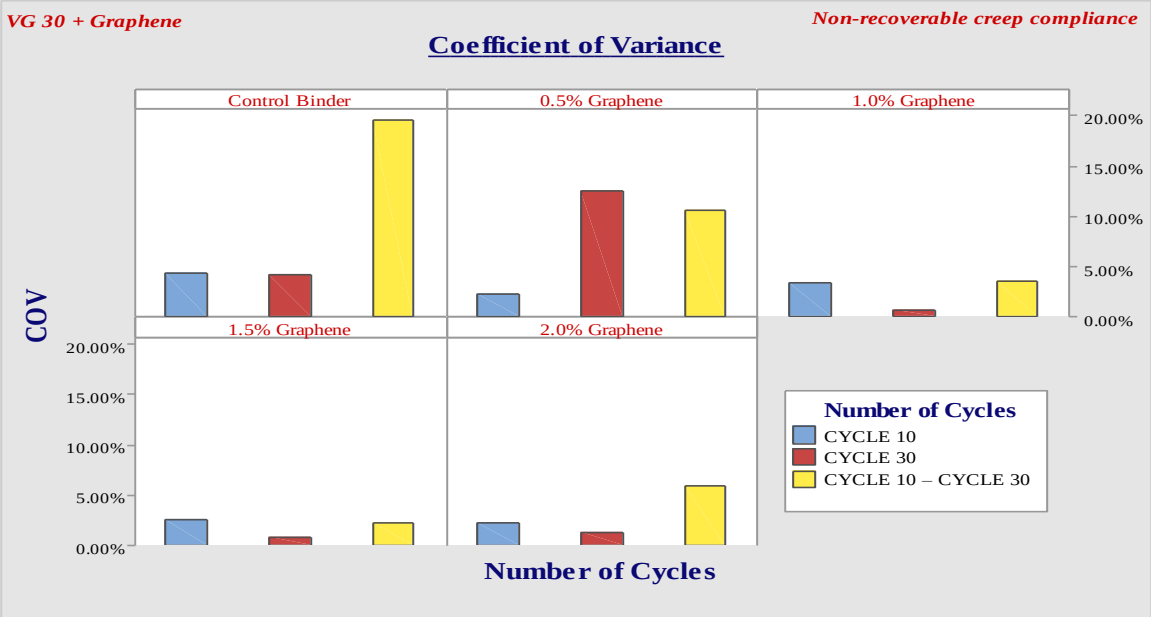

Figure 120 Coefficient of Variation VG30 – Jnr

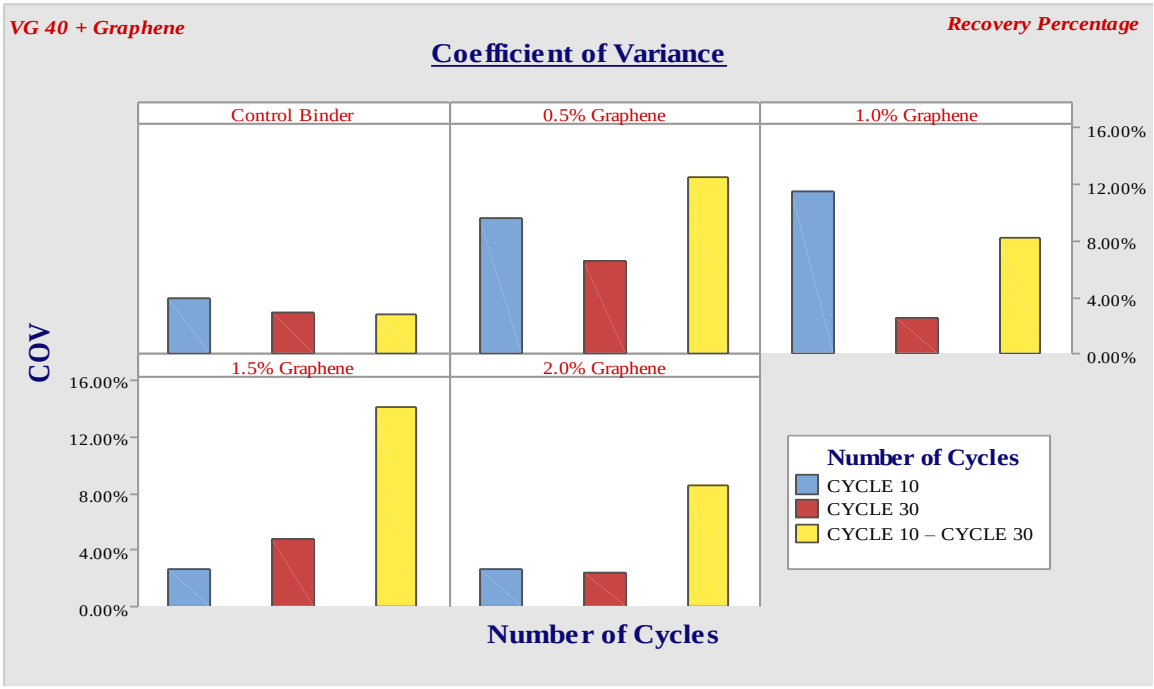

Figure 121 Coefficient of Variation VG40 – R%

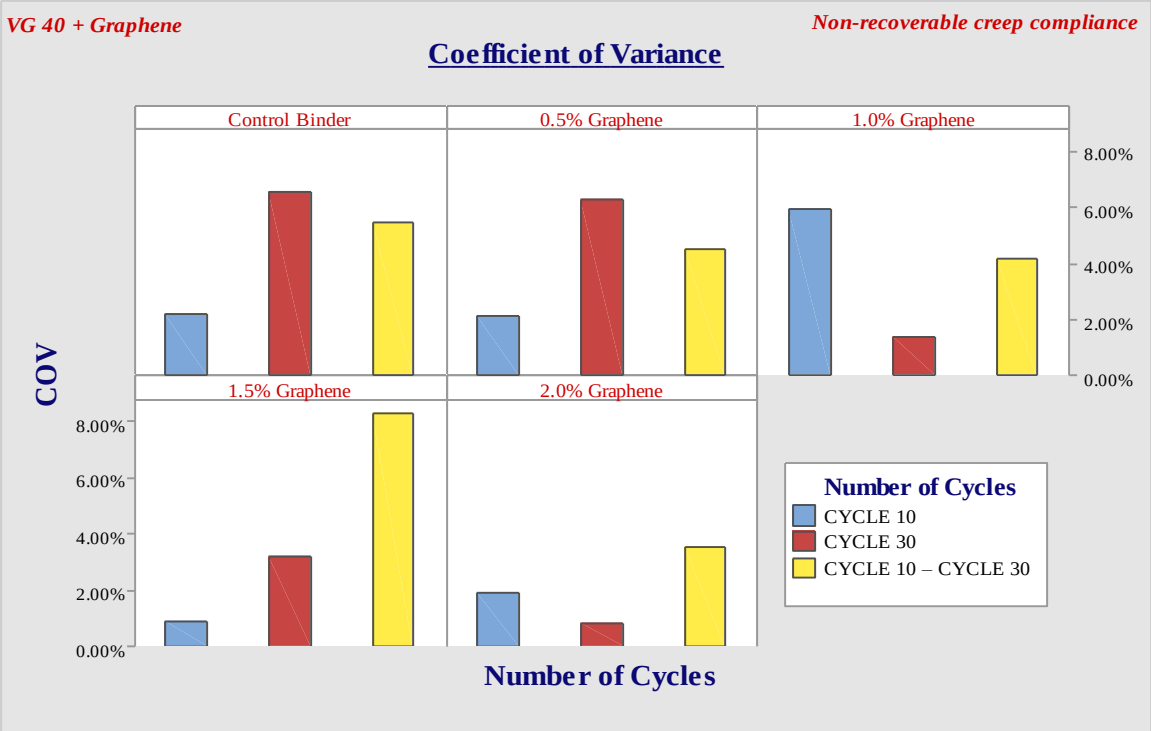

Figure 122 Coefficient of Variation VG40 – Jnr

Table 23 Coefficient of variance VG30

VG30		CYCLE 10	CYCLE 30	CYCLE 10 – CYCLE 30
Control	**R%**	5.78 %	1.68 %	3.72 %
Binder	**Jnr**	4.28 %	4.2 %	19.53 %
0.5%	**R%**	16.4 %	13.44 %	15.87 %
Graphene	**Jnr**	2.27%	12.5 %	10.54 %
1%	**R%**	6.60 %	1.74 %	7.71 %
Graphene	**Jnr**	3.40 %	0.64 %	3.48 %
1.5%	**R%**	8.69 %	1.55 %	8.17 %
Graphene	**Jnr**	2.64 %	0.88 %	2.23 %
2%	**R%**	15.04 %	3.63 %	16.46 %
Graphene	**Jnr**	2.28 %	1.23 %	5.91 %

Table 24 Coefficient of variance VG40

VG40		CYCLE 10	CYCLE 30	CYCLE 10 – CYCLE 30
Control	**R%**	3.86 %	2.97 %	2.83 %
Binder	**Jnr**	2.21 %	6.53 %	5.44 %
0.5%	**R%**	9.56 %	6.58 %	12.47 %
Graphene	**Jnr**	2.14 %	6.27 %	4.49 %
1%	**R%**	11.54 %	2.48 %	8.24 %
Graphene	**Jnr**	5.94 %	1.37 %	4.15 %
1.5%	**R%**	2.70 %	4.78 %	14.17 %
Graphene	**Jnr**	0.91 %	3.18 %	8.29 %
2%	**R%**	2.68 %	2.34 %	8.61 %
Graphene	**Jnr**	1.90 %	0.83 %	3.53 %

4.3.THERMAL CONDUCTIVITY

Graphene has the highest thermal conductivity ever known to the world in the whole universe and has be used to augment the thermal conductivity of a material by forming composites (Wei and Qu 2012). It has been observed that augmenting the thermal conductivity characteristics of the asphalt binder reduces the temperature gradient difference in the asphalt binder and mixture (Zhang et al. 2019). The enhancement of thermal conductivity of asphalt binder is translated into the asphalt mixtures as well which imparts a reduction in the temperature gradient of the pavement and also utilizes less energy in self-healing of asphalt binder pavements (Wang et al. 2017). This enhancement of thermal conductivity of the binder could improve the heat sink effect of the binder and making UHI indifferent from flexible pavement researcher's perspective. The thermal property of the graphene modified asphalt binder tends to show an enhancement in thermal conductivity for both VG30 and VG40 binder. Figure 122 illustrates the thermal conductivity of the graphene modified asphalt binder. The thermal conductivity of the VG30 asphalt binder as observed was 0.1563 W / m.K and with addition of graphene the thermal conductivity of the binder has augmented. The thermal conductivity of 0.5%, 1%, 1.5% and 2% dosages are 0.188 W / m.K, 0.229 W / m.K, 0.237 W / m.K and 0.247 W / m.K respectively. The thermal conductivity has improved

in the asphalt binder by 20.87%, 46.69%, 46.69%, and 51.71% for 0.5%, 1%, 1.5% and 2% respectively. Figure 123 illustrates the thermal conductivity of the graphene modified asphalt binder. The thermal conductivity of the VG40 asphalt binder as observed was 0.1564 W / m.K, there is a negligible difference between thermal conductivity of VG30 and VG40. The thermal conductivity of 0.5%, 1%, 1.5% and 2% dosages are 0.201 W / m.K, 0.225 W / m.K, 0.254 W / m.K and 0.290 W / m.K respectively. The thermal conductivity has improved in the asphalt binder by 28.47%, 44.37%, 62.89% and 85.56% for 0.5%, 1%, 1.5% and 2% respectively, the results are tabulated in Table 25.

Table 25 Thermal conductivity VG30 and VG40

Grade	Thermal Conductivity [W/ m.K]				
	Control Binder	**0.5% Graphene**	**1.0% Graphene**	**1.5% Graphene**	**2.0% Graphene**
VG30	0.1563	0.1889	0.2293	0.2371	0.2479
VG40	0.1564	0.2010	0.2259	0.2548	0.2903

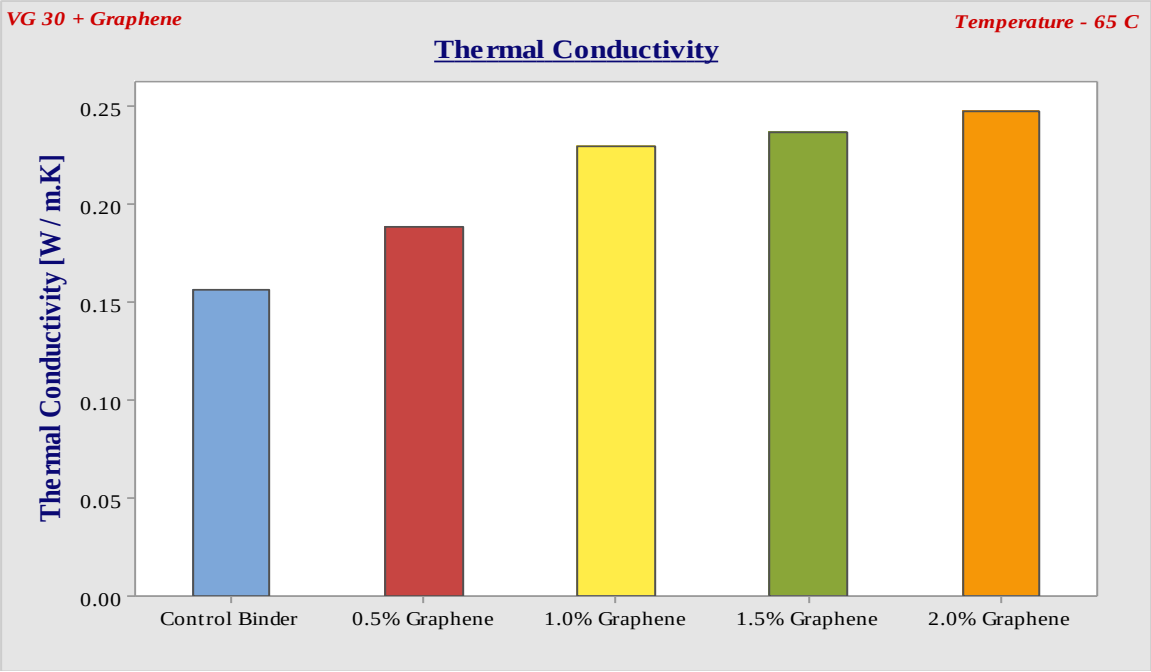

Figure 123 Thermal Conductivity VG30

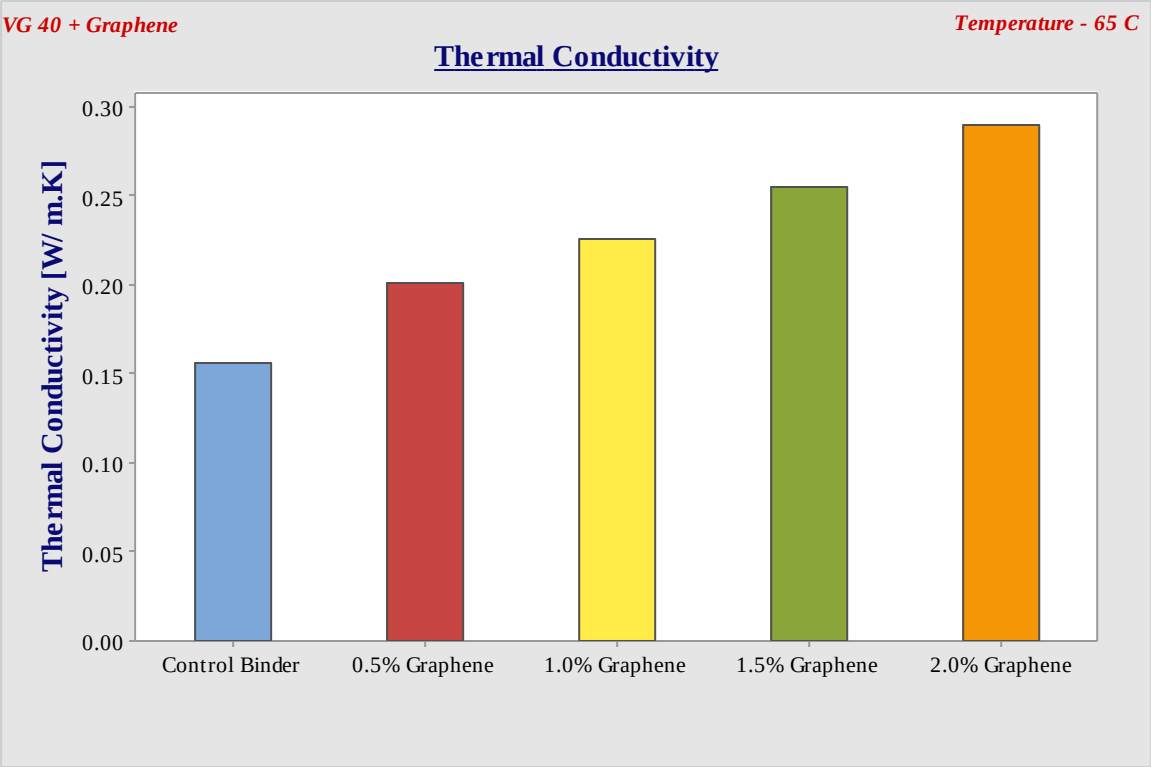

Figure 124 Thermal Conductivity VG40

Chapter 5 STATISTICAL MODELING

5.1.INTRODUCTION

(Peters 2001) describes use of statistical analysis for experimental data as a tool for measuring the similarities or differences between two (more) different materials or same material. One of many statistical tests one of the most sort after and illustrative in characterizing the data set to model the effects of any modification or treatment is analysis of variance (ANOVA). ANOVA analyses the interactions amongst a data set or groups with an independent factor (one-way) or two factors (two-way) or three factors (three-way) .Two-way ANOVA was implemented by (Ali et al. 2018) to establish the significance of adding various waxes and additives with varying grades of asphalt binder. In this study varying proportions / dosages with varying stress levels in the MSCR test were considered to be the two independent factors but the analysis was not a success thus a non-parametric test was utilized. The two-way ANOVA follows six prerequisite assumptions to be qualified by the sample data set (Toothaker and Newman 1994). ANOVA is a parametric test which implies that the data set should be normally distributed and if the sample fails to follow the condition then the results obtained by ANOVA are erroneous, to avoid any discrepancies non-parametric tests such as Wilcoxon, Kruskal Wallis H test, Mann-Whitney test etc., could be implemented (Nahm 2016). In this study Kruskal Wallis H test was used to analyze the effects of proportion and stress level to the asphalt binder. Kruskal Wallis H test is an equivalent to one-way ANOVA and is rank based test (Kruskal and Wallis 1952). The analysis is further discussed below.

5.2.TWO-WAY ANOVA

The significance level of the data set with regard to proportion / dosage of the asphalt and the stress levels applied was observed using SPSS. Before commencing analysis of variance ANOVA there are 6 assumptions that need to be championed. The assumptions and the MSCR test data response in given in Table 26:

Table 26 Assumptions for Two-way ANOVA

Assumption	Description	Response	Remark
Continuity	The measured quantity should be without any discrepancies to the ordinal groups.	The data was in percentage for recovery and kPa^{-1} for Jnr.	Passing
Ordinal variables	The independent variables should consist of two or more categories.	The proportions / dosage consisted of 5 categories and stress level consisted of 8 categories.	Passing
Independent observations	There must not be any relation in the observations in groups and in between the groups.	The data was independent for each group.	Passing
No significant outliers	There should be considerable variation from the mean value. Large varied are terms as outliers	The number of outliers was high as shown in Figure 125.	Failed
Normality	The data should be normally distributed.	The data was not normally distributed, though with the help of transformation data was normalized as shown in Figures .	Failed but normalized by transformation.
Homogeneity	There shall be homogeneity of variance for the categories of the independent variables.	Levene's test was conducted to observe this assumption and null hypothesis of a homogeneous data set was rejected due to significance level less than 0.05.	Failed

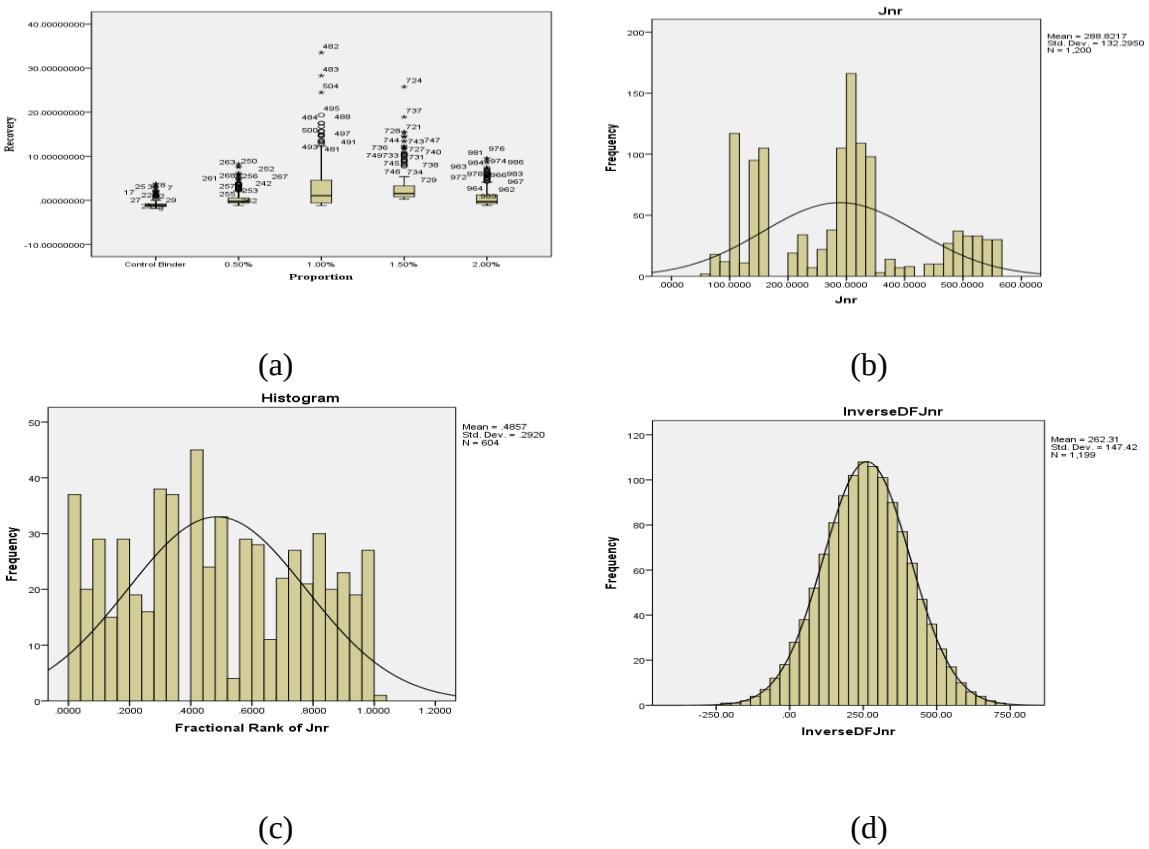

Figure 125 (a) Outliers in the Data Set Represented by Box lot to Show the Data Redundancy Beyond Variance of the Data (b) Raw Data not Observing a Normal Distribution (c) Fractional Ranking Used to Transform into a Normally Distributed Curve by Inverse Differential Function (d) Normal Distribution of the Data by Inverse Differential Function.

After failing to comply to the assumptions of ANOVA a non-parametric test Kruskal – Wallis H test (KH – test) was conducted though the KH - test does not observe the interactions but the KH - test suggests the ranks of the data and the statistical significance of the data.

5.3.KRUSKAL – WALLIS H TEST

The test suggests the ranks of the a particular data set which is either based on the variation from the mean or from the median of the data, the variation from the mean or median depends on the similarity of the data. If the data has a similar shape e.g. a bell curve but without normalization then the data is said to have a rank system based on the variation from the median of the data set and if the data is having an irregular shape as shown in Figure (b), then the data is ranked based on the mean ranking system. The

Kruskal – Wallis H test is followed after fulfilling of four assumptions as listed in Table 27.

Table 27 List of assumptions for Kruskal – Wallis H test

	Assumption	Description	Response	Remark
1.	**Ordinal Scale**	The data should be one dimensional or continuous.	The data is ordinal and one dimensional in nature.	Passed.
2.	**Two or more categorical groups**	The dependent variable should consist of two or more groups.	The data is categorized as per proportion / dosage and stress levels.	Passed.
3.	**Independence of observation**	The data should independent of any relations among the groups and in between the groups.	The data was independent and did not form any relations.	Passed.
4.	**Same variability**	The data should form similar curves for each group.	The data does not conform to similar shapes / similar distribution of the graphs	The ranking is based on the mean ranking system.

Null hypothesis for the test was that the mean ranks of the data are same across all groups and the alternate hypothesis for the data was that mean ranks are not same. Tables 29, 31, 33, 35, 37, 39, 41 and 43 lists the statistical significance of the data, which illustrates that the p-value of the data is less than 0.05 which implies highly significant difference between the mean of the data set for the different dosages and the stress levels categories. Also the Chi-square (χ^2) value is much greater (>>) than the critical Chi-square (χ^2) value as listed in Chi-square (χ^2) tables for degree of freedom 4 and 7 (*number of groups*

– *1)* and level of significance 0.05. Therefore, Type I error is encountered, hence, rejecting the null hypothesis.

Rank as the term indicates the standing of the data point in the data set, in Kruskal Wallis H test the lowest value is categorized as lowest rank. The mean rank suggests the standing of the mean value of the categorical value in the overall data set. Table 28, 30, 32, 34, 36, 38, 40 and 42 list the mean rank of the groups compared. The purpose of mean rank is to illustrate the mean value of the rank wise distribution of the data, the lower the mean rank value lower is the mean value of the group. The mean rank value for control binder is lowest for the dependent variable recovery percentage with a value of 208.28 and 209.07 for VG30 – cycle 10 and VG40 – cycle 10 respectively, similarly for VG30 – 30 cycles and VG 40 – 40 cycles mean rank value for control binder is lowest with 746.86 and 643.3 respectively, 30 cycle test has higher mean rank value than the 10 cycle test due to large data set and data redundancy due to repetition of more cycles in the 30 cycle test. Similarly the mean rank of the stress levels follows with the lowest stress level comprising of highest mean rank for the recovery percentage and the lowest mean rank for the Jnr value. Though, a similar trend is not followed for all the stress levels as the data varies irregularly over the stress levels which could be associated to the efficiency of DSR to apply stresses / strains. The post-hoc pairwise analysis of the data was carried out by two pair independent Kruskal Wallis H test in SPSS as illustrated in the model Figures generated using SPSS in Figures 126 – 133.

Table 28 List pf Ranks - VG30 Cycle 10 (Proportion / Dosage)

VG30 – Cycle 10			
	Proportion	**N**	**Mean Rank**
Recovery Percentage	Control Binder	240	208.28
	0.5% Graphene	240	489.58
	1% Graphene	240	897.74
	1.5% Graphene	240	897.74
	2% Graphene	240	509.17
	Total	1200	
Non-recoverable	Control Binder	240	1080.50

creep compliance	0.5% Graphene	240	691.83
	1% Graphene	240	240.50
	1.5% Graphene	240	240.50
	2% Graphene	240	749.18
	Total	1200	

Table 29 Statistical Tests VG30 Cycle 10 – (Proportion / Dosage)

Test Statistics[a,b]		
	Recovery Percentage	**Non-recoverable creep compliance**
Chi-Square	701.786	1039.224
df	4	4
Asymp. Sig.	<0.05	<0.05
a. Kruskal Wallis Test		
b. Grouping Variable: Proportion		

Table 30 List of Ranks - VG30 Cycle 10 (Stress Levels)

VG30 – Cycle 10			
	Stress_Level	**N**	**Mean Rank**
Recovery Percentage	0.1 kPa	10	64.60
	0.5 kPa	10	67.10
	1.0 kPa	10	64.80
	1.5 kPa	10	30.00
	2.0 kPa	10	36.90
	2.5 kPa	10	39.60
	3.0 kPa	10	6.20
	3.2 kPa	10	14.80
	Total	80	
Non-recoverable creep compliance	0.1 kPa	10	25.50
	0.5 kPa	10	13.40

	1.0 kPa	10	7.60
	1.5 kPa	10	65.50
	2.0 kPa	10	45.50
	2.5 kPa	10	35.50
	3.0 kPa	10	75.50
	3.2 kPa	10	55.50
	Total	80	

Table 31 Statistical Tests VG30 Cycle 10 – (Stress Levels)

Test Statistics[a,b]		
	Recovery Percentage	**Non-recoverable creep compliance**
Chi-Square	71.109	77.163
df	7	7
Asymp. Sig.	<0.05	<0.05
a. Kruskal Wallis Test		
b. Grouping Variable: Stress_level		

Table 32 List of Ranks – VG40 Cycle 10 (Proportion)

VG40 – Cycle 10			
	Proportion	**N**	**Mean Rank**
Recovery Percentage	Control Binder	240	209.07
	0.5% Graphene	240	433.55
	1% Graphene	240	873.70
	1.5% Graphene	240	879.43
	2% Graphene	240	606.75
	Total	1200	
Non-recoverable creep compliance	Control Binder	240	1080.50
	0.5% Graphene	240	838.14
	1% Graphene	240	267.36
	1.5% Graphene	240	214.28

	2% Graphene	240	602.22
	Total	1200	

Table 33 Statistical Tests VG40 Cycle 10 – (Proportion)

Test Statistics[a,b]		
	Recovery Percentage	**Non-recoverable creep compliance**
Chi-Square	666.578	1093.133
df	4	4
Asymp. Sig.	<0.05	<0.05
a. Kruskal Wallis Test		
b. Grouping Variable: Proportion		

Table 34 List of Ranks - VG40 Cycle 10 (Stress Levels)

VG40 – Cycle 10			
	Stress Level	**N**	**Mean Rank**
Recovery Percentage	0.1 kPa	10	72.20
	0.5 kPa	10	62.70
	1.0 kPa	10	61.60
	1.5 kPa	10	37.50
	2.0 kPa	10	34.60
	2.5 kPa	10	34.30
	3.0 kPa	10	12.70
	3.2 kPa	10	8.40
	Total	80	
Non-recoverable creep compliance	0.1 kPa	10	8.80
	0.5 kPa	10	23.80
	1.0 kPa	10	13.90
	1.5 kPa	10	48.40

	2.0 kPa	10	52.60
	2.5 kPa	10	35.50
	3.0 kPa	10	75.20
	3.2 kPa	10	65.80
	Total	80	

Table 35 Statistical Tests VG40 Cycle 10 – (Stress Levels)

Test Statistics[a,b]		
	Recovery Percentage	**Non-recoverable creep compliance**
Chi-Square	70.897	75.358
df	7	7
Asymp. Sig.	<0.05	<0.05
a. Kruskal Wallis Test		
b. Grouping Variable: Stress Level		

Table 36 List of Ranks – VG30 Cycle 30 (Proportion)

VG30 – Cycle 30			
	Proportion	**N**	**Mean Rank**
Recovery Percentage	Control Binder	720	746.86
	0.5% Graphene	720	1535.12
	1% Graphene	720	2886.29
	1.5% Graphene	720	2434.41
	2% Graphene	720	1399.82
	Total	3600	
Non-recoverable creep compliance	Control Binder	720	3232.69
	0.5% Graphene	720	2053.01
	1% Graphene	720	403.00
	1.5% Graphene	720	1038.00

	2% Graphene	720	2275.80
	Total	3600	

Table 37 Statistical Tests VG30 Cycle 30 – (Proportion / Dosage)

Test Statistics[a,b]		
	Recovery Percentage	**Non-recoverable creep compliance**
Chi-Square	1947.391	3249.271
df	4	4
Asymp. Sig.	<0.05	<0.05
a. Kruskal Wallis Test		
b. Grouping Variable: Proportion		

Table 38 List of Ranks – VG30 Cycle 30 (Stress Levels)

VG30 – Cycle 30			
	Stress Level	**N**	**Mean Rank**
Recovery Percentage	0.1 kPa	450	3196.51
	0.5 kPa	450	2335.77
	1.0 kPa	450	1979.94
	1.5 kPa	450	1735.79
	2.0 kPa	450	1536.94
	2.5 kPa	450	1388.08
	3.0 kPa	450	1040.05
	3.2 kPa	450	1190.92
	Total	3600	
Non-recoverable creep compliance	0.1 kPa	450	1282.15
	0.5 kPa	450	1568.23
	1.0 kPa	450	1684.06
	1.5 kPa	450	1789.64
	2.0 kPa	450	1882.81

	2.5 kPa	450	1971.23
	3.0 kPa	450	2081.03
	3.2 kPa	450	2144.84
	Total	3600	

Table 39 Statistical Tests VG30 Cycle 30 – (Stress Levels)

Test Statistics[a,b]		
	Recovery Percentage	**Non-recoverable creep compliance**
Chi-Square	1441.753	237.226
df	7	7
Asymp. Sig.	<0.05	<0.05
a. Kruskal Wallis Test		
b. Grouping Variable: Stress Level		

Table 40 List of Ranks – VG40 Cycle 30 (Proportion)

VG40 – Cycle 30			
	Proportion	**N**	**Mean Rank**
Recovery Percentage	Control Binder	720	653.03
	0.5% Graphene	720	1266.89
	1% Graphene	720	2672.78
	1.5% Graphene	720	2497.93
	2% Graphene	720	1911.87
	Total	3600	
Non-recoverable creep compliance	Control Binder	720	3240.12
	0.5% Graphene	720	2519.29
	1% Graphene	720	561.83
	1.5% Graphene	720	944.22
	2% Graphene	720	1737.05
	Total	3600	

Table 41 Statistical Tests VG40 Cycle 30 – (Proportion / Dosage)

Test Statistics[a,b]		
	Recovery Percentage	**Non-recoverable creep compliance**
Chi-Square	1906.893	3239.565
df	4	4
Asymp. Sig.	<0.05	<0.05
a. Kruskal Wallis Test		
b. Grouping Variable: Proportion		

Table 42 List of Ranks – VG40 Cycle 30 (Stress Levels)

VG40 – Cycle 30			
	Stress Level	**N**	**Mean Rank**
Recovery Percentage	0.1 kPa	450	3229.21
	0.5 kPa	450	2296.83
	1.0 kPa	450	1989.73
	1.5 kPa	450	1735.21
	2.0 kPa	450	1538.17
	2.5 kPa	450	1374.23
	3.0 kPa	450	1052.29
	3.2 kPa	450	1188.34
	Total	3600	
Non-recoverable creep compliance	0.1 kPa	450	1252.97
	0.5 kPa	450	1578.85
	1.0 kPa	450	1767.14
	1.5 kPa	450	1781.77
	2.0 kPa	450	1873.05
	2.5 kPa	450	2042.79
	3.0 kPa	450	2030.73

	3.2 kPa	450	2076.69
	Total	3600	

Table 43 Statistical Tests VG40 Cycle 30 – (Stress Levels)

Test Statistics[a,b]		
	Recovery Percentage	**Non-recoverable creep compliance**
Chi-Square	1463.220	226.451
df	7	7
Asymp. Sig.	<0.05	<0.05
a. Kruskal Wallis Test		
b. Grouping Variable: Stress Level		

Table 44 lists the variance in the recovery percentages for stress level and different proportion of the graphene dosages from χ^2 statistics by employing the formula given in Equation 11. The variance in the VG30 asphalt binder for cycle 10 test was computed to be 5.93% and for VG40 cycle 10 was 5.91% which illustrates that the degree of variation in the data for recovery percentage for different stress levels in both the grades for cycle 10 test was almost equal whereas the variation percentage following the proportion of graphene dosage was ~60% for both the binders. The cycle 30 test results illustrate a higher degree of variance for both the binders of about ~40% for different stress levels and ~55% for different proportions for both the binders, which signifies that 30 cycle test varied in the data values quite significantly. Table 45 lists the variance in the data set of non – recoverable creep compliance which gives the same results as was observed for recovery but varies in the results for stress level values for 30 cycle where it varies only ~ 7% instead of ~40%. The proportion parameter shows data variation of ~90%. Pairwise distribution is given in Figures 126 – 133.

$$\boldsymbol{\eta^2 = \frac{\chi^2}{N-1}} \qquad \textbf{Equation 11}$$

Where,

$\boldsymbol{\eta^2}$ – variance in the data

χ^2 – Chi square value

N – Number of data points.

Table 44 The Degree of Variance $\boldsymbol{\eta^2}$as per $\boldsymbol{\chi^2}$ Statistics for Recovery Percentage

Parameter	**Grade**	**Number of Cycles**	$\boldsymbol{\chi^2}$	**N**	$\boldsymbol{\eta^2}$
Stress Level	VG30	10	71.109	1200	5.93%
	VG40	10	70.897	1200	5.91%
	VG30	30	1441.753	3600	40.05%
	VG40	30	1463.2	3600	40.65%
Proportion	VG30	10	701.787	1200	58.53%
	VG40	10	666.587	1200	55.59%
	VG30	30	1947.391	3600	54.10%
	VG40	30	1906.893	3600	52.98%

Table 45 The Degree of Variance $\boldsymbol{\eta^2}$as per $\boldsymbol{\chi^2}$ Statistics for Non – Recoverable Creep Compliance

Parameter	**Grade**	**Number of Cycles**	$\boldsymbol{\chi^2}$	**N**	$\boldsymbol{\eta^2}$
Stress Level	VG30	10	77.163	1200	6.44%
	VG40	10	75.358	1200	6.29%
	VG30	30	237.226	3600	6.59%

	VG40	30	226.451	3600	6.29%
Proportion	VG30	10	1039.22	1200	86.67%
	VG40	10	1093.13	1200	91.17%
	VG30	30	3249.33	3600	90.28%
	VG40	30	3239.57	3600	90.01%

Figure 126 illustrates that the mean ranks of 0.5% and 2% graphene dosage are in a close vicinity, thus the pairwise comparison with a significance of 1 reiterates the null hypothesis to be true i.e., the mean of the two groups is same. The result signifies that the dosage of 0.5% graphene to VG 30 asphalt is obtains the same recovery percentage effect as does the 2% graphene dosage. Rest all the dosages vary with each other. Figure 127 shows that the mean rank of 1.5% dosage is in the neighborhood of mean rank of 1% graphene dosage and the significance of 1 implies that graphene dosages of 1% and 1.5% to VG30 had a similar effect on reducing the non-recoverable creep compliance (Jnr). Figure 128 illustrates that the 1% and 1.5% dosages obtain a similar effect on the recovery behavior of VG40 asphalt binder and Figure 129 describes that 1% and 1.5% dosages have 93.5% probability to have a similar effect Jnr value of the binder. Both the results mentioned above describe the response of asphalt binder for MSCR – Cycle 10 test. The results of MSCR – Cycle 30 test are further discussed. Figure 130 illustrates that the 0.5% and 2% graphene dosages show a similar effect on the VG30 asphalt binder recovery percentage but only have a probability of 13.4% to be same. Figure 131 illustrates a distinctive result where none of the graphene dosages have a similar effect on VG30 asphalt binder, though it represents a mean rank of 403 for 1% graphene dosage which is the lowest, thus, signifying that 1% graphene dosage has the maximum effect in augmenting the stiffness of the VG30 asphalt binder. Also Figures 132 and 133 shows that none of the binders is having a similar effect of recovery percentage or the Jnr value. The results suggest that the 30 cycle test is more distinctive and provides a more elaborative data set.

Pairwise Comparisons of Proportion

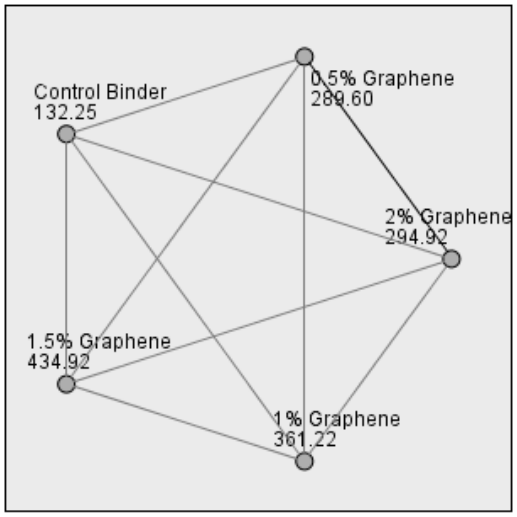

Each node shows the sample average rank of Proportion.

Sample1-Sample2	Test Statistic	Std. Error	Std. Test Statistic	Sig.	Adj.Sig.
Control Binder-0.5% Graphene	-157.355	22.346	-7.042	.000	.000
Control Binder-2% Graphene	-162.675	22.528	-7.221	.000	.000
Control Binder-1% Graphene	-228.975	22.528	-10.164	.000	.000
Control Binder-1.5% Graphene	-302.675	22.528	-13.435	.000	.000
0.5% Graphene-2% Graphene	-5.320	22.346	-.238	.812	1.000
0.5% Graphene-1% Graphene	-71.620	22.346	-3.205	.001	.014
0.5% Graphene-1.5% Graphene	-145.320	22.346	-6.503	.000	.000
2% Graphene-1% Graphene	66.300	22.528	2.943	.003	.033
2% Graphene-1.5% Graphene	140.000	22.528	6.214	.000	.000
1% Graphene-1.5% Graphene	-73.700	22.528	-3.271	.001	.011

Each row tests the null hypothesis that the Sample 1 and Sample 2 distributions are the same.
Asymptotic significances (2-sided tests) are displayed. The significance level is .05.

Figure 126 Pairwise Comparison Kruskal Wallis H test - Recovery Percentage [VG30-Cycle 10]

Pairwise Comparisons of Proportion

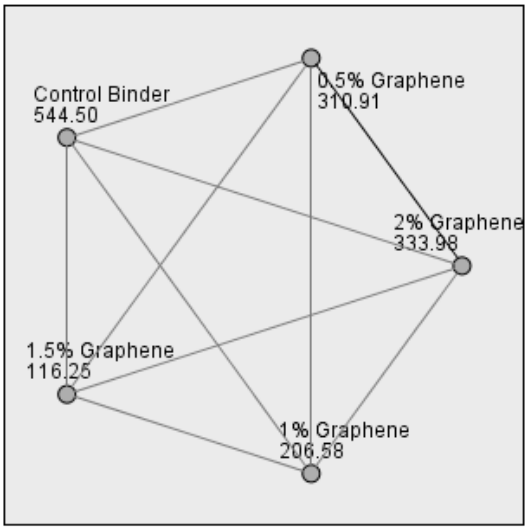

Each node shows the sample average rank of Proportion.

Sample1-Sample2	Test Statistic	Std. Error	Std. Test Statistic	Sig.	Adj.Sig.
1.5% Graphene-1% Graphene	90.333	22.528	4.010	.000	.001
1.5% Graphene-0.5% Graphene	194.661	22.346	8.711	.000	.000
1.5% Graphene-2% Graphene	-217.725	22.528	-9.664	.000	.000
1.5% Graphene-Control Binder	428.250	22.528	19.009	.000	.000
1% Graphene-0.5% Graphene	104.328	22.346	4.669	.000	.000
1% Graphene-2% Graphene	-127.392	22.528	-5.655	.000	.000
1% Graphene-Control Binder	337.917	22.528	15.000	.000	.000
0.5% Graphene-2% Graphene	-23.064	22.346	-1.032	.302	1.000
0.5% Graphene-Control Binder	233.589	22.346	10.453	.000	.000
2% Graphene-Control Binder	210.525	22.528	9.345	.000	.000

Each row tests the null hypothesis that the Sample 1 and Sample 2 distributions are the same.
Asymptotic significances (2-sided tests) are displayed. The significance level is .05.

Figure 127 Pairwise Comparison Kruskal Wallis H test - Jnr [VG30-Cycle 10]

Pairwise Comparisons of Proportion

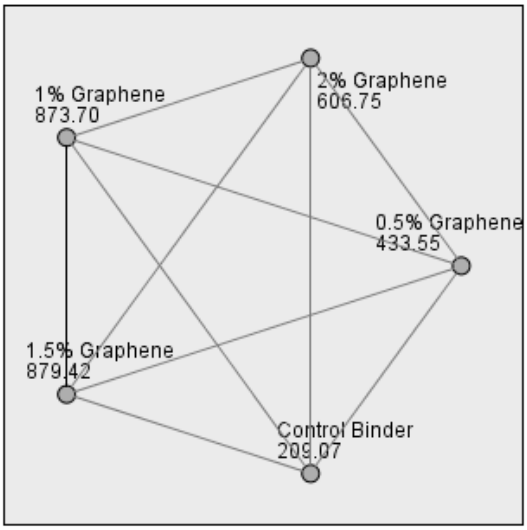

Each node shows the sample average rank of Proportion.

Sample1-Sample2	Test Statistic	Std. Error	Std. Test Statistic	Sig.	Adj.Sig.
Control Binder-0.5% Graphene	-224.483	31.636	-7.096	.000	.000
Control Binder-2% Graphene	-397.675	31.636	-12.570	.000	.000
Control Binder-1% Graphene	-664.633	31.636	-21.009	.000	.000
Control Binder-1.5% Graphene	-670.354	31.636	-21.190	.000	.000
0.5% Graphene-2% Graphene	-173.192	31.636	-5.475	.000	.000
0.5% Graphene-1% Graphene	-440.150	31.636	-13.913	.000	.000
0.5% Graphene-1.5% Graphene	-445.871	31.636	-14.094	.000	.000
2% Graphene-1% Graphene	266.958	31.636	8.438	.000	.000
2% Graphene-1.5% Graphene	272.679	31.636	8.619	.000	.000
1% Graphene-1.5% Graphene	-5.721	31.636	-.181	.856	1.000

Each row tests the null hypothesis that the Sample 1 and Sample 2 distributions are the same.
Asymptotic significances (2-sided tests) are displayed. The significance level is .05.

Figure 128 Pairwise Comparison Kruskal Wallis H test - Recovery Percentage [VG40-Cycle 10]

Pairwise Comparisons of Proportion

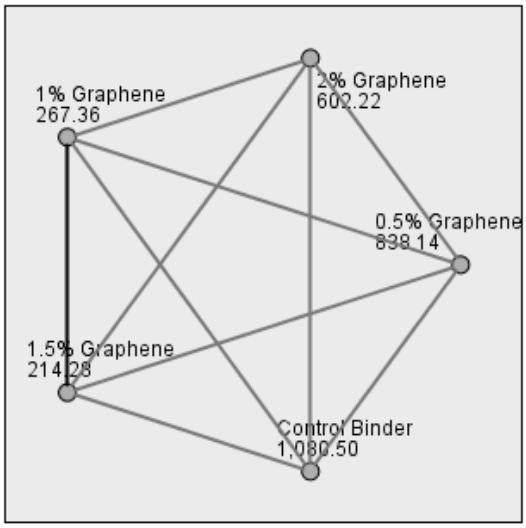

Each node shows the sample average rank of Proportion.

Sample1-Sample2	Test Statistic	Std. Error	Std. Test Statistic	Sig.	Adj.Sig.
1% Graphene-Control Binder	813.138	31.636	25.703	.000	.000
1.5% Graphene-0.5% Graphene	623.858	31.636	19.720	.000	.000
1% Graphene-2% Graphene	-334.858	31.636	-10.585	.000	.000
1.5% Graphene-Control Binder	866.221	31.636	27.381	.000	.000
0.5% Graphene-Control Binder	242.362	31.636	7.661	.000	.000
1% Graphene-0.5% Graphene	570.775	31.636	18.042	.000	.000
2% Graphene-0.5% Graphene	235.917	31.636	7.457	.000	.000
2% Graphene-Control Binder	478.279	31.636	15.118	.000	.000
1.5% Graphene-2% Graphene	-387.942	31.636	-12.263	.000	.000
1.5% Graphene-1% Graphene	53.083	31.636	1.678	.093	.934

Each row tests the null hypothesis that the Sample 1 and Sample 2 distributions are the same.
Asymptotic significances (2-sided tests) are displayed. The significance level is .05.

Figure 129 Pairwise Comparison Kruskal Wallis H test - Jnr [VG40-Cycle 10]

Pairwise Comparisons of Proportion

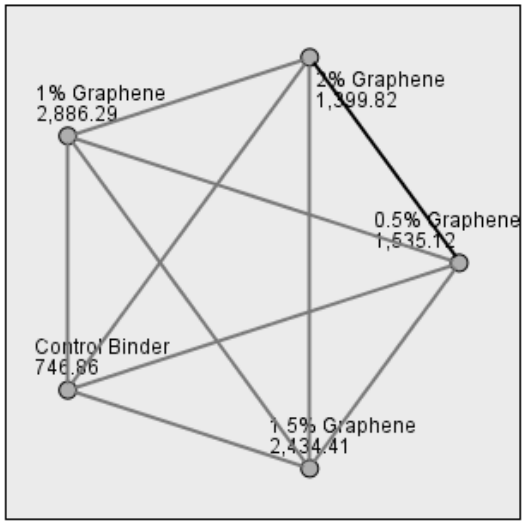

Each node shows the sample average rank of Proportion.

Sample1-Sample2	Test Statistic	Std. Error	Std. Test Statistic	Sig.	Adj.Sig.
Control Binder-2% Graphene	-652.954	54.780	-11.920	.000	.000
Control Binder-0.5% Graphene	-788.256	54.780	-14.390	.000	.000
Control Binder-1.5% Graphene	-1,687.549	54.780	-30.806	.000	.000
Control Binder-1% Graphene	-2,139.422	54.780	-39.055	.000	.000
2% Graphene-0.5% Graphene	135.301	54.780	2.470	.014	.135
2% Graphene-1.5% Graphene	1,034.594	54.780	18.886	.000	.000
2% Graphene-1% Graphene	1,486.468	54.780	27.135	.000	.000
0.5% Graphene-1.5% Graphene	-899.293	54.780	-16.416	.000	.000
0.5% Graphene-1% Graphene	-1,351.167	54.780	-24.665	.000	.000
1.5% Graphene-1% Graphene	451.874	54.780	8.249	.000	.000

Each row tests the null hypothesis that the Sample 1 and Sample 2 distributions are the same.
Asymptotic significances (2-sided tests) are displayed. The significance level is .05.

Figure 130 Pairwise Comparison Kruskal Wallis H test - Recovery Percentage [VG30-Cycle 30]

Pairwise Comparisons of Proportion

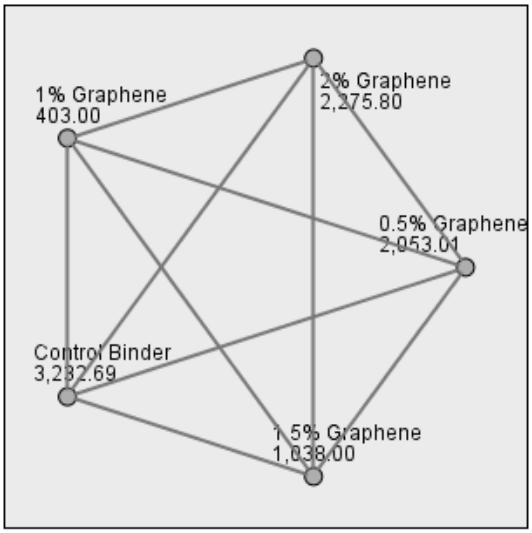

Each node shows the sample average rank of Proportion.

Sample1-Sample2	Test Statistic	Std. Error	Std. Test Statistic	Sig.	Adj.Sig.
1% Graphene-1.5% Graphene	-635.000	54.780	-11.592	.000	.000
1% Graphene-0.5% Graphene	1,650.006	54.780	30.121	.000	.000
1% Graphene-2% Graphene	-1,872.801	54.780	-34.188	.000	.000
1% Graphene-Control Binder	2,829.693	54.780	51.656	.000	.000
1.5% Graphene-0.5% Graphene	1,015.006	54.780	18.529	.000	.000
1.5% Graphene-2% Graphene	-1,237.801	54.780	-22.596	.000	.000
1.5% Graphene-Control Binder	2,194.693	54.780	40.064	.000	.000
0.5% Graphene-2% Graphene	-222.796	54.780	-4.067	.000	.000
0.5% Graphene-Control Binder	1,179.688	54.780	21.535	.000	.000
2% Graphene-Control Binder	956.892	54.780	17.468	.000	.000

Each row tests the null hypothesis that the Sample 1 and Sample 2 distributions are the same.
Asymptotic significances (2-sided tests) are displayed. The significance level is .05.

Figure 131 Pairwise Comparison Kruskal Wallis H test - Jnr [VG30-Cycle 30]

Pairwise Comparisons of Proportion

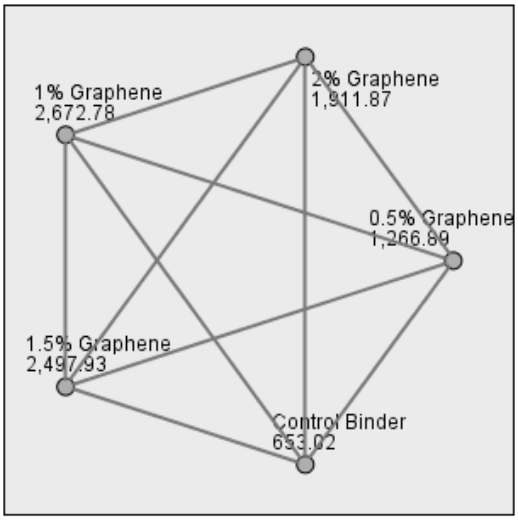

Each node shows the sample average rank of Proportion.

Sample1-Sample2	Test Statistic	Std. Error	Std. Test Statistic	Sig.	Adj.Sig.
Control Binder-0.5% Graphene	-613.864	54.780	-11.206	.000	.000
Control Binder-2% Graphene	-1,258.844	54.780	-22.980	.000	.000
Control Binder-1.5% Graphene	-1,844.908	54.780	-33.679	.000	.000
Control Binder-1% Graphene	-2,019.758	54.780	-36.870	.000	.000
0.5% Graphene-2% Graphene	-644.981	54.780	-11.774	.000	.000
0.5% Graphene-1.5% Graphene	-1,231.044	54.780	-22.473	.000	.000
0.5% Graphene-1% Graphene	-1,405.894	54.780	-25.664	.000	.000
2% Graphene-1.5% Graphene	586.064	54.780	10.699	.000	.000
2% Graphene-1% Graphene	760.914	54.780	13.890	.000	.000
1.5% Graphene-1% Graphene	174.850	54.780	3.192	.001	.014

Each row tests the null hypothesis that the Sample 1 and Sample 2 distributions are the same.
Asymptotic significances (2-sided tests) are displayed. The significance level is .05.

Figure 132 Pairwise Comparison Kruskal Wallis H test - Recovery Percentage [VG40-Cycle 30]

Pairwise Comparisons of Proportion

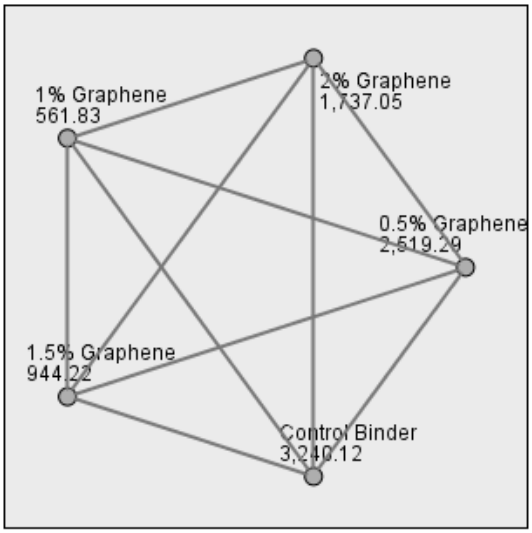

Each node shows the sample average rank of Proportion.

Sample1-Sample2	Test Statistic	Std. Error	Std. Test Statistic	Sig.	Adj.Sig.
1% Graphene-1.5% Graphene	-382.393	54.780	-6.981	.000	.000
1% Graphene-2% Graphene	-1,175.221	54.780	-21.454	.000	.000
1% Graphene-0.5% Graphene	1,957.460	54.780	35.733	.000	.000
1% Graphene-Control Binder	2,678.288	54.780	48.892	.000	.000
1.5% Graphene-2% Graphene	-792.828	54.780	-14.473	.000	.000
1.5% Graphene-0.5% Graphene	1,575.067	54.780	28.753	.000	.000
1.5% Graphene-Control Binder	2,295.894	54.780	41.911	.000	.000
2% Graphene-0.5% Graphene	782.239	54.780	14.280	.000	.000
2% Graphene-Control Binder	1,503.067	54.780	27.438	.000	.000
0.5% Graphene-Control Binder	720.828	54.780	13.159	.000	.000

Each row tests the null hypothesis that the Sample 1 and Sample 2 distributions are the same.
Asymptotic significances (2-sided tests) are displayed. The significance level is .05.

Figure 133 Pairwise Comparison Kruskal Wallis H test - Jnr [VG30-Cycle 30]

Chapter 6 CONCLUSION

Experimental investigation of the augmented physical, rheological and thermal properties of graphene modified asphalt binder was established using BIS codes, ASTM, AASHTO and SHRP guidelines. The statistical significance of the MSCR data obtained from DSR was analyzed with non – parametric statistical tests. The conclusions drafted for the graphene additive asphalt binder is listed below:

1. The softening point of asphalt binder increased by 2℃ with the 0.5% addition of graphene and showed no significant difference on a minimum 2℃ thermometric for both asphalt binder grades.
2. The storage stability of binder was not hampered and continued to be stable in compliance to the separation results for both grades.
3. The absolute viscosity of the binder showed clear signs of increment up to 1% graphene dosage and declined within an increment gap of 0.5% for both VG30 and VG40.
4. The stiffness of binder or complex shear modulus (G^*) augmented two folds approximately and decreased the phase shift angle representing a stiffer viscoelastic state of the asphalt binder for both the graphene modified asphalt binders.
5. Likewise rutting parameter $G^*/\sin\delta$ was enhanced significantly with the modification of graphene nanoparticles to the asphalt binder, with 1% being the optimum.
6. The frequency sweep test established an augmented relation between frequency and rheological parameters. Also the black space diagrams illustrated a heightened level of significance for 1% graphene modified asphalt binder.
7. MSCR test is a function of recovery percentage to the non – recoverable creep of the asphalt binder, following which 1% graphene modified binder showed augmented results in terms of recovery percentage and permanent deformation.
8. Jnr *diff* plummeted to two digit values for 1% graphene from a three digit Jnr *diff* value of the control binder
9. Stress sensitivity measured over a spectrum of eight stress levels illustrated a far lesser difference between 0.5 kPa and 3.2 kPa than 0.1 kPa and 3.2 kPa. The

magnitude of difference between the stress levels was lower for Jnr values and higher for recovery percentage for graphene modified binder.

10. The coefficient of variance for the MSCR test cycle 10 and cycle 30 varied moderately, thus establishing a firm idea about the difference in means of the data observed.
11. Thermal conductivity of the asphalt binder augmented with every increment of graphene with highest augmentation of about 85% for 2% graphene dosage.
12. The data obtained from the MSCR test 10 cycle and 30 cycle was neither homogeneous nor normally distributed and had a significant number of outliers. Thus the results were non – parametric.
13. Kruskal – Wallis H test was used to analyze the data with a non – parametric rank based approach, where χ^2 and p – value represented a Type I error in the data which signifies that null hypothesis is be rejected.
14. The null hypothesis is rejected for both 10 cycle and 30 cycle tests and a pairwise comparison showed that the population developed few significant relations for cycle 10 test but none for cycle 30 test which signifies that the cycle 30 data is more distinctive.
15. Addition of graphene augmented various parameters of the asphalt binder and requires more research to garner its possibilities to develop a rut resistant asphalt concrete pavement and thermally engaging surface to reduce UHI.

REFERENCES

Airey, G., Rahimzadeh, B., and Collop, A. (2002). "Linear viscoelastic limits of bituminous binders." *Journal of the Association of Asphalt Paving Technologists - Volume - 71* , 89-115.

Ali, A. W., Kim, H. H., Mazumder, M., Lee, M.-S., and Lee, S.-J. (2018). "Multiple Stress Creep Recovery (MSCR) characterization of polymer modified asphalt binder containing wax additives." *International Journal of Pavement Research and Technology*.

Baochang , Z. a., Man, X., Dewen, Z., and H, Z. (2009). "The effect of styrene butadiene rubber or montmorillonite modification." *Construction and Building Materials, 23*, 3112 - 3117.

Becker, Y., Méndez , M. P., and Rodríguez, Y. (2001). "Poly Modified Asphalt." *Vision Technologica,* 39-50.

Behnood, A., and Gharehveran, M. M. (2019). "Morphology, rheology, and physical properties of polymer-modified asphalt binders." *European Polymer Journal* , 766–791.

Chuah, S., Pan, Z., Sanjayan, J. G., Wang, C. M., and Duan, W. H. (2014). "Nano reinforced cement and concrete composites and new perspective from graphene oxide." *Construction and Building Materials*, 113-124.

Compton, O. C., Jain, B., Dikin, D. A., Abouimrane, A., Amine, K., and Nguyen, S. T. (2011). "Chemically Active Reduced Graphene Oxide with Tunable C/O Ratios." *ACS Nano*, 4380–4391.

Coplantz, J. S., Yapp, M. T., and Finn, F. N. (1993). *"Review of relationships between modified asphalt properties and pavement performance - SHRP - A - 631."* National academy of sciences: Washington, DC

Cucalon, L. G., Kaseer, F., Arámbula-Mercado, E., Martin, A. E., Morian, N., Pournoman, S., and Hajj, E. (2018). "The crossover temperature: significance and application towards engineering balanced recycled binder blends." *Road Materials and Pavement Design*, 2164-7402.

D'Angelo, J. A. (2009). "Effect of Polyphosphoric Acid on Asphalt Binder Properties." *Transportation Research Circular E-C160 - Polyphosphoric Acid Modification of Asphalt Binders: A Workshop*, Transportation Research Board: Minneapolis, Minnesota 27-39.

Ebrahim, A., and El-MaatyBehiry, A. (2012). "Fatigue and rutting lives in flexible pavement." *Ain Shams Engineering Journal*, 367-374.

Eda, G., and Chhowalla, M. (2010). "Chemically Derived Graphene Oxide TowardsLarge-Area Thin-Film Electronics and Optoelectronics." *Advanced materials*, 2392-2415.

Fanga, H., Haddock, J. E., White, T. D., and J, A. (2004). "On the characterization of flexible pavement rutting using creep model-based finite element analysis." *Finite Elements in Analysis and Design*, 49-73.

Faruk, A. N., Lee, S. I., Zhang, J., Naik, B., and Walubita, L. F. (2015). "Measurement of HMA shear resistance potential in the lab: The SimplePunching Shear Test." *Construction and Building Materials*, 62-72.

Ghavanini, F. A., and Theander, H. (2015, January 26). *"Graphene feasibility and foresight study for transport infrastructures."* Chalmers Indusriteknik: Sweden

Hjort, M., Haraldsson, M., and Jansen, J. M. (2008). *"Road Wear from Heavy Vehicles – an overview."* NVF-rapporter: Sverige

Hossain, Z., Ghosh, D., Zaman, M., and Hobson, K. (2016). "Use of the Multiple Stress Creep Recovery (MSCR) Test Method to Characterize Polymer- Modified Asphalt Binders." *Journal of Testing and Evaluation VOL. 44*.

Huang, Y. H. (2004). *"Pavement Analysis and Design."* Uiversity of Kentucky, Upper Saddle River, NJ 07458: Prentics Hall, Pearson Education, Inc.

IS 73:2013. (2013). *"Indian code of Paving Bitumen."* Beureu of Indian Standards: New Delhi

Jain, S., Joshi, Y. P., and Goliya, S. S. (2013). "Design of Rigid and Flexible Pavements by Various Methods & Their Cost Analysis of Each Method." *Int. Journal of Engineering Research and Application* , 119-123.

Jeffry, S. A., Jaya , R. P., Abdul Hassan , N., Yaacob , H., Mirza , J., and Hasyyat, S. (2018). "Effects of nanocharcoal coconut-shell ash on the physical and rheological properties of bitumen." *Building and construction materials*, 1-10.

Jhonson, D. (2019, June 4). "Where Does Graphene Go From Here?" *IEEE Spectrum*.

Johra, F. T., Lee, J.-W., and Jung, W.-G. (2014). "Facile and safe graphene preparation on solution based platform." *Journal of Industrial and Engineering Chemistry* , 2883–2887.

Karnati, S. R., Oldham, D., Finni, E. H., and Zhang, L. (2019). "Surface functionalization of silica nanoparticles to enhance aging resistance of asphalt binder." *Construction and Building Materials* , 1065–1072.

Kim, H., Abdala, A. A., and Macosko, C. W. (2010). "Graphene/Polymer Nanocomposites." *Macromolecules*, 6515–6530.

Kim, S.-S. (2005). "Direct Measurement of Asphalt Binder Thermal Cracking." *Journal of Materials in Civil Engineering*.

Kruskal, W. H., and Wallis, W. A. (1952). "Use of Ranks in One-Criterion Variance Analysis." *American Statistical Association - Volume 47, Issue 260*.

Lee, C., Wei, X., Kysar, J. W., and Hone, J. (2008). "Measurement of the Elastic Properties and Intrinsic Strengthof Monolayer Graphene." *Science*, 321-385.

Lewandowski, L. H. (1994). "Polymer modification of paving asphalt binder." *Rubber chemistry and technology*, 447-480.

Li , Y., Wu, S., and Amirkhanian, S. (2018). "Investigation of the graphene oxide and asphalt interateraction and its effect on asphalt pavement." *Construction and building materials*, 572-584.

Li, C., Wu, S., Tao, G., and Xiao, Y. (2016). "Initial Self-Healing Temperatures of Asphalt Mastics Based on Flow Behavior Index." *Materials*, 917-932.

Liu , X., Li , T., and Zhang, H. (2018). "Short-term aging resistance investigations of polymers and polyphosphoric acid modified asphalt binders under RTFOT aging process." *Construction and building materials*, 787-794.

Liu, K., Zhang, K., and Shi, X. (2018). "Performance evaluation and modification mechanism analysis of asphalt binders modified with graphene oxide." *Construction and Building Materials*, 880–889.

Mallick, R. B., Chen, B.-L., and Bhowmic, S. (2009). "Harvesting energy from asphalt pavements and reducing the heat island effect." *International Journal of Sustainable Engineering*, 214-228.

Moghaddam , T. B., and Baaj, H. (2018). "Rheological characterization of high-modulus asphalt mix with modified asphalt binders." *Construction and building materials*, 142 - 152.

Moghaddam, T. B., Karim, M. R., and Abdelaziz, M. (2011). "A review on fatigue and rutting performance of asphalt mixes." *Scientific Research and Essays* , 670-682.

Nahm, F. S. (2016). "Nonparametric statistical tests for the continuous data: the basic concept and the practical use." *Korean J Anesthesiolv.69(1)*.

Peters , C. A. (2001). "Statistics for Analysis of Experimental Data." In *Environmental Engineering Processes Laboratory Manual.* Champaign, IL: S. E. Powers, Ed.

Petersen, J. C., Robertson, R. E., Branthaver, J. F., Harnsberger, P. M., Duvall, J. J., Kim, S. S., . . . Glover, C. J. (1987). *"Basic characterization and evaluation - Volume 4; Test methods."* Natiional Academy of science: Washington, DC

Polacco, G., Filippi, S., Merusi, F., and Stastna, G. (2015). "A review of the fundamentals of polymer-modified asphalts: Asphalt/polymer interactions and principles of compatibility." *Advances in Colloid and Interface Science - volume 224*, 72-112.

Saboo, N., and Kumar, P. (2015). "A study on creep and recovery behavior of asphalt binders." *Construction and Building Materials* , 632–640.

Santagata, E., Baglieri, O., Tsantilis, L., and Dalmazzo, D. (2012). "Rheological Characterization of Bituminous Binders Modified with Carbon Nanotubes." *Procedia - Social and Behavioral Sciences - Volume 53*, 546-555.

Sha, Q.-l. (2006). "The premature damage of bituminous pavement on expressway and the counter measures." *Journal of Changsha University of Science & Technology - Natural Science- volume - 03*.

Shafabakhsh, G. H., Sadeghnejad, M., and Sajed, Y. (2014). "Case study of rutting performance of HMA modified with waste rubber powder." *case studies in sonstruction materials*, 69-76.

Shirzad , S., Hassan, M. M., Aguirre , M. A., Mohammad, L. N., Cooper Jr, S., and Negulescu, I. I. (2019). "Rheological properties of asphalt binder modified with recycled asphalt materials and light-activated self-healing polymers." *Construction and building materials*, 187-195.

Singh, K. L., Kumar, P., and Mehndiatta, H. C. (2006). *"Rheological behaviour of bituminous binders for indian conditions."* IIT Roorkee: Roorkee

Singh, M., Kumar, P., and Maurya, M. R. (2013). "Effect of aggregate types on the performance of neat and EVA-modified asphalt mixtures." *International Journal of Pavement Engineering*, 163-173.

Sinha, V., Singh, H., and Shekhar, S. (2007). "Rutting in Flexible Pavements – A CASE STUDY." *J. Indian Roads Cogress*, 177-191.

Soenena , H., Blombergb, T., Pellinenc , T., and Laukkanenc, O.-V. (2013). "The multiple stress creep-recovery test: a detailed analysis of repeatability and reproducibility." *Road Materials and Pavement Design*, 2-11.

Soleimani, A., Walsh, S., and A, S. (2009). "Asphalt Cement Loss Tangent as Surrogate Performance Indicatorfor Control of Thermal Cracking." *Transportation Research Record, ,* 39-46.

Sybilski, D., Soenen, H., Gajewski, M., Chailleux, E., and Bankowski, W. (2013). "Binder Testing." In M. N. Partl, E. Chailleux, H. U. Bahia, F. Canestrari, C. Roche, H. D. Benedetto, . . . D. Sybilski , *Advances in Interlaboratory Testing and Evaluation of Bituminous Materials: State-of-the-Art Report of the RILEM Technical Committee 206-ATB* (15-63). Springer Netherlands.

Terrel, R. L., and Epps, J. A. (1988). *"User manual on additives and modifiers in asphalt binder."* National Pavement Asphalt Association

Toothaker , L. E., and Newman, D. (1994). "Nonparametric Competitors to the Two-Way ANOVA." *Journal of Educational and Behavioral Statistics - Volume 3*, 237 - 273.

Tyson, B. M., Abu Al Rub, R. K., Yazdanbakhsh, A., and Grasley, Z. (2011). "A quantitative method for analyzing the dispersion and agglomerationof nano-particles in composite materials." *Composites: Part B 42*, 1395–1403.

Vissche, J. D., Paez-Dueñas, A., Cabanillas, P., Carrera, V., Cerny, R., Durand, G., . . . Lancaster, I. (2016). "European round robin tests for the Multiple Stress Creep Recovery Test and contribution to the development of the European standard test method." *6th Eurasphalt & Eurobitume Congress* ., E&E Congress 2016: Prague, Czech Republic

Wang, Z., Dai, Q., Guo, S., Wang , R., Ye , M., and Yap , Y. K. (2017). "Experimental investigation of physical properties and accelerated sunlight-healing performance of flake graphite and exfoliated graphite nanoplatelet modified asphalt materials." *Construction and Building Materials* , 412–423.

Wei, W., and Qu, X. (2012, 8). "Extraordinary Physical Properties of Functionalized." *Small*, 2138–2151.

Yildrim, Y. (2007). "Polymer modified asphalt binders." *Construction and building materials*, 67-72.

Yin, Y., Huang, W., and LvXiang, J. (2018). "UnifiedConstruction of Dynamic Rheological Master Curve of Asphalts and Asphalt Mixtures." *International Journal of Civil Engineering - Volume 16, Issue 9*, 1057–1067.

Yinfei, D., Jiaqi, C., Zheng, H., and Weizheng, L. (2018). "A review on solutions for improving rutting resistance of asphalt pavement and test methods." *Construction and Building Materials - Volume 168*, 893-905.

Yuan, Q., Lin, C.-T., and A, K. W. (2019). "All-carbon devices based on sp2-on-sp3 configuration." *APL Mater*.

Zani , L., Giustozzi, F., and Harvey, J. (2017). "Effect of storage stability on chemical and rheological properties of polymer-modified asphalt binders for road pavement construction." *Construction and Building Materials*, 326–335.

Zhang, D., Chen, M., Wu, S., and Ria, M. (2019). "Thermal and rheological performance of asphalt binders modified with expanded graphite/polyethylene glycol composite phase change material (EP-CPCM)." *Construction and Building Materials*, 83–91.

Zhang, R., and Zhu, H. (2018). "Potential Applications and Perspectives." In H. Zhu, Z. Xu, D. Xie, and Y. Fang, *Graphene: Fabrication, Characterizations, Properties and Applications* (233-249). Academic Press.

Zhen, Z., and Zhu, H. (2018). "Structure and Properties of Graphene." In H. Zhu, Z. Xu, D. Xie, and Y. Fang, *Graphene: Fabrication, Characterizations, Properties and Applications* (1-12). Academic Press.

Zhu, Y., Stoller, M. D., Cai, W., and Vel, A. (2010). "Exfoliation of Graphite Oxide in Propylene Carbonate and Thermal Reduction of the Resulting Graphene Oxide Platelets." *ACS Nano*, 1227–1233.

raft_-_5-_corrections_-_22_July_2019_-_Moeed_-_AKC_Review-1.docx

ORIGINALITY REPORT

11%	4%	7%	7%
SIMILARITY INDEX	INTERNET SOURCES	PUBLICATIONS	STUDENT PAPERS

PRIMARY SOURCES

1	Kefei Liu, Kun Zhang, Xianming Shi. "Performance evaluation and modification mechanism analysis of asphalt binders modified by graphene oxide", Construction and Building Materials, 2018 Publication	1%
2	Yuanyuan Li, Shaopeng Wu, Serji Amirkhanian. "Investigation of the graphene oxide and asphalt interaction and its effect on asphalt pavement performance", Construction and Building Materials, 2018 Publication	<1%
3	www.tandfonline.com Internet Source	<1%
4	Submitted to Universiti Teknologi MARA Student Paper	<1%
5	Submitted to La Trobe University Student Paper	<1%
	Submitted to Universiti Teknologi Petronas	

6	Student Paper	<1%
7	Submitted to University of Nottingham Student Paper	<1%
8	Dong Zhang, Meizhu Chen, Shaopeng Wu, Martin Riara, Jiuming Wan, Yuanyuan Li. "Thermal and rheological performance of asphalt binders modified with expanded graphite/polyethylene glycol composite phase change material (EP-CPCM)", Construction and Building Materials, 2019 Publication	<1%
9	ascelibrary.org Internet Source	<1%
10	hrcak.srce.hr Internet Source	<1%
11	Submitted to National University of Singapore Student Paper	<1%
12	Hui Yao, Zhanping You, Liang Li, Chee Huei Lee, David Wingard, Yoke Khin Yap, Xianming Shi, Shu Wei Goh. "Rheological Properties and Chemical Bonding of Asphalt Modified with Nanosilica", Journal of Materials in Civil Engineering, 2013 Publication	<1%